Nanocapsules loaded hydrogels for intra-articular and intra-peritoneal drug delivery

Bhanu Teja Surikutchi, M.S (Pharm.), MBA

Thesis submitted to the University of Nottingham and Universidade de Santiago de Compostela for the degree of Doctor of Philosophy

October 2019

Table of contents

1. Introduction 24

1.1 Local drug delivery 24

1.1.1 Formulation approaches for local delivery 25

1.2 Intra-articular (IA) delivery 30

1.2.1 Osteoarthritis (OA) – anatomy and pathology of disease 30

1.2.2 OA – current treatment regimen & approaches 31

1.2.3 Introduction to IA delivery 33

1.2.4 Shortcomings of marketed IA formulations 34

1.2.5 Formulation strategies employed to overcome the shortcomings of IA formulations 35

1.3 Introduction to intra-peritoneal (IP) local delivery 40

1.3.1 Clinical approaches for IP delivery – HIPAC & PIPAC 41

1.3.2 Challenges associated with IP delivery 42

1.3.3 Anatomy and physiology of peritoneum 43

1.3.4 Formulation strategies employed for IP delivery 44

1.4 Objective and scope of project 48

2. Development and evaluation of nanocapsules-loaded hydrogels for intra-articular drug delivery 50

2.1 Materials 53

2.2 Methods 54

2.2.1 Preparation and characterization of HA NCs 54

2.2.2 Preparation and characterization of NCs loaded Fn-HA gels 56

2.2.3 *In vitro* release studies 58

2.2.4 Evaluation of local residence and biodistribution 60

2.2.5 Evaluation of *in vivo* efficacy 62

2.3 Results and discussion 64

2.3.1 Development and characterization of DXM NCs 64

2.3.2 Development and characterization of Fn-HA gel loaded with DXM NCs 70

2.3.3 *In vitro* release studies 74

2.3.4 Evaluation of local residence and biodistribution after IA administration of ^{111}In labelled NCs 77

2.3.5 Evaluation of anti-inflammatory efficacy of Fn-HA gel containing DXM NCs in AIA rats 83

2.4 Conclusions 92

3. Development and evaluation of nanocapsules-loaded enzymatically / physically crosslinked gels for intra-peritoneal drug delivery 94

3.1 Materials 98

3.2 Methods 98

3.2.1 Preparation and characterization of DiR NCs 98

3.2.2 Preparation and optimization of Fn-HA and 2′-dC-*N*4-C_8 gels containing DiR NCs 100

3.2.3 Characterization of Fn-HA and 2′-dC-*N*4-C_8 gels containing DiR NCs 101

3.2.4 *In vivo* local residence and biodistribution studies 102

3.3 Results and discussion 104

3.3.1 Preparation and characterization of DiR NCs 104

3.3.2 Development and optimization of NCs-loaded 2′-dC-*N*4-C_8 gel 106

3.3.3 Characterization of Fn-HA and 2′-dC-*N*4-C_8 gels 109

3.3.4 *In vivo* local residence and biodistribution studies using IVIS® fluorescence imaging 117

3.4 Conclusion 123

4. Intra-peritoneal delivery – Development and evaluation of covalently cross-linked hydrogels incorporated with NCs 125

4.1 Materials 128
4.2 Methods 128
4.2.1 Preparation and optimization of covalently crosslinked hydrogels 128
4.2.2 Characterization of covalently crosslinked hydrogels 131
4.2.3 *In vivo* local residence and biodistribution studies 133
4.2.4 Incorporation of DCX into NCs 134
4.3 Results and discussion 136
4.3.1 Preparation and optimization of covalently cross-linked hydrogels 136
4.3.2 Characterization of PEG-MAL – thiol gels 146
4.3.3 *In vivo* local residence and biodistribution studies 151
4.3.4 Incorporation of DCX into NCs 158
4.4 Conclusions 161
5. Conclusions and Future work 164
5.1 Conclusions 164
5.1.1 Development of NCs-loaded hydrogel for IA delivery 166
5.1.2 Development of NCs-loaded hydrogel for IP delivery 167
5.2 Future work 170
5.2.1 Further development & evaluation of DXM NCs-loaded Fn-HA gel 170
5.2.2 Further development & evaluation of DCX NCs-loaded PEG-MAL – thiol gel 171
6. References 173

Declaration

Unless otherwise acknowledged, the work presented in this thesis is my own. No part has been submitted for any other degree at The University of Nottingham or any other institution.

As the project was part of the NanoFar doctorate programme, part of experimental work was done at University of Santiago de Compostela.

This doctoral dissertation was conducted under the supervision of:

Dr Maria José Alonso Fernández, Full Professor, Department of Pharmaceutical Technology, University of Santiago de Compostela, Spain

Dr Maria Marlow, Associate Professor, School of Pharmacy, University of Nottingham, UK

Dr José Crecente Campo, Research scientist, Department of Pharmaceutical Technology, University of Santiago de Compostela, Spain

Dr Anna Grabowska, Professor of Cancer Microenvironment, Faculty of Medicine & Health Sciences, University of Nottingham, UK

Bhanu Teja Surikutchi

October 2019

Acknowledgements

Life is a canvas on which we paint the colours of happiness, grief, enthusiasm, mercy, anxiety, kindness and many other feelings. It always drives us into situations, which change our thought process and help us to grow every day. Change is the only thing in the world that never changes. I am recollecting these phrases as these were the thoughts that motivated me to start my PhD. I am extremely grateful for the society where I brought up to cultivate this thinking in me.

I express my sincere respect and gratitude to my supervisors, Dr. Maria Marlow at the University of Nottingham, Dr. Maria José Alonso and Dr. José Crecente Campo at Universidad de Santiago de Compostela, Spain for the supervision and guidance that they have offered me during the course of my Ph.D. I'm also thankful to my co-supervisor at University of Nottingham, Dr Anna Grabowska for her guidance on *in vivo* intra-peritoneal studies. I would also like to express my thanks to European Commission, Education, Audiovisual and Culture Executive Agency (EACEA), Erasmus Mundus programme, NanoFar doctorate funding. It has given me an opportunity to work, explore and connect with people working in different domains from different countries. This opportunity gave me exposure to multiple cultures, which has broaden my mind. Without the support of NanoFar, it would not be possible for me to this PhD.

In vivo studies that were performed during this PhD were only possible with the support from collaborators. Dr Edgar Pérez-Herrero, Dr Araceli Delgado, Dr Carmen Evora and Dr Patricia García-García supported me with the *in vivo* intra-articular biodistribution studies at Universidad de La Laguna, Spain. Additionally, Jennifer Fernández, Olalla Ramil Gómez and Dr Maria José Armada from Universidade da Coruña, Spain, have supported me with the *in vivo* intra-articular efficacy studies. Dr Irene Golán Cancela and Dr José A. Costoya from Universidad de Santiago de Compostela, Spain also supported me with *in vivo* intra-peritoneal IVIS® imaging studies. I am thankful to all of them who gave me tremendous support with the execution of animal experiments, data analysis, and interpretation.

I would also like to thank Belen Cuesta and Balbina Fernández for their technical support during my stay at Universidad de Santiago de Compostela, Spain. Additionally, the technical support offered by Esmé Ireson and Paul cooling from Boots Science Building was remarkable. I am also thankful to Dr. Christopher Parmenter from Nano and Microscale Research Centre (NMRC) at the University of Nottingham, UK, for his support with electron microscopy.

Professional excellence is difficult to achieve without moral support from family and friends. Thankfulness is a small word to give credits to my parents, Badarinath Surikutchi and Naga Hymavathi, who gave me life and shaped me to whom I am today. I am grateful to them for everything. My wife, Radha has been supportive and understanding. During the most crucial last year of my PhD, she gave me strength during the times when I was low and she was always there with me to share happy moments. I am very thankful to her. I also thank my sister Bhavya whose happiness makes me smile. Special thanks to my friend Maruthi Prasanna, who has been supportive personally at all times. The time I spent with him in Santiago de Compostela was remarkable. I also thank my NanoFar colleagues and alumni for their guidance.

Abstract

In this thesis, composite hydrogels containing polymeric nanocapsules (NCs) were developed and evaluated for sustained drug delivery through intra-articular (IA) and intra-peritoneal (IP) administrations, for the treatment of osteoarthritis (OA) and peritoneal malignancies. IA corticosteroids or hyaluronic acid (HA) injections are prescribed to manage the moderate stage of OA. Despite their long clinical use, the therapeutic efficacy of these formulations is often limited because of their short joint residence time. Nanoparticles, after IA administration, could penetrate into the synovial membrane and show enhanced efficacy. They have been incorporated into hydrogels to form composite systems to further enhance joint retention. In this study, dexamethasone (DXM), a model anti-inflammatory agent, has been incorporated into hyaluronic acid (HA) NCs to yield a maximum drug loading of 6 mg/mL. These DXM NCs were found to have a particle size, PDI and zeta potential of 250 ± 30 nm, 0.2 and -17 ± 3 mV respectively, which were stable up to 1 month at 2 – 8 ºC. Further, a fibrin (Fn) – HA hydrogel, previously developed in our lab, was optimized to incorporate up to 34% w/w of DXM NCs. Oscillatory amplitude and frequency sweep tests performed on Fn-HA gel showed a viscoelastic behaviour comparable to commercial IA hydrogels. An *in vitro* release study performed on DXM NCs-loaded Fn-HA gel exhibited a DXM release of up to 70% in 48 h. Further, *in vivo* local residence and biodistribution studies, performed with ^{111}In-labelled NCs indicated that the NCs were cleared through popliteal lymph nodes from the knee cavity and that this behaviour was not influenced by the presence of the Fn-HA gel. A long and short-term anti-inflammatory efficacy study performed in antigen induced arthritis (AIA) rats showed no beneficial anti-inflammatory activity, as observed from knee diameters and synovial histology. Hence, the developed formulation did not overcome the current challenge associated with ineffective steroid anti-inflammatory IA injections.

Another part of the thesis involved the development and evaluation of a composite formulation for IP drug delivery in the management of peritoneal malignancies. IP administration of chemotherapeutic drugs would be beneficial in patients with peritoneal malignancies. Nanoparticles could be used as potential drug delivery strategy for IP administration because of their potential

to offer higher tumour penetration. Incorporation of nanoparticles in the hydrogel delays their clearance from the IP cavity and provides sustained release. Hence, in chapters 3 and 4, different hydrogels have been developed for IP delivery to incorporate NCs. A fluorescent dye, DiR, was first incorporated into HA NCs to allow the determination of *in vivo* local residence and biodistribution through IVIS® imaging in immunodeficient BALB/c nude mice. Further, two different hydrogels, Fn-HA gel and a self-assembling 2′-dC-*N*4-C_8 gel, were optimized to incorporate 30% w/w of DiR NCs. Fn-HA gel, upon IP administration showed fluorescence up to 2 weeks, which was confirmed through *ex vivo* analysis as uptake of the NC by the liver. Hence, it was concluded that Fn-HA gel failed to retain the NCs in the peritoneal cavity. This finding triggered the development of a covalently cross-linked hydrogel that could offer better sustained release. Branched poly(ethylene glycol) (PEG) polymers, 4-arm PEG norbornene (PEG-NB) and 4-arm PEG maleimide (PEG-MAL), were selected to develop covalently cross-linked hydrogels. A linear PEG was chemically modified to include thiol-end groups through an ester linkage to form a cross-linker, PEG-SH. PEG-NB and PEG-SH underwent photocrosslinking reaction to form a hydrogel, which was mediated by photoinitators LAP or Irgacure® 2959 in presence of UV. However, DiR was degraded in the gel due to incompatibility with the photoinitiators. Alternatively, PEG-MAL reacted with PEG-SH to form a hydrogel through Michael-type addition reaction, incorporating DiR NCs without degradation of DiR. *In vitro* release studies showed that PEG-MAL – thiol gel (10% w/w PEG-MAL concentration with equimolar PEG-SH) showed 45% cumulative DiR release in 5 days. IVIS® imaging study showed that this hydrogel resided in the IP cavity between 24 h and 1 week, after implantation in the cavity through a surgical procedure. This *in vivo* study also demonstrated the biodegradability and tolerability of PEG-MAL – thiol gel within the experimental timeframe. DCX, a model chemotherapeutic agent was then incorporated into NCs, which were then incorporated into PEG-MAL – thiol gel to yield a final DCX concentration of 0.9 mg/mL. The *in vitro* release study showed a cumulative DCX release of 45 % in 2 days, indicating that the hydrogel has shown control over the DCX release. In summary, PEG-MAL – thiol gel showed potential residence in the IP cavity and demonstrated the controlled release of DCX.

Abbreviations

% EE	Percentage entrapment efficiency
% ID	Percentage injected dose
$^{111}InCl_3$	Indium chloride (radioactive isotope of Indium)
2′-dC-N4-C_8	*N*-4-octanoyl-2′-deoxycytidine
AIA	Antigen induced arthritis
AUC	Area under curve
BSA	Bovine serum albumin
BZT	Benzethonium chloride
$CaCl_2$	Calcium chloride
CRP	C-reactive protein
Cryo-TEM	Cryogenic transmission electron microscopy
DCX	Docetaxel
DiR	1,1"-dioctadecyl-3,3,3",3"-tetramethylindotricarbocyanine iodide
DLS	Dynamic light scattering
DTPA-PE	1,2-dimyrisoyl-sn-glycero-3-phosphoethanolamine-*N*-diethylenetriaminepentaacetic acid
DTT	Dithiothreitol
DXM	Dexamethasone
ECM	Extracellular matrix
ELISA	Enzyme-linked immunosorbent assay
FCA	Freund’s complete adjuvant
FIB-SEM	Focussed ion bean scanning electron microscopy
Fn	Fibrin
GMP	Good manufacturing practice
HA	Hyaluronic acid
HA-ADH	HA functionalized with adipic dihydrazide-end groups
HA-CHO	HA functionalized with aldehyde-end groups
HIPEC	Hyperthermal intra-peritoneal chemotherapy
HPLC	High-performance liquid chromatography
IA	Intra-articular
IP	Intra-peritoneal

KCl	Potassium chloride
KH_2PO_4	Potassium phosphate monobasic
Labrafac	Labrafac^{TM} Lipophile WL 1349
LAP	Lithium phenyl-2,4,6-trimethylbenzoylphosphinate
LDA	Laser Doppler anemometry
Lipocol	Lipocol 40-HCO (PEG 40-hydrogenated castor oil)
mBSA	Methylated bovine serum albumin
$MgCl_2$	Magnesium chloride
Na_2HPO_4	Sodium phosphate dibasic
NaCl	Sodium chloride
NaOH	Sodium hydroxide
NCs	Nanocapsules
NMR	Nuclear magnetic resonance
NSAIDS	Non-steroidal anti-inflammatory agents
NTA	Nanoparticle tracking analysis
OA	Osteoarthritis
PBS	Phosphate buffer saline
PCL	Poly(caprolactone)
PDI	Polydispersity index
PDPA	poly(oligoethylene glycol methacrylate)-poly(2-(diisopropylamino)ethyl methacrylate
PECT	poly (e-caprolactone-co-1,4,8-trioxa [4.6]spiro-9-undecanone)-poly(ethylene glycol)-poly (e-caprolactone-co-1,4,8-trioxa [4.6]spiro-9-undecanone))
PEG	Poly(ethylene glycol)
PEG-MAL	4-arm poly(ethylene glycol) maleimide
PEG-NB	4-arm poly(ethylene glycol) norbornene
PEG-SH	Poly(ethylene glycol) with mercaptopropionate-end groups
PEVA	Poly(ethylene-vinyl acetate)
PGA	Poly(glycolic acid)
PIPAC	Pressurized intra-peritoneal aerosol chemotherapy
PLA	Poly(lactic acid)

PLGA	Poly(lactic-co-glycolic acid)
PRP	Platelet rich plasma
PVA	Poly(vinyl alcohol)
PVDF	Polyvinylidine difluoride
SD-NCs	Nanocapsules prepared by solvent displacement
SE-NCs	Nanocapsules prepared by self-emulsification
SIPF	Simulated intra-peritoneal fluid
SSF	Simulated synovial fluid
UV	Ultraviolet
VEGF	Vascular endothelial growth factor

List of figures

Figure 1.1 Schematic representation of different types of thermosensitive hydrogels used for local drug delivery. (a) Hydrogels prepared from micelles, incorporated with a hydrophobic drug; (b) Hydrogels prepared through synthesis of novel thermosensitive hydrogel materials, containing larger hydrophobic domain for high drug loading; (c) Hydrogels incorporated with liposomes, nanoparticles or microparticles; (d) Hydrogel formed by association of polymer and surfactant to form mixed micelles; (e) Hydrogels incorporated with nanocrystals (Adapted from reference (23)) 27

Figure 1.2 Schematic representation of anatomical changes that occur in a typical articulating joint, affected with osteoarthritis. Degeneration and fibrillations on the cartilage, formation of subchondral cysts and inflammation of synovial membrane with thickening of joint capsule that are commonly observed radiological investigation are indicated here. 31

Figure 1.3 Schematic representation of current standard of care employed in the management of OA, indicating the strategies employed from mild to severe stage of disease (from left to right). (Adapted from reference (42)).....32

Figure 1.4 Schematic illustration of leaky nature of the synovial membrane. Small molecules are exchanged between synovial cavity and systemic circulation through blood and lymph capillaries, whereas large molecules undergo preferential lymphatic drainage upon IA injection. 35

Figure 1.5 Illustration of fate of nano and microparticles after IA administration. (a) Nanoparticles can be phagocytosed by type A synoviocytes from the peritoneal cavity, which would be helpful for their penetration into subsynovium to retain longer in the cavity. (b) Targeted nanoparticles can selectively penetrate into the articular cartilage, which would be helpful in cartilage regeneration. (c) Microparticles penetrate neither into subsynovium nor into articular cartilage, rather retain longer within the synovial cavity. (Adapted from reference (73)) 38

Figure 1.6 Schematic representation of different clinically relevant techniques for IP drug delivery. Conventional IP chemotherapy involves use of administration of chemotherapeutic agents at regular intervals, whereas metronomic IP chemotherapy involves continuous administration without drug-

free periods. PIPAC and HIPEC involves administration of chemotherapeutic agents under high pressure or high temperature respectively, for effective tissue penetration. Hydrogels containing micro or nanoparticles are also suggested as potential drug delivery strategy in the future for prolonged retention and sustained efficacy after IP administration. (Adapted from reference (105)).....42
Figure 2.1 A representative polarized microscopic image obtained from isolated NCs, prepared by solvent displacement, using lecithin as a surfactant. Presence of birefringence indicates the recrystallization of DXM.....65
Figure 2.2 Microscopic images of self-emulsifying nanoemulsions. Immediately after the preparation, combinations VII, VIII and IX showed the recrystallization of DXM, while combinations I, III, IV, V and VI indicated the instability of nanoemulsion due to phase separation.....68
Figure 2.3 Schematic representation of optimized manufacturing process for preparation of self-emulsifying DXM NCs.....69
Figure 2.4 Influence of the molecular weight and concentration of HA on the colloidal stability of DXM NCs. Particle size was measured after preparing the DXM NCs and at different time points during their storage at 2-8°C. Except HA (40 kDa) at 0.25% w/w, all other formulations showed increase in size after 28-day storage ($p < 0.05$, Dunnett's multiple comparison test). (Each value is a Mean ± SD of 3 preparations).....69
Figure 2.5 Optimization of Fn-HA gel to incorporate DXM NCs. Gels were prepared at increasing concentrations of fibrinogen and thrombin. Images were captured after preparation of gels at different time points, where (a) indicates Gel-1 after 6 min; (b) indicates Gel-2 after 6 min; (c) indicates Gel-3 after 6 min; (d) indicates Gel-4 after 4 min, and (e) indicates Gel-5 after 2 min. Gel-4 and Gel-5 have formed the gels in presence of DXM NCs.....72
Figure 2.6 Rheology of Fn-HA gel containing DXM NCs, performed by oscillatory amplitude sweep using parallel plate assembly at 25 ºC. Viscoelastic property of the gel was confirmed by presence of a LVE region, where G' was > G". Presence of crossover point indicates the mechanical breakdown of the gel at > 10% strain. (Data represented as Mean ± SD, n = 3).....73
Figure 2.7 Rheology of Fn-HA gel containing DXM NCs, performed by oscillatory frequency sweep using parallel plate assembly at 25 ºC. A steady increase in G' and G" indicates the viscoelastic properties of the gel. No

crossover point indicates that the elastic property of the gel was retained in the frequency range tested. (Data represented as mean ± SD, n = 3) 74
Figure 2.8 Colloidal stability of DXM NCs in SSF, determined by incubating them in SSF at 37 °C for 48 h, measuring the particle size at regular intervals. No significant change in particle size was observed after 48 h of incubation ($p > 0.05$, Dunnett's multiple comparison test). (Each value is a Mean ± SD, n = 3).....75
Figure 2.9 *In vitro* release study, showing the % cumulative release of DXM from DXM NCs, determined using dialysis membrane (7 kDa cutoff), which was further incubated in SSF at 37 ºC. (Each value is a Mean ± SD, n = 3) ...76
Figure 2.10 *In vitro* release study, showing the % release of DXM from Fn-HA gel containing DXM NCs, incubated in SSF at 37 ºC. (Each value is a Mean ± SD, n = 3) 77
Figure 2.11 Radiolabel stability of ^{111}InNCs, determined by incubating them with SSF at 37 ºC. At each time point, samples were centrifuged with Amicon® filters to separate and quantify free ^{111}In from ^{111}In bound to NCs. (Each value is a Mean ± SD, n = 3) 78
Figure 2.12 Local residence of ^{111}In labelled NCs, administered alone or in Fn-HA gel, represented as Mean ± SEM of %ID remaining at injection site after IA administration in (a) healthy and (b) arthritic rats (n=3 rats/group), as determined by a gamma counter probe (Captus®, Nuclear Iberica). A physical mixture of NCs alone and NCs loaded in Fn-HA gel with $^{111}InCl_3$ were used as controls (n=3 rats/group). 80
Figure 2.13 Biodistribution of ^{111}InNCs, administered alone or in Fn-HA gel, represented as Mean ± SEM of %ID/g obtained from various organs at (a) 6 h, (b) 24 h and (c) 72 h after IA administration (n=3 rats/group), using a gamma counter (Cobra II, Packard). A physical mixture of NCs alone and NCs loaded in Fn-HA gel with $^{111}InCl_3$ were used as controls (n=3 rats/group).....82
Figure 2.14 Evolution of the (a) left and (b) right knee diameters and (c) the body weight in a 28-day efficacy study performed in arthritic AIA rats. Treatments administered by the IA route were: free DXM (group 4), DXM-loaded NCs (group 5) and Fn-HA gel containing DXM-loaded NCs (group 6) in AIA rats. Healthy rats (group 1) were used as negative control. Untreated AIA rats (group 2) and AIA rats treated with Fn-HA gel containing blank NCs (group

3) were used as other controls for the study. Data represented as Mean ± SEM (n=6 rats/group).....85
Figure 2.15 Evolution of the knee diameter (b) and the body weight (a) in a 14-day efficacy study performed in arthritic AIA rats. Treatments administered by the IA route were: free DXM alone (group 3) and Fn-HA gel containing DXM NCs (group 4) in AIA rats. Healthy rats (group 1) and untreated AIA rats (group 2) were used as controls for the study. Data represented as Mean ± SEM (n=8 rats/group) 86
Figure 2.16 Serum CRP values obtained from 28-day evaluation study, during the course of disease induction and treatment, measured by collecting the blood samples from retro-orbital plexus of rats, followed by ELISA test. Data represented as Mean ± SEM (n=6 rats/group). No significant differences were obtained between the groups, except between negative control and non-treated AIA group without any treatment (*$p < 0.05$, two-way ANOVA, Dunnett's multiple comparison test).....87
Figure 2.17 Microscopic slides obtained from 28-day anti-inflammatory efficacy study, showing the histology of cross-sections obtained from left knees of rats related to different groups, stained with Masson's trichome stain at 3 different magnifications. ST, M, FC and TP indicates synovial tissue, meniscus, femoral condyle and tibial plateau respectively.....89
Figure 2.18 Histological scores obtained by double-blind analysis of (a) synovium and (b) cartilage cross-sections obtained on 28th day of the study. DXM NCs and Fn-HA gel containing DXM NCs have shown significant differences from untreated AIA group (* $p \leq 0.05$ done Mann-Whitney post-hoc analysis), while no significant differences between the groups were seen with cartilage cross-sections.....90
Figure 2.19 Histological scores obtained by double-blind analysis of (a) synovium and (b) cartilage cross-sections obtained on 14th day of the study. No significant differences between the groups were seen with both synovial and cartilage cross-sections.....91
Figure 3.1 Optimization of 2′-dC-N4-C_8 gel to incorporate NCs, showing the increasing concentrations of a gelator, from 0.3 to 20% w/w, while the concentration of NCs was kept constant at 30% w/w. Gelator was first dissolved in the PBS (0.01 M, pH 7.4) at 60 ºC, and a suspension of NCs in PBS (0.01 M,

pH 7.4) was added to it after cooling the solution between 40 – 45 ºC. The formation of hydrogel was evaluated by vial inversion, performed after leaving the gels for 24 h at room temperature. Gels were not formed at (a) 0.3 %w/w, (b) 1 %w/w and (c) 2 %w/w gelator concentration, while gelator concentrations at (d) 3 %w/w, (e) 4 %w/w and (f) 20 %w/w showed gel formation.....108

Figure 3.2 Rheology performed immediately after the preparation of Fn-HA gel and 24 h after preparation of 2′-dC-N4-C_8 gel. (a) Oscillatory amplitude sweeps of Fn-HA and 2′-dC-N4-C_8 gels performed within the strain range of 0.1 to 100 % at a fixed frequency of 10 rad s^{-1}, 25 ºC. (b) 2′-dC-N4-C_8 gels showing significantly higher G' and G" ($p < 0.05$, paired t-test). Data represented as Mean ± SD (n = 3).....111

Figure 3.3 Rheology of 2′-dC-N4-C_8 gel, performed after 24 h of preparation: (a) Oscillatory amplitude sweep study showing the influence of incorporation of NCs on mechanical properties of the 2′-dC-N4-C_8 gel, performed within the strain range of 0.1 to 100 % at a fixed frequency of 10 rad s^{-1}, 25 ºC. (b) Time-dependent recovery performed on 2′-dC-N4-C_8 gel, by running 4 cycles of each constituting a strain of 0.5% for 20 min and 500% for 5 min, at 25 ºC. 113

Figure 3.4 Cryo-TEM images of Fn-HA (a & b) and 2′-dC-N4-C_8 gels (c & d). Fn-HA gel was spotted on to the grid immediately after mixing NCs and gel components in a syringe, whereas sample for 2′-dC-N4-C_8 gel was spotted onto the grid immediately after addition of NCs into 2′-dC-N4-C_8 solution at 40 – 45 ºC. Samples were left undisturbed at room temperature for 3 – 5 min on the grid before freezing. Images were captured after cryogenic freezing in liquid ethane at – 90 ºC using Cryoplunge®.....114

Figure 3.5 *In vitro* release of DiR from Fn-HA and 2′-dC-N4-C_8 gels, determined by incubating them in SIPF at 1:3 and 1:9 dilutions respectively, at 37 ºC. Data indicates the fluorescence intensity obtained as the sum of free and NCs bound DiR, represented as Mean ± SD (n=3).....117

Figure 3.6 *In vivo* pilot studies to determine the optimum concentration of DiR required for IVIS® imaging. (a) First pilot study performed at 25 ppm DiR concentration, showing the fluorescence acquired with time among the groups administered with DiR alone, DiR NCs, Fn-HA gel + blank NCs and Fn-HA gel + DiR NCs (n = 2 mice/group). Each image shows a negative control and 2 mice respective to that group. (b) Second pilot study performed at 5 ppm DiR

concentration, showing the fluorescence acquired with time among the groups administered with negative control, DiR alone, DiR NCs, Fn-HA gel + blank NCs and Fn-HA gel + DiR NCs (n = 1 mouse/group), represented as 1 to 5 respectively in the 0 h image. All images were captured at λ_{exc} = 745 nm and λ_{em} = 820 nm.....120
Figure 3.7 *In vivo* IVIS® imaging study to determine the local residence and biodistribution of Fn-HA gel containing DiR NCs. (a) Compilation of images showing the fluorescence acquired with time among the groups administered with negative control, DiR alone, DiR NCs and Fn-HA gel + DiR NCs (n=5 mice/group). (b) Compilation of images related to various organs, obtained after sacrificing the mice 2 weeks after IP administration. All images were captured at λ_{exc} = 745 nm and λ_{em} = 820 nm.....122
Figure 4.1 Schematic representation of chemical reaction involved in the synthesis of PEG-SH crosslinker. The linear PEG (MW: 3350, n = 74.7 repeating units) was refluxed with mercaptopropionic acid, in presence of *p*-toluenesulfonic acid and DTT in toluene.. 137
Figure 4.2 Chemical structure of fluorescent dye, DiR, showing the conjugated double bonds, which are susceptible to degradation by photoinitiators, LAP and Irgacure® 2959 in the presence of UV 142
Figure 4.3 Schematic representation of Michael-type addition reaction involved in formation of PEG-MAL – thiol gel (MW of PEG-MAL = 10 kDa, n = 53.3 repeatiting units; MW of PEG-SH = 3350, n' = 74.7 repeating units).....145
Figure 4.4 FIB-SEM images of (a) PEG-Mal – thiol gel frozen under liquid nitrogen using metal mirror freezer (b) PEG-MAL – thiol gel milled at higher beam currents, showing the clusters of NCs. Scale bar indicates 10 µm.....147
Figure 4.5 (a) Gelation kinetics of PEG-MAL – thiol gel as determined by oscillatory rheology performed on parallel plate assembly at 0.5 Hz frequency, 0.5% strain, 0.5 mm gap and 25 ºC, showing the increase of G' and G" with time. (b) A comparison of Fn-HA, 2′-dC-N4-C8 and PEG-MAL – thiol gels, showing a significant difference of G' ($p < 0.05$, Tukey's multiple comparison test). Data represented as mean ± SD (n = 3) 148
Figure 4.6 *In vitro* release study showing the release of DiR from PEG-MAL – thiol gels, as estimated by fluorescence analysis from each time point. Gels were prepared at 5 and 10% w/w concentrations of PEG-MAL and equimolar

concentrations of PEG-SH, followed by incubation under 1:25 dilution in SIPF at 37 ºC. Data represented as mean ± SD (n=3).....151
Figure 4.7 *In vivo* IVIS® imaging study performed on mice (set 1) (a) Compilation of images acquired after 0, 4 and 24 h of administration, showing the fluorescence obtained from DiR alone, DiR NCs and DiR NCs + PEG-MAL – thiol gel groups. Mouse administered with isotonic trehalose solution as negative control is also represented in the image (b) Compilation of images acquired from organs obtained after sacrificing the mice at 24 h time point, showing the fluorescence prominently from liver in case of DiR NCs and DiR NCs + PEG-MAL – thiol gel groups. Gels retrieved from the peritoneal cavity after 24 h, indicating the fluorescence, are also shown here.....155
Figure 4.8 *In vivo* IVIS® imaging study performed on mice (set 2) (a) Compilation of images acquired after 0, 4, 24, 48, 96 h and 1 week of administration, showing the fluorescence obtained from DiR alone, DiR NCs and DiR NCs + PEG-MAL – thiol gel groups. Mouse administered with isotonic trehalose solution as negative control is also represented in the image (b) Compilation of images acquired from organs obtained after sacrificing the mice at 1 week time point, showing the fluorescence prominently from liver in case of DiR NCs and DiR NCs + PEG-MAL – thiol gel groups.....156
Figure 4.9 Biodistribution obtained from IVIS® imaging study after administration of negative control, DiR alone, DiR NCs and DiR NCs + PEG-MAL – thiol gel after IP administration. (a) Average radiance obtained from various organs acquired after sacrificing the mice up on 24 h of IP administration. IP cavity has shown remnants of DiR NCs + PEG-MAL – thiol gel, whose average radiance is also represented here. Data represented is mean ± SEM (n = 2). (b) Average radiance obtained from various organs acquired after sacrificing the mice up on 1 week of IP administration. Data represented is mean ± SEM (n = 4).....157
Figure 4.10 Optimization of DCX loading in NCs. Incorporation of DCX at (a) 12 mg/mL and (b) 7.5 mg/mL has shown recrystallization as seen by birefringence, while (c) 3 mg/mL did not show any recrystallization 159
Figure 4.11 *In vitro* release study showing the release of DCX from PEG-MAL – thiol gel, as determined by extracting the DCX from the media, followed by HPLC analysis from each time point. Gels contain 10% w/w PEG-MAL and an

equimolar concentration of PEG-SH, incubated under 1:25 dilution in SIPF at 37 ºC. Data represented as mean ± SD (n = 3).....161

List of tables

Table 1.1 List of various biodegradable and non-biodegradable polymers that have been explored as implantable drug delivery systems (Adapted from reference ((27))) 28

Table 1.2 Examples of local drug delivery systems evaluated for various routes of administration and sites of local delivery. *ND means information not disclosed. (Adapted from reference ((27)))....29

Table 1.3 List of anti-inflammatory products approved by US FDA for IA administration, their labelled dose and the range of usual dosage employed for OA. *Zilretta® is an injectable microsphere formulation, supplied as 32 mg powder in a vial, along with 5 mL dispersant for injection. (Source: Orange book, 2019).....33

Table 2.1 Final composition of the optimized formulation composition of NCs, prepared by self-emulsification method. 55

Table 2.2 Colloidal properties of NCs prepared by solvent displacement, using lecithin as a surfactant. (Each value is a mean ± SD of 3 preparations). 65

Table 2.3 Colloidal properties of NCs prepared by solvent displacement, using Tween® 80 as a surfactant. (Each value is a mean ± SD of 3 preparations) 66

Table 2.4 Screening of oils and surfactants used to prepare self-emulsifying nanoemulsions. * Each combination involved mixing of DXM (0.6% w/w) with respective oil (30% w/w) and surfactant (20% w/w) to form a nanoemulsion with water (36% w/w). Each of these mixtures had 13% w/w of ethanol as a co-solvent for DXM. Last two columns indicate the recrystallization and phase separation, as observed visually and microscopically after the preparation of respective mixture. 67

Table 2.5 Influence of concentration and molecular weight of HA on % EE and drug loading of DXM, a compilation of data from DXM NCs immediately after preparation, and after storage at 2 - 8 °C for 2 weeks (Each value is a Mean ± SD of 3 preparations) 70

Table 2.6 Optimization of gel components for incorporation of DXM NCs. Concentrations of fibrinogen and thrombin evaluated to incorporate DXM NCs are tabulated. 34% w/w of DXM NCs was loaded into all the gels, which yielded

an equivalent dose of 2.04 mg/mL of DXM. This was equivalent to therapeutic dose of 1 mg/kg, considering IA administration volume of 100 µL. 72
Table 3.1 Composition of simulated intraperitoneal fluid 100
Table 3.2 Colloidal properties of NCs after incorporation of DiR at different concentrations. % EE, determined by isolating the NCs immediately after preparation, followed by extracting the DiR in ethanol and quantifying the fluorescence at an emission wavelength of 785 nm, is also shown here. Each value is represented as Mean ± SD (n = 3) 106
Table 3.3 Colloidal stability of NCs during the preparation of 2′-dC-N4-C_8 gel, determined by exposing the suspension of NCs in PBS (0.01 M, pH 7.4) between 40 – 45 °C for 10 min. Data represented as Mean ± SD (n = 3) 109
Table 3.4 Resistance to dilution study performed by incubating Fn-HA and 2′-dC-N4-C_8 gels in SIPF at 37 ºC under different dilutions. Gels were monitored each day up to 48 h after incubation. Gels that were swollen and remain undissolved as intact gels were considered to be tolerated (n = 3/gel/dilution). 116
Table 4.1 Composition of PEG-NB – thiol gel, prepared by mixing the solutions of individual gel components in PBS under bench-top UV light exposure (365 nm, 5 mW/cm^2) in a syringe mould 130
Table 4.2 Composition of PEG-MAL – thiol gel, prepared by mixing the solutions of individual gel components in citrate buffer, 0.1 M, pH 5.0 in a syringe mould 131
Table 4.3 UV stability of NCs, as determined by incubating the suspension of DiR NCs in PBS, followed by exposing them to UV for 5 min at 25 ºC. No significant changes in colloidal properties ensures the UV stability of NCs. Data represented as Mean ± SD (n = 3) 138
Table 4.4 Compatibility study to determine the photostability of DiR NCs with individual gel components before and after exposure to UV. Each mixture was prepared in same proportions as present in the gel, at 25 ºC (n=1). Incompatibility was evaluated by reduction in fluorescence intensity units after exposure to UV. (*Composition indicates respective mixtures prepared in 0.01 M PBS, pH 7.4) 141

Table 4.5 Experimental parameters evaluated to determine the influence of nature and concentration of photoinitiators and UV exposure times on photostability of DiR NCs.....142
Table 4.6 Determination of colloidal stability of DiR NCs up on incubation in buffers with different pH, at 25 ºC. Data is represented as mean ± SD (n = 3) 144
Table 4.7 Colloidal properties, % EE and drug loading of DCX loaded NCs. Data represented as mean ± SD (n = 3).....159

1. Introduction

This introductory chapter reviews the importance of local drug delivery and the various formulation strategies employed for effective local delivery in the management of osteoarthritis and peritoneal malignancies. The role of intra-articular (IA) injections in the management of osteoarthritis is explained here, highlighting the shortcomings of marketed formulations. Moreover, the importance of intra-peritoneal (IP) delivery of chemotherapeutic agents in the treatment of peritoneal malignancies is also described along with the challenges associated with IP chemotherapy and various formulation strategies that have been evaluated to date. The objectives and the scope of the thesis, aimed at treating unmet clinical needs associated with osteoarthritis and peritoneal malignancies through local delivery, are explained.

1.1 Local drug delivery

Based on the method of administration, drug delivery can be classified into systemic or local. Systemic drug delivery is generally administered through oral or parenteral, where pharmacologically active compounds are distributed throughout the body by the circulatory system. In contrast, local drug delivery is achieved through administration of pharmacologically active compounds within a restricted area of the body or specific tissue, where the disease is located. Local drug delivery is advantageous when the scope of the disease is restricted to an organ or a cavity within the body. It provides better access to the drug in comparison to systemic delivery, which usually delivers only a proportion of the drug to the site of interest. Moreover, local delivery offers reduced side effects, as the access of therapeutic agent to untargeted regions of the body is usually restricted (1-3).

Local drug delivery is achieved through injection, implantation, inhalation or topical application. Depending on site of administration, local delivery might lead to rapid clearance, providing reduced therapeutic effect than expected. Intra-ocular, intra-nasal, intra-articular, and intra-peritoneal are the common local delivery approaches where rapid clearance of therapeutic molecules is the major challenge (4-7). Various formulation strategies are employed in order to retain the therapeutic agents for prolonged periods at the site of administration.

Hydrogels, implants, *in situ* forming depots, micro and nanoparticles are most commonly used formulation strategies to control the release of therapeutic agent from the delivery system and to retain the drug at the site of administration for prolonged periods (8-11).

Local delivery is also employed to achieve enhanced tissue penetration. Biological membranes such as skin, mucous layers, blood-brain barrier, connective tissues around neurons etc., act as barriers for diffusion of therapeutic agents. They allow only molecules with suitable physicochemical properties. Delivery of therapeutic agents locally at the site of interest would enhance the tissue penetration and accessibility of the molecule at the site. Formulations such as nanoparticles have been designed to enhance the tissue penetration after local delivery (12).

1.1.1 Formulation approaches for local delivery

From a formulation perspective, nanoparticles, microparticles, hydrogels, implants, *in situ* depots and polymeric films are widely explored for local drug delivery.

Nanoparticles offer greater surface area-to-volume ratio, which enhances the binding to biological membranes, eventually favours the tissue penetration (13, 14). Moreover, they also offer additional benefits of targeting through surface functionalization with various ligands or cell penetrating peptides (15-17). Ruoslahti published a consolidated review on various peptides, explaining the role of peptides in tumour homing, tumour penetration. It was emphasized that peptides are well suited for nanoparticle targeting because of their relatively easy synthesis, non-immunogenicity and target specificity (16).Nanoparticles have also considerable interest in local drug delivery to mucosa because of their enhanced retention and tissue penetration. Mucus is a viscous secretion present as a layer on the lung airways, gastrointestinal tract and other tissues. It undergoes continuous turnover and clears foreign particles as a part of the body's natural defence (18). Nanoparticles have been designed to bind to the mucosa and penetrate into the underlying tissue for local delivery. For example, budesonide nanosuspension coated with Pluronic F-127 of approximately 200 nm size has shown mucosal binding and enhanced tissue penetration in

comparison to 2 µm sized particles coated with polyvinylpyrollidone in a mouse model of inflammatory bowel disease. They have found that micron sized particles are too large to penetrate the colorectal mucus prior to clearance (19). Mucosal binding of nanoparticles has also been evaluated for prolonged retention. Kaldybekov *et al.* developed mucoadhesive PLGA-PEG nanoparticles by incorporating maleimide functionality on the surface of nanoparticles. Maleimide functionality favoured the mucoadhesion through Michael-type addition reaction of the nanoparticles with inherent thiol residues present in the mucins present on the mucosal surfaces of urinary bladder. In addition, they reported that these particles were non-irritant to mucosal surfaces through a slug mucosal irritation test. This could find applications for local drug delivery in the treatment of urinary bladder cancer and interstitial cystitis (20).

Hydrogels are another class of formulations for local drug delivery, which are capable of swelling in aqueous environments, imbibing large volumes of water. The porosity, biocompatibility and ability to incorporate various particles makes them attractive tools for controlled local drug delivery. Thermosensitive hydrogels have been widely explored, customizing them to achieve variable properties. Hydrophobic drugs have been dissolved or dispersed in the hydrogel matrix to achieve controlled drug delivery. Figure 1.1 shows various types of thermosensitive hydrogels that have been explored for local drug delivery. For example, Berrada *et al.* developed a thermosensitive hydrogel from chitosan and β-glycerophosphate, to incorporate camptothecin for intra-tumoural drug delivery. Camptothecin shows adverse systemic toxicity due to its conversion to a toxic carboxylate form in the serum. Local delivery of camptothecin through intra-tumoural injection in a hydrogel significantly delayed the tumour growth with minimal systemic toxicity (21). Hydrophobic molecules are often loaded in hydrogels, dispersing them as fine crystals in the hydrogel matrix. Alternatively, drugs have been first incorporated into polymeric nano or microcarriers to incorporate them further into a hydrogel matrix in the interest of attaining further control over the release. Recently, Palmese *et al.* published a consolidated review on hybrid hydrogels, which are incorporated with micro or nanoparticulate systems, and their applications in biomedical research (22).

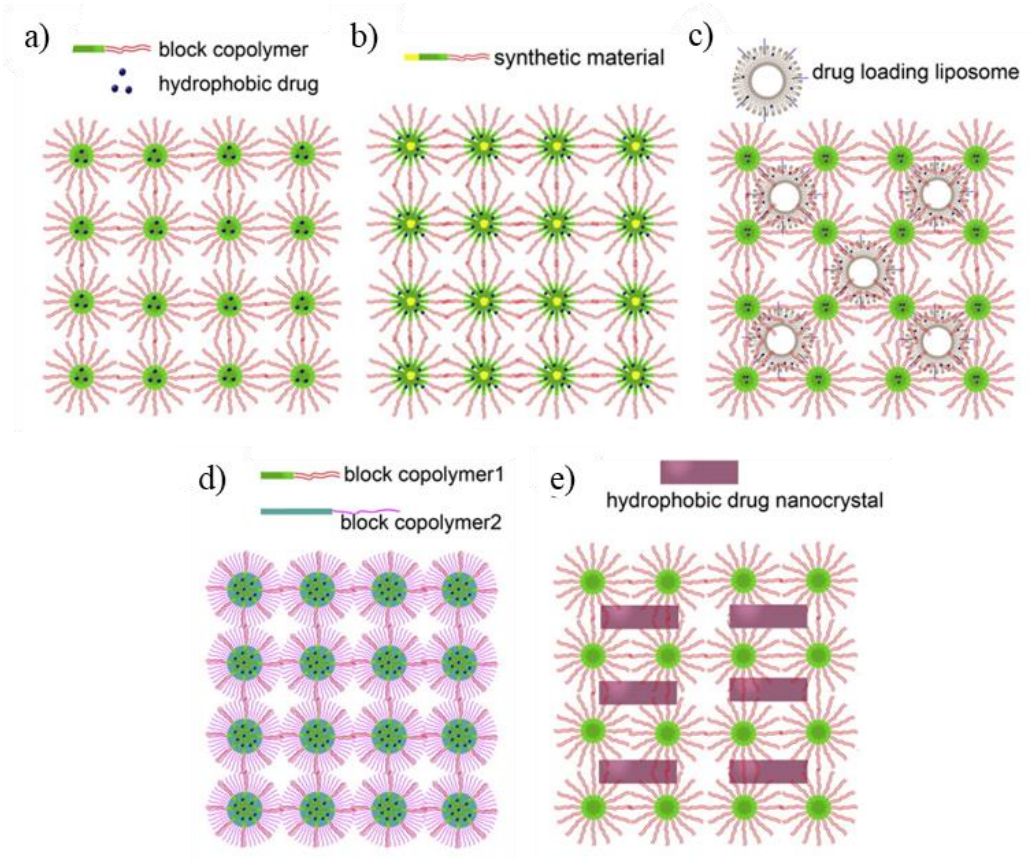


Figure 1.1 Schematic representation of different types of thermosensitive hydrogels used for local drug delivery. (a) Hydrogels prepared from micelles, incorporated with a hydrophobic drug; (b) Hydrogels prepared through synthesis of novel thermosensitive hydrogel materials, containing larger hydrophobic domain for high drug loading; (c) Hydrogels incorporated with liposomes, nanoparticles or microparticles; (d) Hydrogel formed by association of polymer and surfactant to form mixed micelles; (e) Hydrogels incorporated with nanocrystals (Adapted from reference (23))

Microparticulate drug delivery systems are advantageous than nanoparticles for local delivery, if the release of active components is driven by gradual dissolution or erosion from a depot. These particles offer lower surface area-to-volume ratio in comparison to nanoparticles, which reduces the amount of drug released in unit time (11). Paclimer® microparticles, prepared by incorporating paclitaxel in polyphosphoester particles showed a six-fold reduction in tumour volume doubling rate of non-small cell lung tumours after intra-tumoural injection. Enhanced anti-tumour effect was found to be due to the sustained release of paclitaxel from the microparticles (24). Microparticles have gained importance in local drug delivery to the lungs through inhalation. Bronchodilators are usually administered in the particle size range of 1 – 3 µm. However, these particles tend to aggregate in dry powder inhalers, compromising the dispersion performance. Hence, porous polymeric

microparticles have been designed to achieve greater dispersion and controlled release. Poly(lactic-co-glycolic acid) (PLGA) has been widely explored polymer for sustained, local delivery to lung because of its biocompatibility and established safety profile (25, 26).

Implants were first investigated in 1960s for controlled drug release for both localised and systemic drug delivery. However, the first clinical use of an implant was in 1990 with approval of Norplant®, which was designed to implant in the superficial plane beneath the upper arm for controlled systemic delivery of levonorgestrel for female contraception. Various polymers, from synthetic and natural origins, have been developed to design implants as biodegradable or non-degradable drug delivery systems. Table 1.1 shows various biodegradable and non-biodegradable polymers that have been explored for implants.

Table 1.2 shows some examples of local drug delivery systems, which were evaluated for various routes of administration.

Table 1.1 List of various biodegradable and non-biodegradable polymers that have been explored as implantable drug delivery systems (Adapted from reference ((27)))

Biodegradable polymers for implants	**Non-biodegradable polymers for implants**
Poly(lactic acid) (PLA)	Poly(siloxanes)
Poly(glycolic acid) (PGA)	Poly(ethylene-vinyl acetate) (PEVA)
Poly(lactic-co-glycolic acid) (PLGA)	Poly(urethanes)
Poly(caprolactone)	Chitosan
Poly(phosphazenes)	Cellulose
Poly(anhydrides)	Silk
Poly(amides)	-

Table 1.2 Examples of local drug delivery systems evaluated for various routes of administration and sites of local delivery . *ND means information not disclosed. (Adapted from reference ((27)))

Product	Route of administration	Drug	Material	Indication
Gliadel® wafers	Intra-tumoural	Carmustine	Silicone	Glioblastoma
Oncogel®	Intra-tumoural	Paclitaxel	PLGA-PEG-PLGA	Oesophageal cancers
GemRIS®	Intra-vesicular	Gemcitabine	ND*	Non-muscle invasive bladder cancer
Estring®	Intra-vaginal	Estradiol	Silicone	Menopausal symptoms
Ocusert®	Intra-ocular	Pilocarpine, Alginic acid	PEVA	Open angle glaucoma
Retisert®	Intra-ocular	Fluocinolone	Poly(vinyl alcohol) (PVA)	Non-infectious uveitis
Vitasert®	Intra-ocular	Ganciclovir	PVA, PEVA	Retinitis in HIV patients
Ozurdex®	Intra-vitreal	Dexamethasone	PLGA	Macular oedema

With the importance of local delivery and various formulations approaches employed for local delivery described, these later sections will focus on local delivery to the synovial cavity in the knee and peritoneal cavity through IA and IP administration. Current gaps in IA and IP drug delivery are discussed, to explain the rationale for the aims and objectives of thesis.

1.2 Intra-articular (IA) delivery

1.2.1 Osteoarthritis (OA) – anatomy and pathology of disease

Osteoarthritis (OA) is a progressive, degenerative disease that affects the articulating joints (28), which not only affects the elder population, but also affects younger people who are involved in activities associated with prolonged high mechanical stress. The prevalence of OA is expected to increase in the next decades, especially in the obese population, which is associated with their lifestyle changes. Age is another factor that contributes to OA. It affects approximately 25 % of population above 60 years (29). Women are more prone to OA and approximately 18 % of the population above 60 years are affected. This is a consequence of inherent hormonal changes associated with age related oestrogen deficiency (30).

A typical articular joint consists of a fibrous capsule, enclosing the adjacent bones. The joint cavity is filled with a viscous synovial fluid that gives lubrication for free joint movement (31). Synovial membrane consists of areolar tissue, adipocytes, fibroblasts and a discontinuous layer of synoviocytes. There are two types of synoviocytes, A and B. Synoviocytes A act as macrophages that clear the molecules through phagocytosis, while synoviocytes B synthesize HA for lubrication (32-34). OA brings anatomical changes in the affected joint, which are associated with extreme pain and disability to perform routine physical activities (35). Anatomical changes in the joint are characterized by degeneration of articular cartilage, subchondral bone sclerosis and formation of osteophytes. Additionally, changes in synovium, menisci, peri-articular muscle and ligaments are the hallmarks of disease progression (36). Figure 1.2 shows the schematic representation of anatomical changes in the joint during osteoarthritis. Although, OA can occur in many articular joints, knees, hips, spine and hand are most commonly affected. Age, obesity, lifestyle, occupational stress, history of joint injury and misalignment of joints are the common risk factors associated with OA (37). Unfortunately, patients do not experience pain or associated symptoms before significant cartilage damage. It is estimated that patients have no experience of pain up to 40 % of cartilage loss, as seen by radiological changes. These cartilage changes often lead to bone damage in the later stage (38).

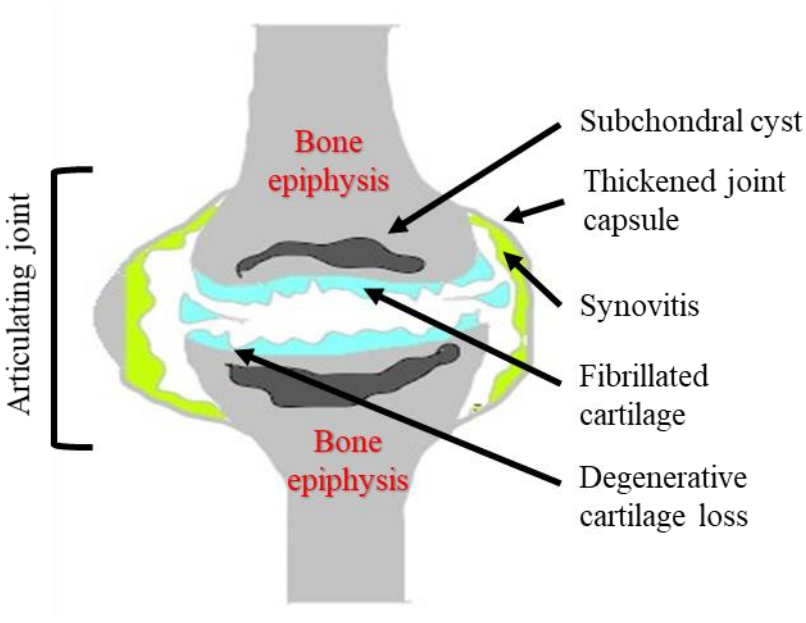


Figure 1.2 Schematic representation of anatomical changes that occur in a typical articulating joint, affected with osteoarthritis. Degeneration and fibrillations on the cartilage, formation of subchondral cysts and inflammation of synovial membrane with thickening of joint capsule that are commonly observed radiological investigation are indicated here.

Research has been extensively done on understanding the molecular pathways involved in mediation of pain and degeneration. Cartilage is an avascular and aneural tissue and hence does not directly involved in pain mediation. However, structural changes in associated tissues such as formation of osteophytes, subchondral cysts, and synovial membrane trigger local pain mediation pathways. Various proinflammatory mediators such as prostanoids, nerve growth factors and nitric oxide, are present due to tissue damage that activates peripheral nociceptors (39, 40). The information is being transmitted to the dorsal root ganglion, through the spinothalamic tract to cortical centres of the brain to perceive the pain (41).

1.2.2 OA – current treatment regimen & approaches

Currently there are no approved disease modifying agents available for OA. Hence, treatments are generally associated with the symptomatic management of the disease. Treatment options are generally chosen based on the stage of the disease (42). Figure 1.3 shows the current standard of care employed in the management of OA. Early stage is often managed through non-pharmacological treatments, which include lifestyle changes, reducing the body weight, use of joint supportive braces and moderate exercises. Moderate stage of the disease is

treated through pharmacological treatments such as oral or topical non-steroidal anti-inflammatory agents (NSAIDS), analgesics, nutritional supplements, and IA injections. IA injections can be hyaluronic acid (HA) preparations, which act as viscosupplements without any pharmacologically active compound or corticosteroids. Alternatively, platelet rich plasma (PRP) is another procedure employed to mediate healing and remodelling of the cartilage. PRP is obtained by concentrating the platelets in plasma by centrifuging the autologous blood, which will be injected into the joint (43). This is known to activate endogenous thrombin and IA collagen, which secretes growth factors that help to heal the cartilage (44, 45). Finally, the severe stage of the disease, which is non-responsive to non-pharmacological or pharmacological measures, is treated by surgical intervention. Joint replacement is the most common approach, while osteotomy and joint fusion are alternatives based on age and severity (46-48).

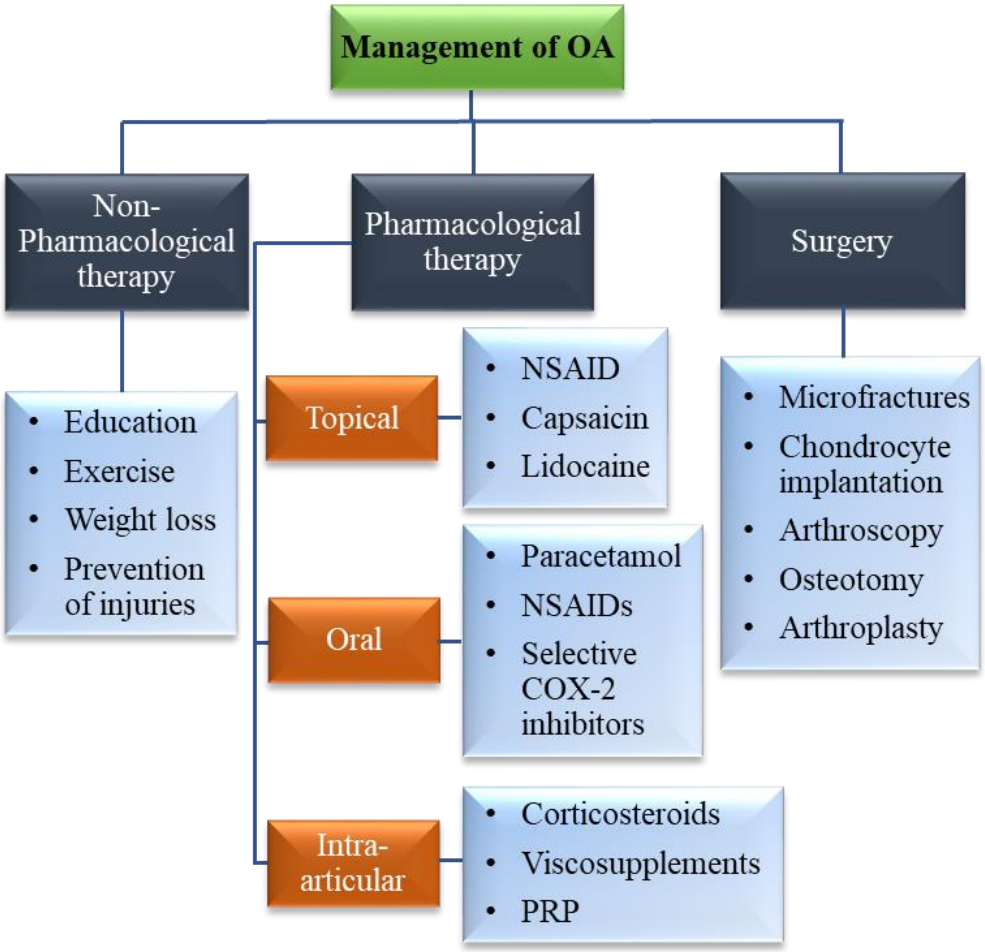


Figure 1.3 Schematic representation of current standard of care employed in the management of OA, indicating the strategies employed from mild to severe stage of disease (from left to right). (Adapted from reference (42))

1.2.3 Introduction to IA delivery

In this section, IA therapy for local delivery to the articular joint is discussed in detail. IA injections are not first line treatments but are preferred as the last non-operative alternative when other conservative modalities have failed. For the first time in 1951, Hollander *et al.* introduced the concept of IA injection of hydrocortisone (49). Later, various steroidal molecules have been investigated along with HA injections. Currently approved IA injections can be broadly classified into corticosteroids and HA injections, which do not contain any pharmacologically active ingredient. Table 1.3 shows the list of anti-inflammatory products, which are approved by US FDA for IA delivery. Moreover, a lot of small molecules, proteins and peptides for cartilage regeneration are being explored in clinical trials. Maudens *et al.* lists various molecules alone or in a drug delivery system, that are in clinical trials (50).

Table 1.3 List of anti-inflammatory products approved by US FDA for IA administration, their labelled dose and the range of usual dosage employed for OA. *Zilretta® is an injectable microsphere formulation, supplied as 32 mg powder in a vial, along with 5 mL dispersant for injection. (Source: Orange book, 2019)

Product	**Dosage form**	**Brand name**	**Dose (mg/ml)**	**Range of usual dosage**
Betamethasone acetate + Betamethasone sodium phosphate	Aqueous suspension	Celestone® Soluspan® Betaject®	3 + 3	1.5 – 6
Methylprednisolone acetate	Aqueous suspension	Depo-Medrol® Solu-Medrol™	20 or 40 or 80	4 – 40
Triamcinolone acetonide	Aqueous suspension	Kenalog®-40 Zilretta®*	40	5 – 40

Triamcinolone diacetate	Aqueous suspension	Aristocort® Forte	40	5 – 40
Triamcinolone hexacetonide	Aqueous suspension	Aristospan®	20	5 – 40
Dexamethasone sodium phosphate	Aqueous solution	Adrenocot® Decadron® phosphate	4 or 10	2 – 6

1.2.4 Shortcomings of marketed IA formulations

Despite the long history of clinical use and cost-effectiveness of IA injections, actual clinical benefits associated with these treatments is still debatable (51-53). IA administered corticosteroids are rapidly clear from the joint (54). Pharmacokinetic profile of IA administered molecules of molecular weight < 10,000 Da is expected to be similar to non-IV parenteral administration (55, 56). The reason for this rapid clearance was explained by leaky ultrastructure of synovium (Figure 1.4). Water and protein in synovial fluid is completely replaced within a period of 2 h (57). Wernecke *et al.* reported that the residence times of commonly used corticosteroids in the joint was from hours to a few days (58). Alternatively, hyaluronic acid (HA) injections are usually marketed as medical devices, which act as viscosupplements that reduce the friction in the joint. The symptomatic relief obtained from these HA injections is also limited because of degradation of HA by endogenous enzymes such as hyaluronidase in the joint (59-61). HAs of higher crosslinking densities are also designed to reduce the degradation and increase the residence (62). However, the clinical outcomes did not bring significant long term benefits associated with pain, which would help to perform routine physical activities (63).

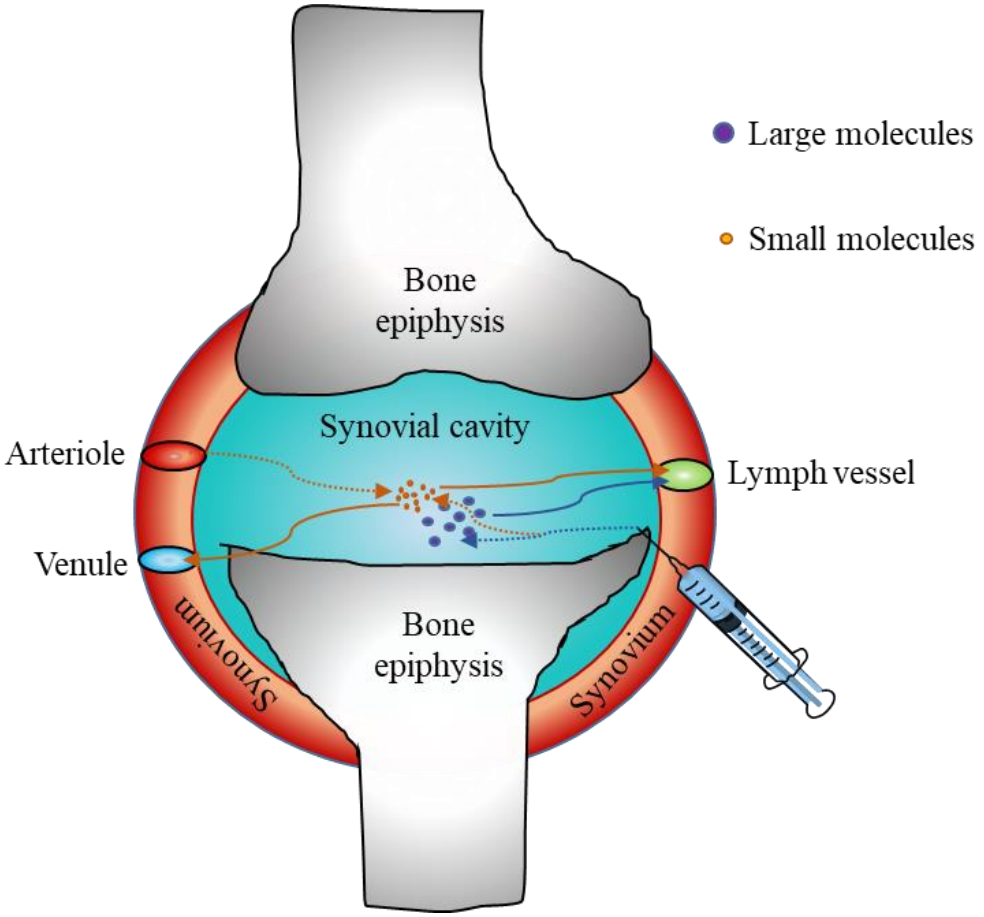


Figure 1.4 Schematic illustration of leaky nature of the synovial membrane. Small molecules are exchanged between synovial cavity and systemic circulation through blood and lymph capillaries, whereas large molecules undergo preferential lymphatic drainage upon IA injection.

1.2.5 Formulation strategies employed to overcome the shortcomings of IA formulations

As retention of active components in the joint is the major challenge associated with IA delivery, various formulation strategies have been employed to achieve longer retention and sustained release including suspensions, hydrogels, nano and microparticles. (64-66).

1.2.5.1 IA suspensions

Being hydrophobic molecules, corticosteroids are relatively easy to be formulated as suspensions. Triamcinolone acetonide and hexacetonide, methylprednisolone acetate, betamethasone acetate and betamethsone sodium phosphate are commercially available as suspensions. These suspensions were expected to undergo dissolution in the joint cavity to elicit desired therapeutic effect. Among these suspensions, triamcinolone has shown longer IA duration of action up to 21 days as a hexacetonide salt form (58). Although, suspensions

retain the drug longer than soluble formulations, the therapeutic effect elicited by marketed formulations still do not ameliorate the symptoms associated with pain. The residence time and the interaction of the drug molecules from these formulations with local inflammatory cascade is not enough (67, 68).

1.2.5.2 Microparticles for IA delivery

Microspheres are another type of drug delivery system that has shown prominent benefits in extending the residence time in the joint. Particle size has been reported as one of the crucial factors for determining the extent of retention in the joint after IA injection. Smaller particles tend to escape from the cavity faster than the larger particles. Pradal *et al.* evaluated the IA residence of fluorescent dye, DiD, loaded poly(lactic acid) particles at 3 different sizes, in presence and absence of HA gel. They have found that 300 nm and 3 µm particles were rapidly cleared from the joint, while 10 µm particles retained longer. They have also observed that incorporation of particles in a HA hydrogel helped in further retention of particles (69). Flexion therapeutics Ltd., an American biopharmaceutical company has developed a sustained release PLGA based microsphere formulation of Triamcinolone acetonide with a median particle diameter of 42 – 52 µm. This formulation was successful in controlling the release of triamcinolone, showing the quantifiable drug concentrations 12 weeks after IA administration (70). This has been marketed with a brand name Zilretta®. This is the first and the only approved formulation for extended release of any IA corticosteroid.

Synovial macrophages tend to phagocytose the particles < 10 µm without eliciting a neutrophil response. Horisawa *et al.* compared the synovial phagocytosis of fluorescently labelled PLGA micro and nanoparticles. They have found that 265 nm PLGA nanoparticles were phagocytosed by macrophages in the joint within 3-7 days, while 26 µm PLGA microparticles were not phagocytosed and were retained in the cavity. However, they have made an interesting observation that retention in the cavity is not directly related to the therapeutic effect. Phagocytosed PLGA nanoparticles were able to penetrate into the subsynovium, where inflammatory mediators elicit their response. They have concluded that PLGA nanoparticles were more suitable to elicit anti-inflammatory response after IA administration (71).

1.2.5.3 Nanoformulations for IA delivery

Microparticles tend to reside longer in the joint. However, efficacy of microparticles is limited by the release of the drug from the formulation, which is again dependent on the degradation of the polymer matrix. Once released, the drug molecules must penetrate into the local tissues such as synovium and cartilage in order to interact with inflammatory cascade to elicit an anti-inflammatory action (72). Microparticles cannot dictate the further interaction of drug molecules with the tissues. However, nanoparticles have the capability to penetrate into the synovial membrane and interact with tissue associated inflammatory reactions. Hence, nanoparticles have also gained importance for IA drug delivery.

A range of nanoformulations has been explored for IA delivery, which include polymeric or lipidic nanoparticles and liposomes. The fate of nano and microparticulate formulations after IA injection would be different. Nanoparticles undergo phagocystosis by type A synoviocytes that engulf them into the cell, whereas microparticles are retained in the synovial fluid adhering to the cartilage or synovium. Alternatively, targeted nanoparticles can also permeate into the articular cartilage, which is majorly employed for cartilage regeneration (73). Figure 1.5 schematically explains the fate of nanoparticles and microparticles after IA injection.

Periyasamy *et al.* assigned the localization of nanocarriers within various anatomical structures of the joint based on their size (74). They have explained that nanocarriers of size < 250 nm may also penetrate into the sub-synovium through the cell-junctions. Interestingly, carriers of even a smaller size (< 60 nm) are capable of entering the extracellular matrix (ECM) of cartilage by convective transport during the compression of cartilage. Active ingredients, which are intended for cartilage repair could penetrate into the ECM of the cartilage through this mechanism. For example, micelles are small enough in diameter to penetrate the ECM and hence would be appropriate for this purpose. Otherwise, active ingredients that are intended to reduce the pain and inflammation, and whose site of action is in the synovium or in the sub-synovium, delivery systems of slightly higher particle size domains such as polymeric or lipidic nanoparticles and liposomes are appropriate.

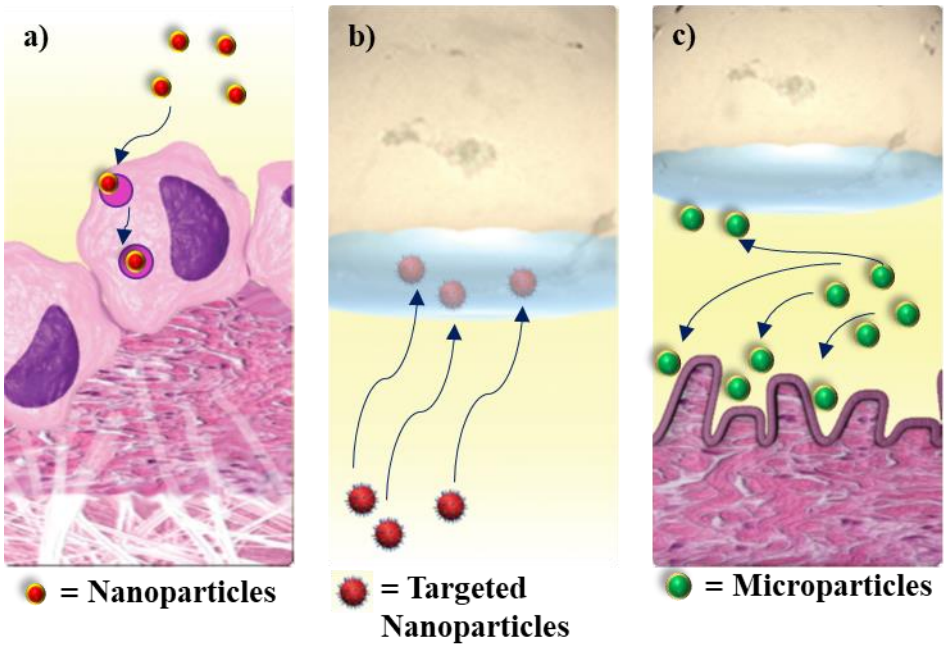


Figure 1.5 Illustration of fate of nano and microparticles after IA administration. (a) Nanoparticles can be phagocytosed by type A synoviocytes from the peritoneal cavity, which would be helpful for their penetration into subsynovium to retain longer in the cavity. (b) Targeted nanoparticles can selectively penetrate into the articular cartilage, which would be helpful in cartilage regeneration. (c) Microparticles penetrate neither into subsynovium nor into articular cartilage, rather retain longer within the synovial cavity. (Adapted from reference (73))

Despite nanoparticles being able to penetrate into sub-synovial tissue, they are still susceptible to rapid clearance from the joint. To combat this issue yet benefiting the size related advantages of nanoparticles, composite systems have been explored using hydrogels to retard nanoparticles' release and clearance from the IA joint.

1.2.5.4 Studies that employed the combination of nanoparticles and hydrogels

Morgen *et al.* synthesized a nanoparticle that can ionically crosslink with endogenous HA to form a hydrogel. Nanoparticles (approximately 100 nm) were designed to contain a neutral polymer core and a cationic polymer coat. Fluorophore was incorporated into these particles to determine their residence in the knee after IA injection. It was found that 74 % of fluorescence was still evident from the knee after 7 days of administration. This has proved that, hydrogels can retard the release of nanoparticles into the joint, which would retard their clearance (75). In another study, Kang *et al.* incorporated micelles, formed by self-assembly of PEG and kartogenin (chondrogenesis inducer), into a HA hydrogel for increasing the IA residence and sustained release. Gels were

formed by covalent crosslinking of PEG chains from self-assembled micelles to HA. IA injection of this hydrogel reduced the progression of OA in surgically induced OA rat model (76). Similarly, Kim *et al.* synthesized cationic PLGA-Eudragit nanoparticles containing piroxicam, a non-steroidal anti-inflammatory agent, that can crosslink with endogenous HA to extend increase the IA retention. *In vivo* pharmacokinetic estimation showed that the drug concentration in the joint was 3.2 fold and 1.8 fold higher than drug solution and neutrally charged nanoparticles respectively (77). Nanoparticles in presence of a hydrogel have shown a sustained release, prolonged retention and enhanced therapeutic effect in the joint. Hence, these studies have illustrated that composite hydrogel containing nanoparticles have the potential for prolonged retention and sustained anti-inflammatory effect after IA administration.

As explained earlier, IA corticosteroids are mostly available in the market as aqueous suspensions in different salt-forms (table 1.3). They were designed as highly hydrophobic compounds in order to reduce the dissolution rate of those molecules in the synovial cavity. In contrast, dexamethasone (DXM) is commercially available as a hydrophilic salt-form, DXM sodium phosphate, as an aqueous solution for injection. DXM in its native form is hydrophobic, which makes it difficult to solubilize in its free state into an aqueous solution. Polymeric nanocapsules (NCs), which consists of an oil core and a polymer coat offers higher loading of hydrophobic drugs such as DXM in their native state (78). Development of a NCs formulation would favour incorporation of DXM, a model drug, in its native state. In addition, NCs could be transported by synovial macrophages into sub-synovium, where DXM could elicit its anti-inflammatory action. As explained earlier, NCs alone could be rapidly cleared from the joint, which can be retarded by incorporating them into a hydrogel. Hence, a hydrogel that incorporates DXM-loaded NCs also need to be developed in order to control the release of NCs into the synovial cavity.

1.3 Introduction to intra-peritoneal (IP) local delivery

IP local delivery is performed to treat malignancies and peritoneal adhesions (7). The most common cause for formation of peritoneal adhesions is the insertion of catheters into the peritoneal cavity for peritoneal dialysis (79). Various polymers and hydrogels have been explored to prevent the formation of peritoneal adhesions (80, 81). In this section, the focus is on peritoneal malignancies and different strategies to treat them. Malignancies associated with abdominal and pelvic organs are one of the leading forms of cancer, accounting for about 8-9 % of cancer deaths (82). In this chapter, the focus is peritoneal malignancies. These primary cancers which are associated with any of the peritoneal organs are highly aggressive and exhibit metastasis within the peritoneal cavity and other peritoneal organs (83, 84). Unfortunately, in most of the cases these primary cancers fail to demonstrate early clinical symptoms, leading to delayed diagnosis. Many cases show large amounts of tumour nodules over peritoneal surfaces at the time of first diagnosis (85). Peritoneal carcinomatosis, one of the most dissociative forms of metastasis, brings extreme pain and discomfort due to accumulation of ascites fluid and bowel obstruction (86). In majority of cases, microvascular permeability of peritoneum to water, small solutes and proteins gets increased due to the secretion of vascular endothelial growth factor (VEGF), cytokines and chemokines in the surrounding tissue (87, 88). Increased permeability leads to generation of albumin-rich ascites fluid within the cavity. It is believed that formation of ascites fluid is associated with lymphatic obstruction, and osmotic water transport following the drainage of proteins from leaky microcapillaries (89).

The standard of care for the treatment of these peritoneal malignancies is a cytoreductive surgery of macroscopic tumours (90). Intravenous (IV) chemotherapy is also given perioperatively or postoperatively to treat untraceable microscopic tumours to avoid recurrence (91). Clinical studies suggest that chemotherapy if given along with cytoreductive surgery offers better solutions than individual treatments (92, 93). These conventional IV chemotherapies are non-specific and pose severe side-effects, compromising the quality of life of patients (94). Moreover, achieving effective local drug concentrations by IV therapy is a significant challenge (95, 96). Hence, direct

administration of chemotherapeutic agents into the peritoneal cavity has been evaluated. It was found that that intra-peritoneal (IP) administration of chemotherapeutic drugs offers pharmacokinetic advantages in comparison to the IV route. Dedrick *et al.* summarized the pharmacokinetic principles behind IP administration and showed the potential to attain higher local concentrations in comparison to systemic administration. They reported clinical advantage after IP administration of 5-fluorouracil and methotrexate, as observed by the higher peritoneal concentrations of both the drugs after IP administration (97). Shimada *et al.* compared the pharmacokinetic parameters of docetaxel after IP and IV administration in mice bearing gastric cancer. The concentration of docetaxel in the peritoneal cavity and solid tumour was significantly higher for IP administered group than IV equivalent. Plasma area under curve (AUC) after IP administration was similar to IV administration, indicating no additional systemic toxicity (98). In another study, Mohamed *et al.* showed the pharmacokinetic advantage and tissue distribution of paclitaxel after IP administration with isotonic 6% hetastarch solution and 1.5% dextrose peritoneal dialysis solution. They reported that the fluid clearance from the peritoneal cavity was lower with hetastarch, which was also reflected in higher area under curve (AUC) ratio of peritoneal to plasma paclitaxel (99).

1.3.1 Clinical approaches for IP delivery – HIPAC & PIPAC

IP administration carries the therapeutic agent near to hypoxic regions which are difficult to reach by the IV route (100). Although none of the chemotherapeutic products are approved for IP administration, many compounds including, doxorubicin, fluorouracil, paclitaxel and platinum-based compounds have been explored for IP therapy (101-104). In current clinical practice, IP administration is achieved by repeated instillation through catheters. In the extensive review on IP delivery, Dakwar *et al.* described various procedures that are employed in the clinic for IP administration. These procedures involve perfusion of chemotherapeutic agents under hyperthermic conditions (HIPEC) or pressurized aerosol pumps (PIPAC) (105). Figure 1.6 shows the various approaches that are employed in the clinic for IP administration. It also highlights the incorporation of nanoparticles in a hydrogel as a potential strategy to achieve prolonged IP retention.

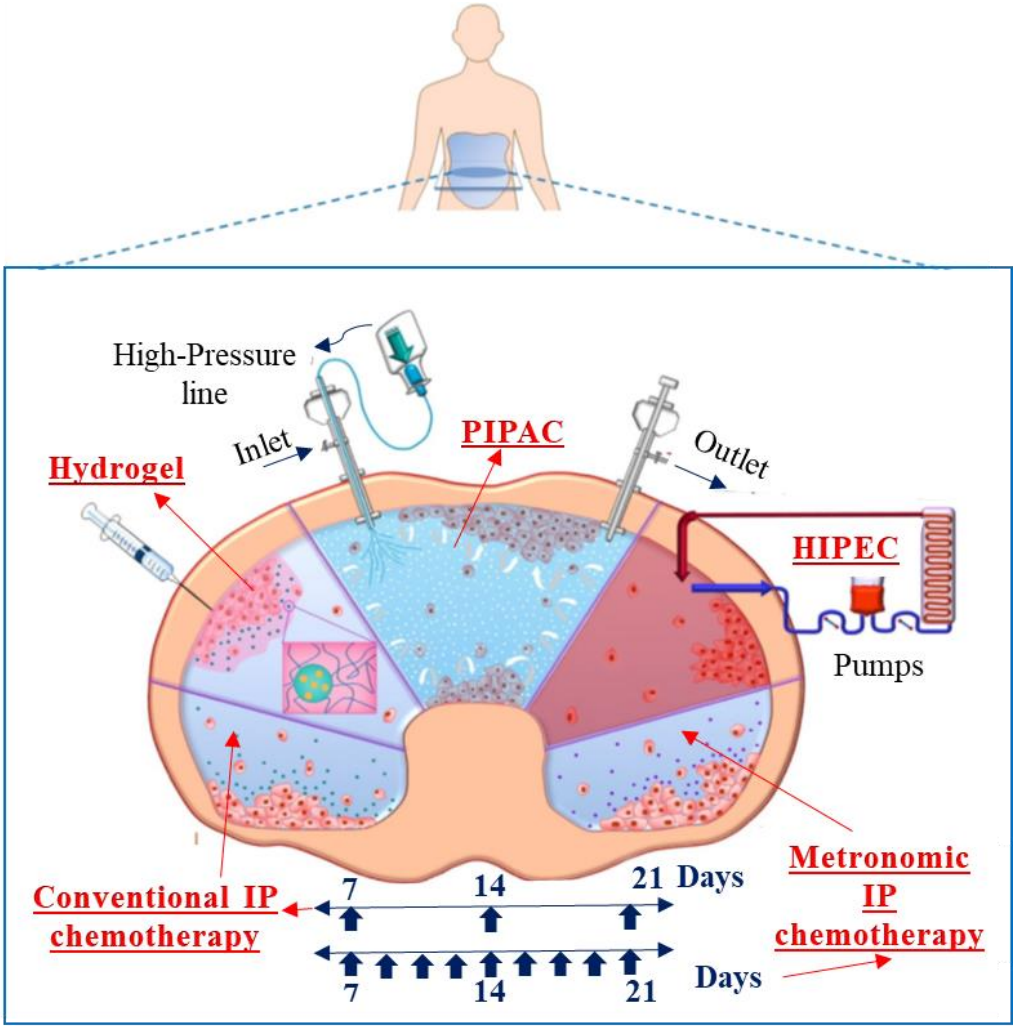


Figure 1.6 Schematic representation of different clinically relevant techniques for IP drug delivery. Conventional IP chemotherapy involves use of administration of chemotherapeutic agents at regular intervals, whereas metronomic IP chemotherapy involves continuous administration without drug-free periods. PIPAC and HIPEC involves administration of chemotherapeutic agents under high pressure or high temperature respectively, for effective tissue penetration. Hydrogels containing micro or nanoparticles are also suggested as potential drug delivery strategy in the future for prolonged retention and sustained efficacy after IP administration. (Adapted from reference (105)).

1.3.2 Challenges associated with IP delivery

Although, IP delivery of chemotherapeutic agents has shown significant pharmacokinetic and pharmacodynamic advantage, there are certain challenges that are associated with IP delivery. These challenges can be classified into two types: challenges associated with the delivery approach, and challenges associated with rapid clearance of molecules from the cavity. The current conventional IP chemotherapy delivery approach might cause issues associated with IP catheters. As explained before, current clinical practice of IP chemotherapy involves installation of catheters for HIPEC and PIPAC. Walker

et al. assessed that in a clinical trial of GOG172 for IP chemotherapy, where 34 % of patients discontinued IP chemotherapy due to catheter related complications. These complications were related to infections, catheter leakage, pain and bowel perforations (94, 106). Moreover, in many cases stretching and distention of abdomen was observed due to additional volume input into the IP cavity through catheters. This might cause extreme pain and discomfort (107).

Another challenge associated with IP delivery is the rapid clearance of molecules form the cavity. IP administered chemotherapeutic agents were rapidly cleared from the cavity, showing marginal therapeutic benefits than expected. Dedrick *et al.* explained that the IP chemotherapeutic agents did not meet expected pharmacokinetic advantage due to poor coverage of serosal surface during the irrigation and poor tissue penetration (108). To understand the reason behind short residence and rapid clearance from the peritoneal cavity, we need to understand the anatomy and physiology of the peritoneum.

1.3.3 Anatomy and physiology of peritoneum

Peritoneal membrane has an average total surface area of 1.5 m^2, which covers the visceral, abdominal and pelvic organs (109). This membrane is composed of several layers of connective tissue. The first layer consists of mesothelium which secretes surface hyaluronan which protects the membrane from physical damage and surface adhesion. There is a submesothelial basement membrane which supports the mesothelial cells and separates them from interstitial space. Blood vessels percolate through the interstitial space, whose endothelial cells regulate the movement of fluid and molecules through and from the peritoneal cavity. Peritoneal membrane is not a classical semi-permeable membrane. It is highly permeable to water, small molecules and proteins (95, 110). This characteristic feature of peritoneal membrane makes it is feasible to perform peritoneal dialysis as an alternative to artificial kidney dialysis (111). Peritoneal dialysis is a renal replacement therapy that can be performed at home for patients with end-stage kidney disease. Relatively small chemotherapeutic molecules can easily get exchanged between peritoneal cavity and systemic circulation through the peritoneal membrane with the assistance of inserted catheters (112).

Peritoneal fluid fills the peritoneal cavity, providing an external aqueous environment rich in proteins and electrolytes, to the peritoneal organs. Under normal osmatic conditions, fluid exchange happens through diffusion of water into the cavity, which is compensated by reabsorption of fluid into the blood or lymph vessels that are fenestrated through the interstitial space (113). Under cancerous conditions, osmatic pressure builds up in the abdominal cavity due to high protein content as a result of leaky blood vessels associated with the tumour. High osmotic pressure drives further water input into the cavity, raising the total peritoneal fluid volume. This fluid is called ascites fluid, which is a common manifestation in patients with peritoneal malignancies (88, 89).

All these features explain the dynamic nature of the peritoneal cavity. Hence, retention of the chemotherapeutic agents is the major challenge in order to attain desired therapeutic outcomes. Development of controlled release drug delivery systems with prolonged retention would be helpful not only to achieve desired pharmacokinetic and pharmcodynamic benefits, but also reduce the complications associated with IP administered catheters.

1.3.4 Formulation strategies employed for IP delivery

Nano and microparticulate formulations, hydrogels, and implants have been explored as potential strategies for prolonging the residence time and effectiveness of chemotherapeutic agents. In this section, rationale for using these formulations, and their challenges are discussed.

1.3.4.1 Particulate formulations – Nano & micro formulations

Micro and nanoparticulate formulations have been developed for attaining the longer retention and controlled release after IP administration. Both micro and nanoparticles have some advantages and disadvantages. By virtue of their size, microparticles tend to be retained longer in the peritoneal cavity. Kohane *et al.* compared the retention of 250 µm and 265 nm particles made of PLGA after IP administration. They have found that microparticles were retained in the peritoneum up to 2 weeks, while nanoparticles were cleared within 2 days of IP administration (114). Tsai *et al.* compared the clearance of paclitaxel loaded PLGA microspheres (6 µm) with paclitaxel loaded gelatin nanoparticles (900 nm) and found that microspheres showed slower clearance from the peritoneum

(115). Rapid clearance of nanoparticles from the IP cavity can be attributed to the capillary pores of vasculature and lymphatic duct openings into the peritoneal cavity. Lymphatic drainage represents the major clearance route for nanoparticles, which seems inevitable after IP administration (116, 117). Particles > 500 nm might accumulate in the lymph nodes, while smaller particles would enter the systemic circulation.

Although microparticles are retained relatively longer in the IP cavity, there are potential risks of peritoneal adhesions and local inflammation with microparticles (114, 118). In contrast, nanoparticles do not cause peritoneal adhesions while offering advantages of tumour penetration. Nanoparticles can be designed to penetrate into biological membranes for intracellular delivery (119, 120). Simón-Gracia *et al.* synthesized pH responsive paclitaxel loaded polymerosomes, which have shown significantly higher accumulation in the tumour parenchyma after IP administration. They have used a diblock copolymer, poly(oligoethylene glycol methacrylate)-poly(2-(diisopropylamino)ethyl methacrylate (PDPA), to design pH responsive polymerosomes that can selectively release the cargo intra-cellularly in the tumour mass (121).

In the interest of advantages and disadvantages of micro and nanoparticles, there has been a dilemma in deciding the optimum sized particles for IP delivery. A formulation that offers an optimum balance between the local retention, avoiding peritoneal adhesions and achieving the desired therapeutic efficacy is required.

1.3.4.2 Hydrogels

Injectable biodegradable hydrogels have been explored for IP local drug delivery. Physically cross-linked, thermosensitive hydrogels formed by sol-gel phase transition and chemically cross-linked hydrogels formed by covalent crosslinking, have been evaluated (122, 123). A thermosensitive hydrogel prepared using a triblock copolymer, poly(ethylene glycol)-poly(caprolactone)-poly(ethylene glycol) (PEG-PCL-PEG), containing 5-fluorouracil was IP administered for local chemotherapy of colorectal peritoneal carcinomatosis. CT26 cells were injected into the murine abdominal cavity to induce the tumour.

Five days after the induction, the first treatment dose was given, which was followed by another treatment a week later. Significant reduction in size and number of tumour nodules was observed after sacrificing the mice on the 20th day after initial administration (124). Although, a significant reduction in tumour nodules was observed, once per week dosing was performed in this study, which might be difficult in a clinical setting. Repeated dosing might be due to the poor tolerance of physically cross-linked thermosensitive hydrogels to high dilutions. In contrast, covalently cross-linked hydrogels tend to tolerate high dilutions. Hence, they have also been explored for administration into peritoneal cavity.

Bajaj G *et al.* chemically modified HA in order to form functionalized derivatives that can covalently crosslink each other upon physical mixing in an aqueous medium. HA-adipic dihydrazide (HA-ADH) and HA-aldehyde (HA-CHO) were synthesized to form a hydrogel that can incorporate paclitaxel particles in the micrometer size range . This was administered IP to form an *in situ* crosslinkable hydrogel that would release the paclitaxel particles upon gradual degradation. These particles would undergo further dissolution to show chemotherapeutic effect. They have found that the HA gel was able to be retained up to 14 days in the IP cavity. However, this retention was not translated into therapeutic effect due to poor dissolution of paclitaxel after being released from the gel (125). In another study, Sun *et al.* incorporated paclitaxel as nanocrystals instead of micron-sized particles into the same covalently cross-linked hydrogel. They have observed a significant increase in survival of ovarian cancer bearing mice in comparison to Taxol® for the microparticulate paclitaxel incorporated HA gel. Increased efficacy was attributed to greater dissolution and cellular uptake of paclitaxel particles (126). Hence, the consensus in the literature is that hydrogels in combination with nanoparticles give better therapeutic outcomes.

1.3.4.3 Hydrogels containing nanoparticles

Composite systems have been designed by incorporating the nanoparticles into a hydrogel. Alternatively, nanoparticles have been modified to self-assemble into a hydrogel after IP administration. These composite systems delays the clearance of nanoparticles from the IP cavity, as the rate of release of

nanoparticles into the cavity depends on the degradation of the hydrogel. Based on this hypothesis, various composite hydrogels have been designed and evaluated in the literature. For example, linoleic acid was first coupled with Pluronic F-127 (Plu-CLA) to form a self-assembling polymer to form a hydrogel at body temperature. Plu-CLA nanoparticles were then prepared to incorporate docetaxel, which were then injected into BALB/c mice with TMK1 human gastric cancer cells to form a hydrogel in the IP cavity. It was observed that the hydrogel has shown significant reduction in metastatic peritoneal nodules and increased the survival (127). Xu *et al.* have prepared paclitaxel nanoparticles, which can self-assemble to form a thermosensitive hydrogel after IP administration. An amphiphilic copolymer, (PECT, poly (e-caprolactone-co-1,4,8-trioxa [4.6]spiro-9-undecanone)-poly(ethylene glycol)-poly (e-caprolactone-co-1,4,8-trioxa [4.6]spiro-9-undecanone)) was used to confer self-assembling properties to the nanoparticles. Paclitaxel loaded PECT gel was shown to be biocompatibility and tolerated as a drug delivery system for IP chemotherapy. It was found to be retained for up to 8 days, as evaluated by a fluorescence imaging study. In addition, an efficacy study performed in a peritoneal carcinomatosis model has shown a significant suppression in tumour growth and metastasis in comparison to a Taxol® group for the .paclitaxel loaded PECT gel (128). In another study, docetaxel loaded polymeric nanoparticles were first prepared with a copolymer polylactic acid (PLA)-Pluronic L35-PLA. These nanoparticles were then incorporated into a thermosensitive hydrogel prepared with PLA-L64-PLA. IP administration of this hydrogel has suppressed the tumour growth and increased the survival in peritoneal carcinomatosis model (129).

All the previously described hydrogels were thermosensitive hydrogels with nanoparticles. Alternatively, nanoparticles were also incorporated into these covalently crosslinked hydrogels for further retention. Cho *et al.* prepared a covalently cross-linked HA hydrogel, incorporating cisplatin containing HA nanoparticles. They have observed retention of the gel up to 4 weeks, showing the sustained release of platinum. They have also reported the receptor mediated endocytosis of cisplatin containing HA particles into tumour cells. This hydrogel met all the desired properties of a sustained release drug delivery

system for IP delivery. Unfortunately, in a mouse model of IP tumour, this formulation did not show desired anti-tumor efficacy. In fact, authors have reported a slight increase in tumour burdens at a later time point, which was attributed to degradation products of the formulation (130). Hence, there is a need to develop a composite hydrogel that contain nanoparticles, aimed at IP delivery of chemotherapeutic agent for prolonged period with desired therapeutic efficacy.

1.4 Objective and scope of project

The overall aim of Ph.D. project is to design and evaluate a composite drug delivery system, which involves development of NCs that can incorporate hydrophobic drugs, and a hydrogel, which can incorporate these NCs for sustained local drug delivery. Two different cavities, the articular joint and the peritoneal cavity, were considered in the interests of answering the therapeutic needs associated with osteoarthritis and peritoneal malignancies. The focus of this project is to develop and evaluate a composite hydrogel containing NCs for prolonged retention and sustained drug delivery in the articular joint and peritoneal cavity. First objective was to develop the NCs formulation, which involves selection and optimization of different excipients, and method of preparation to ensure reasonable drug entrapment efficiency, drug loading and colloidal stability. *In vitro* release studies were then carried out to understand the performance of formulation in presence of simulated biological fluids. Further objective was to determine the *in vivo* retention of NCs after incorporation in a hydrogel. Hence, NCs were either radiolabelled or fluorescence tagged to administer in articular joint or peritoneal cavity. Final objective was to evaluate the therapeutic efficacy after IA administration of dexamethasone, a model anti-inflammatory agent, loaded formulation in antigen induced arthritis (AIA) rats. For IP delivery, docetaxel, an anti-cancer agent, was chosen to incorporate in the NCs and then incorporated in a hydrogel. *In vitro* tests were performed to evaluate its potential as an IP sustained drug delivery system.

- In **chapter 2**, HA coated NCs were developed to incorporate therapeutically relevant doses of dexamethasone exploring solvent evaporation and self-

emulsification techniques. Further, drug loading, entrapment efficiency, colloidal stability and *in vitro* release were evaluated. A radiolabel marker, ^{111}In, was loaded into NCs and IA administered to determine their local residence and biodistribution after incorporation in a fibrin (Fn)-HA gel. Anti-inflammatory efficacy was then evaluated after IA administration in antigen induced arthritis (AIA) rats.

- **Chapter 3** focusses on evaluation of NCs loaded in a hydrogel for IP drug delivery. Physically cross-linked hydrogels, Fn-HA and *N*-4-octanoyl-2′-deoxycytidine (2′-dC-*N*4-C_8), were optimized and evaluated to incorporate NCs. Fn-HA and 2′-dC-*N*4-C_8 represents hydrogels formed by two different mechanisms: enzyme mediated crosslinking and self-assembly respectively. DiR, a near-infrared fluorescent dye, was incorporated into NCs. Dye loading, dye entrapment efficiency and colloidal stability of DiR NCs was evaluated. Rheological properties and *in vitro* release studies was performed on Fn-HA and 2′-dC-*N*4-C_8 gels, after incorporation of DiR NCs. Local residence and biodistribution was determined using IVIS® fluorescence imaging in BALB/c nude mice after IP administration.
- In **chapter 4**, a covalently crosslinked hydrogel was designed and developed, aiming to withstand the dynamic environment associated with high fluid turnover present in the peritoneal cavity. Poly(ethylene glycol) based hydrogels, formed by two crosslinking mechanisms, photo-crosslinking and Michael addition reaction, were evaluated to incorporate DiR NCs. Photostability of the dye was evaluated after incorporation of DiR NCs in the PEG gel, and then *in vitro* DiR release studies were performed. An *in vivo* local residence and biodistribution was determined using IVIS® fluorescence imaging in BALB/c nude mice after IP administration. Docetaxel, an anti-cancer agent, was first incorporated into NCs, which were then incorporated into the PEG gel. *In vitro* release studies were then performed to establish the potential of DCX NCs loaded PEG gel for IP drug delivery.
- Finally, in **chapter 5**, findings described in chapters 2, 3 and 4 will be summarized and discussed with a focus on their future therapeutic application in OA and peritoneal malignancies.

2. Development and evaluation of nanocapsules-loaded hydrogels for intra-articular drug delivery

Osteoarthritis (OA) is a progressive, degenerative disease that affects the articulating joints (28), which is associated with extreme pain and disability to perform routine physical activities (35). Currently, only symptomatic treatments based on the stage of the disease are available (42). Early stage is often managed through non-pharmacological treatments, which include lifestyle changes, reducing the body weight, use of joint supportive braces and moderate exercises. Moderate stage of the disease is treated with oral or topical non-steroidal anti-inflammatory agents (NSAIDS), analgesics, nutritional supplements, and intra-articular (IA) injections. Severe stage of the disease is treated by surgical intervention, which commonly includes joint replacement (46-48).

IA injections are not first line treatments but are preferred as the last non-operative alternative when other conservative modalities have failed. Currently approved IA injections can be broadly classified into corticosteroids and viscosupplementations (HA injections without any pharmacologically active ingredient). Despite the long history of clinical use and cost-effectiveness of IA injections, their actual clinical benefits are still under debate (51-53). IA administered corticosteroids rapidly clear from the joint because of the leaky ultrastructure of synovium (54). Water and protein in synovial fluid is completely replaced within a period of 2 h (57), and the residence times of commonly used corticosteroids are from hours to few days (58). Hence, various formulation strategies have been employed to achieve longer retention and sustained release of IA injections. Suspensions, hydrogels, nano and microparticles were commonly explored drug delivery systems (64-66).

Among particulate delivery systems, both micro and nanoparticles have been well explored. Particle size of the delivery system has been reported as one of the crucial factors for determining the extent of retention in the joint after IA injection. Nanoparticles tend to escape from the cavity faster than the microparticles (69). Synovial macrophages tend to phagocytose particles < 10 µm, whereas microparticles > 10 µm tend to reside longer in the joint. However,

efficacy of microparticles is limited by the poor penetration into the local tissues such as synovium and cartilage in order to interact with local inflammatory cascade to elicit anti-inflammatory action (72). Nanoparticles have the capability to penetrate into the synovial membrane and interact with tissue associated inflammatory reactions. Hence, nanoparticles have also gained importance for IA drug delivery despite of their relatively higher clearance rates. To overcome their rapid clearance, nanoparticles have been incorporated into hydrogels to form composite systems for sustained release (discussed in section 1.2.5.4). Hence, in this study, we aimed to synthesize a composite system of nanocapsules (NCs) loaded into a hydrogel for IA injection.

NCs are drug delivery vehicles, which consists of a polymeric shell enveloping an oil core (78). They are versatile drug delivery systems that can harbour lipophilic molecules in the oily core and hydrophilic drugs in the polymeric shell. In this chapter, we have developed and evaluated polymeric NCs generated by solvent displacement and self-emulsification (or spontaneous emulsification) methods to incorporate a model anti-inflammatory agent, dexamethasone (DXM).

Hydrogels are complex matrices formed by 3D crosslinking of polymer chains in an aqueous or semi-aqueous environment. Because of their networked internal structure, they allow entrapment of drug, micro or nanoparticles, cells, proteins, and other biological molecules. In most of the cases, hydrogels that are used for IA delivery are pre-formed injectable or *in situ* forming systems (131, 132). Fibrin (Fn) hydrogels are a class of *in situ* forming hydrogels that have been well explored both in regenerative medicine and as drug delivery systems. Cells, nucleic acids, and other biologically active components have been incorporated in these hydrogels (133, 134). It was observed that networks formed from Fn have a positive impact on osteoarthritis. Tisseel®, a Fn sealant was found to favour chondrogenesis of articular cartilage (135). Additionally, hyaluronic acid (HA) is an endogenous lubricant present in synovial fluid. Hydrogels formed from a combination of Fn and HA have interpenetrating networks that offer higher drug loading and mechanical properties. HA has been chemically modified to offer various biomedical applications in combination with Fn (136-138). We hypothesize that a hydrogel formed from Fn and HA

could offer both chondrocyte-friendly properties of fibrin and lubricant properties of HA in the knee joint.

Previously, in our lab, a Fn-HA gel capable of incorporating NCs (prepared by the solvent displacement technique) was developed. These NCs had a limited capacity to encapsulate DXM. In this work, we have developed new NCs, prepared by both solvent displacement and self-emulsyfing techniques, capable of encapsulating a higher loading of DXM. In addition, we have optimized the amount of NCs loaded into the gel. After the development of this composite formulation, *in vivo* local residence, biodistribution and anti-inflammatory efficacy were evaluated in antigen induced arthritis (AIA) rat model.

Aim

To develop and evaluate a composite formulation containing DXM NCs in a Fn-HA gel in the management of arthritis.

Hypothesis

The use of a composite formulation may show enhanced local residence time of an anti-inflammatory agent after IA administration, and hence this could benefit its overall performance.

Objectives

1. To develop and characterize polymeric nanocapsules with HA, loading a model anti-inflammatory agent, DXM
2. To optimize the incorporation of DXM NCs in Fn-HA gel
3. To evaluate the *in vitro* release of DXM from NCs and Fn-HA gel
4. To radiolabel ^{111}In to HA NCs and evaluate their residence time & biodistribution
5. To evaluate the anti-inflammatory efficacy of Fn-HA gel containing DXM NCs

2.1 Materials

Fibrinogen and thrombin, both from human blood plasma were purchased from Sigma-Aldrich, Spain. Different molecular weights of HA (research grade), 41-65 kDa, 500-749 KDa and 1.01-1.8 MDa, were purchased from Lifecore, USA. DXM (99.7% purity), Tween® 80 and Castor oil, all good manufacturing practice (GMP) grades, were purchased from Acofarma, Spain. Lipocol® HCO-40 was obtained from Lipo chemicals, USA. Labrasol and Labrafac™ Lipophile WL1349 (EP and USP compliant grades) were procured from Gattefossé, France. Phosphatidylcholine enriched soy lecithin (EPIKURON® 145 V) was a free sample from Cargill, Spain. Extra pure virgin olive oil was purchased from Acros Organics, Belgium. Kolliphor® RH 40 (GMP grade) was purchased from BASF, Germany. Benzethonium chloride (BZT) was purchased from Spectrum, USA. Oleylamine, HEPES, Bovine serum albumin (BSA) (≥ 98%), sodium chloride (NaCl), calcium chloride dihydrate ($CaCl_2$. $2H_2O$), potassium chloride (KCl), sodium phosphate dibasic (Na_2HPO_4), and potassium phosphate monobasic (KH_2PO_4) of ≥ 99% purity, were acquired from Sigma-Aldrich, Spain. mBSA and Freund's complete adjuvant (FCA) were purchased from Sigma-Aldrich, Spain. Marketed DXM sodium phosphate injection (Kern Pharma, Spain) was purchased at local pharmacy. Enzyme linked immunosorbent assay (ELISA) kit for rat C-reactive protein (CRP) was obtained from Alpha diagnostic international, USA. Masson's trichome staining kit was purchased from Sigma-Aldrich, Spain. 1,2-dimyrisoyl-sn-glycero-3-phosphoethanolamine-*N*-diethylenetriaminepentaacetic acid (14:0 DTPA-PE) was purchased from Avanti polar lipids, Inc., USA. $^{111}InCl_3$ was obtained from PerkinElmer (USA) and Mallinckrodt Pharmaceuticals (USA). Amicon® Ultra centrifugal filters (0.5 mL, 10 kDa cutoff) were purchased from Merck, Spain. In-house ultrapure (Milli-Q) was used throughout the experiments. All organic solvents used were of high-performance liquid chromatography (HPLC) grade.

2.2 Methods

2.2.1 Preparation and characterization of HA NCs

2.2.1.1 Preparation of DXM-loaded HA NCs

HA NCs loaded with DXM, a model anti-inflammatory drug, were prepared by two different methods, solvent displacement and spontaneous emulsification.

Solvent evaporation technique for preparation of polymeric NCs (SD-NCs) was adopted from the procedure earlier described by our group (78). Two different surfactants, lecithin and Tween® 80 were evaluated. Briefly, DXM (4 or 6 or 8.1 mg), lecithin (5.625 mg) or Tween® 80 (15 mg), oleylamine (1.125 mg), BZT (1 mg), and olive oil (50 mg) were dissolved in 5 mL of ethanol. Then, the organic phase was injected through a needle (23 G) to 10 mL of aqueous phase containing 2.5 mg of HA 700 kDa, and kept under magnetic stirring at 900 rpm during 10 minutes at room temperature. Further, ethanol was removed by evaporation under vacuum (Rotavapor Heidolph, Germany). Final volume was adjusted to 5 mL with ultrapure water.

DXM-loaded NCs were also prepared by self-emulsification technique (SE-NCs). Formulation optimization was performed by selecting various oils and surfactants, based on their capacity to solubilize DXM, followed by mixing them in different DXM-loaded NCs were also prepared by self-emulsification technique (SE-NCs). Formulation optimization was performed by selecting various oils and surfactants, based on their capacity to solubilize DXM, followed by mixing them in different proportions in order to produce the nanoemulsions. Tween® 80, Labrasol and Kolliphor® RH 40 were used as surfactants at 20% w/w, while Labrafac, castor oil and olive oil were used as oils at 10 – 30% w/w. Lipocol 40-HCO was used as a co-surfactant at 10% w/w, to attain colloidal stability. In addition, HAs, 40 kDa (0.1, 0.25 and 0.5% w/w) and 700 kDa (0.1% w/w), were screened in order to form the shell of the NCs with optimum colloidal stability. The optimized composition for SE-NCs is shown in Table 2.1.

The optimized formulation of NCs consists of Labrafac™ Lipophile WL 1349 (from now-onwards it is written as Labrafac), Tween® 80 and Lipocol® HCO-40 (from now-onwards it is written as Lipocol) as oil and surfactants

respectively. For a 3 g batch size, 18 mg of DXM, 600 mg of Tween® 80, 300 mg of Labrafac and 300 mg of Lipocol were mixed together to form a drug-surfactant mixture. An amount of 3 mg of BZT was dissolved separately in 500 µL of ethanol and this solution was added to drug-surfactant mixture to assist solubilization of DXM and impart positive charge to the nanoemulsions. A volume of 1050 µL of water was then injected into this composition, under stirring at 1500 rpm, using a syringe. This process led to formation of a cationic nanoemulsion. An amount of 7.5 mg of HA (40 kDa) was separately dissolved in 330 µL of water and this was added to the nanoemulsion, allowing the formation of a polymeric coating through electrostatic interaction, to form NCs.

Table 2.1 Final composition of the optimized formulation composition of NCs, prepared by self-emulsification method.

Ingredients	**Chemical names**	**Composition (% w/w)**
DXM	Dexamethasone	0.6
Tween® 80	Polyoxyethylene sorbitan monoleate	20
Lipocol	PEG-40 Hydrogenated Castor oil	10
Labrafac	Medium chain triglycerides	10
BZT	Benzethonium chloride	0.1
Ethanol	Ethyl alcohol	13.15
HA (40 KD)	Glucosaminoglycan	0.25
Water	-	45.9

2.2.1.2 Determination of physicochemical properties

The mean hydrodynamic diameter (size) and polydispersity index (PDI) of the HA NCs obtained by both preparation procedures were measured after dilution (50×) with ultrapure water by dynamic light scattering (DLS) at 25 °C with an angle of detection at 173°. The zeta potential was measured by laser Doppler anemometry (LDA) using the same dilution. Both DLS and LDA analysis were performed in a Zetasizer®, NanoZS, Malvern Instruments, Malvern, UK.

2.2.1.3 Determination of encapsulation efficiency and drug loading

The encapsulation efficiency (% EE) of DXM was determined after the isolation of the SD-NCs by ultracentrifugation at 30,000×*g* for 1 h at 15 °C (Avanti® J-E, Ultracentrifuge, Beckman Coulter, USA). As SE-NCs were comparatively

larger in size, they were separated by centrifugation at relatively lower speed, 18,000×*g* for 1 h at 15 °C (Hettich, Universal 32R, Germany). The amounts of DXM in supernatant (isolated NCs), liquid underneath and non-isolated NCs (before centrifugation) were quantified by HPLC as described here.

To extract DXM from each of these samples, a pre-weighed quantity (approx. 20 mg) of the respective sample was diluted in 1 mL of ethanol, followed by vortex shaking for 3 min. The samples were analyzed by HPLC using a method adapted from the literature (139). The HPLC system consisted of a VWR-Hitachi LaChrom Elite® system equipped with a UV detector L-2400 set at 239 nm and a reverse phase SunFire column 186002560, 100Å, C18 (4.6 ID × 250 mm, pore size 5 μm), Waters, USA. The mobile phase was a mixture of methanol and ultrapure water (65%:35% v/v), isocratic, with the flow rate of 1 mL/min. The column was set at 30 °C and the injection volume was 20 μL. The standard calibration curves of DXM were linear in the range of 1-1000 μg/mL (r^2 = 0.999). Samples were transferred into auto-sampler vials, capped and placed in the HPLC auto-sampler. The concentration of DXM obtained from these samples was used to calculate the % EE and drug loading using equation 2.1 and 2.2 respectively.

$$\% \text{ EE} = \frac{\text{Amount of DXM in isolated destructed NCs}}{\text{Total DXM}} \times 100 \quad \text{.....Equation 2.1}$$

$$\text{Drug loading} = \frac{\text{Amount of DXM in NCs}}{\text{Volume of NCs}} \quad \text{.....Equation 2.2}$$

2.2.2 Preparation and characterization of NCs loaded Fn-HA gels

2.2.2.1 Optimization of incorporation of NCs in Fn-HA gel

The Fn-HA gel was prepared by thrombin mediated enzymatic polymerization. The following stock solutions were prepared for the gel formation.

- A lyophilized powder of human blood derived fibrinogen was dissolved in 0.15 M solution of NaCl at 37 °C to attain a concentration of 25 mg/mL, aliquoted and stored at -20 °C. Before each experiment, an aliquot was thawed to 37 °C for not more than 2 h before the gel preparation.

- A lyophilized powder of human blood derived thrombin was dissolved in 0.01 M phosphate buffer saline (PBS), kept at 4 °C, to a concentration of 100 NIH-U/mL. BSA was added as a stabilizer to an equivalent final concentration of 1% w/w. Aliquotes were made and stored at -20 °C. Before each experiment, an aliquot was thawed to 37 °C for not more than 2 h before the gel preparation.

- HA of, 700 kDa and 1.5 MDa MW, were dissolved separately in HEPES buffer (0.02 M HEPES, 0.1 M NaCl, 10^{-4} M $CaCl_2$, pH 7.4) to obtain a concentration of 0.65% w/v for each of these solutions. A 1:1 mixture of these solutions was prepared to give a ready-to-use mix (HAs) for gel preparation.

The optimization of Fn-HA gel was performed based on the therapeutic dose requirements of DXM. DXM has been explored for management of arthritis in the doses ranging from 0.5 to 1.2 mg/kg in various animal models. Therefore, we aimed to incorporate 34% w/w NCs in the Fn-HA gel, yielding a DXM dose equivalent to 1 mg/kg after IA administration. SE-NCs loaded with DXM (from now onwards called as DXM NCs) were incorporated in the gel. The concentration of gel components was optimized to ensure the gel formation after addition of DXM NCs. This was performed by sequentially increasing the concentrations of fibrinogen and thrombin from Gel-1 to Gel-5, compensating the concentrations of HAs mix (table 2.7). The components were mixed in a vial and gel formation was observed by tilting the vial after every 30 seconds up to maximum of 6 minutes.

2.2.2.2 Rheology studies

Modular compact rheometer (MCR302, Anton Paar GMBH, Austria) was used to perform dynamic rheology measurements using a parallel plate assembly (25 mm diameter rotating shaft, PP25). Approximately, 300 µL of gel-4 was placed on the center of the fixed plate. Fn-HA gel samples were prepared by combining mixtures of fibrinogen, DXM NCs and HAs solutions to form a premix. Later, this premix was loaded in the syringe and thrombin was then taken into the loaded syringe. Mixing of components was performed my moving the plunger of the syringe six to seven times. This mixture was then extruded out of the syringe within 2 min onto the plate to avoid gel formation inside the syringe barrel. Gel samples were then allowed to set for 5 min over the plate without

any intervention. After 5 min, the rotating shaft was allowed to come in contact with the gel. Measurement gap between fixed plate and rotating parallel plate was fixed for all the samples to be 0.5 mm. All measurements were recorded at 25 °C. Oscillatory amplitude sweeps were performed in the strain range of 0.1% to 100% at constant frequency of 10 rad s^{-1}. Storage modulus (G') and loss modulus (G") were recorded for gel-4. Similarly, oscillatory frequency sweep runs were recorded in the angular frequency range of 0.1 to 100 s^{-1}.

2.2.3 *In vitro* release studies

2.2.3.1 Preparation of simulated synovial fluid (SSF)

The simulated synovial fluid (SSF) was prepared using the composition described in the literature (140). In brief, NaCl, KCl, Na_2HPO_4 and KH_2PO_4 were added to the water to attain concentrations of 0.017 M, 0.0027 M, 0.01 M and 0.00176 M respectively. HA (1.5 MDa) was added to this salt solution at a concentration of 3 mg/mL, and mixed well to dissolve. pH of the final solution was adjusted to 7.4 using 0.1 N HCl or NaOH.

2.2.3.2 Stability of NCs in SSF

The stability of DXM NCs was evaluated in SSF at 37 °C. NCs were added to SSF in the proportion of 1:4 (200 mg/mL) and mixed well to form a suspension. This suspension was incubated at 37 °C for 48 h. The particle size was evaluated at regular intervals as per the procedure mentioned in section 2.2.1.2.

2.2.3.3 In vitro release of DXM from DXM NCs in SSF

Three different approaches have been explored for determining the release of DXM from DXM NCs: dialysis tubing, centrifugation and gel chromatography columns. DXM released into the medium was quantified using a HPLC-based analytical method, as mentioned in section 2.2.1.3. All the samples were filtered using 0.22 µm polyvinylidene difluoride (PVDF) filters before analysing the DXM content by HPLC. Filter compatibility of DXM with PVDF was ensured by separately running the calibration curve of DXM post-filtration.

SnakeSkin™ 7 kDa MWCO dialysis tubing (Thermo Scientific™, Spain) was used for evaluating the release of DXM from DXM NCs. 1 mL of isolated DXM NCs were diluted to 4 mL with milli-Q water and this NCs suspension was loaded into the dialysis bag, which was further clamped on both sides. A

suspension of DXM, prepared in 0.01 M PBS pH 7.4 containing 0.1% w/v Tween® 80, was used as a control. Three repeats of each of DXM NCs and DXM suspension were prepared. Later, these dialysis bags were immersed in 800 mL of PBS, pH 7.4, maintained at 37 °C in USP type II dissolution apparatus (Turu Grau DT-6, Spain). At 0.5, 1, 1.5, 4, 6 and 24 h, 10 mL of media was withdrawn, which was then replaced with fresh medium. 350 µL of each sample was diluted with 650 µL of ethanol to extract DXM for HPLC analysis. At the end of the study, 20 µL of sample from the dialysis bag were withdrawn and diluted to 1 mL with ethanol to determine the percentage recovery of DXM.

Centrifugation was also used to determine the release of DXM from DXM NCs. Briefly, 152 µL of NCs were suspended in 600 µL of SSF, and this suspension was incubated at 37 °C for 48 h under horizontal shaking at 150 rpm. Three samples were kept for each timepoint, starting from 2, 8, 24 and 48 h. At each timepoint, samples were centrifuged at 18,000×*g* for 1 h at 15 °C. NCs from the supernatant were separated and size of NCs was evaluated after centrifugation using the method mentioned in section 2.2.1.2. 100 µL of underneath liquid was collected and diluted to 1 mL with ethanol, which was then filtered to calculate DXM content by HPLC.

Alternatively, Sephadex G-25 PD-10 gel chromatography columns (GE healthcare Lifesciences, USA) were also explored to estimate the release of DXM from DXM NCs. A volume of 152 µL of NCs were suspended in 600 µL of 0.01 M PBS, pH 7.4, and this suspension was incubated at 37 °C for 48 h under horizontal shaking at 150 rpm. At each timepoint, from 2, 8, 24 to 48 h , 1 mL of sample was passed through the column under gravity. Twenty fractions of 0.5 mL each were collected from the column. First ten fractions were analyzed by DLS as described in section 2.2.1.2, to determine the particle size, which indicated the presence of NCs in the media. Based on the gravity, fractions containing intact NCs were expected to be eluted in the initial phase, while free DXM that would be released during the study was expected to elute in the later fractions. Fractions free of NCs were analyzed by HPLC for estimation of free DXM.

2.2.3.4 In vitro release of DXM from Fn-HA gel loaded with DXM NCs in SSF

In vitro release of DXM from Fn-HA gel was determined by forming an *in situ* hydrogel by injecting the gel components in SSF. A volume of 130 µL of SSF was placed in a 500 µL microtube and warmed to 37 °C. Later, µL of gel components, containing 34 µL of NCs, were added to the microtube gently, by introducing the needle down to the bottom of the tube. Gel formation happened at the bottom of the tube, leaving some quantity of SSF over the gel. At each timepoint (6, 18, 24, 30 and 48 h.), 50 µL aliquots were collected and diluted to 1 mL with ethanol before analysing by HPLC. All the samples were filtered using 0.22 µm polyvinylidene difluoride (PVDF) filters before analysing the DXM content by HPLC.

2.2.4 Evaluation of local residence and biodistribution

2.2.4.1 Radiolabelling of HA NCs with ^{111}In

A radiolabel marker, ^{111}In was attached to HA NCs using a linker DTPA-PE. DTPA-PE was first incorporated into NCs by dissolving DTPA-PE (0.08% w/w of NCs) in chloroform (0.6% w/w of NCs). For example, a 3 g batch size of NCs will have 0.24 mg of DTPA-PE in 20 µL of chloroform. A volume of 20 µL of this solution was mixed with the 480 µL solution of BZT in ethanol and further incubated with 0.16-1 mCi (6-37 MBq) of $^{111}InCl_3$ for 30 minutes. In another vial, 600 mg of Tween® 80, 300 mg of Labrafac and 300 mg of Lipocol were weighed. A solution of 500 µL of BZT and ^{111}In coupled DTPA-PE was then added to this. Further manufacturing process is similar to the self-emulsifying NCs, as mentioned in section 2.2.1.1. ^{111}In labelled NCs were then isolated by filtration/centrifugation at 18000g using Amicon® filters & radiolabeling efficiency was determined.

2.2.4.2 Determination of radiolabeling efficiency & radiolabel stability

Labelled NCs were expected to remain in the upper compartment of the device after centrifugation. The activity of both fractions was measured with a gamma counter (Cobra II, Packard). Efficiency was determined using equation 2.3:

$$\% \text{ Labelling efficiency} = \frac{\text{Activity of filter with isolated NCs}}{\text{Total activity}} \text{ X } 10 \quad \text{..Equation 2.3}$$

Further, radiolabel stability was assessed by incubating labelled NCs with SSF (1:4 v/v), at 37 °C under horizontal agitation. Samples were collected at 1 h, 6 h, 24 h and 2, 3, 7 and 13 days from the time of incubation. Free ^{111}In was determined using Amicon® filters, as explained above.

2.2.4.3 Animals

All experiments were performed using healthy female Sprague Dawley rats (130-290 g) in accordance to E.C. (2010/63/EU) on care and use of animals in experimental procedures. All experiments were approved by the local Research Ethics Committee (CEIBA) of Universidad de La Laguna. Animals were caged in metabolic cages under controlled conditions, supplied with food and water *ad libitum*.

2.2.4.4 Evaluaiton of local residence of NCs after IA injection

The residence time of the free NCs and NCs-containg Fn-HA gel was evaluated in healthy and AIA rats. Arthritis was induced by IA injection of an antigen, as described in the literature (141, 142). Briefly, two doses of FCA (1 mL, 1 mg/ml solution) were received by each animal sub-cutaneously, for immunopotentiation on 21st and 14th day before induction of arthritis. Later, arthritis was induced by IA administration of BSA (100 µL, 10 mg/ml) in the left knee of each rat on day 0 in all the groups except group 1. On day 1, treatment was given by IA administering 100 µL of respective sample to each group (~ 1 µCi, 37 KBq). For the free ^{111}In NCs group, 34 mg of ^{111}In NCs were diluted to 100 µL in water for injection before IA administration. The right knee of all rats received normal saline as a control.

Both, healthy and AIA rats were divided into 4 groups (3 rats/group). Two groups received ^{111}In labelled NCs alone and Fn-HA gel containing ^{111}In labelled NCs. Two control groups received a physical mixture of blank NCs and free $^{111}InCl_3$, and a physical mixture of blank NCs loaded Fn-HA gel and free $^{111}InCl_3$. Rats was kept under anaesthesia with isoflurane/oxygen with their body temperature maintained at 37 °C during the whole procedure. DXM was incorporated into the test formulations for AIA rats.

Retention of NCs was tracked by assessing the remaining radioactivity periodically at the injection site up to 14 days using an external gamma counter

probe (Captus®, Nuclear Iberica, Nucliber S.A., Spain). To measure the remaining radioactivity, rat's knee joint was placed in contact with the detector. At each time point, four consecutive readings were performed and the peak at 254 keV was integrated to acquire cumulative events registered over 1 min. Mean of these readings were considered to be the remaining radioactivity (% injected dose (% ID)) at that particular time point. The value obtained at time 0 was assumed to be 100% administered dose. The animals were set free after revival from anaesthesia.

2.2.4.5 Evaluation of biodistribution of NCs after IA injection

The biodistribution of NCs was evaluated with and without Fn-HA gel in AIA rats. Arthritis was induced as explained in section 2.2.4.4. Rats were divided into 4 groups (3 rats/group). ^{111}In labelled NCs with and without Fn-HA gel forms the two test groups, while a physical mixture of blank NCs and $^{111}InCl_3$, with and without Fn-HA gel forms the two control groups. Each group was allocated to 6 h, 24 h and 72 h time points to sacrifice and harvest the organs. As a whole, 36 animals were used for this study (4 groups x 3 rats/group x 3 time points). 100 µL of each formulation was administered IA which is equivalent to radioactivity of ~ 1 µCi, 37 KBq.

At each time point, animals were euthanized in CO_2 chamber and organs were harvested to measure the radioactivity in the gamma counter (Cobra II, Packard). Standards to correct the natural decay were prepared by taking an aliquot from injected formulation. Blood samples were collected by cardiac puncture. Harvested organs include spleen, heart, liver, lung, kidneys, popliteal and inguinal lymph nodes, femur, knee, tibia and bladder. Radioactivity was determined with respect to injected dose (100%), per gram of tissue (% ID/g).

2.2.5 Evaluation of *in vivo* efficacy

2.2.5.1 A 28-day evaluation study

The efficacy of DXM NCs was evaluated in AIA female Lewis rats. 30 rats were acquired from Charles River, Germany. They were housed in polypropylene cages under standard controlled conditions (24 ± 1 °C, 12 h light/dark cycle), and fed with commercial chow and acidified drinking water *ad libitum*. They were separated into 6 groups (5 rats/group) and left undisturbed for a week for

acclimatization. As explained in section 3.2.1.4, two doses of FCA were received by each animal, first on 21st day and again on 14th day before the induction of arthritis, for immunopotentiation. Later, arthritis was induced by IA administration of BSA in the left knee of each rat on day 0 in all the groups except group 1. On day 2, respective treatment (test or control) was administered to arthritic knee, while right knee of all rats received normal saline as a control. Group 1 (negative control) and Group 2 (AIA group) received normal saline in both the knees. Group 3 (AIA/blank NCs + Gel) received a hydrogel loaded with blank NCs. DXM sodium phosphate injection (4 mg/ml), a marketed formulation, was administered in group 4 (AIA/DXM) as a treatment control. Group 5 (AIA/DXM-NCs) received DXM NCs alone, while group 6 (AIA/DXM-NCs + Gel) received Fn-HA hydrogel loaded with DXM NCs. 100 µL of injection volume was adopted in all groups except group 4, where 50 µL of formulation was used (equivalent to 1 mg of DXM per kg body weight of rat).

The response to the treatment was evaluated by determining specific physical, biochemical and histochemical parameters. The reduction in knee diameter with time was evaluated by goniometer, as an indicator of swelling and inflammation. The serum levels of circulating CRP, a non-specific biochemical marker for inflammation, was evaluated by collecting the blood samples from retro-orbital plexus. On day 28, animals were euthanized, and knee joint was excised for histochemical analysis. Morphological changes in synovial membrane and articular cartilage was evaluated by hematoxylin-eosin (H-E) stain. A systematic double blind histological score was allocated to rank the potential outcomes of the treatment.

2.2.5.2 A 14-day evaluation study

A 14-day efficacy study was performed with a similar protocol as mentioned in section 2.2.5.2 with some modifications. In this study, treatment was given to rats on day 1 after induction of arthritis, rather than day 2. Moreover, 32 animals were allocated into 4 groups (8 rats/group). Non-suffering animals constitute the group 1 (negative control), while suffering, yet not treated animals constitute the group 2 (AIA group). Test groups include marketed DXM formulation (group 3 - AIA/DXM) and Fn-HA hydrogel loaded with DXM NCs (group 4 -

AIA/DXM-NCs + Gel). Knee diameters and body weights were measured till 14 days after the induction of arthritis. On 14th day, rats were euthanized to harvest the synovial membranes and cartilages and treat them with hematoxylin-eosin (H-E) stain. A systematic double-blind histological score was allocated to rank the potential outcomes of the treatment.

2.3 Results and discussion

2.3.1 Development and characterization of DXM NCs

DXM has been evaluated as an anti-inflammatory agent for the treatment of OA in animal models. The dose usually administered in rats by the IA route has been 0.5 - 1.2 mg/kg in a volume of 50 - 100 µL (143-145). Moreover, based on the previous studies performed in our laboratory, the maximum amount of NCs that can be loaded into Fn-HA gel was 35 % w/w (146). Considering these factors, it was estimated that the targeted dose of DXM in the suspension of NCs was 5 mg/mL. The solvent displacement and self-emulsification methods were explored for preparation of NCs.

Solvent displacement is a commonly employed procedure for preparing polymeric NCs (147). This process involves the preparation of an oil phase containing an active ingredient, surfactactants and oil in an organic solvent. This oil phase is then emulsified under stirring to form a nanoemulsion. An aqueous solution of polymer is then added to this nanoemulsion to form NCs. The organic solvent is then evaporated to concentrate the NCs (148, 149). Self-emulsifying is another technique which makes use of high amounts of surfactants in order to favour the process of emulsification and stabilization. The mixture of oil and surfactants also facilitates the solubilization of hydrophobic drugs (150).

2.3.1.1 Preparation and optimization of NCs by solvent displacement technique

First, NCs were prepared by solvent displacement method using lecithin as a surfactant. Three formulations (SD-LF1, SD-LF2, SD-LF3) were prepared at three different concentrations of DXM (4, 6 and 8 mg/ml) and colloidal properties were evaluated after preparation. There was no significant impact of the DXM concentration on colloidal properties of NCs (Table 2.2), however, as

evaluated by polarized microscopy, DXM was precipitated from NCs (Figure 2.1).

Table 2.2 Colloidal properties of NCs prepared by solvent displacement, using lecithin as a surfactant. (Each value is a mean ± SD of 3 preparations).

Formulation	Conc. of DXM (mg/ml)	Size (nm)	PDI	Zeta potential (mV)
SD-LF1	8.1	130 ± 4	0.2	-27 ± 7
SD-LF2	6	161 ± 5	0.2	-31 ± 1
SD-LF3	4	143 ± 10	0.2	-29 ± 2

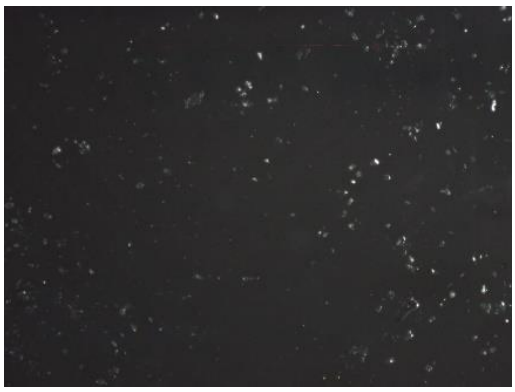


Figure 2.1 A representative polarized microscopic image obtained from isolated NCs, prepared by solvent displacement, using lecithin as a surfactant. Presence of birefringence indicates the recrystallization of DXM.

As DXM was precipitated with lecithin containing NCs, Tween® 80 was considered as an alternative surfactant and NCs were prepared with same method at two different DXM concentrations, 8 (SD-TF1) and 6 mg/ml (SD-TF2) (table 2.4). Similar to lecithin formulations, no considerable impact of DXM concentration on the colloidal properties was observed (Table 2.3). However, recrystallization of DXM was also observed with these Tween® 80 based NCs.

Table 2.3 Colloidal properties of NCs prepared by solvent displacement, using Tween® 80 as a surfactant. (Each value is a mean ± SD of 3 preparations)

Formulation	Conc. of DXM (mg/ml)	Size (nm)	PDI	Zeta potential (mV)
SD-TF1	8.1	178 ± 3	0.2	-42 ± 2
SD-TF2	6	176 ± 4	0.2	-42 ± 1

The recrystallization of DXM might be due to the low solubility of DXM in the mixture of oils & surfactants. NCs prepared by solvent displacement had low amount of these components, leading to precipitation of DXM. Alternatively, NCs prepared by self-emulsification use higher amounts of surfactants and oils. These agents are known to enhance the solubility of lipophilic drugs. Hence, various surfactants and oils were shortlisted based on solubility of DXM for preparation of self-emulsifying NCs.

2.3.1.2 Preparation and optimization of NCs by self-emulsifiication technique

The first step in this process was the selection of suitable oil and surfactants which can solubilize DXM and provide emulsion stability. Moghimipour *et al.* determined the solubility of DXM in various oils, surfactants and co-surfactants for preparation of a microemulsion. Labrafac, Tween® 80, Labrasol and Capryol 90 have shown relatively high DXM solubility (151). In our study, Tween 80, Labrasol and Kolliphor® RH 40 were evaluated as surfactants, while olive oil, labrafac and castor oil were used as oils.

DXM, the oil and a surfactant were mixed in different combinations, and apparent solubility was first observed using a microscope, for absence of traces of undissolved DXM. Unfortunately, DXM was not soluble in any of the studied mixtures. Hence, ethanol was used as a cosolvent. Nanoemulsions were then prepared by adding water to these mixtures under stirring. As shown in Table 2.4, recrystallization and phase separation were observed, visually and microscopically, under certain experimental conditions. Namely, combinations VII, VIII and IX showed DXM precipitation. While, combinations I, III, IV, V and VI showed phase separation due to emulsion instability. The presence of DXM crystals and phase separation was also confirmed through microscopy (Figure 2.2). Combination II showed neither precipitation of DXM nor phase

separation. Hence, from combination II, Tween® 80 and Labrafac were selected as surfactant and oil respectively.

Table 2.4 Screening of oils and surfactants used to prepare self-emulsifying nanoemulsions. * Each combination involved mixing of DXM (0.6% w/w) with respective oil (30% w/w) and surfactant (20% w/w) to form a nanoemulsion with water (36% w/w). Each of these mixtures had 13% w/w of ethanol as a co-solvent for DXM. Last two columns indicate the recrystallization and phase separation, as observed visually and microscopically after the preparation of respective mixture.

Mixture*	**Surfactant (20% w/w)**	**Oil (30% w/w)**	**Recrysta-llization**	**Phase separation**
I	Tween® 80	Olive oil	No	Yes
II	Tween® 80	Labrafac	No	No
III	Tween® 80	Castor oil	No	Yes
IV	Labrasol	Olive oil	No	Yes
V	Labrasol	Labrafac	No	Yes
VI	Labrasol	Castor oil	No	Yes
VII	Kolliphor® RH 40	Olive oil	Yes	No
VIII	Kolliphor® RH 40	Labrafac	Yes	No
IX	Kolliphor® RH 40	Castor oil	Yes	No

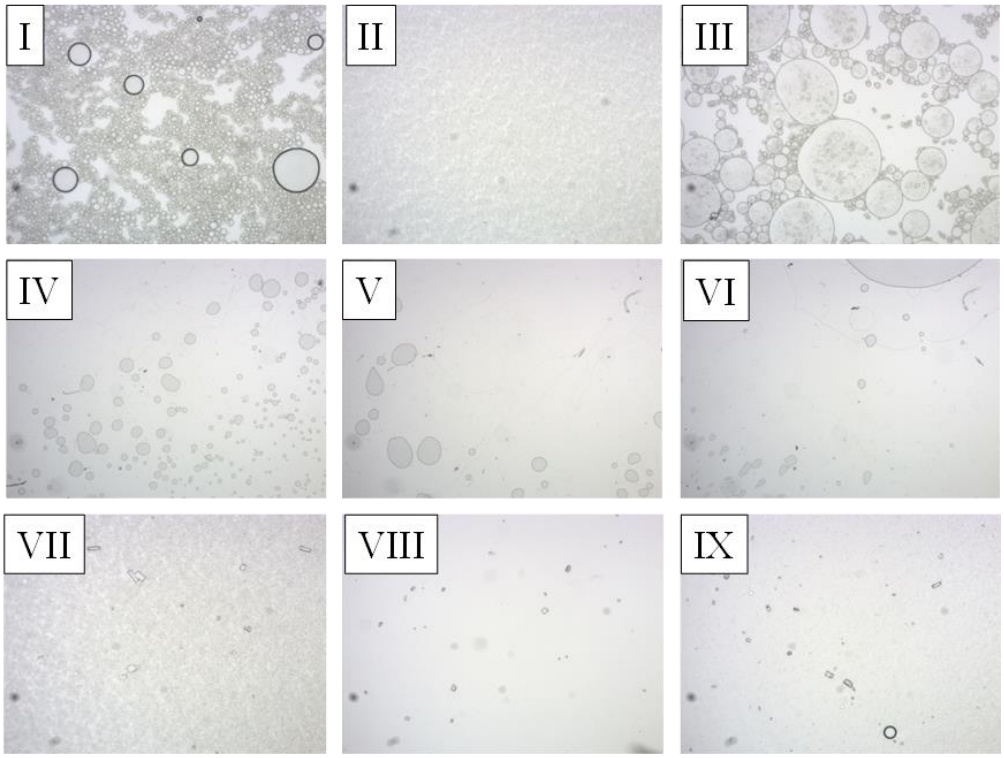


Figure 2.2 Microscopic images of self-emulsifying nanoemulsions. Immediately after the preparation, combinations VII, VIII and IX showed the recrystallization of DXM, while combinations I, III, IV, V and VI indicated the instability of nanoemulsion due to phase separation.

Once surfactant and oil were identified, proportions of Tween® 80 and labrafac were varied to achieve a stable colloidal dispersion. Tween® 80 was used at 10, 15 and 20% w/w, while Labrafac was used at 10, 20 and 30% w/w. A co-surfactant, Lipocol was incorporated into the nanoemulsions prepared from combination II (Table 2.4) at 10 and 15% w/w concentration. Ethanol was added at 13.15% w/w as a co-solvent for DXM. None of the nanoemulsions showed precipitation up to 6 mg/mL DXM concentration. Among the nanoemulsions evaluated, Tween® 80, Labrafac and Lipocol produced nanoemulsions with reproducible colloidal properties at 20, 10 and 10% w/w respectively.

In order to obtain NCs from this nanoemulsion, 0.1% w/w BZT was dissolved in ethanol and added to the mixture of Tween® 80, labrafac and lipocol. The resulting positively-charged nanoemulsion was then, mixed with an aqueous solution of HA (negatively-charged) (0.25% w/w, 40 kDa) leading to the formation of NCs (Figure 2.3). Size, PDI and zeta potential of these optimized HA NCs were found to be 250 ± 30 nm, 0.2 and –17 ± 3 mV respectively (n = 3).

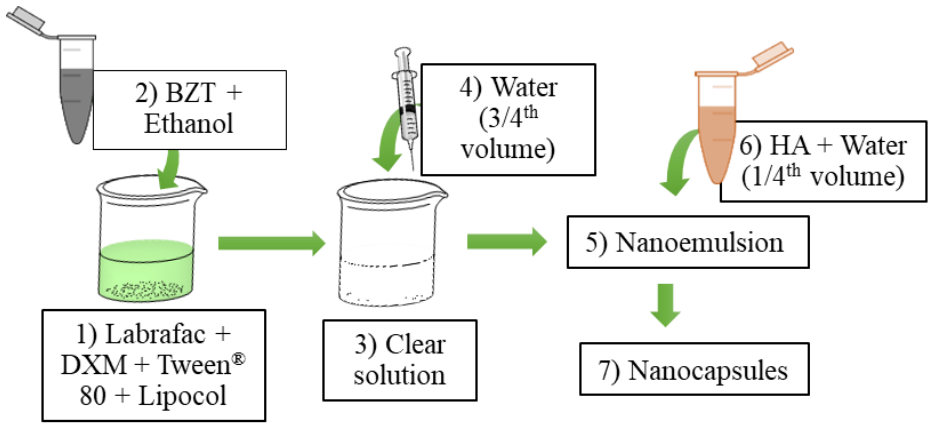


Figure 2.3 Schematic representation of optimized manufacturing process for preparation of self-emulsifying DXM NCs

After obtaining stable DXM-loaded NCs, the influence of molecular weight and concentration of HA on the colloidal parameters of the NCs was evaluated. NCs were prepared with two different molecular weights of HA, where 40 kDa HA was evaluated at 3 different concentrations, 0.1, 0.25 and 0.5% w/w and 700 kDa HA was evaluated at 0.1% w/w only. Further increase in concentration of 700 kDa HA caused handling difficulties associated with viscosity of HA. Moreover, colloidal stability was also evaluated by storing these NCs up to 4 weeks at 2 – 8 °C (Figure 2.4). No major changes in size was observed until day 14, among all compositions. However, on day 28 formulation containing 0.25% w/w of HA (40 kDa) remained stable, while other formulations tend to show an increase in size ($p < 0.05$, Dunnett's multiple comparison test). Hence, 40 kDa HA at 0.25% w/w was selected.

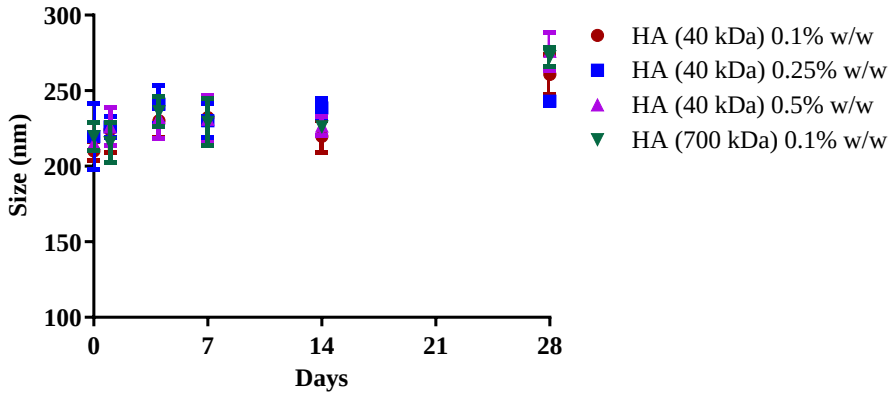


Figure 2.4 Influence of the molecular weight and concentration of HA on the colloidal stability of DXM NCs. Particle size was measured after preparing the DXM NCs and at different time points during their storage at 2-8°C. Except HA (40 kDa) at 0.25% w/w, all other formulations showed increase in size after 28-day storage ($p < 0.05$, Dunnett's multiple comparison test). (Each value is a mean ± SD of 3 preparations)

2.3.1.3 Determination of entrapment efficiency – influence of HA

The results presented in table 2.5 indicate that the MW and concentration of HA did not have an impact on the % EE of DXM. However, after 2 weeks of storage at 2 - 8 °C, NCs containing 0.1% w/w of HA, both 40 and 700 kDa, showed reduction in drug loading. Recrystallization of DXM was also observed in these samples. Lower concentration of HA might lead to discontinuous coating of globule surface, triggering the precipitation of DXM from oil phase. Moreover, high molecular weight HA (700 kDa) might also cause discontinuous coating due to non-uniform polymer deposition. Abellán-Pose *et al.*, also observed that use of high molecular weight polyglutamic acid (PGA), hampered the uniform polymer deposition onto the surface of docetaxel loaded nanoemulsion droplets (149). Hence, DXM-loaded NCs prepared with 40 kDa HA at a concentration of 0.25 % w/w were the most adequate in terms of drug loading and stability (Figure 2.4, Table 2.5).

Table 2.5 Influence of concentration and molecular weight of HA on % EE and drug loading of DXM, a compilation of data from DXM NCs immediately after preparation, and after storage at 2 - 8 °C for 2 weeks (Each value is a Mean ± SD of 3 preparations)

Polymer	**Concentration (% w/w)**	**% EE**	**Initial drug loading (mg/mL)**	**Drug loading after 2 weeks, 2-8 °C (mg/mL)**	**% Loss of DXM**
HA (40 KD)	0.1	41 ± 1	5.3 ± 0.6	4.4 ± 1.4	18 ± 15
	0.25	46 ± 6	5.3 ± 0.1	5.5 ± 0.1	0 ± 0
	0.5	49 ± 2	5.3 ± 0.1	5.3 ± 0.1	1 ± 1
HA (700 KD)	0.1	39 ± 6	5.0 ± 0.1	4.3 ± 0.1	14 ± 2

2.3.2 Development and characterization of Fn-HA gel loaded with DXM NCs

DXM-loaded NCs described in the previous section were incorporated into the hydrogel in order to obtain a composite formulation, suitable for prolonged retention and sustained release in the synovial cavity.

2.3.2.1 Optimization of incorporation of DXM NCs in Fn-HA gel

Fibrinogen is a natural blood coagulation factor which gets activated in presence of thrombin, to form a Fn network, which is responsible for clot formation (152). Fn scaffolds have been well explored for drug delivery (153). Nanoparticles containing growth factors, cells, therapeutic proteins and small molecules have been incorporated into fibrin gels for tissue regeneration and therapeutic purposes. For example, Zhou *et al.*, loaded chitosan nanoparticles in Fn gel for local delivery of recombinent human epidermal growth factor for wound healing (154). In another study, a fibrin network in combination with poly(ether)urethane-polydimethylsiloxane was developed to incorporate poly(lactic-co-glycolic acid) (PLGA) nanoparticles, loaded with vascular endothelial growth factor and basic fibroblast growth factor for wound healing (155).

Fibrin along with HA has been previously designed in our lab to form a Fn-HA gel, which could incorporate NCs loaded with an antagonist for galactin-3, a proinflammatory cascade initiator, for the treatment rheumatoid arthritis, as well as DXM (146). In this work it was hypothesized that the presence of HA in the Fn-HA gel might also help treating inflammatory arthritis, as HA has been historically used as an IA non-pharmacological agent in the management of OA (62).

In this study, we have adopted and further optimized this Fn-HA gel in order to incorporate NCs containing a high loading of DXM (final dose of 1 mg/kg). Concentrations of fibrinogen, thrombin and HAs were tuned to incorporate DXM NCs, ranging from Gel-1 to Gel-5 (Table 2.6). Figure 2.5 shows the images of gel compositions captured after mixing. Gel-1, Gel-2 and Gel-3 did not show formation of a gel after 6 minutes of mixing. While, Gel-4 showed gelation after 4 minutes and Gel-5 showed gelation after 2 minutes. Although gel formation was observed with compositions corresponding to both Gel-4 and Gel-5, Gel-4 was selected because of its reasonable slow gelation time, which allows mixing of gel components in the syringe before IA injection. In contrast, gelation time was too fast (< 2 min) for Gel-5 which led to formation of gel inside the syringe barrel, causing needle blockage. Moreover, it is desirable to keep the concentration of thrombin as low as possible as high concentrations of

this compound may stimulate proinflammatory processes in synovial tissues (156, 157).

Table 2.6 Optimization of gel components for incorporation of DXM NCs. Concentrations of fibrinogen and thrombin evaluated to incorporate DXM NCs are tabulated. 34% w/w of DXM NCs was loaded into all the gels, which yielded an equivalent dose of 2.04 mg/mL of DXM. This was equivalent to therapeutic dose of 1 mg/kg, considering IA administration volume of 100 µL.

Ingredient (% w/w)	Gel-1	Gel-2	Gel-3	Gel-4	Gel-5
Fibrinogen	6	12	18	24	36
Thrombin	2	4	6	8	12
HAs mix	58	50	42	34	18

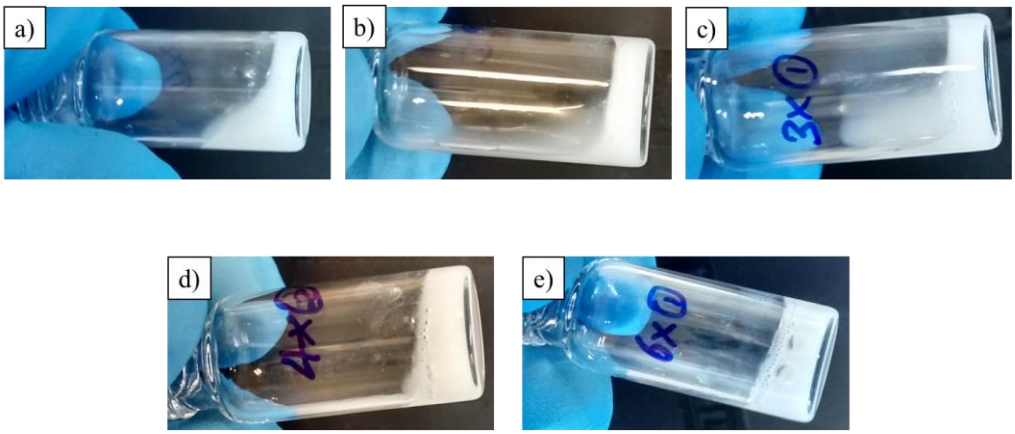


Figure 2.5 Optimization of Fn-HA gel to incorporate DXM NCs. Gels were prepared at increasing concentrations of fibrinogen and thrombin. Images were captured after preparation of gels at different time points, where (a) indicates Gel-1 after 6 min; (b) indicates Gel-2 after 6 min; (c) indicates Gel-3 after 6 min; (d) indicates Gel-4 after 4 min, and (e) indicates Gel-5 after 2 min. Gel-4 and Gel-5 have formed the gels in presence of DXM NCs

2.3.2.2 Rheology of DXM NCs loaded Fn-HA gel

Rheology is a useful tool to determine the structural properties of hydrogels. In general, hydrogels are known to exhibit viscoelastic behaviour. Oscillatory rheology studies are performed to derive storage modulus, G' which corresponds to elastic behaviour, and loss modulus, G" which corresponds to the flow properties of the material (158). G' and G" of Fn-HA gel were recorded using oscillatory amplitude and frequency sweeps. Amplitude sweep studies showed that G' is higher than G", indicating the elastic behaviour of the gel at lower strains (Figure 2.6). However, increasing strains led to reduction in G'. A crossover point was observed at 10% strain, indicating the mechanical breakdown of the gel. It is considered that after the crossover point, gel loses its

elastic behaviour and exhibits a flow property like a viscous liquid. Fn-HA gel is considered to behave like an elastic material at strains lower than crossover point, and this region is called linear viscoelastic (LVE) region (159). Beyond this point, it should be interpreted that flow properties of the gel dominate over the elastic properties.

Frequency sweep of Fn-HA gel was recorded at a fixed low strain value, which indicated a steady rise in both G' and G" values (Figure 2.7). This is a known phenomenon exhibited by viscous polymeric materials. However, it should be noted that G' and G" did not cross over in the whole frequency range, indicating that the elastic behaviour of the material is persistent with increasing frequency. These results are in consistent with viscoelastic behaviour that hydrogels exhibit typically (160).

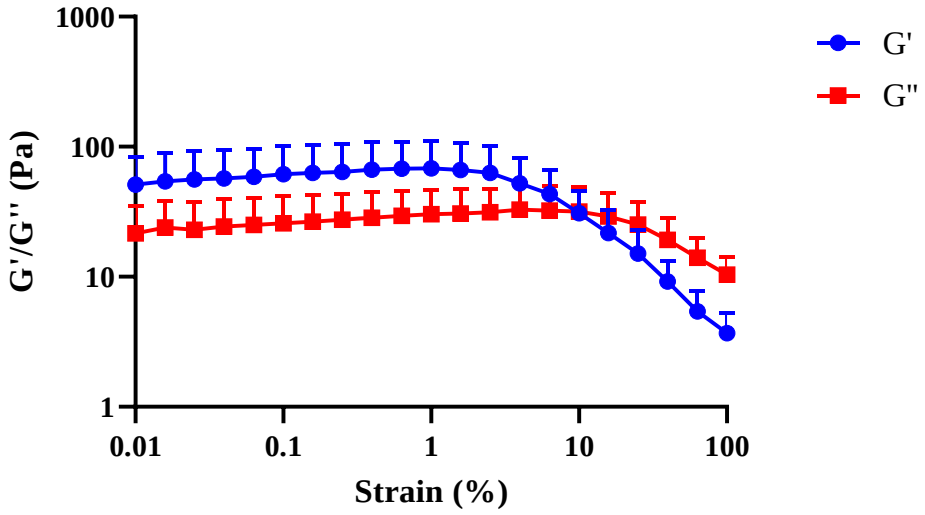


Figure 2.6 Rheology of Fn-HA gel containing DXM NCs, performed by oscillatory amplitude sweep using parallel plate assembly at 25 ºC. Viscoelastic property of the gel was confirmed by presence of a LVE region, where G' was > G". Presence of crossover point indicates the mechanical breakdown of the gel at > 10% strain. (Data represented as Mean ± SD, n = 3)

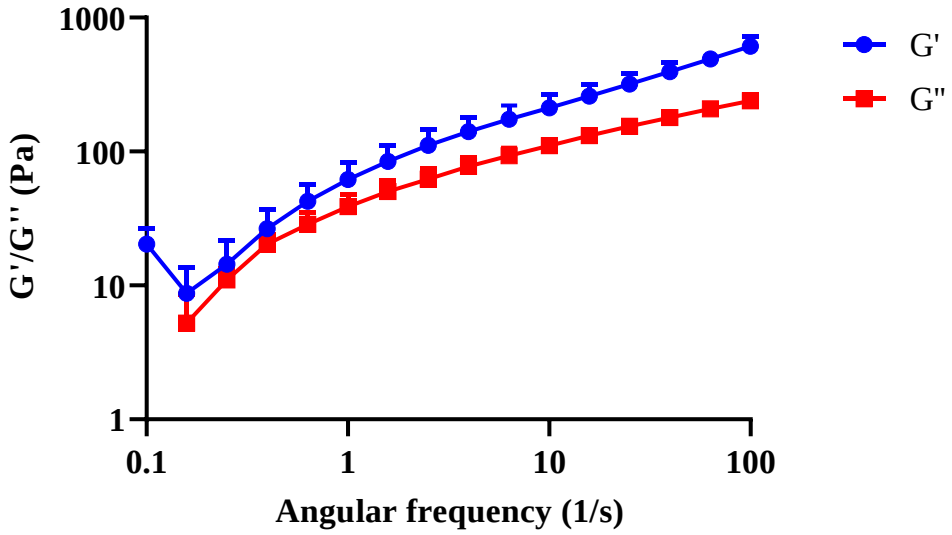


Figure 2.7 Rheology of Fn-HA gel containing DXM NCs, performed by oscillatory frequency sweep using parallel plate assembly at 25 ºC. A steady increase in G' and G" indicates the viscoelastic properties of the gel. No crossover point indicates that the elastic property of the gel was retained in the frequency range tested. (Data represented as mean ± SD, n = 3)

2.3.3 *In vitro* release studies

2.3.3.1 In vitro release of DXM from DXM NCs in SSF

DXM release studies from DXM-loaded NCs were carried out in simulated synovial fluid (SSF) using three different methods, as mentioned in section 2.2.3.3. The integrity of NCs in SSF was first ensured by checking the stability of NCs in SSF (section 2.2.3.2). As shown in Figure 2.8, although, a slight size increase was observed at 2 h, this size was retained for at least 48 h.

To calcuate the amount of DXM released, the first step was to isolate the NCs from the free DXM. Different methods were evaluated for this separation. Using ultracentrifugation, it was found that approximately 70% of DXM was released in the the first sampling point. Moreover, the size of isolated NCs changed from 250 ± 30 nm to 550 ± 150 nm, and the PDI from 0.2 to 1.0, indicating the instability of NCs towards centrifugation. This indicates the inefficiency of this method in establishing the release profile of DXM.

Gel chromatography columns, another approach for estimation of DXM release was also found to be unsuitable for estimation of DXM release. NCs were destabilized by column matrix. Size of NCs was changed drastically from 250

± 30 nm to > 1000 nm, while the PDI increased from 0.2 to 1, indicating the incompatibility of NCs towards PD-10 columns.

The use of a dialysis membrane was also explored to study the release of DXM from NCs. Figure 2.9 shows the cumulative release of DXM over 24 h, established using a dialysis membrane. As a control, a DXM suspension was also dialyzed. Approximately 3-5% of DXM was released from control sample of DXM suspension and from the NCs, respectively. Unfortunately, a significant amount of DXM was found to be associated to the dialysis membrane, a fact that led us to discard the experimental approach. This is in agreement with previous reports describing the adhesion of lypophilic molecules to dialysis membranes (161, 162).

Based on the experimental difficulties for assessing the release of DXM from the NCs, the decision was to study the release of the drug from the final delivery system, the DXM-loaded NCs containing hydrogel, as described in the following section.

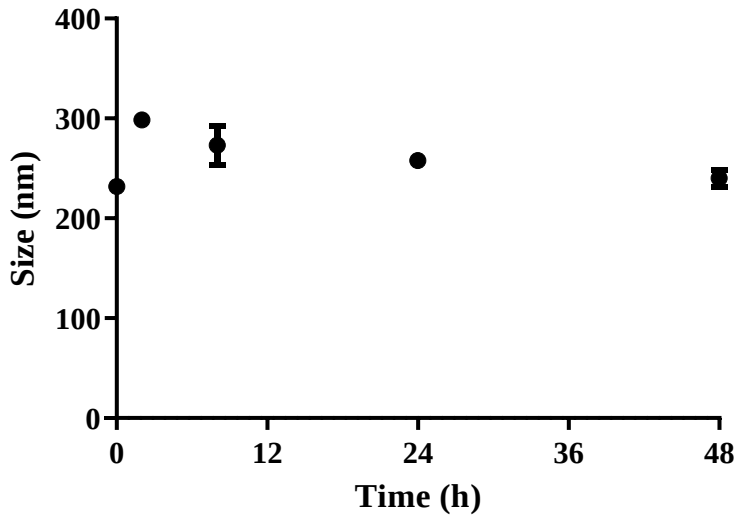


Figure 2.8 Colloidal stability of DXM NCs in SSF, determined by incubating them in SSF at 37 °C for 48 h, measuring the particle size at regular intervals. No significant change in particle size was observed after 48 h of incubation ($p > 0.05$, Dunnett's multiple comparison test). (Each value is a Mean ± SD, n = 3)

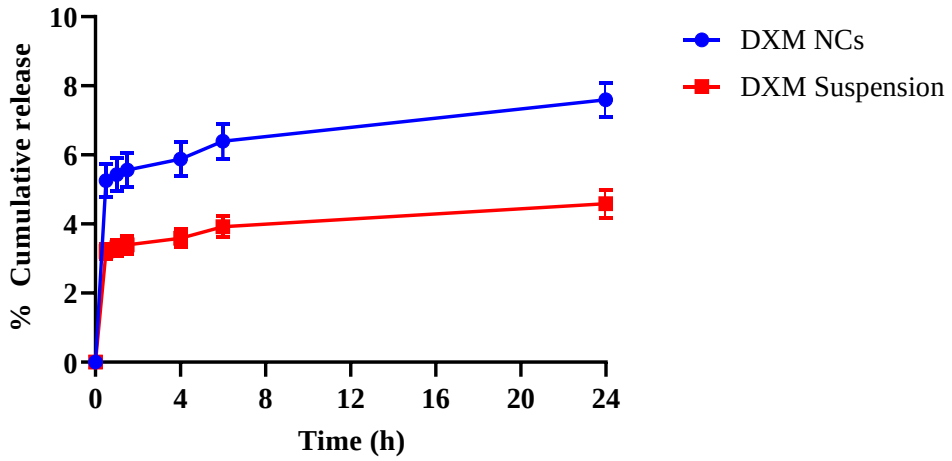


Figure 2.9 *In vitro* release study, showing the % cumulative release of DXM from DXM NCs, determined using dialysis membrane (7 kDa cutoff), which was further incubated in SSF at 37 ºC. (Each value is a Mean ± SD, n = 3)

2.3.3.2 In vitro release of DXM from Fn-HA gel containing DXM NCs in SSF

The DXM release from the final system, Fn-HA gel containing DXM-loaded NCs, in SSF, was determined as described in section 2.2.3.4. The results in Figure 2.10 indicate that DXM was gradually released reaching a 70% of DXM release. However, it should be noted that the amount of DXM estimated at each timepoint was an additive of free DXM and DXM entrapped in NCs that were also released from the gel. Hence, % release of DXM was considered to reflect the simultaneous process of gel degradation and DXM release (free or encapsulated) from the formulation.

It is known that the degradation of Fn gel networks is influenced by temperature, pH and presence of electrolytes. Nair *et al.*, reported that the pH and ionic strength of the medium affect the network structure by influencing the Fn assembly, while temperature influences both Fn monomer generation and Fn assembly (163). The presence of electrolytes in SSF and the temperature (37 °C) might have contributed to its degradation. Initiation of degradation might have led to formation of pores in the swollen hydrogel matrix, increasing the permeability of the gel. Chiu *et al.*, observed that presence of pores in Fn-thrombin networks determine their permeability, which is a function of their concentrations (164). In summary, the presence of electrolytes, temperature and formation of pores which might have led to the degradation of the gel and the release of free and encapsulated DXM into the medium.

On the other hand, with regard to the relase of DXM from the NCs, based on previous reports, it could be speculated that the release is governed by the partition of the drug between the oily core of the NCs and the surrounding medium.

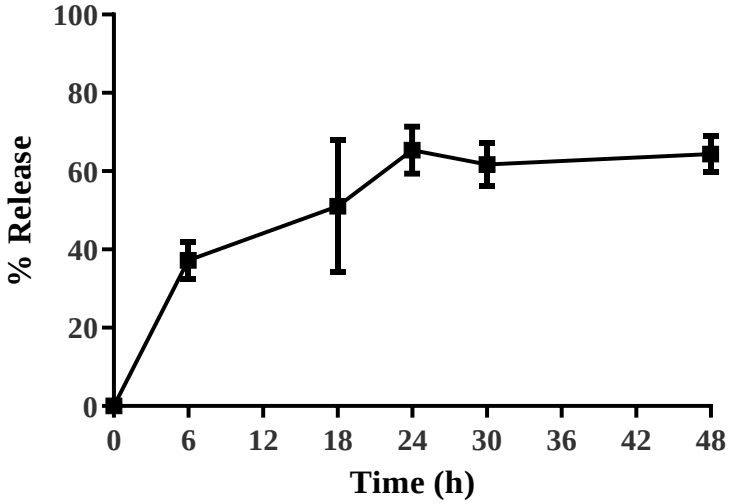


Figure 2.10 *In vitro* release study, showing the % release of DXM from Fn-HA gel containing DXM NCs, incubated in SSF at 37 ºC. (Each value is a Mean ± SD, n = 3)

2.3.4 Evaluation of local residence and biodistribution after IA administration of ^{111}In labelled NCs

2.3.4.1 Labelling of NCs with ^{111}In

Radiolabels have been in use in the clinic for various diagnostic and therapeutic purposes, highlighting their relative tolerability (165, 166). Labelling of nanoparticles using a radioactive ligand is a common approach to evaluate their biodistribution and local residence. ^{111}In, ^{99m}Tc, ^{67}Ga, ^{131}I, ^{188}Re are commonly used radioligands for tracking their biodistribution (167, 168). Our lab has previously studied the biodistribution of polyethylene glycol-polyglutamic acid (PEG-PGA) NCs labelled with ^{111}In. The incorporation of the radiolabel to the NCs was mediated by a metal chelating agent DTPA-PE (169). The same labelling protocol was adapted in this study, as explained in section 2.2.4.1.

In the first step, the assesemnt of the physicochemical properties of the NCs after incorporation of the linker DTPA-PE was performed. The results showed that the size of NCs was slightly reduced from 250 ± 30 nm to 215 ± 20 nm. Although, not statistically significant ($p > 0.05$, Student's t-test), this slight

reduction could be attributed to the amphiphilic nature and surface localization of DTPA-PE (170). The PDI and zeta potential were remained unchanged at 0.2 and –15 ± 3 mV respectively.

In the second step, ^{111}In was tagged to DTPA-PE as mentioned in section 2.2.4.1. The labelling efficiency of ^{111}In was determined by separating the free and bound ^{111}In and was found to be 97.8 ± 1.1 %. The association of the label to the NCs was stable, leaking only 4% of ^{111}In after 13 days of incubation in SSF (Figure 2.11).

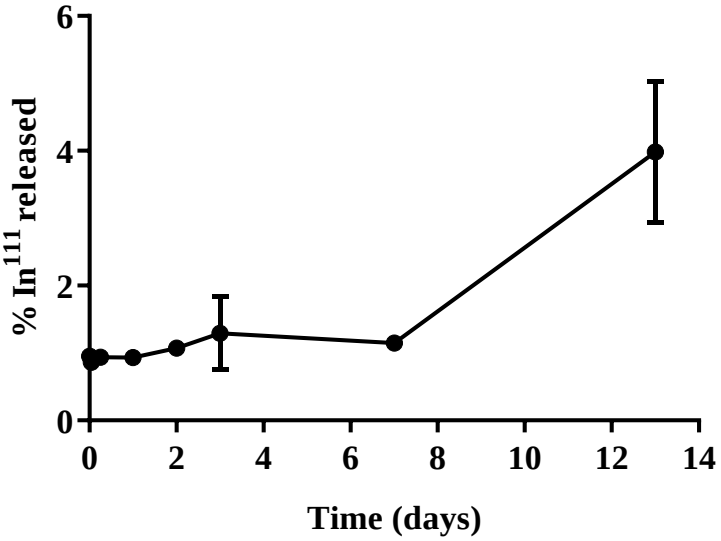


Figure 2.11 Radiolabel stability of ^{111}InNCs, determined by incubating them with SSF at 37 ºC. At each time point, samples were centrifuged with Amicon® filters to separate and quantify free ^{111}In from ^{111}In bound to NCs. (Each value is a Mean ± SD, n = 3)

2.3.4.2 Evaluation of local residence after IA administration

Once NCs were radiolabelled and characterized, the ability of these ^{111}In NCs to retain in the synovial cavity after IA injection was evaluated in presence and absence of Fn-HA gel. A physical mixture of NCs and free $^{111}InCl_3$ was used as a control for NCs, whereas a mixture of NCs loaded in Fn-HA gel and free $^{111}InCl_3$ was used as a control for gel sample.

The residence time of the NCs at injection site obtained by tracking the residual radioactivity in presence and absence of Fn-HA gel is shown in Figure 2.12. After 14 days of administration, radioactivity was observed from all the groups with no significant differences between them ($p > 0.05$, one-way ANOVA, Tukey's multiple comparison test). The control groups also showed retention

similar to NCs group and NCs-loaded Fn-HA gel group, which might be due to the potential interaction of $^{111}InCl_3$ with blank NCs. Association of ^{111}In with blank NCs in the control groups might led to retention profile similar to NCs and NCs-loaded Fn-HA gel group. Additionally, $^{111}InCl_3$ might have precipitated into indium oxide, which has lower solubility under physiological conditions (171). Formation of indium oxide at the injection site might led to higher radioactivity than expected. Similar phenomenon has also been observed by Abellan-Pose *et al*., where $^{111}InCl_3$ was precipitated as indium oxide, after subcutaneous administration in rats (169).

It was also observed that there were no significant differences in % ID remaining at injection site between the NCs group and the NCs-loaded Fn-HA gel group ($p > 0.05$, one-way ANOVA and Tukey's multiple comparison test). It was anticipated that Fn-HA gel could retain the NCs longer in the cavity, driven by its gradual degradation. However, no difference in residual radioactivity signifies that Fn-HA gel did not retard the release of loaded NCs. Release of NCs could be due to rapid enzymatic or mechanical degradation of the gel. Although, Fn-HA gel has shown comparable rheological properties (Figure 2.6) to commercial HA based IA injections Ostenil® and GO-ON®, it did not tolerate the mechanical forces exerted by weight bearing knee joint (172).

Enzymatic degradation is another phenomenon that fibrin mediated hydrogels encounter. Despite of the fact that the fibrin-derived hydrogels are well explored as tissue regeneration matrices, they might face rapid enzymatic degradation *in vivo*. Ahmed *et al.*, found that matrix metalloproteinases and plasminogen activators, which are predominantly expressed in arthritic joints, are responsible for early degradation of fibrin gels (173). As discussed in the literature, the major drawback of fibrin hydrogels is that, they susceptible to protelolytic degradation *in vivo*, which might be responsible for premature degradation of Fn-HA gel (174). Synovial cavity is an enzyme rich environment. As an indigenous viscosifier also, hyaluronic acid undergoes continuous degradation and rejuvenation within the cavity (61). These enzymatic activities increase many folds in AIA rats because of the prevailing inflammatory activity (60, 175). These factors might also contribute to the degradation of Fn-HA gel.

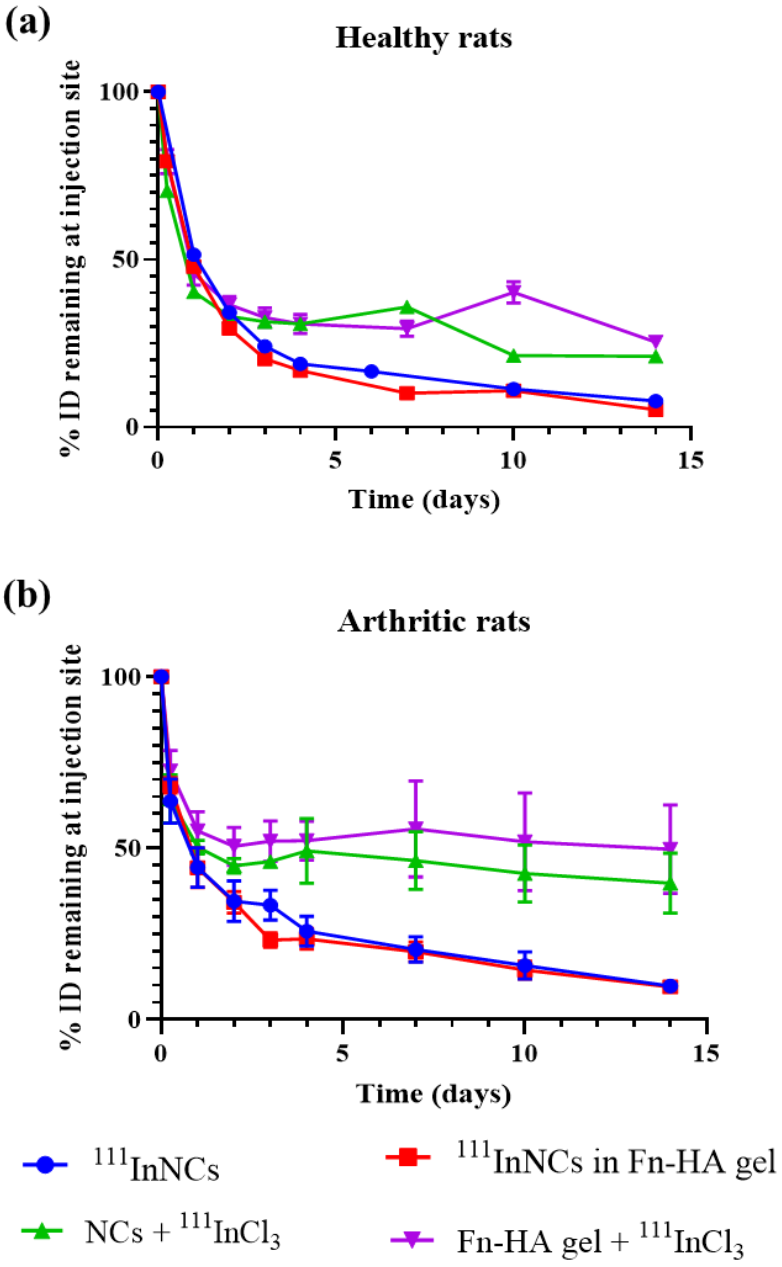


Figure 2.12 Local residence of ^{111}In labelled NCs, administered alone or in Fn-HA gel, represented as Mean ± SEM of %ID remaining at injection site after IA administration in (a) healthy and (b) arthritic rats (n=3 rats/group), as determined by a gamma counter probe (Captus®, Nuclear Iberica). A physical mixture of NCs alone and NCs loaded in Fn-HA gel with $^{111}InCl_3$ were used as controls (n=3 rats/group).

2.3.4.3 Evaluation of biodistribution after IA administration

The biodistribution of NCs from injection site was studied by calculating the % ID from different organs at certain timepoints after administration. The values obtained were normalized by considering the weight of each organ collected. Figure 2.13 shows the % ID/g obtained from different organs at 6, 24 and 72 h. Overall, the data indicate a rapid drainage of the NCs from the IA cavity to the

lymphatics, irrespective of the presence of the gel. Both groups, ^{111}In-NCs and ^{111}In-NCs loaded Fn-HA gel, showed higher radioactivity levels in popliteal lymph nodes at 6 and 24 h, than the corresponding controls. However, the high variation in the values obtained led to the absence of statistically significant differences between the groups.

The clearance of NCs from the joint and subsequent biodistribution of NCs into popliteal lymph nodes could be attributed to the dynamic environment of the synovial cavity. Constant exchange of fluid, small and large molecules occur continuously through lymph ducts and capillary beds encircling the cavity. This phenomenon becomes more prominent in arthritic joint because of underlying inflammatory activity (176). Moreover, tissue residing macrophages and actively recruiting macrophages from circulatory system are also prominent in the synovial cavity (177). These macrophages might phagocytize the NCs, an even fragments of the eroding gel, clearing them from the cavity. These results are in accordance to the previous reports on the clearance of nanoparticles from the synovial cavity. For example, Pradal *et al.*, discussed the size driven escape of fluorescently labelled poly(lactic acid) nanoparticles from the knee joint into surrounding lymph nodes, after IA administration (69). They observed that 300 nm particles were cleared rapidly from the healthy and inflammed joint, while 3 µm particles were cleared from inflammed joint only. The 10 µm particles were completely retained in the cavity irrespective of inflammation state of the joint. The authors attributed the rapid clearance of small particles to the phagocytosis by macrophages. Additionally, as explained before, Fn-HA gel might have undergone rapid mechanical or enzymatic degradation, which led to release of NCs into the synovial cavity. Hence, biodistribution pattern observed by NCs-loaded Fn-HA gel group was similar to NCs group.

Therefore the overall conclusion from this study is the drainage of the delivery system from the IA cavity to the lymphatics. The fact that the gel did not have any effect in this drainage could be because it was rapidly degraded and/or the uptake of NCs and degrading gel by macrophages. Irrespective of the mechanism of drainage the results led us to discard the potential of the developed system as a long-acting IA delivery system.

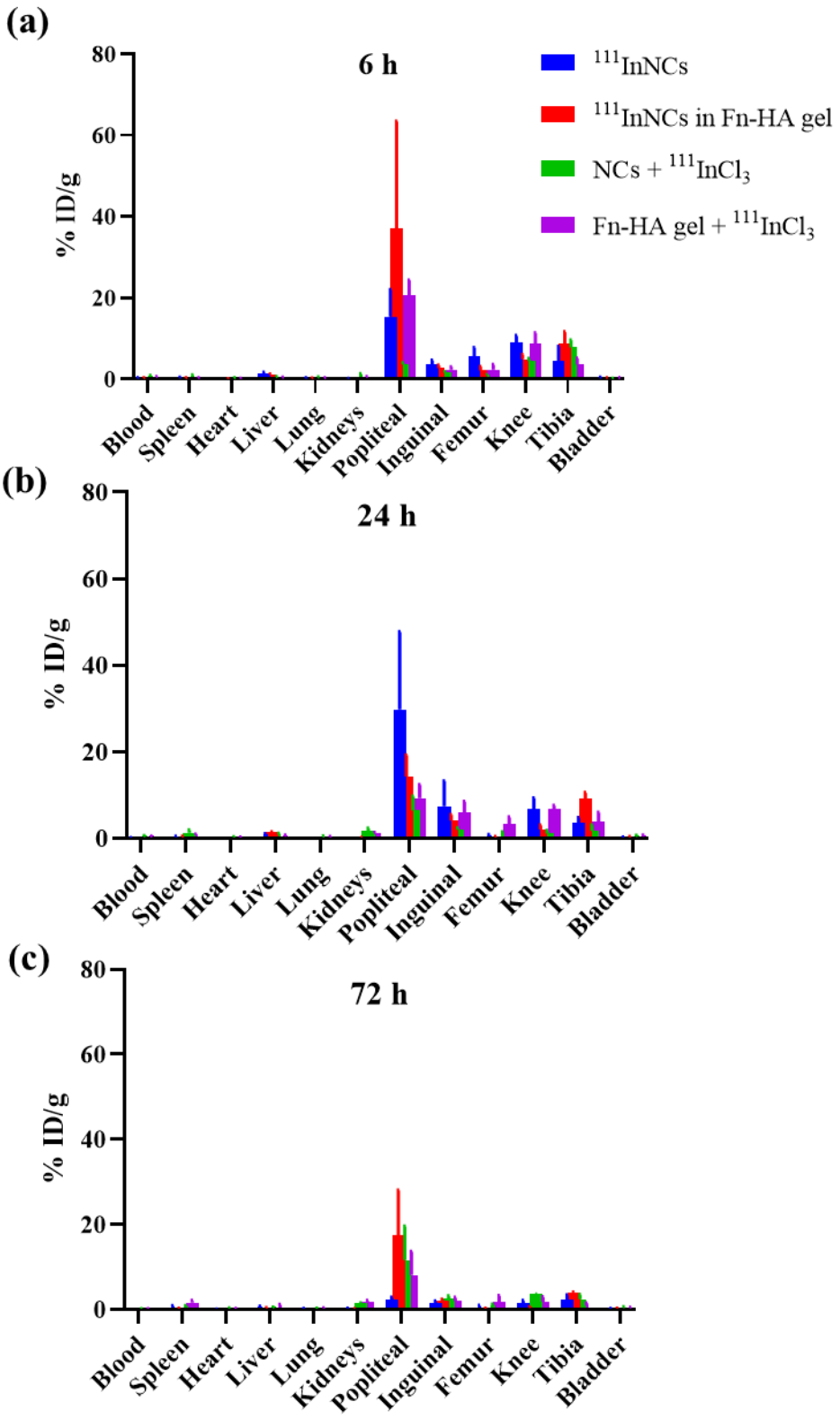


Figure 2.13 Biodistribution of ^{111}InNCs, administered alone or in Fn-HA gel, represented as Mean ± SEM of %ID/g obtained from various organs at (a) 6 h, (b) 24 h and (c) 72 h after IA administration (n=3 rats/group), using a gamma counter (Cobra II, Packard). A physical mixture of NCs alone and NCs loaded in Fn-HA gel with $^{111}InCl_3$ were used as controls (n=3 rats/group).

2.3.5 Evaluation of anti-inflammatory efficacy of Fn-HA gel containing DXM NCs in AIA rats

The efficacy of the formulations designed was evaluated in animal models (AIA) where arthritis was generated using an antigen. The efficacy of DXM NCs and Fn-HA gel containing DXM NCs was evaluated in two separate studies. The first efficacy study was 28-days long, while the second efficacy study was 14-days long, both after single IA administration.

The 28-day long study was designed to evaluate the response to IA administration of Fn-HA gel containing DXM NCs, administered on second day after induction of arthritis. In contrast, in the 14-day long study, DXM treatment was administered one day after induction of arthritis, so that extent of damage due to AIA induction was limited. Physical parameters such as body weights and knee diameters of animals were monitored throughout both the studies.

2.3.5.1 Evaluation of physical and biochemical parameters in response to DXM treatment

Figure 2.14 (c) and Figure 2.15 (a) show the evolution of the animal's weight during the 28-day and 14-day efficacy studies, respectively. Slight reduction in body weight was seen after the induction of arthritis in all groups except the negative control. This might be due to the inflammatory and metabolic activity in animals. Body weights appear to regain during treatment, maybe due to the administration of steroids. Winter *et al.*, reported a similar pattern of changes in the body weight during the course of disease induction and treatment with anti-inflammatory agents in adjuvant induced arthritis model (178).

Figure 2.14 (a) shows an initial increase in knee diameter in both, right and left knees, due to the volume injected into the joint cavity. However, knee diameters of left joint ramped up sharply in all groups except the negative control group, indicating the initiation of a profound inflammatory activity in the knee. In the 28-day study, the left knee diameters were gradually reduced in all groups, including the groups untreated with DXM (group 2 and 3). This phenomenon can be attributed to inherent healing response shown by rats with time. No additional benefit was observed in response to DXM treatment in terms of knee diameters, as seen in groups 4, 5 and 6. Similar results were observed in the 14-

day study (Figure 2.15). These findings are not aligned with the literature on anti-inflammatory effects of IA DXM. For example, Elron-Gross *et al.*, reported the anti-inflammatory activity of an IA liposomal DXM formulation alone and in combination with diclofenac (179). In another study, Zhang *et al.*, reported that DXM incorporated in a cross-linked HA gel showed anti-inflammatory and chondroprotective effects after single IA injection into rat knees, in a surgery induced arthritis model (131). Heard *et al.*, also reported that DXM exhibited anti-inflammatory activity and prevented the development of post-traumatic osteoarthritis after single IA injection (145).

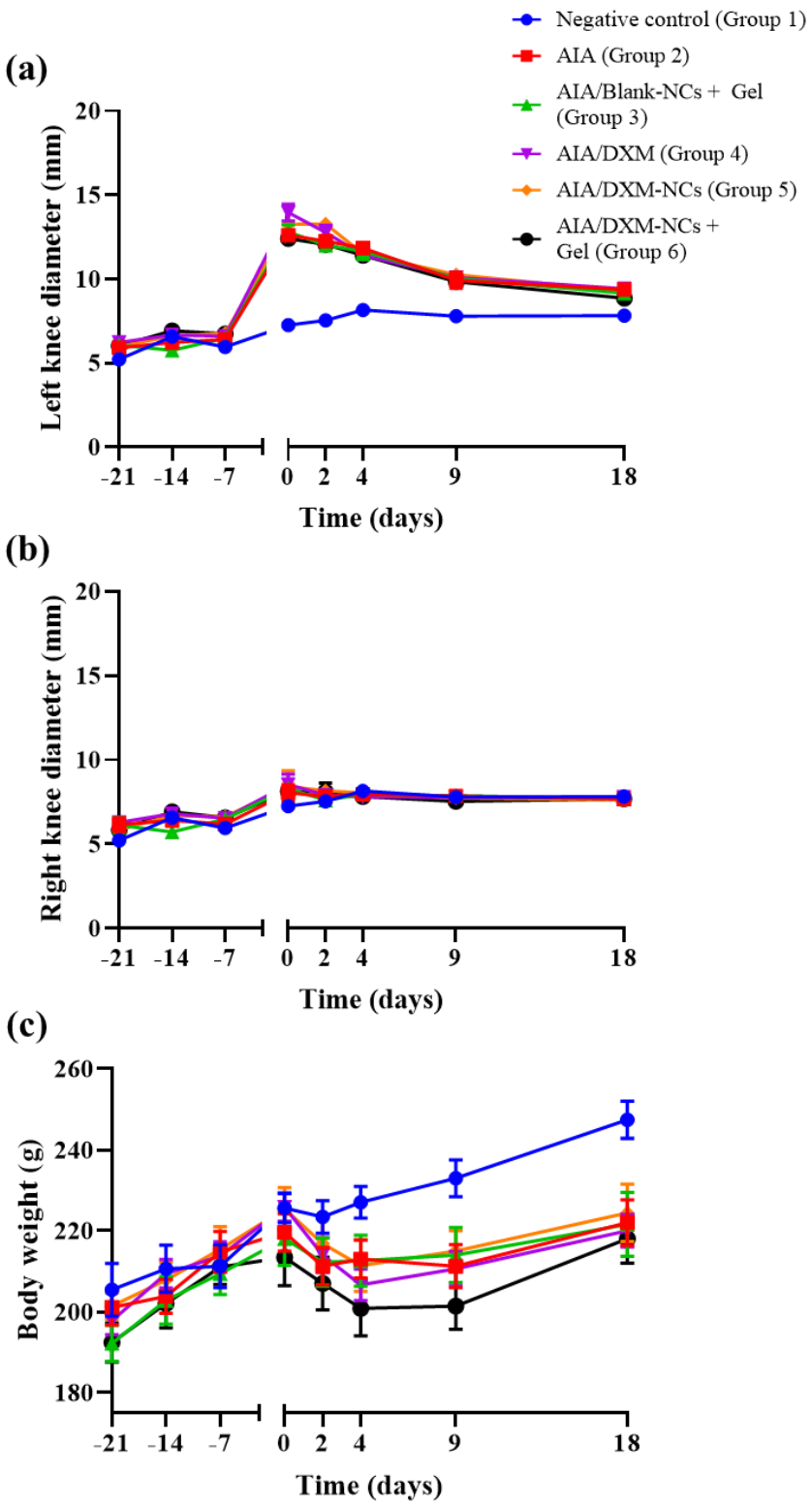


Figure 2.14 Evolution of the (a) left and (b) right knee diameters and (c) the body weight in a 28-day efficacy study performed in arthritic AIA rats. Treatments administered by the IA route were: free DXM (group 4), DXM-loaded NCs (group 5) and Fn-HA gel containing DXM-loaded NCs (group 6) in AIA rats. Healthy rats (group 1) were used as negative control. Untreated AIA rats (group 2) and AIA rats treated with Fn-HA gel containing blank NCs (group 3) were used as other controls for the study. Data represented as Mean ± SEM (n=6 rats/group)

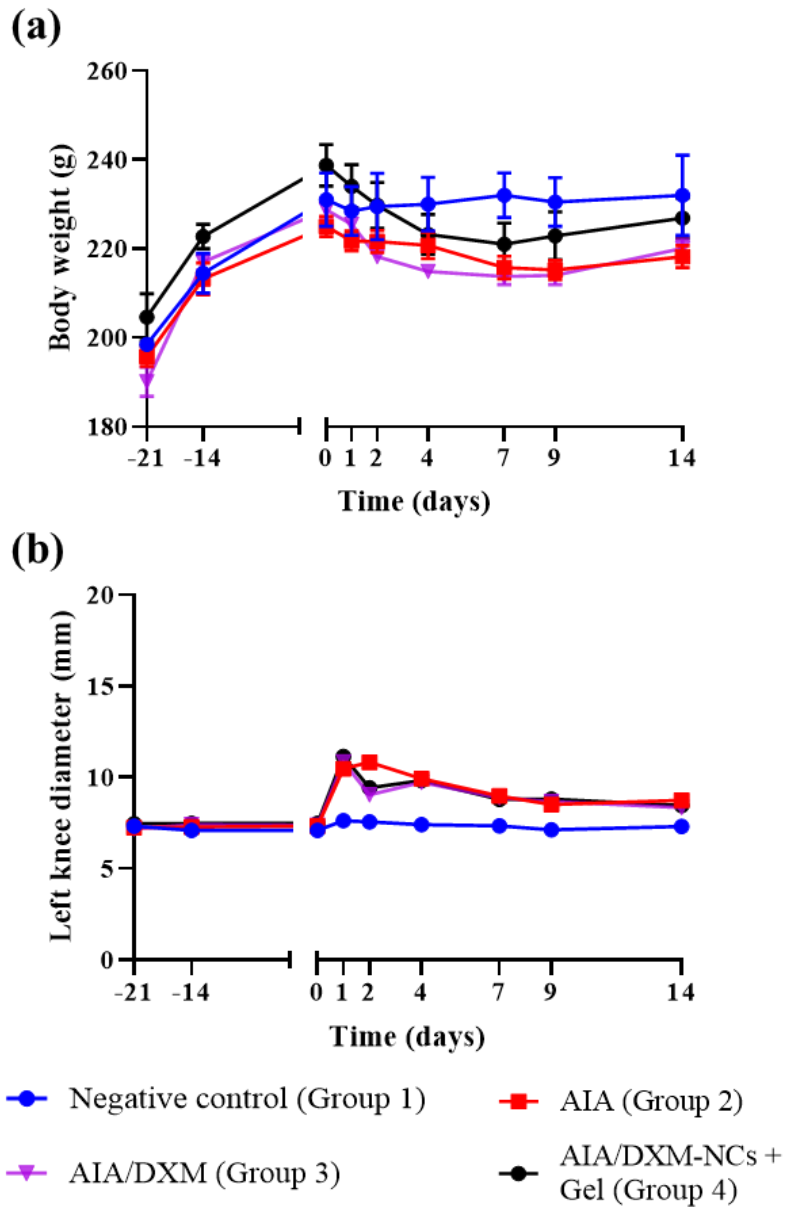


Figure 2.15 Evolution of the knee diameter (b) and the body weight (a) in a 14-day efficacy study performed in arthritic AIA rats. Treatments administered by the IA route were: free DXM alone (group 3) and Fn-HA gel containing DXM NCs (group 4) in AIA rats. Healthy rats (group 1) and untreated AIA rats (group 2) were used as controls for the study. Data represented as Mean ± SEM (n=8 rats/group)

Serum CRP values were also monitored in the 28-day study as an indicator of systemic inflammatory activity (180). Figure 2.16 shows the CRP values monitored from day 1 to day 18 after induction of arthritis. An increase in CRP values were observed in all AIA groups in comparison to negative control, indicating the increased inflammatory activity. These CRP values were slightly reduced on day 2 and, then, maintained for the duration of the study with the exception of the non treated AIA group which showed the highest CRP values.

The local administration of DXM in the knee might not have reflected in the CRP, which is a systemic parameter. Similar scenario was also reported by Čeponis *et al.*, where liposomal clondronate, led to low levels of synovial hyperplasia, TNF-α and tissue fixed macrophages after IA injection. However, the effect of clondronate was not reflective in reducing the serum CRP values after IA administration (181). To understand the influence of IA DXM on serum CRP values, Schade *et al.*, established a dose-response relationship. These authors found that DXM shows a biphasic sinusoidal dose-response curve for serum CRP values, after IA administration in AIA rats in the dose range of 0.001 mg/kg to 1 mg/kg (182). Hence, the anti-inflammatory response of DXM on CRP values is not an inversely proportional linear relationship. These findings support the non-response of CRP values towards IA DXM injection.

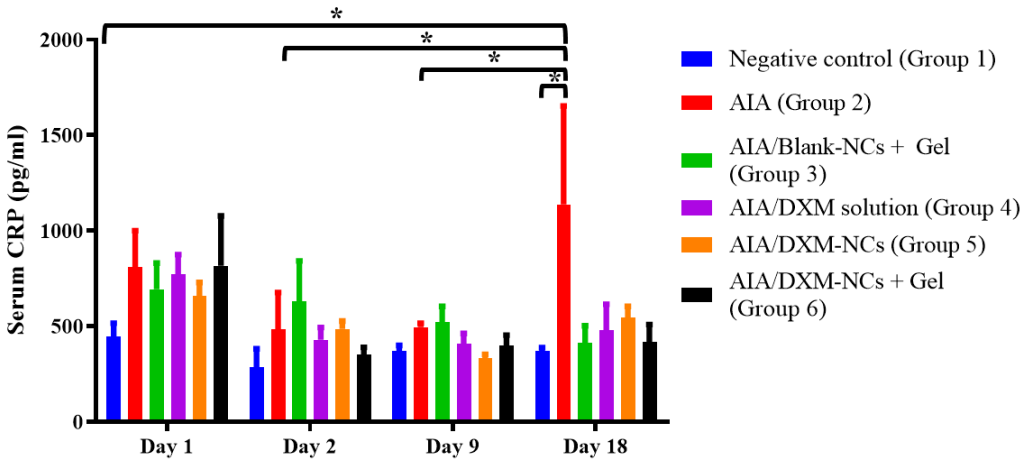


Figure 2.16 Serum CRP values obtained from 28-day evaluation study, during the course of disease induction and treatment, measured by collecting the blood samples from retro-orbital plexus of rats, followed by ELISA test. Data represented as Mean ± SEM (n=6 rats/group). No significant differences were obtained between the groups, except between negative control and non-treated AIA group without any treatment (*$p < 0.05$, two-way ANOVA, Dunnett's multiple comparison test)

2.3.5.2 Evaluation of histological changes in response to DXM treatment

Histological scores obtained from the synovial and cartilage tissue sections obtained through double-blind scoring, after 28 days indicated a significant tissue disruption associated with induction of arthritis in comparison to negative control (Figure 2.18). In addition, a significant reduction of the synobial histology score was observed in groups treated with DXM NCs and Fn-HA gel containing DXM-loaded NCs, as compared to the untreated group 2. As expected from the literature (63), no beneficial effects were observed in cartilage

sections after DXM treatments. Figure 2.17 shows a representative synovial tissue section from each group. No significant differences in cartilage tissue scores among the test & untreated groups. Similarly, the histological scores of synovial membrane and cartilage from 14-days long study did not show any statistical differences between the marketed DXM formulation and DXM NCs loaded Fn-HA gel.

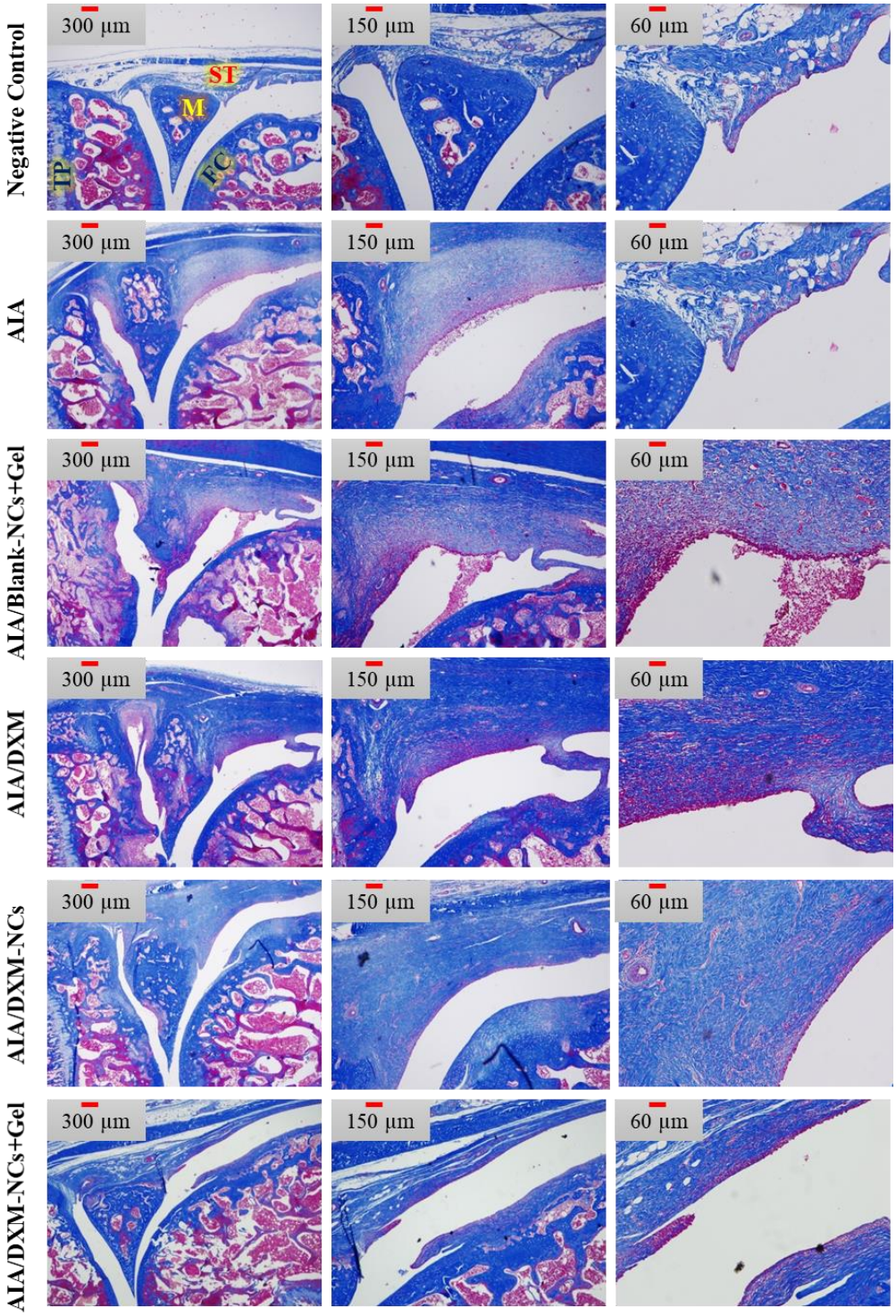


Figure 2.17 Microscopic slides obtained from 28-day anti-inflammatory efficacy study, showing the histology of cross-sections obtained from left knees of rats related to different groups, stained with Masson's trichome stain at 3 different magnifications. ST, M, FC and TP indicates synovial tissue, meniscus, femoral condyle and tibial plateau respectively

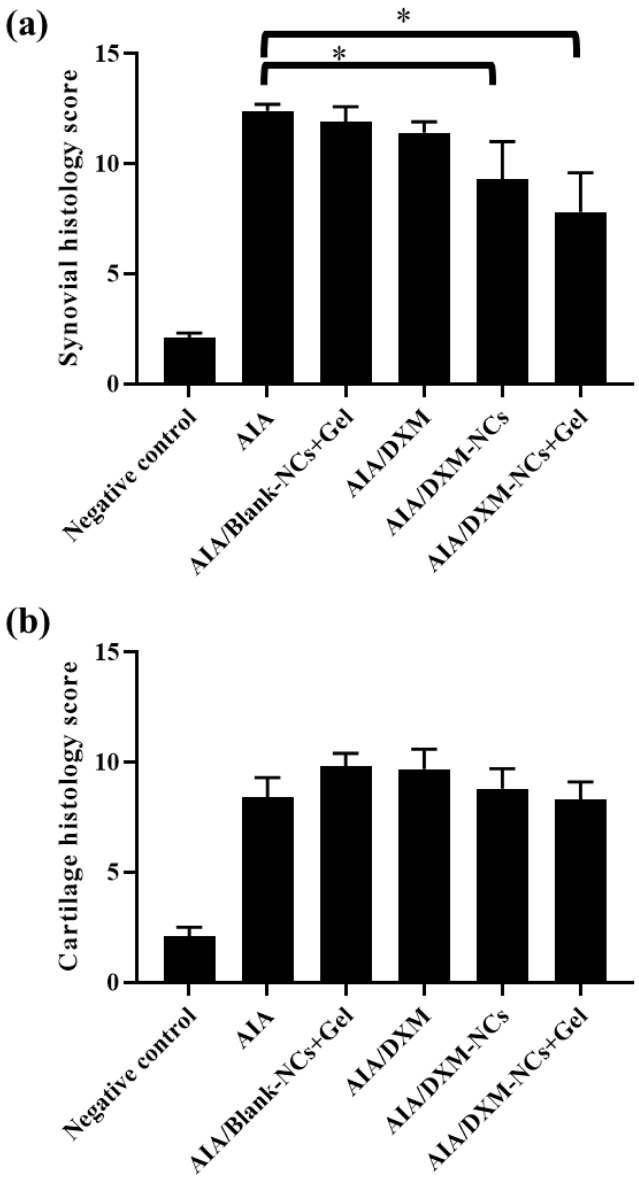


Figure 2.18 Histological scores obtained by double-blind analysis of (a) synovium and (b) cartilage cross-sections obtained on 28th day of the study. DXM NCs and Fn-HA gel containing DXM NCs have shown significant differences from untreated AIA group (* $p \leq 0.05$ done Mann-Whitney post-hoc analysis), while no significant differences between the groups were seen with cartilage cross-sections.

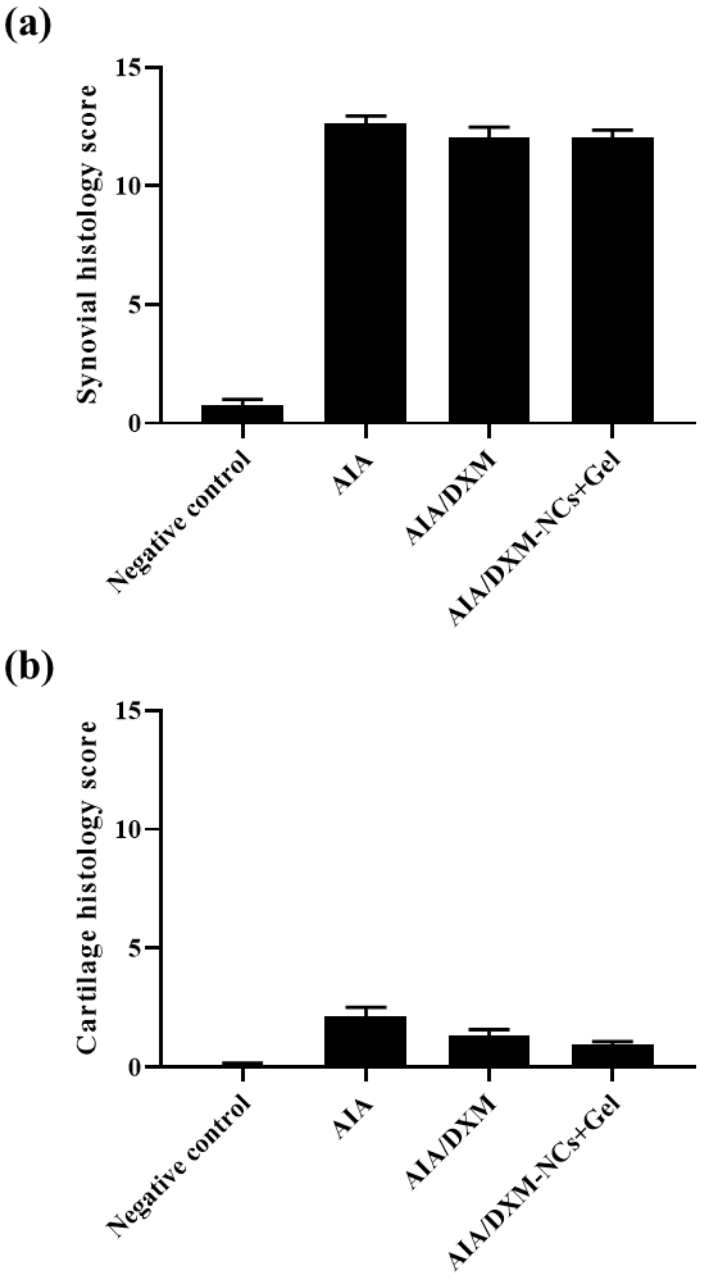


Figure 2.19 Histological scores obtained by double-blind analysis of (a) synovium and (b) cartilage cross-sections obtained on 14th day of the study. No significant differences between the groups were seen with both synovial and cartilage cross-sections.

Overall, these results indicate that the anti-inflammatory activity was not appreciable for any DXM treatment, either in an early phase (14-days) or in a late phase (28-days) study. The fact that the DXM marketed formulation did not also show beneficial anti-inflammatory activity, would support the ineffectiveness of existing steroid formulations towards management of arthritis as reported in the literature (72). However, the type of disease model could influence the study outcome. For example, in a study performed by Zang *et al.*, IA administration of DXM, alone or in presence of a crosslinked HA hydrogel showed a significant improvement in histology scores of arthritis rats at comparatively lower doses of 0.01 mg/kg and 0.025 mg/kg. This study was performed in an anterior cruciate ligament transection (ACLT) surgery model for OA (131).

2.4 Conclusions

Herein we report the development of a composite hydrogel formulation containing HA NCs-loaded with a model anti-inflammatory drug, DXM. DXM-loaded NCs with an adequate drug loading (DXM concentration: 6 mg/mL) were incorporated in a Fn-HA gel, and the resulting composite showed a viscoelastic behaviour comparable to commercial HA injections. *In vitro* release studies showed a sustained release of DXM, up to 70% in 48 h. *In vivo* studies involving the IA administration of the system to rats indicated that the NCs were cleared through popliteal lymph nodes from the knee cavity and that this behaviour was not influenced by the presence of the hydrogel. An *in vivo* efficacy study performed in AIA rats showed no beneficial anti-inflammatory activity, as observed from knee diameters and synovial histology. Failure to show anti-inflammatory activity was unexpected based on the literature, and could be partially attributed to potential rapid degradation of Fn-HA gel.

Acknowledgements

In vivo local residence and biodistribution studies were performed in collaboration with Patricia García-García [1,2], Edgar Pérez-Herrero[1,2] and Araceli Delgado[1,2]

In vivo efficacy studies were performed in collaboration with Fernández-Rodríguez JA[3], Ramill-Gómez O[3] and López-Armada MJ[3]

[1] Department of Chemical Engineering and Pharmaceutical Technology, University of La Laguna, La Laguna 38200, Tenerife, Spain

[2] Institute of Biomedical Technologies (ITB), Center for Biomedical Research of the Canary Islands (CIBICAN), University of La Laguna, La Laguna 38071, Tenerife, Spain

[3] Aging and Inflammation Research Lab, Instituto de Investigación Biomédica de A Coruña (INIBIC), Complexo Hospitaloario Universitario A Coruña (CHUAC), Sergas, Universidade da Coruña (UDC), 15006, A Coruña, Spain

3. Development and evaluation of nanocapsules-loaded enzymatically/physically crosslinked gels for intra-peritoneal drug delivery

In the previous chapter, DXM NCs were developed and incorporated into a Fn-HA gel for IA delivery. This formulation was unable to show prolonged retention and beneficial anti-inflammatory effects in the AIA rat model. Hence, the composite formulation of Fn-HA gel containing DXM NCs was not suitable for the synovial joint. To further explore the potential of this formulation for localised drug delivery, another route of administration, intra-peritoneal delivery, was evaluated. The peritoneal cavity (a fluid rich sac, which encloses visceral organs in the abdominal cavity) is a dynamic environment with a high turnover of fluid, where the sustained delivery of therapeutic agents will be beneficial. Many researchers have explored this route of administration for delivering chemotherapeutic agents in treatment of cancers associated with peritoneal membrane or other organs in the peritoneal cavity. In addition, the peritoneal cavity is commonly accessed to perform peritoneal dialysis (111). However, the common problem associated with peritoneal dialysis is formation of adhesions. Hydrogels containing no pharmacologically active compounds have been explored for preventing the formation of post-surgical fibrotic adhesions (183-186) (187-189).

Many of these primary cancers which are associated with the organs in the cavity are highly aggressive and exhibit metastasis within the peritoneal cavity and also with other peritoneal organs (190). Routine strategy for the treatment of these peritoneal malignancies is a cytoreductive surgery of macroscopic tumours. Intravenous (IV) chemotherapy can also be given perioperatively or postoperatively to treat untraceable microscopic tumours to avoid recurrence (191). These conventional chemotherapies are non-specific and pose severe side effects, compromising the quality of life of patients. Moreover, achieving effective local drug concentrations by IV therapy is a significant challenge (192). It has been demonstrated that intra-peritoneal (IP) administration of chemotherapeutic drugs offers pharmacokinetic advantages in comparison to the IV route (98). Shimada *et al.* compared the pharmacokinetic parameters of

docetaxel after IP and IV administration in mice bearing gastric cancer. The concentration of docetaxel in the peritoneal cavity and the solid tumour was significantly higher for IP administered group than IV arm. The plasma area under curve (AUC) after IP administration was similar to IV administration, indicating no additional systemic toxicity (98). Although no chemotherapeutic products are approved for IP administration, many compounds including, doxorubicin, fluorouracil, paclitaxel and platinum-based compounds have been explored for IP therapy. In the current clinical practice, IP administration is achieved by repeated instillation through catheters. These procedures involve perfusion of chemotherapeutic agents under hyperthermic conditions (193, 194) or pressurized aerosol pumps (195, 196). It is extremely challenging to provide long-term repeated administrations through indwelling catheters, due to pain and infection-related problems for the patient. This challenge poses a need for developing sustained release chemotherapeutic formulations for IP delivery, which can avoid installation of catheters. Novel drug delivery systems, aimed at prolonging the duration of action of these agents have been explored using nanoparticles (NPs) (197, 198), nanocrystals (199), liposomes (200), microspheres (114), and hydrogels (201).

Among particulate drug delivery systems, micro and nanoparticles demonstrate some benefits and disadvantages. As described in section 1.3.4.1, microparticles show relatively slow dissolution than nanoparticles because of their lower surface area to volume ratio. Moreover, they do not undergo phagocytosis because of their relatively larger size. However, microparticles pose potential risks to form adhesions and inflammation in the peritoneal cavity (118). In contrast, nanoparticles do not cause peritoneal adhesions and they are relatively tunable to offer higher tumour penetration. Tumour penetrating and cell penetrating peptides are often surface-decorated onto nanoparticles to achieve high tumour penetration and intracellular delivery (16). However, nanoparticles can be phagocytosed by peritoneal macrophages to clear them from the cavity (105). Incorporation of nanoparticles in the hydrogel delays their clearance from the IP cavity, as the rate of release of nanoparticles into the cavity depends on the degradation of the hydrogel. For example, Silveira et al. incorporated doxorubicin functionalized mesoporous silica nanoparticles (MSNs) into

Pluronic F127 hydrogels to achieve prolonged release for the treatment of prostate cancer. The composite system had a gelation temperature of 21 ºC, which allowed in situ gelation upon IP administration to form a depot. They reported significant reduction in aggressive tumour nodules. Interestingly, the intrinsic cardiotoxicity of doxorubicin has been significantly reduced because of its sustained release after local administration in the peritoneal cavity (202). Similarly, as explained in section 1.3.4.3, Xu *et al.* and Fan *et al.* also reported sustained delivery of nanoparticles after incorporation in a hydrogel (128, 129).

However, development of a sustained drug delivery system for IP cavity does not necessarily ensure beneficial therapeutic outcomes. Therapeutic efficacy of a composite drug delivery system depends on complex range of factors, which include rate of release of NCs from the hydrogel, effective penetration and delivery of chemotherapeutic agents into the tumour mass, degradation etc. For example, as described in section 1.3.4.3, Cho et al. reported compromised therapeutic efficacy despite of sustained release shown by the composite formulation of cisplatin-containing HA nanoparticles, incorporated in a covalently crosslinked HA gel. They reported a slight increase in tumour burdens at later time point, which was attributed to degradation products of the formulation (130). Hence, there is a need for exploring various composite systems that can yield a biocompatible hydrogel incorporated with nanoparticles, aiming prolonged IP delivery and desired therapeutic efficacy.

In this chapter, we have developed and evaluated two different hydrogel formulations that can incorporate HA NCs. An enzymatically cross-linked Fn-HA gel developed in the previous chapter (section 2.3.2) was chosen as one of the hydrogels, as it was proven to be biocompatible and biodegradable in the animal models (sections 2.3.4 and 2.3.5). Alternatively, a self-assembled hydrogel formed by a hydrogelator, *N*-4-octanoyl-2′-deoxycytidine (from now onwards called as 2′-dC-*N*4-C_8), was considered for the study. 2′-dC-*N*4-C_8 was previously developed in our lab and was subsequently evaluated for protein delivery and prevention of protein aggregation (203, 204). Štaka *et al.* incorporated C-14 Gemcitabine-loaded HA NCs into the self-assembling 2′-dC-*N*4-C_8 hydrogel and demonstrated an *in vitro* controlled release for > 1 month (205). Hence, this was selected as another hydrogel to incorporate NCs.

DiR, a near-infrared fluorescent marker, was first incorporated into NCs that were developed before (section 2.3.1). DiR NCs were then incorporated into both Fn-HA and 2′-dC-*N*4-C_8 gels. Rheology, electron microscopy was performed on these hydrogels to understand their structural features. Further, resistance to dilution and *in vitro* release were evaluated. Finally, *in vivo* biodistribution and local residence were evaluated with one of the hydrogels that contain DiR NCs using IVIS® imaging in nude mice.

Aim

To develop and evaluate enzymatically/physically cross-linked hydrogels containing DiR NCs for sustained IP delivery

Hypotheses

1. Incorporation of DiR in the NCs would demonstrate their *in vivo* local residence and biodistribution after IP administration through IVIS® imaging
2. Fn-HA gel or 2′-dC-*N*4-C_8 gel would entrap DiR NCs and favour the slower release of the same
3. Incorporation of NCs in a hydrogel would prolong the residence time of the formulation in the IP cavity

Objectives

1. To incorporate DiR into HA NCs and determine the entrapment efficiency
2. To incorporate DiR NCs into an Fn-HA gel
3. To optimize the concentrations of the self-assembling 2′-dC-*N*4-C_8 hydrogelator to form a hydrogel, incorporating DiR NCs
4. To characterize the DiR NCs loaded Fn-HA and 2′-dC-*N*4-C_8 gels and determine the *in vitro* release of DiR NCs
5. To determine the optimal dose of DiR required for IVIS® imaging
6. To evaluate the *in vivo* biodistribution and local residence of selected gel containing DiR NCs, using IVIS® imaging

3.1 Materials

Fluorescent label, 1,1"-dioctadecyl-3,3,3",3"-tetramethylindotricarbocyanine iodide (DiR) was purchased from Thermo Fisher Scientific, Spain. Fibrinogen, thrombin, sodium hyaluronate (HA), Tween® 80, Lipocol® HCO-40, Labrafac™ Lipophile WL1349, benzethonium chloride (BZT), HEPES and bovine serum albumin were acquired from the same sources as described in section 2.1. Sodium chloride (NaCl), sodium azide, calcium chloride dihydrate ($CaCl_2$. $2H_2O$), potassium chloride (KCl), magnesium chloride ($MgCl_2$), sodium phosphate dibasic (Na_2HPO_4), potassium phosphate monobasic (KH_2PO_4) of ≥ 99 % purity was purchased from Sigma-Aldrich, UK. Phosphate buffer saline tablets (0.01 M) were also procured from Sigma-Aldrich, UK. A self-assembling gelator, 2′-dC-*N*4-C_8, was synthesized in-house (206). All organic solvents used were HPLC grade. In-house ultrapure (Milli-Q) or endotoxin-free water was used throughout the experiments. Laboratory glassware was previously sterilized in an autoclave (Systec, Germany) prior to *in vivo* experiments.

3.2 Methods

3.2.1 Preparation and characterization of DiR NCs

3.2.1.1 Preparation of DiR loaded NCs

Self-emulsifying HA NCs containing DiR were prepared by a slight modification of the previously described method (section 2.2.1.1). A working standard, 1000 ppm of DiR was prepared by diluting the stock solution (2.5 mg/mL of DiR in ethanol) in ethanol. To prepare DiR NCs, Tween® 80, Labrafac and Lipocol were first weighed in an empty glass vial and mixed to form an oil-surfactant mixture. A solution of BZT in ethanol was then prepared and added to this mixture to attain a final concentration of 1 mg/mL of NCs. The DiR stock solution was then added and mixed well. The amount of stock solution added was based on the final concentration of DiR in NCs. For example, 270, 360, or 540 µL was added to attain 90, 120 and 180 ppm DiR NCs, assuming a 3 g batch size. Finally, a $3/4^{th}$ volume of water was added to this mixture to form a nanoemulsion. An aqueous solution of HA (40 kDa) was

separately prepared at a concentration of 22 mg/mL in remaining 1/4th volume of water, which was then added to the nanoemulsion to form DiR NCs.

3.2.1.2 Determination of physicochemical properties

The mean hydrodynamic diameter(size) and polydispersity index (PDI) of DiR NCs were measured after dilution (50×) with ultrapure water by dynamic light scattering (DLS) at 25 °C with an angle of detection at 173°. The zeta potential was measured by laser doppler anemometry (LDA) after diluting the samples (50×) with ultrapure water. DLS and LDA analysis was performed using a Zetasizer and NanoZS, Malvern respectively Instruments, Malvern, UK.

Mean particle size and its distribution were also evaluated by nanoparticle tracking analysis (NTA) (NanoSight Ltd., Malvern Instruments, UK). NCs were pumped through a fine capillary into the sample chamber after 10000x dilution in Milli-Q water. The light scattered by the floating NCs was visualized through 20x magnification under a microscope. A fixed camera operating at 30 frames per second (fps) captured a video of NCs floating by Brownian motion. This video was then analysed on a frame-to-frame basis to process the data obtained from the pattern of motion. Data obtained were averaged and processed to yield D90, D50 and D10 values, which represents around 1 million particles captured.

3.2.1.3 Determination of entrapment efficiency

The encapsulation efficiency (% EE) of DiR was determined after the isolation of DiR NCs by centrifugation at 18,000×*g* for 1 h at 15 °C (Hettich, Universal 32R, Germany). A calibration curve of DiR in ethanol was prepared and fluorescence intensity was measured using a microplate reader (Tecan Infinite® 200 plate reader) at excitation and emission wavelengths of 745 and 795 nm respectively. The amount of DiR in the supernatant (isolated NCs), liquid underneath and the non-isolated (before centrifugation) NCs were quantified by measuring the amount of fluorescence obtained from each fraction after approximately 50x dilution in ethanol. The exact amount of dilution was calculated by weighing the sample before dilution. Equation 3.1 was used to determine % EE.

$$\% \text{ EE} = \frac{\text{Amount of DiR in isolated NCs}}{\text{The total amount of DiR}} \text{ X } 100 \quad \text{.....Equation 3.1}$$

3.2.1.4 Preparation of simulated intraperitoneal fluid (SIPF)

Simulated IP fluid (SIPF) was prepared based on the composition described in the literature (207). Table 3.1 shows the composition of SIPF. BSA was first dissolved by adding the whole amount to 75 % volume of water under stirring, then NaCl, KCl, $CaCl_2$, $MgCl_2$, Sodium azide, Na_2HPO_4, and KH_2PO_4 were added to this solution. The final volume was made up with water after adjusting the pH to 7.4.

Table 3.1 Composition of simulated intraperitoneal fluid

Component	**Weight (g)**
Sodium Chloride (NaCl)	7.00
Potassium Chloride (KCl)	0.20
Calcium Chloride (Anhydrous) ($CaCl_2$)	0.14
Magnesium Chloride (Anhydrous) ($MgCl_2$)	0.05
Sodium Azide	0.50
Disodium Phosphate (Anhydrous) (Na_2HPO_4)	1.44
Mono Potassium Phosphate (KH_2PO_4)	0.24
Bovine serum albumin (BSA)	30.00
Water	q.s to 1 L

3.2.2 Preparation and optimization of Fn-HA and 2′-dC-*N*4-C_8 gels containing DiR NCs

3.2.2.1 Preparation of DiR NCs loaded Fn-HA gel

Fn-HA gel was prepared with the same procedure as described in section 2.2.2.1. DiR NCs at a concentration of 30 % w/w were incorporated into the Fn-HA gel.

*3.2.2.2 Optimization of DiR NCs-loaded 2′-dC-*N*4-C_8 gel*

2′-dC-*N*4-C_8 is a supramolecular gelator, which forms a hydrogel in water using a heating/cooling cycle (204). 2′-dC-*N*4-C_8 was first weighed out into a glass vial and phosphate buffer saline (0.01 M, pH 7.4) was added. The vial was heated to 60 ± 5 °C with stirring. Stirring was continued until no solid remained. At this stage, a fine dispersion of the gelator in water was observed. This was

cooled to and held at 40 – 45 °C, then DiR NCs to this solution. After the addition of DiR NCs, the entire solution was cooled to room temperature under stirring to form a hydrogel. Colloidal stability of DiR NCs at 40 – 45 °C was ensured by exposing them to the said temperature at equivalent dilution in PBS in absence of gelator, followed by measuring the size and PDI using DLS as described in section 3.2.1.2.

The concentration of gelator was optimized to incorporate at least 30 % w/w of DiR NCs. Gels were prepared at 0.3, 1, 2, 3, 4 and 20% w/w of gelator concentrations in PBS. Gels were prepared in 2 mL HPLC glass vials at a final volume of 500 µL, incorporating 150 mg of DiR NCs. The formation of a hydrogel was evaluated by vial inversion one day after preparation. Compositions which did not show any flow after inverting the vial were considered to form a stable hydrogel.

3.2.3 Characterization of Fn-HA and 2′-dC-*N*4-C_8 gels containing DiR NCs

3.2.3.1 Rheology

Rheology was performed for 2′-dC-*N*4-C_8 gels using a modular compact rheometer (MCR302, Anton Paar GMBH, Austria). A 7 mL aluminum cup (14.5 mm internal diameter) and a four-bladed vane (ST10-4V-8.8/97.5, Anton Paar GMBH, Austria) assembly were used for all the measurements. A fixed volume of 2 mL was used for all samples, which were prepared in the aluminum cups directly using the same method as described in section 3.2.3.1. Measurements were recorded at a 4 mm gap from the bottom at 25 °C. Storage modulus (G') and loss modulus (G") were recorded in oscillatory amplitude and frequency sweeps. Oscillatory amplitude sweep was performed in the strain range of 0.1% to 100% at a constant frequency of 10 rad s^{-1}. Time-dependent recovery studies were also performed for 2′-dC-*N*4-C_8 by alternating the strain between 1 % and 500 % for 20 min and 5 min respectively, per each cycle. 4 such cycles were recorded to observe the structural changes in the gel.

3.2.3.2 Cryo-Transmission electron microscopy (TEM) imaging

Samples were prepared on carbon grids which were made hydrophilic by argon plasma cleaning (in a Fischione Model 1020 Plasma Cleaner) prior to use.

Samples were spotted onto the grid with a Cryoplunge® (CP3 Gatan Inc) and were instantaneously frozen using liquid ethane, creating a frozen-hydrated sample in a thin film of vitreous ice.

A drop (approx. 10 µl) of diluted suspension of blank NCs in water (50 X) was spotted on the grid, which was then blotted for 2 seconds before freezing. Fn-HA gel and 2′-dC-*N*4-C_8 gels were prepared as explained in section 3.2.2. For loading the Fn-HA gel onto the grid, a drop of gel mixture was spotted immediately after the addition of thrombin. For 2′-dC-*N*4-C_8 gel, grids were spotted with the mixture of a gelator, NCs and PBS at 40 – 45 °C, while the mixture was still in the solution state. Both gel samples were left undisturbed for 3 – 5 minutes before blotting and freezing, to allow gel formation.

Image acquisition was performed on a JEOL Ltd JEM-2100F microscope with a Gatan 914™ Cryo-tomography holder, fitted with a Gatan Orius™ camera.

3.2.3.3 Resistance of hydrogels to dilution

The ability of Fn-HA and 2′-dC-*N*4-C_8 gels to withstand the dilution was observed by incubating the gels in SIPF at 37 °C. Three dilutions were considered at gel: SIPF ratios of 1:3, 1:9 and 1:25. The integrity of gels after incubation was evaluated by visual observation.

*3.2.3.4 In vitro release of DiR from Fn-HA and 2′-dC-*N*4-C_8 gels*

In vitro release of DiR from Fn-HA and 2′-dC-*N*4-C_8 gels was determined by incubating the DiR NCs loaded gels with SIPF at 37 °C. Gels were incubated at maximum tolerated dilution corresponding to each gel. Fn-HA gel was incubated at 1:3 dilution, while the 2′-dC-*N*4-C_8 gel was incubated at 1:9 dilution. At each time point, 50 µl of samples were collected and diluted with ethanol accordingly. Fluorescence intensity was recorded with the same procedure as described in section 3.2.1.3. Three repeat samples were undertaken at each time point.

3.2.4 *In vivo* local residence and biodistribution studies

Local residence and biodistribution studies were performed on Fn-HA gel rather than 2′-dC-*N*4-C_8 gel based on its *in vivo* tolerability as established previously

(chapter 2.3.4 and 2.3.5). Fn-HA gel samples for *in vivo* were prepared as previously described.

3.2.4.1 Animals and image acquisition

All experiments were performed on immunodeficient BALB/c nude mice (Janvier laboratories, France) under the animal protocol no. 15005AE/07/FUN01/FIS02/JACP1. Mice were housed in specific pathogen-free conditions, according to the Federation of European Laboratory Animal Science Associations (FELASA) guidelines.

Images were acquired after inducing sedation with isoflurane from XGI-8 Gas Anesthesia Unit (Caliper Life Sciences, USA). Fluorescence (λ_{exc} = 745 nm/ λ_{em} = 820 nm) was acquired with the IVIS® spectrum imaging system (Caliper Life Sciences, Perkin-Elmer, USA) at different time intervals.

3.2.4.2 Pilot studies: Optimization of DiR concentration for IVIS® imaging

Two pilot studies were performed to identify the optimum concentration of DiR for imaging. In the first pilot study, 200 µL of the sample containing DiR equivalent to 25 ppm was injected per animal. Nine animals were classified into 5 groups, consisting of a negative control (1 animal injected with isotonic trehalose solution), DiR alone (2 animals injected with DiR in isotonic trehalose solution), DiR NCs (2 animals injected with DiR NCs suspended in isotonic trehalose solution), Fn-HA gel + blank NCs (2 animals) and Fn-HA gel + DiR NCs (2 animals). . Images were acquired on the dorsal and ventral side of the animal at 0, 2, 4, 6, 24, 48, 72, and 96 h and finally on the 27th day.

In the second pilot study, 200 µL of the sample containing DiR equivalent to 5 ppm was injected per animal. DiR NCs containing 18 ppm DiR were prepared by reducing the amount of DiR that was incorporated into the oil phase during the preparation of NCs. These 18 ppm DiR NCs were expected to yield a final concentration of 5 ppm after incorporation in a hydrogel. Five animals were classified into 5 groups (1 animal/group), consisting of negative control, DiR alone, DiR NCs, Fn-HA gel + blank NCs and Fn-HA gel + DiR NCs. Images were acquired on the dorsal and ventral side of the animal at 0, 2, 4, 6, 24, 48, 72 and 96 h.

3.2.4.3 Pivotal study: Determination of local residence and biodistribution

Once the optimum concentration of DiR was identified, a pivotal study was performed in 20 mice, classifying them into 4 groups (5 animals/group):- a negative control, DiR alone, DiR NCs and Fn-HA gel + DiR NCs. 200 µL of the sample containing DiR equivalent to 5 ppm was injected per animal. Images were acquired on the dorsal and ventral side of the animal at 0 h, 4 h, 24 h, 96 h, 1 week and 2 weeks. Additionally, on the 14^{th} day, animals were sacrificed, and organs were harvested to acquire fluorescence from brain, lung, liver, spleen, and kidneys.

3.3 Results and discussion

In the previous chapter, the development and evaluation of the composite formulation focused only on Fn-HA gel, which ultimately did not exhibit appreciable *in vivo* efficacy. Hence, in this chapter, another class of hydrogel, which is a self-assembling 2′-dC-*N*4-C_8 gel, has also been developed and evaluated along with Fn-HA gel for a different route of administration. Development strategy involved incorporation of a fluorescent marker, DiR, into NCs, which would be helpful to evaluate its local residence and biodistribution after IP administration. Once DiR NCs have been prepared and characterized, they were incorporated into both the hydrogels. Later, these hydrogels were further characterized for rheology, resistance to dilution and *in vitro* DiR release studies. The Fn-HA gel hydrogels was selected for *in vivo* evaluation of local residence and biodistribution after IP administration through IVIS® fluorescence imaging.

3.3.1 Preparation and characterization of DiR NCs

HA NCs prepared using the procedure described in section 2.3.1, were used to incorporate DiR. DiR is one of the various near-infrared dyes, which have been in use for fluorescence assisted *in vivo* tracking. The longer emission wavelength of DiR favours whole-body imaging of animals without the influence of autofluorescence (208). Being an amphiphilic molecule, DiR will be incorporated into both the lipid and surfactant phases of the NC. This phenomenon enables researchers to incorporate this into biphasic membrane and vesicular systems for *in vivo* tracking. For example, Zhang *et al.* incorporated

DiR into lipophilic bilayers of PEG-coated liposomal nanoprobes. These nanoprobes were designed to carry a monoclonal antibody PGN635, specific to overexpressing phosphatidylserine moieties of endothelial cells in the tumour vasculature. Incorporation of DiR into lipophilic bilayers of liposomes helped to perform fluorescence imaging to evaluate tumour targeting in MDA-MB231 breast cancer-bearing mice (209). In another study, DiR was incorporated into salbutamol sulfate liposomes with a particle size of 57 ± 21 nm. The distribution of liposomes in the rat lungs was assessed at different time points, from 15 min to 48 h using an IVIS® imaging system. It was found that DiR liposomes showed persistent disposition throughout the tracheobronchial tree, which was seen even at 48 h. However, the total radiant efficiency of DiR was found to reduce with time, indicating the gradual clearance of liposomes (210). Hence, DiR has been used as a successful marker for the determination of local residence and distribution. In our study, NCs have a lipidic core that favours incorporation of DiR.

DiR NCs were prepared at three different concentrations of DiR, yielding final concentrations of 180, 120 and 90 ppm. Colloidal properties of NCs were evaluated after incorporation of DiR. Table 3.2 compares the size, PDI and zeta potential of NCs before and after DiR incorporation. The incorporation of DiR influenced the particle size depending on its concentration. It was found that DiR NCs with the highest DiR concentration had the lowest particle size, while PDI and zeta potential were unchanged. 90 ppm DiR NCs have a particle size of 200 ± 15 nm, while 120 ppm and 180 ppm DiR NCs have sizes of 181 ± 10 and 174 ± 15 nm respectively. Reduction in the size of NCs with DiR could be attributed to its amphiphilic properties. This would incorporate DiR at oil-water interface and behave like a surfactant to reduce the particle size of NCs. Bastiat *et al.* found that incorporation of near IR fluorescent dyes, Dil and DiO, has shown reduction in the interfacial tension between Labrafac and water, as measured by drop tensiometer device. It was observed that increasing concentration of these dyes further reduced the interfacial tension, demonstrating their amphiphilic surfactant-like properties (211). DiR also belongs to class of indocarbocyanine dyes, similar to Dil and DiO. Hence, DiR

might have shown similar behaviour of reducing the Labrafac-water interfacial tension.

Entrapment efficiency (% EE) of DiR in NCs was also evaluated at 3 different concentrations of DiR, by measuring the fluorescent intensity of isolated NCs after centrifugation. Table 3.2 also shows the % EE of DiR. It was observed that 42 – 46 % of DiR was entrapped into NCs, irrespective of the initial concentration of DiR in the tested concentration range. Percentage recovery, calculated by comparing the theoretical concentration of DiR against the sum of entrapped and unentrapped DiR, was > 90 %. Appreciable recovery values validate the efficiency of the manufacturing process. Yu et al. have studied the influence of nature of surfactant on % EE of DiR in poly(lactide)-d-α-tocopheryl polyethylene glycol 1000 succinate (PLA-TPGS) nanoparticles. They have seen a maximum DiR % EE of 48.4 ± 3.3 %, which is comparable to our data (212).

Table 3.2 Colloidal properties of NCs after incorporation of DiR at different concentrations. % EE, determined by isolating the NCs immediately after preparation, followed by extracting the DiR in ethanol and quantifying the fluorescence at an emission wavelength of 785 nm, is also shown here. Each value is represented as Mean ± SD (n = 3)

Sample	Size(nm)	PDI	Zeta potential (mV)	% EE
Blank NCs	250 ± 30	0.2	-17 ± 3	-
90 ppm DiR NCs	200 ± 15	0.2	-17 ± 3	42 ± 6
120 ppm DiR NCs	181 ± 10	0.2	-17 ± 3	46 ± 5
180 ppm DiR NCs	174 ± 15	0.2	-17 ± 3	42 ± 4

3.3.2 Development and optimization of NCs-loaded 2′-dC-*N*4-C_8 gel

As DiR was successfully incorporated into NCs, further development involves incorporation of these DiR NCs into hydrogels. First, DiR NCs were incorporated into Fn-HA gel using the same method as described in section 2.2.2. No further optimization was required for the incorporation of DiR NCs into Fn-HA gel. Alternatively, a self-assembling 2′-dC-*N*4-C_8 gel was then developed and optimized to incorporate DiR NCs.

2′-dC-*N*4-C_8 gels are nucleoside based self-assembling networks that can be prepared by simple heating to 60 °C, followed by cooling to room temperature. Nucleoside based gelators self-assemble through hydrogen bonding, π stacking and the solvophobic forces created by a hydrophobic side chain (213). Skilling *et al.* have chemically modified 2′-deoxycytidine and 2′,3′ dideoxycytidine, with hydrophobic fatty acid side chains that can form fibrous networks upon self-assembly (204). During this optimization, various acyl chains have been incorporated to tune the solubility and gel formation ability of these derivatives. 2′-dC-*N*4-C_8 was found to be water-soluble derivative that can form hydrogels without any organic solvent (206). This gelator has been previously explored as an injectable self-assembling hydrogel for protein delivery and prevention of protein aggregation (203). Moreover, Štaka *et al*. have previously evaluated incorporating C-14 Gemcitabine-loaded HA NCs into the self-assembling 2′-dC-*N*4-C_8 hydrogel. They demonstrated an *in vitro* controlled release for > 1 month (205). However, they were able to incorporate a maximum of 8% w/w NCs in the 2′-dC-*N*4-C_8 gel. The focus of that study was to develop intra-tumoural drug delivery system for C-14 Gemcitabine. However, in our study we explored this 2′-dC-*N*4-C_8 gel for IP administration. Higher doses of chemotherapeutic agents might be required for IP administration, as the clearance rates of the molecules are comparatively higher from the IP cavity. Dedrick *et al.* explained that the IP chemotherapeutic agents did not meet expected pharmacokinetic advantage due to poor coverage of serosal surface during the irrigation and poor tissue penetration (108). Hence, we aimed to incorporate at least 30% w/w of NCs into 2′-dC-*N*4-C_8 gel, similar to Fn-HA gel. Moreover, the NCs that we developed has a particle size of 250 ± 30 nm, in contrast to 40 or 80 nm particles that they used for intra-tumoural delivery.

Hence, we optimized the 2′-dC-*N*4-C_8 gel by evaluating the ability of hydrogelator to form a hydrogel at different concentrations, after incorporating NCs. The concentration of the gelator was increased, while the concentration of NCs was kept constant at 30% w/w. Gels were prepared with the procedure described in section 3.2.2.2 and kept them at room temperature for 24 h. On the next day, those vials were inverted to evaluate the gel formation in presence of NCs. 2′-dC-*N*4-C_8 gelator tends to form gels in aqueous solutions at

concentrations > 0.5 % w/w, as observed previously (214). However, presence of NCs along with the gelator in the medium influenced the gel formation. It was observed that in presence of 30% w/w NCs, gels were not formed at 0.3, 1 and 2% w/w gelator concentrations. Further, an increase in concentration of gelator from 3 – 20 % w/w showed the gel formation (Figure 3.1). Hence, the lowest concentration of gelator required to form a gel i.e. 3% w/w was progressed. No leakage of fluid was observed after gel formation, indicating that the NCs were successfully incorporated into the 2′-dC-*N*4-C_8 gel.

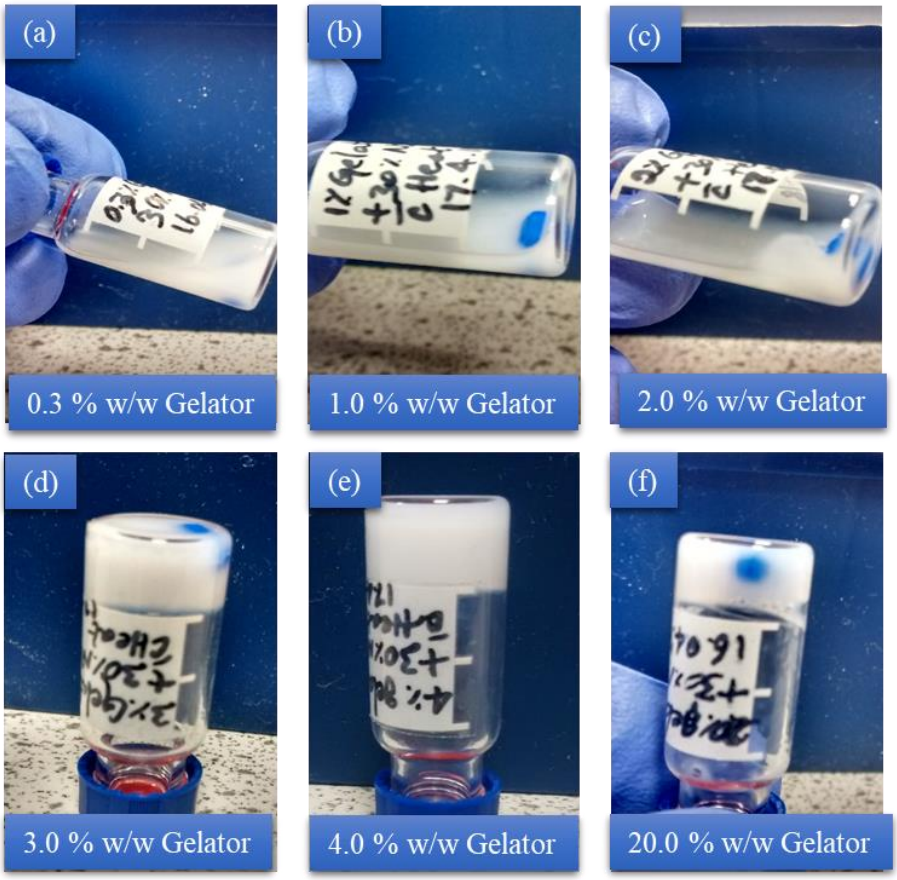


Figure 3.1 Optimization of *2′-dC-N4-C_8* gel to incorporate NCs, showing the increasing concentrations of a gelator, from 0.3 to 20% w/w, while the concentration of NCs was kept constant at 30% w/w. Gelator was first dissolved in the PBS (0.01 M, pH 7.4) at 60 ºC, and a suspension of NCs in PBS (0.01 M, pH 7.4) was added to it after cooling the solution between 40 – 45 ºC. The formation of hydrogel was evaluated by vial inversion, performed after leaving the gels for 24 h at room temperature. Gels were not formed at (a) 0.3 %w/w, (b) 1 %w/w and (c) 2 %w/w gelator concentration, while gelator concentrations at (d) 3 %w/w, (e) 4 %w/w and (f) 20 %w/w showed gel formation

Incorporation of NCs in 2′-dC-*N*4-C_8 gel exposes them to heating and cooling cycles during the preparation. Hence, it was essential to evaluate the colloidal stability of these NCs during the manufacturing process. NCs were suspended

in PBS (0.01 M, pH 7.4), which was then heated to temperatures between 40 – 45 °C for 10 min. These conditions simulate the manufacturing process of 2′-dC-*N*4-C_8 gel while excluding the gelator. The absence of gelator in this mixture did not lead to gel formation after cooling the mixture to room temperature, which made the DLS measurements feasible. Table 3.3 shows the colloidal properties of NCs, before and after exposing them to heat. No differences in particle size and PDI were observed after thermal exposure, indicating their colloidal stability during the gel preparation.

Table 3.3 Colloidal stability of NCs during the preparation of 2′-dC-N4-C_8 gel, determined by exposing the suspension of NCs in PBS (0.01 M, pH 7.4) between 40 – 45 °C for 10 min. Data represented as Mean ± SD (n = 3)

Colloidal properties	**NCs immediately after preparation**	**NCs after heat exposure**
Size (nm)	250 ± 30	260 ± 25
PDI	0.2	0.2
Zeta potential (mV)	-17 ± 3	-17 ± 3

3.3.3 Characterization of Fn-HA and 2′-dC-*N*4-C_8 gels

Once NCs were successfully incorporated into Fn-HA and 2′-dC-*N*4-C_8 gels, they were characterized for rheology, electron microscopy, resistance to dilution and *in vitro* release studies.

3.3.3.1 Rheology

Rheology illustrates the structural and mechanical properties of hydrogels. Fn-HA gel containing 30% w/w NCs was previously characterized for rheology (section 2.3.2.2). In this section, the 2′-dC-*N*4-C_8 gel that contains 30% w/w NCs characterized through oscillatory rheology. Rheology of 2′-dC-*N*4-C_8 gel has been extensively studied by Skilling *et al*. They have reported the viscoelastic behaviour, showing G' > G". At the gelator concentration of 0.5% w/v, no crossover point was observed during the oscillatory amplitude sweep study, which proved that the gel was mechanically stable up to a relatively high strain range of 5%. Hence, they have validated the potential of this gelator as an intra-tumoural drug delivery system (214). Štaka *et al.* reported the rheology of 2′-dC-*N*4-C_8 gel after incorporation of HA NCs at three different concentrations,

2, 4 and 8% w/v. Gels were evaluated at the gelator concentration range of 0.5 to 3% w/v. They have observed that incorporation of HA NCs increased the G' values, at 2% and 4% w/v of NCs. Interestingly, at 2.5% w/v gelator concentration, 10 fold increase in G' was observed. However, incorporation of NCs did not form gels at 0.5% w/v gelator concentration. This study demonstrated influence of incorporation of HA NCs on rheology of a low molecular weight gelator, 2′-dC-*N*4-C_8, for the first time (205). In this study, we have also incorporated HA NCs into 2′-dC-*N*4-C_8 gel. However, the particle size and composition of NCs were different. Moreover, the proportion of NCs we incorporated into 2′-dC-*N*4-C_8 gel was 30% w/w, in contrast to maximum of 8% w/v that was tested previously. Hence, it was interesting to evaluate the rheology of 2′-dC-*N*4-C_8 gel.

Oscillatory amplitude sweep performed on NCs-loaded 2′-dC-*N*4-C_8 gel showed G' > G", indicating viscoelastic behaviour, which was compared to Fn-HA gel. Figure 3.2 (a) shows the oscillatory amplitude sweeps of 2′-dC-*N*4-C_8 and Fn-HA gels. G' and G" values of 2′-dC-*N*4-C_8 gel at 0.01% strain was found to be higher than Fn-HA gel, indicating its relatively higher mechanical properties (Figure 3.2 (b)). However, these G' values of 2′-dC-*N*4-C_8 gel was found to be lower than Štaka *et al*. For example, they have reported that at a gelator concentration of 3% w/v, G' values were approximately 23,000, 6000 and 4000 Pa, at 2, 4 and 8% w/v of NCs respectively. They have explained that 2′-dC-*N*4-C_8 gelator, being an amphiphilic molecule, might participate in the oil-water interface of NCs, which could reduce the involvement of gelator in the formation of gel network. Higher concentration of NCs in the gel increase the involvement of gelator in their oil-water interface, thus forming weak gel networks. (212). The G' of 2′-dC-*N*4-C_8 gel, which contains 30% w/w of NCs showed much lower value of approximately 1000 Pa in line with the previous study that increasing NCs' concentration in the gel decreases the G' values.

Although G' value of 2′-dC-*N*4-C_8 gel was significantly lower than the previously reported gels, we have found that these G' and G" values were higher than the gels without NCs (Figure 3.3 (a)). The role of NCs in enhancing mechanical properties is not clear. However, we speculate that the presence of additional surfactants in the NCs might enhance the solubility of the gelator in

the aqueous phase. At 3% w/w gelator concentration, the gelator was not completely soluble in the aqueous media; rather it forms an oil-like dispersion at higher temperatures, during the preparation. The presence of amphiphilic gelator might increase the gelator solubility and contribute to the formation of relatively stronger gels. However, as described earlier, the G' 2′-dC-*N*4-C_8 gel, containing 30% w/w of NCs was far lower than the reported gels with lower concentration of NCs.

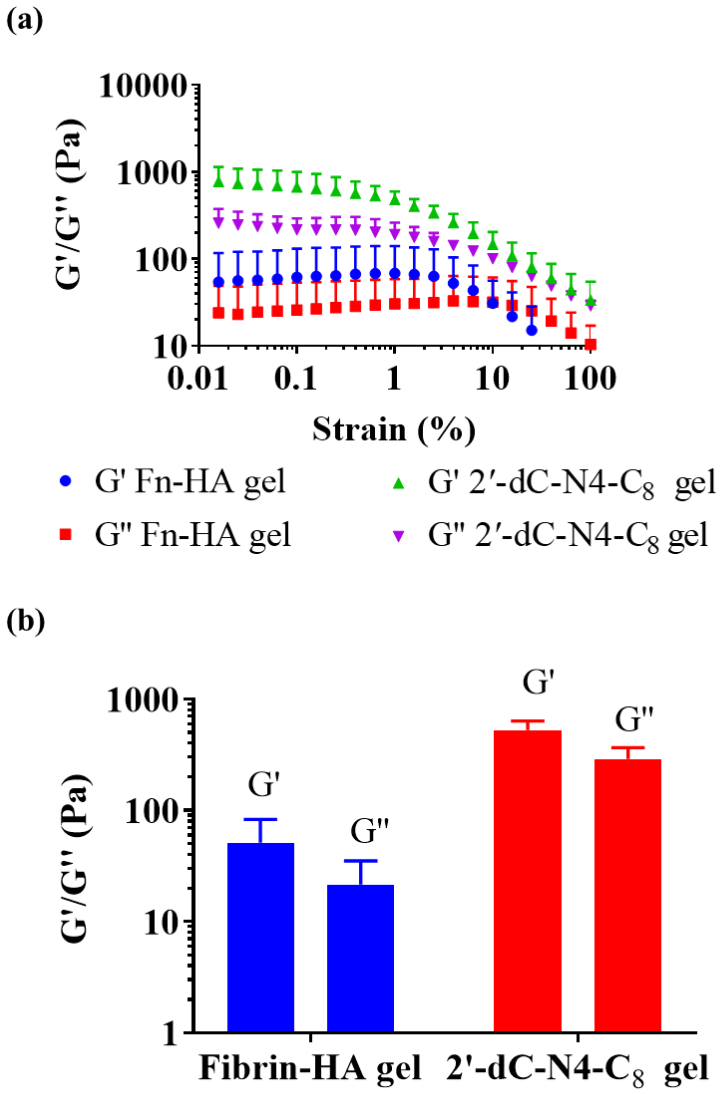


Figure 3.2 Rheology performed immediately after the preparation of Fn-HA gel and 24 h after preparation of *2′-dC*-N4-C_8 gel. (a) Oscillatory amplitude sweeps of Fn-HA and *2′-dC*-N4-C_8 gels performed within the strain range of 0.1 to 100 % at a fixed frequency of 10 rad s^{-1}, 25 ºC. (b) *2′-dC*-N4-C_8 gels showing significantly higher G' and G" ($p < 0.05$, paired t-test). Data represented as Mean ± SD (n = 3).

Interestingly, 2′-dC-*N*4-C_8 gel also showed self-healing behavior, which was previously reported by Skilling *et al.*, (204). When 2′-dC-*N*4-C_8 gel was exposed to high and mild strains in cyclic fashion as described in section 3.2.3.1, it showed a time-dependent recovery. As represented in Figure 3.3 (b), 2′-dC-*N*4-C_8 gel only partially recovered its G' after subjecting it to higher strain (500%) for 5 min. Recovery ratio was calculated as described by Chen *et al.*, which was the ratio of average G' values after recovery to the initial average G' value (215). The recovery ratio was found to be 0.17, which indicated that the extent of recovery was low in the experimental timeframe. The recovery ratio obtained was far lower than Skilling *et al*., where complete recovery was observed at a ratio of 0.70 with 2′-dC-*N*4-C_8 gelator without the NCs. The presence of NCs in the gel matrix might not favor reassembly of the gelator molecules. In summary, it can be concluded that the rheology of the NCs-loaded 2′-dC-*N*4-C_8 gel showed weaker mechanical strength and disrupted self-healing behavior than previously reported values.

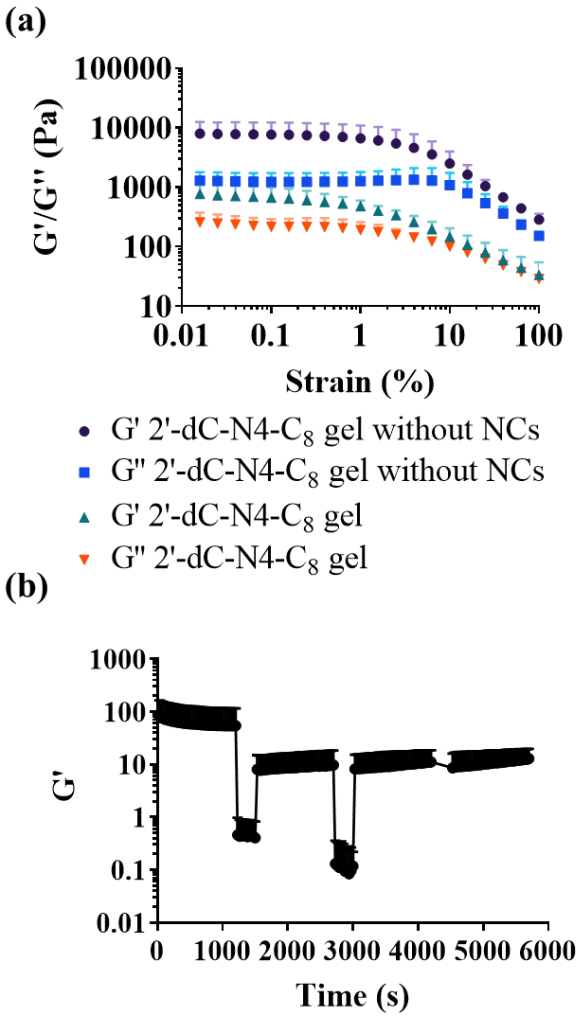


Figure 3.3 Rheology of *2′-dC-N4-C8* gel, performed after 24 h of preparation: (a) Oscillatory amplitude sweep study showing the influence of incorporation of NCs on mechanical properties of the *2′-dC*-N4-*C8* gel, performed within the strain range of 0.1 to 100 % at a fixed frequency of 10 rad s^{-1}, 25 ºC. (b) Time-dependent recovery performed on *2′-dC-N4-C8* gel, by running 4 cycles of each constituting a strain of 0.5% for 20 min and 500% for 5 min, at 25 ºC.

3.3.3.2 Cryo-TEM imaging and NTA analysis

Electron microscopy helps to capture the internal structure of the hydrogels. Physically cross-linked hydrogels might show fibrous internal structures. For example, cryo-TEM images acquired from 2′-dC-*N*4-C_8 gel containing gemcitamine NCs have also shown similar fibrous structures (205). The presence of these fibers was found to be the result of self-assembly process that drives the network formation. We have performed the cryo-TEM imaging according to the procedure described in section 3.2.3.2. Cryo-TEM images of Fn-HA and 2′-dC-*N*4-C_8 gels showed the presence of NCs after their incorporation in both the gels. NCs were clearly visible as small circular objects residing inside and on the surface of the TEM grid (Figure 3.4 (c) and (d)). Fn-

HA gel did not show a continuous network-like structure, where gel fibers were discrete strands as shown in Figure 3.4 (a). In contrast, 2′-dC-*N*4-C_8 gel has shown a network like structure formed by long inter-twining hair-like fibers (Figure 3.4 (b)). According to our observation, the property of fiber formation has been retained with the 2′-dC-*N*4-C_8 gelator after incorporation of NCs. However, as observed in the images, the size distribution of NCs was not homogenous in both the gels. Cryo-TEM images of NCs also showed heterogeneity before incorporation in both the gels, which was not seen in the PDI from DLS measurements. Hence, it was necessary to determine whether the heterogeneity in NCs was a result of cryo-TEM sample processing or it is their inherent property, which was not seen in DLS. We therefore have used nanoparticle tracking analysis (NTA) to further characterize and understand the heterogeneity of NCs.

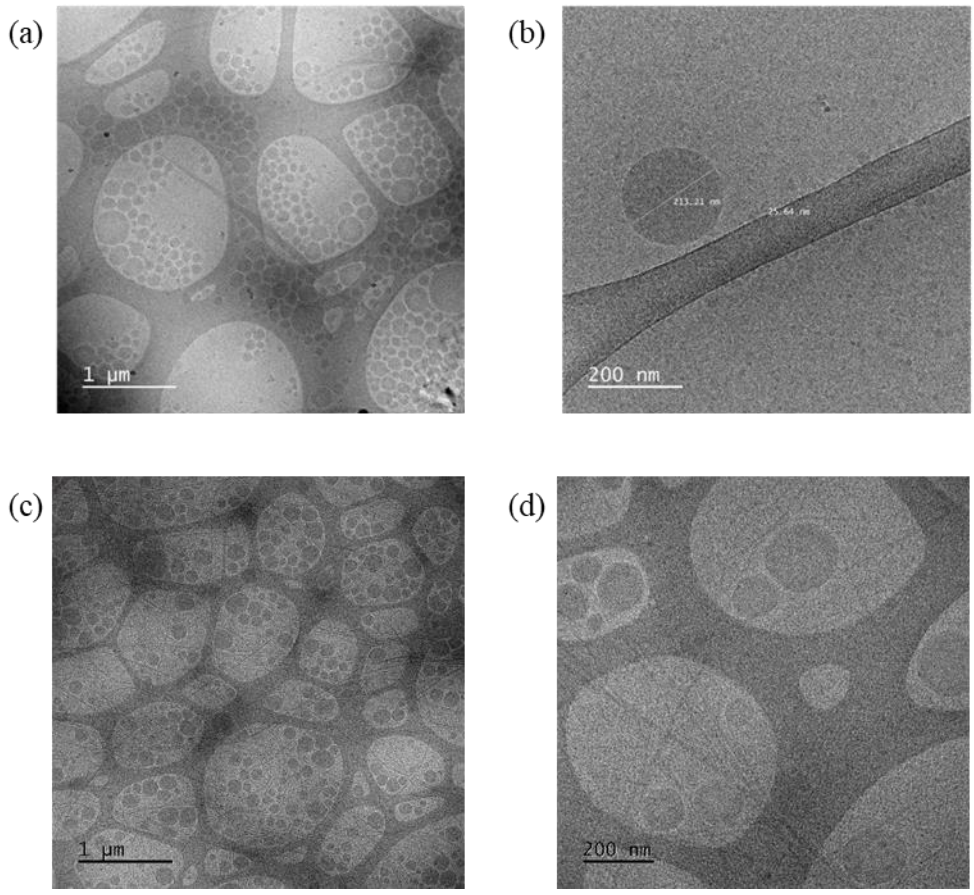


Figure 3.4 Cryo-TEM images of Fn-HA (a & b) and *2′-dC*-N*4*-*C*$_8$ gels (c & d). Fn-HA gel was spotted on to the grid immediately after mixing NCs and gel components in a syringe, whereas sample for *2′-dC*-N*4*-*C*$_8$ gel was spotted onto the grid immediately after addition of NCs into *2′-dC*-N*4*-*C*$_8$ solution at 40 – 45 ºC. Samples were left undisturbed at room temperature for 3 – 5 min on the grid before freezing. Images were captured after cryogenic freezing in liquid ethane at – 90 ºC using Cryoplunge®

NTA is a method of visualizing and analysing particles suspended in the medium, by relating their Brownian motion to particle size. NTA helps to determine the particle size distribution by obtaining D90, D50 and D10 values. D90, D50, and D10 correspond to the upper limit of particle size, which contains 90, 50 and 10% of total number of particles in the sample. Larger the differences in D90, D50 and D10 signifies the heterogeneity in the sample. In this procedure, a laser was focused onto the sample containing nanoparticles, which is scattered by virtue of their size. The scattered light was captured by the camera, which records the movement of each particle by following the scattering light coming from respective suspended particles. Based on Stokes-Einstein equation, rate of particle movement is related to the sphere-equivalent hydrodynamic radius (216, 217). As this technique requires highly diluted sample, NCs were diluted 10000x in milli-Q water before the analysis. D90, D50 and D10 values obtained from NTA were 250 ± 20, 168 ± 10, 106 ± 3 nm respectively. D90 of NCs can be correlated with Z-average size obtained based on intensity measurements from DLS. However, D50 and D10 values indicate that around 50 % by number of particles have sizes ≤ 168 ± 10 nm, while 10% by number of particles have sizes ≤ 106 ± 3 nm. This additional information through light on the heterogeneity of the sample, which DLS cannot evaluate. Hence, it was concluded that the heterogeneity of NCs observed in cryo-TEM images was not induced by sample processing; rather it was the inherent property of NCs.

3.3.3.3 Resistance of gels to dilution

IP cavity is a dynamic environment with high fluid turnover rates. Small and large molecules get cleared from the cavity rapidly (218). Hydrogels and other depot drug delivery systems also face a similar challenge of rapid clearance because of these fluid turnover rates (7). Accordingly, it is very important to evaluate the resistance of hydrogels to dissolve at high dilutions. For example, Bajaj *et al.* performed an *in vitro* release study by incubating 300 µL of paclitaxel nanocrystals-loaded covalently cross-linked HA hydrogel with 20 mL of PBS, containing bovine serum albumin and hyaluronidase for determination of *in vitro* release (125). This formulation showed a prolonged release *in vitro*, which was reflected after IP administration in mice. Hence, in this study, Fn-

HA and 2′-dC-*N*4-C_8 gels were evaluated for resistance to dissolve after exposing them to different dilutions in SIPF at 37 °C. Gels that were swollen but remain undissolved as intact gels in the media were considered to have tolerance to dilution. As shown in Table 3.4, 2′-dC-*N*4-C_8 gel tolerated 1:9 dilution whereas Fn-HA gel only tolerated a 1:3 dilution.. Interestingly, at 1:9 dilution, 2′-dC-*N*4-C_8 hydrogel gelled the whole incubated media, when left undisturbed. This might be because the 2′-dC-*N*4-C_8 gelator dissolves in the media from the initial gel to then gel the whole media at lower concentration. This is feasible as the gelator minimum concentration is 0.5 mg/mL as reported by Skilling *et al.* (214). However, both 2′-dC-*N*4-C_8 and Fn-HA gels did not tolerate high dilution at 1:25.

Table 3.4 Resistance to dilution study performed by incubating Fn-HA and *2′-dC*-N*4-C₈* gels in SIPF at 37 ºC under different dilutions. Gels were monitored each day up to 48 h after incubation. Gels that were swollen and remain undissolved as intact gels were considered to be tolerated (n = 3/gel/dilution).

Gel: SIPF	**Fn-HA gel**	**2′-dC-*N*4-C₈ gel**
1:3	Tolerated	Tolerated
1:9	Dissolved	Tolerated
1:25	Dissolved	Dissolved

3.3.3.4 In vitro release studies

After determining the resistance of Fn-HA and 2′-dC-*N*4-C_8 gels to dilution, it was then necessary to follow the dissolution of these gels with NCs at the maximum tolerated dilution. DiR NCs were first loaded into both Fn-HA and 2′-dC-*N*4-C_8 gels, which were further incubated in SIPF at 37 ºC at 1:3 and 1:9 dilutions respectively. Fluorescence intensity that was determined from SIPF at regular intervals and was considered to be reflective of gel degradation. Fluorescence intensity was obtained after extracting the DiR upon diluting the SIPF in ethanol. The fluorescence measurements were a sum of contributions from free DiR and DiR NCs that were released into the media. As shown in Figure 3.5, Fn-HA gel showed a gradual release up to 40 % in 48 h at 1:3 dilution, while 2′-dC-*N*4-C_8 gel showed a complete rapid release of DiR within 24 h at 1:9 dilution. Rapid dissolution of the of 2′-dC-*N*4-C_8 gel could be attributed to the relatively weak interactions associated with physically

assembled hydrogels. The networks formed by this kind of low molecular weight gelators tend to assemble, dissociate and reassemble depending on the concentration of gelator per unit volume. Hirst *et al.* explained that self-assembly is derived by the degree of assosiation and solubility of the gelator. They have explained that the self-assembly was an interplay between molecular design and spatial organization of gelator units driven by concentration in the medium (219). Hence, as the dilution increases, the concentration of gelator per unit volume reduces, which tend to make loose networks. Formation of loose networks upon dilution cannot uphold the NCs within the hydrogel, leading to their release into the media. As a result, the *in vitro* release estimated for 2′-dC-*N*4-C_8 gelator was found to be rapid. Although Fn-HA gel showed slower release at 1:3 dilution, the relevance of this release profile in a dynamic IP environment is not appreciable, as it did not tolerate higher dilution.

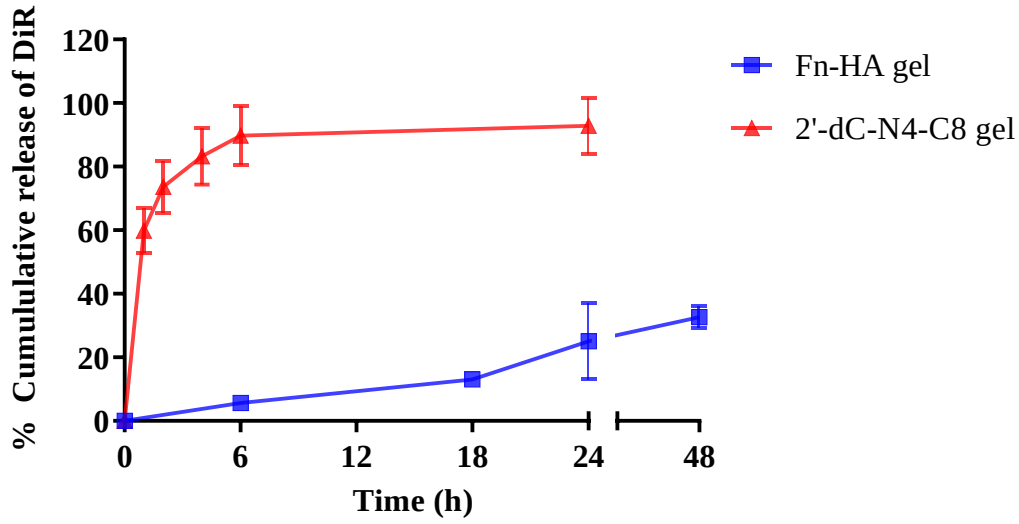


Figure 3.5 *In vitro* release of DiR from Fn-HA and 2′-dC-N4-C_8 gels, determined by incubating them in SIPF at 1:3 and 1:9 dilutions respectively, at 37 ºC. Data indicates the fluorescence intensity obtained as the sum of free and NCs bound DiR, represented as Mean ± SD (n=3)

3.3.4 *In vivo* local residence and biodistribution studies using IVIS® fluorescence imaging

IVIS® imaging is a well-known imaging technique for the determination of biodistribution and efficacy in various animal models. Fluorescence or bioluminescence dyes can be effectively used with this system. For example, Hutteman *et al.*, used a near IR fluorescent probe, IntegriSense® 680, and IVIS® imaging to determine the biodistribution and colorectal metastasis.

Approximately, 50% of colorectal cancer cases develop liver metastasis. However, it was difficult to track the metastasis during the surgery, leading to unexercised tumour mass remaining in the liver. Intra-operative and *ex vivo* fluorescence imaging with the help of integrin αvβ3-directed probe enabled them to detect metastasized tumour mass during the surgery (220). Alternatively, IVIS® imaging also employs bioluminescence probes for determining the efficacy of IP administered chemotherapeutic agents (221, 222). Vassileva *et al.*, evaluated the tumour suppression potential of paclitaxel-loaded chitosan-egg-phosphatidylcholine based implantable drug delivery system using bioluminescence imaging. They have implanted luciferase gene expressing human ovarian carcinoma cells into peritoneal cavity of mice, which allowed the determination of tumour suppression with time (223). In our study, we explored fluorescence imaging to estimate the local residence and biodistribution of gel containing DiR NCs upon IP administration. We have chosen Fn-HA gel rather than 2′-dC-*N*4-C_8 gel because of it's proven *in vivo* tolerability when administered through IA route (section 2.3.4 and 2.3.5). In contrast, 2′-dC-*N*4-C_8 gel had not been administered in any animal model and hence the tolerability of this gel in mice was unknown..

3.3.4.1 Determination of optimal DiR concentration

In order to determine IP residence and biodistribution, the optimal concentration of DiR that gives neither undetectable nor supersaturating fluorescence signal was first identified through two pilot studies. The concentrations of DiR that were employed for first and second pilot studies were 25 and 5 ppm respectively. Figure 3.6 (a) shows the first pilot study where 9 mice were classified into 4 groups. The four groups were DiR alone, DiR NCs, Fn-HA gel + blank NCs and Fn-HA gel + DiR NCs, each containing 2 mice. The ninth mouse was assigned as negative control, which received an isotonic trehalose solution. Except the group which has received Fn-HA gel + blank NCs, all other groups showed DiR distribution throughout the body after 6 h of administration. Signal saturation was observed while capturing images, showing the fluorescence even after 27 days in all the groups. The concentration of DiR was far higher than required. Hence, in the second pilot study, the concentration of DiR was arbitrarily reduced to $1/5^{th}$ of initial concentration (5 ppm). To achieve this concentration,

DiR NCs were prepared at concentration of 18 ppm, 5 times lower than 90 ppm DiR NCs. Particle size, PDI and zeta potential of these 18 ppm DiR NCs was found to be 235 ± 15 nm, 0.2 and –17 ± 3 mV respectively, which was not significantly different from NCs with higher DiR NCs (Table 3.2). Figure 3.6 (b) shows the images obtained from the second pilot study at different time points, up to 96 h. Each image represents 1 mouse from each of the 5 groups, consisting of negative control, DiR alone, DiR NCs, Fn-HA gel + blank NCs and Fn-HA gel + DiR NCs. At this concentration, fluorescence obtained from mice has shown a reduction with time, which represents the clearance of the molecule. Images were captured without signal saturation. Hence 5 ppm DiR was found to be optimal concentration for IVIS® imaging.

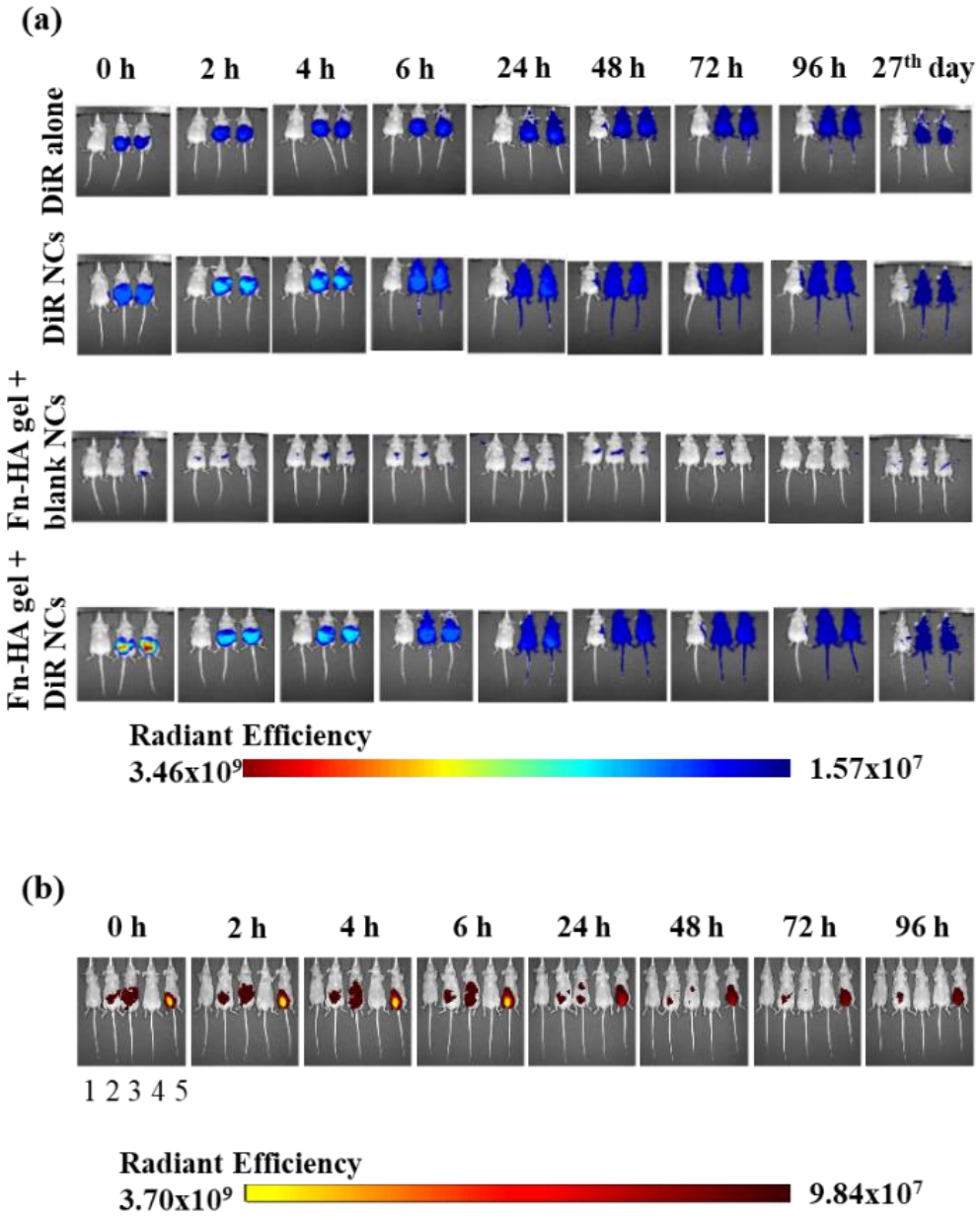


Figure 3.6 *In vivo* pilot studies to determine the optimum concentration of DiR required for IVIS® imaging. (a) First pilot study performed at 25 ppm DiR concentration, showing the fluorescence acquired with time among the groups administered with DiR alone, DiR NCs, Fn-HA gel + blank NCs and Fn-HA gel + DiR NCs (n = 2 mice/group). Each image shows a negative control and 2 mice respective to that group. (b) Second pilot study performed at 5 ppm DiR concentration, showing the fluorescence acquired with time among the groups administered with negative control, DiR alone, DiR NCs, Fn-HA gel + blank NCs and Fn-HA gel + DiR NCs (n = 1 mouse/group), represented as 1 to 5 respectively in the 0 h image. All images were captured at λ_{exc} = 745 nm and λ_{em} = 820 nm

3.3.4.2 Determination of local residence and biodistribution

After identifying the optimal DiR concentration, local residence and biodistribution of Fn-HA gel were studied in 20 mice using the protocol mentioned in section 3.2.4.3. Figure 3.7 (a) shows the compilation of images captured at different time points up to 2 weeks after administration. Each image slide shows the set of 5 animals representing that group. As expected, no fluorescence was seen in the negative control group, which has received an isotonic trehalose solution. DiR alone group has shown some fluorescence after 4 h and 24 h of administration, which was disappeared later. However, both the groups administered with DiR NCs and Fn-HA gel + DiR NCs have shown fluorescence from the abdominal cavity up to 2 weeks, indicating the presence of NCs. This indicates the ability of DiR NCs to retain longer in the body. The fluorescence could come from the IP cavity or from the liver. As the liver is the known destination of nanoparticulate drug delivery systems after IP administration , it was difficult to identify exact localization of fluorescence signal Figure 3.7 (a). Indeed, Kohane *et al.* reported that PLGA nanoparticles of 265 nm were transported to liver and spleen after 2 days of IP administration. They identified that the macrophage driven phagocytosis was the reason behind this accumulation (114). In another study, Yang *et al.*, also found that Pegylated negatively charged graphene oxide nanoparticles of 450 nm also accumulated in the liver and spleen after IP administration (198).

Hence, mice from all groups were sacrificed after 2 weeks and whole organs were imaged to capture the fluorescence. Figure 3.7 (b) shows the compilation of images obtained from brain, lung, liver, spleen, and kidneys, representing mice from all groups. Interestingly, liver has shown fluorescence while other organs did not show any signal (Figure 3.7 (b)). As IVIS® is a qualitative technique, it was difficult to estimate the relative proportion of fluorescence from IP cavity and the liver at the end of the study. Based on the understanding from the *in vitro* release and resistance to dilution studies, it is highly unlikely for the Fn-HA gel to reside in the IP cavity for 2 weeks. Moreover, no physical remnants of the gel were found from the IP cavity after 2 weeks. Hence, the fluorescence obtained after 2 weeks cannot be attributed to the residence of Fn-HA gel in the IP cavity.

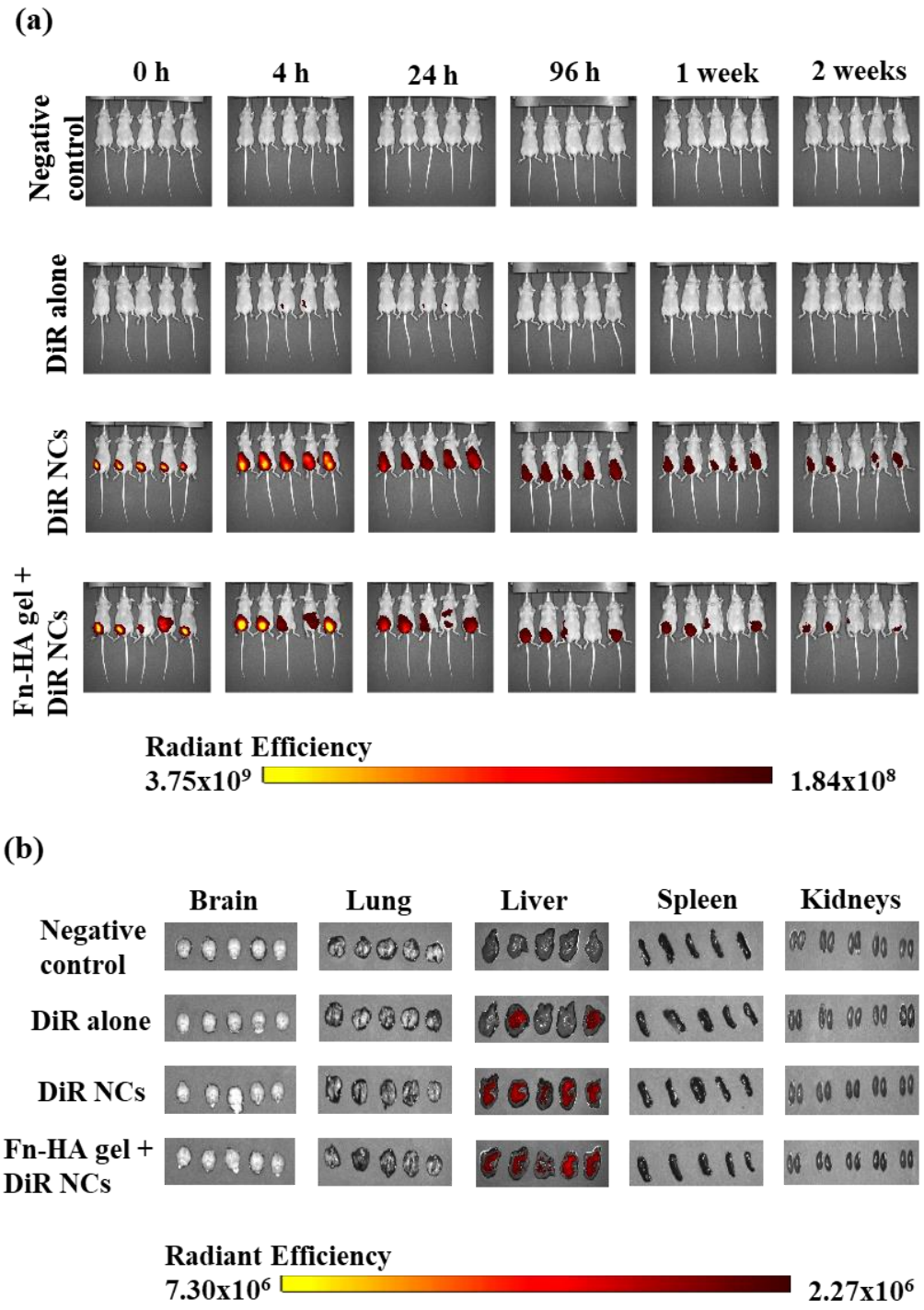


Figure 3.7 *In vivo* IVIS® imaging study to determine the local residence and biodistribution of Fn-HA gel containing DiR NCs. (a) Compilation of images showing the fluorescence acquired with time among the groups administered with negative control, DiR alone, DiR NCs and Fn-HA gel + DiR NCs (n=5 mice/group). (b) Compilation of images related to various organs, obtained after sacrificing the mice 2 weeks after IP administration. All images were captured at λ_{exc} = 745 nm and λ_{em} = 820 nm

3.4 Conclusion

A fluorescent dye, DiR, was successfully incorporated into HA NCs. The incorporation of DiR reduced the size of NCs as a function of its concentration, which was attributed to its amphiphilic properties. Two different hydrogels, Fn-HA, and 2′-dC-*N*4-C_8 gels were optimized to incorporate 30 %w/w of DiR NCs. Both Fn-HA and 2′-dC-*N*4-C_8 gels did not show appreciable resistance to degrade at higher dilutions in SIPF. Rheology of 2′-dC-*N*4-C_8 gel has shown higher G' and G" values, indicating its higher mechanical properties over Fn-HA gel. However, G' values of 2′-dC-*N*4-C_8 gel containing 30% w/w NCs were significantly lower than previously reported gels, which contain 2-8% w/v of NCs. Reduction in mechanical properties was attributed to the interaction between gelator and NCs. *In vitro* release studies suggest that the release of DiR was rapid from 2′-dC-*N*4-C_8 gel, showing a complete release in 24 h. Based on its proven *in vivo* tolerability, Fn-HA gel was chosen for *in vivo* study for determination of *in vivo* local residence and biodistribution upon IP administration. Two pilot studies performed in immunodeficient BALB/c nude mice suggested that the optimum concentration of DiR for IVIS® imaging was 5 ppm. A pivotal local residence and biodistribution study performed in 20 mice showed a strong fluorescence signal from the mice which have received DiR NCs and Fn-HA + DiR NCs up to 2 weeks, in contrast to DiR alone which was not traceable after 24 h. Upon sacrificing the mice after 2 weeks, the liver has only shown the fluorescence among other organs that were imaged. As IVIS® is a qualitative technique, it was difficult to differentiate the fluorescence between the peritoneal cavity and the liver. However, based on the results obtained from *in vitro* release and resistance to dilution studies, it was highly unlikely that the Fn-HA gel could retain up to 2 weeks in the IP cavity. Hence, the fluorescence signal at 2 weeks time point was considered majorly from the liver, which was the most probable uptake of NCs. Therefore, it was understood that combating the dynamic IP environment requires a robust hydrogel that is resistant to high dilutions and retains NCs for longer. Hydrogels formed by covalent crosslinking could be the probable solution for obtaining longer retention in the IP cavity.

Acknowledgements

Fluorescence assisted IVIS® imaging study for determination of *in vivo* local residence and biodistribution was performed in collaboration with Irene Golán Cancela[1] and José A. Costoya[1]

[1] Molecular oncology laboratory, Departamento de Fisioloxia, Facultade de Medicina and Centro de Investigación en Medicina Molecular y Enfermedades Crónicas (CiMUS), Instituto de investigación Sanitaria de Santiago de Compostela (IDIS), Universidade de Santiago de Compostela, Santiago de Compostela, 15706, Spain.

4. Intra-peritoneal delivery – Development and evaluation of covalently cross-linked hydrogels incorporated with NCs

In the previous chapter, it was found that both enzymatically crosslinked Fn-HA gel, and self-assembling 2′-dC-N_4-C_8 gel were not suitable for prolonged drug delivery because of their weak resistance to dilution in the fluid-rich, dynamic IP cavity. Hence, there is a need for development of a more robust hydrogel that can withstand higher dilutions and gradually release the NCs. This chapter will describe the development of a covalently crosslinked hydrogel that was designed to withstand higher dilutions.

Covalently cross-linked hydrogels have been explored for various biomedical applications (224). They are formed by covalent bonds, which are relatively stable against dilution in comparison to physically cross-linked hydrogels (225, 226). High levels of crosslinking density associated with these hydrogels offer higher mechanical strengths than physically cross-linked hydrogels (227). Covalent crosslinking can be achieved through three dimensional addition polymerization of monomers or by inducing a chemical reaction through pH, heat, ionizing or non-ionizing radiation. Based on the type and degree of crosslinking, various properties such as gelation time, porosity, elastic modulus, swellability and degradation time can be tuned to achieve the required the physicochemical properties (228). However, *in vivo* tolerability of these hydrogels is a concern. The crosslinkers that mediate covalent bonding such as glutaraldehyde, formaldehyde, potassium persulfate and other epoxy compounds are often toxic (229, 230).

Although, covalently cross-linked hydrogels might have toxic initiators and are less likely to be biodegradable, a significant amount of research has been carried out on synthesizing biocompatible and biodegradable hydrogels for various biomedical applications. Hyaluronic acid (HA) has been chemically modified with aldehyde and hydrazide groups to form covalent crosslinks. Emoto *et al.* found that the covalently crosslinked gel formed from aldehyde and hydrazide modified HAs, containing cisplatin was retained even after 28 days post IP administration, exhibiting a significant reduction in peritoneal tumour nodules

(231). In another study, Cho *et al.* prepared a covalently cross-linked HA hydrogel, incorporating cisplatin containing HA nanoparticles. They have observed to be retained by the gel for up to 4 weeks, showing the sustained release of platinum. They have also reported the receptor mediated endocytosis of cisplatin containing HA particles into tumour cells. This hydrogel met all the desired properties of a sustained release drug delivery system for IP delivery. Unfortunately, in a mouse model of IP tumour, this formulation did not show desired anti-tumor efficacy. In fact, authors have reported a slight increase in tumour burdens at a later time point, which was attributed to degradation products of the formulation (130). Similarly, another hydrophilic, biocompatible polymer, poly(ethylene glycol) (PEG) has been chemically functionalized to undergo covalent crosslinking to form hydrogels. Three different strategies have been employed to obtain covalently crosslinked PEG gels. They include photo-irradiation of linear or branched PEG polymers, free radical polymerization of PEG acrylates, and specific chemical reactions such as Michael addition, click chemistry, condensation and enzymatic reactions (232). Although covalently crosslinked PEG gels were widely explored for biomedical applications, to our knowledge they have not been explored to incorporate nanoparticles for IP delivery of chemotherapeutic agents.

In this chapter, we have developed and screened two different types of covalently cross-linked PEG gels, prepared by UV crosslinking and Michael addition reactions for IP delivery of model chemotherapeutic agent, docetaxel (DCX). DiR NCs that were prepared as described in section 3.2.1.1, were incorporated into both types of PEG gels. A suitable PEG gel that provides DiR photostability was selected, which was then characterized for gelation kinetics, resistance to dilution, electron microscopy and *in vitro* release studies. We have also evaluated the *in vivo* local residence and biodistribution of a selected PEG gel using IVIS® imaging upon IP administration. Additionally, docetaxel (DCX), a model chemotherapeutic agent, was also incorporated into NCs and then loaded into the selected covalently cross-linked hydrogel. The ability of this composite hydrogel to gradually release DCX was evaluated *in vitro*.

Aim

Development and evaluation of covalently cross-linked hydrogel containing DCX NCs for longer retention in the IP cavity and establish its potential application for IP chemotherapy.

Hypotheses

1. Covalently cross-linked hydrogels could entrap DCX and DiR NCs and prolong their release
2. Covalently crosslinked system would show *in vitro* release and resistance to dilution superior to enzymatically or physically crosslinked hydrogels
3. Covalently crosslinked hydrogel would be biodegradable, biocompatible and demonstrate prolonged residence in the IP cavity after *in vivo* administration

Objectives

1. To synthesise a thiol-functinalized PEG crosslinker that can form covalently cross-linked hydrogels with chemically modified, branched PEG polymers.
2. To synthesize PEG based hydrogels that can incorporate DiR NCs
3. To characterize DiR NCs loaded PEG hydrogels *in vitro* and identify a potential hydrogel that can be evaluated *in vivo*
4. To perform *in vivo* local residence and biodistribution study of the selected hydrogel containing DiR NCs
5. To incorporate DCX, a model chemotherapeutic agent, into NCs and load them further into the selected hydrogel
6. To evaluate the *in vitro* performance of DCX NCs loaded hydrogel and hence establish its potential for treatment of peritoneal cancers

4.1 Materials

DCX (98% purity) was purchased form Acros Organics, Thermo Fisher scientific, UK. PEG (molecular weight (MW): 3350) and fluorescent label, 1,1”-dioctadecyl-3,3,3”,3”-tetramethylindotricarbocyanine iodide (DiR) was purchased from Thermo Fisher Scientific, UK. 4-arm PEG maleimide (PEG-MAL, MW: 10 kDa) was purchased from Advanced BioChemicals, LLC, USA, while 4-arm PEG norbornene (PEG-NB, MW: 10 kDa), *p*-toluenesulfonic acid, dithiothreitol (DTT), 3-mercaptopropionic acid, sodium chloride (NaCl), sodium azide, calcium chloride dihydrate ($CaCl_2$. $2H_2O$), potassium chloride (KCl), magnesium chloride ($MgCl_2$), sodium phosphate dibasic (Na_2HPO_4), potassium phosphate monobasic (KH_2PO_4) was purchased from Sigma-Aldrich®, UK. Phosphate buffer saline (PBS, 0.01 M) tablets were also procured from Sigma-Aldrich®, UK. 1 M Tris buffer (pH 8.0) was purchased from Thermo Fisher Scientific, UK. Photoinitiators, Lithium phenyl-2,4,6-trimethylbenzoylphosphinate (LAP) and 2-Hydroxy-4′-(2-hydroxyethoxy)-2-methylpropiophenone (Irgacure® 2959) were purchased from Sigma-Aldrich®, UK. Pancreatin powder produced from exocrine cells of porcine pancreas and lyophilized powder of esterase from porcine liver (≥ 15 units/mg solid) were also purchased from Sigma-Aldrich®, UK. All organic solvents used were HPLC grade. In-house ultrapure (Milli-Q) or endotoxin-free water was used throughout the experiments. Laboratory glassware was previously sterilized in autoclave (Systec, Germany) prior to *in vivo* experiments.

4.2 Methods

4.2.1 Preparation and optimization of covalently crosslinked hydrogels

4.2.1.1 Synthesis of mercaptopropionate PEG crosslinker

PEG (MW: 3350) (1 g, 2 mmol), 3-mercaptopropionic acid (0.424 g, 40 mmol), *p*-toluenesulfonic acid (7.6 g, 0.4 mmol) and DTT (15.4 g, 1 mmol) were dissolved in toluene (20 mL) in a reaction flask. This mixture was refluxed under nitrogen and stirring for 24 h. Toluene was then evaporated under vacuum and the polymer was precipitated thrice in cold acetone, which was kept at –20 °C for at least 15 min. Precipitated product was then dried, under vacuum at room

temperature, for 2 days to remove the acetone and the weight was recorded to determine the yield. Formation of thiol-functionalized PEG-SH was confirmed by running ^{1}H nuclear magnetic resonance (NMR) spectrum on a Bruker 400 Ultrashield at 400 MHz at 25 °C in deuterated water (D_2O).

4.2.1.2 Preparation of UV crosslinkable PEG-NB – thiol gel

A thiol-ene hydrogel was prepared by radical-mediated photopolymerization between 4-arm PEG-NB and PEG-SH (molar ratio of thiol:ene was 1:1) (Table 4.1). LAP or Irgacure® 2959 was used as a photoinitiator under bench-top ultraviolet (UV) light source (365 nm, 5 mW/cm^2). Gels were prepared in a customized injection mould, prepared by cutting-off the tip of a 1 mL disposable syringe having a 5 mm diameter. The syringe barrel acts as the wall, while top surface of the piston acts as the base of the mould. PEG-NB, PEG-SH and LAP were first dissolved separately in PBS (0.01 M, pH 7.4). These solutions were then mixed in respective proportions in a mould, along with the suspension of previously prepared DiR NCs as described in section 3.2.1.1, to achieve a concentration of 30% w/w of NCs. UV light was then irradiated onto this mixture to form a hydrogel. Unless specifically mentioned, gel volume was fixed at 50 µL (table 4.1).

4.2.1.3 Optimization of UV crosslinkable PEG-NB – thiol gel

Photoinitiators that were used for UV crosslinking are highly reactive and might interact with the fluorophore, DiR. Hence, optimization of PEG-NB – thiol gel was performed by evaluating the percentage recovered of DiR after hydrogel preparation. Based on the pilot studies performed to identify the optimum DiR concentration for IVIS® imaging, a successful hydrogel should recover > 80% of DiR after preparation (section 3.3.4.1). Hydrogels were prepared at different UV exposure times, ranging from 30 s to 5 min, using LAP or Irgacure® 2959 as photoinitiators. These hydrogels were then dissolved in different solutions - ethanol, acetonitrile, dimethyl sulfoxide, 1M hydrochloric acid, 1M sodium hydroxide and pH 3 citrate buffer and the percentage DiR recovered was determined using fluorimetry as described in section 3.2.1.3. Pancreatin (50 mg/mL in 0.01 M PBS, pH 7.4) and esterase (5 mg/mL in 1M Tris buffer, pH 8.0) were also evaluated as alternative media for degradation of the hydrogel enzymatically.

After the identification of a suitable media for degradation of PEG-NB – thiol gel, compatibility study was also performed to determine the potential degradation of DiR with different gel components. The fluorescent intensity of DiR NCs was first measured in PBS (0.01 M, pH 7.4), which was taken as a reference. Different mixtures were then prepared by mixing DiR NCs with various gel components in the same proportions as used for gel preparation and then exposed them to a UV light source (365 nm, 5 mW/cm^2) for 5 min. These mixtures included DiR NCs + LAP, DiR NCs + LAP + PEG-NB, DiR NCs + LAP + PEG-SH, DiR NCs + PEG-NB + PEG-SH. Finally, a mixture of DiR NCs + LAP + PEG-NB + PEG-SH was also prepared, which was not exposed to UV light. The fluorescence intensities of all these mixtures were measured, which were then compared to the reference value obtained from DiR NCs in PBS (0.01 M, pH 7.4). Mixtures that showed drastic reduction in fluorescent intensity were considered to be incompatible.

Table 4.1 Composition of PEG-NB – thiol gel, prepared by mixing the solutions of individual gel components in PBS under bench-top UV light exposure (365 nm, 5 mW/cm^2) in a syringe mould

Ingredients	Amount (mg)	Concentration (% w/w)
PEG-NB	5.00	10.00
PEG-SH	3.63	7.26
LAP or Irgacure® 2959	0.01	0.02
DiR NCs	15.00	30.00
PBS (0.01 M, pH 7.4)	q.s to 50 µL	q.s

4.2.1.4 Preparation and optimization of PEG-MAL – thiol gel

PEG-MAL – thiol gel was prepared by Michael addition reaction initiated by simple mixing of aqueous buffer solutions of PEG-MAL and PEG-SH (molar ratio of maleimide:thiol was 1:1). pH of the buffer was optimized to obtain a rate of reaction that can ensure uniform mixing of gel components and maintain the colloidal stability of DiR NCs. As the rate of reaction is slower at lower pH, colloidal stability of DiR NCs was screened by suspending the DiR NCs in various low pH buffers, followed by determination of particle size and PDI

using the method described in section 3.2.1.2. A buffer that ensures colloidal stability was selected for the preparation of the hydrogel.

After the pH optimization, PEG-MAL – thiol gel was prepared at 5 and 10% w/w concentrations of PEG-MAL. PEG-MAL and PEG-SH were separately dissolved in the buffer. A suspension of DiR NCs was then diluted in the buffer and added to PEG-SH solution. This mixture of DiR NCs and PEG-SH solution was added into the injection mould and PEG-MAL solution was added to it. This whole mixture was then mixed through 3-4 syringe piston stokes and left undisturbed at room temperature for at least 2 h to form the hydrogel. Table 4.2 shows the composition of PEG-MAL – thiol gel at 5 and 10% w/w concentrations of PEG-MAL.

Table 4.2 Composition of PEG-MAL – thiol gel, prepared by mixing the solutions of individual gel components in citrate buffer, 0.1 M, pH 5.0 in a syringe mould

Ingredients	**Gel prepared at 5% w/w PEG-MAL concentration**		**Gel prepared at 10% w/w PEG-MAL concentration**	
	(% w/w)	**Amount (mg)**	**(% w/w)**	**Amount (mg)**
PEG-MAL	5.00	2.50	10.00	5.00
PEG-SH	3.63	1.82	07.26	3.63
DiR NCs	30.00	15.00	30.00	15.00
Citrate buffer (0.1 M, pH 5.0)	q.s	q.s to 50 µL	q.s	q.s to 50 µL

4.2.2 Characterization of covalently crosslinked hydrogels

4.2.2.1 Stability of DiR in PEG gels

Stability of DiR after the incorporation of DiR NCs in PEG gels was determined by dissolving the hydrogel, followed by estimation of DiR content using fluorimetry. As per the optimization studies performed in section 4.3.1.2, porcine esterase was selected to dissolve both the PEG gels. In order to estimate the DiR content, first gels were incubated in an aqueous buffer solution of porcine esterase (5 mg/mL in 1M Tris buffer, pH 8.0) at room temperature for 12 h. Appropriate dilutions were then made in ethanol to estimate the DiR

content against calibration standards using fluorimetry as described in section 3.2.1.3.

4.2.2.2 Determination of gelation kinetics through rheology

Viscoelastic properties of PEG gel were determined using modular compact rheometer (MCR302, Anton Paar GMBH, Austria). A parallel plate assembly (25 mm diameter rotating shaft, PP25) at 25 ºC was used for all the measurements. Gelation kinetics were characterised by monitoring the increase of storage modulus (G') and loss modulus (G") with time at fixed 0.5 mm gap, 0.5 Hz frequency and 0.5% strain. PEG-MAL – thiol gel prepared at 10% w/w PEG-MAL concentration was used for the study. 21.78 mg of PEG-SH and 90 mg of NCs that corresponds to 300 µL of PEG-MAL – thiol gel, was added to 120 µL of citrate buffer (0.1 M, pH 5.0) to form a mixture of PEG-SH and NCs. A solution of PEG-MAL was then prepared by dissolving 30 mg of PEG-MAL in 90 µL of citrate buffer (0.1 M, pH 5.0). The viscoelastic properties were recorded after addition of the mixture of PEG-SH and NCs to the bottom plate of the rheometer. It was then programmed to record the G' and G" every 15 s, until 1800 s. The solution of PEG-MAL in citrate buffer was added after 60 s from the start of experiment. The gelation time was considered to be the crossover point of G' and G", and the maximum G' achieved during the study was used to compare the mechanical properties.

4.2.2.3 Resistance to dilution

The ability of PEG gels to withstand dilutions was observed by incubating the gels in SIPF at 37 ºC. PEG-MAL – thiol gels prepared at 5% and 10% w/w PEG-MAL concentrations were used for the study. Three dilutions were considered at gel: SIPF ratios of 1:3, 1:9 and 1:25. Integrity of gels after incubation was evaluated by visual observation.

4.2.2.4 Cryogenic focussed ion beam scanning electron microscopy (cryo-FIB-SEM)

Cryo-FIB-SEM was used to observe the presence of NCs after incorporation in PEG-MAL – thiol gel. PEG-MAL – thiol gel was first plunge frozen in liquid nitrogen using a metal mirror freezer. This was then transferred under liquid nitrogen to the sample shuttle of a cryo-SEM system (Quorum PPT 2000,

Quorum Technologies). The sample was then Pt coated in the preparation chamber using a sputter for 60 seconds, which was later introduced into the FIB-SEM (FEI Quanta 3D, FEI). The sample was initially milled using a current of 1-3 nA to obtain a rough cut. Further milling was performed at lower currents (0.3 nA – 50 pA) to avoid milling artefacts. To improve the image acquisition, Pt precursor was deposited onto the milled segments using a gas injector (set to 27 °C) whenever required. To further resolve the interference obtained from amorphous ice, samples were sublimed by raising the temperature to -90 °C whenever required.

4.2.2.5 In vitro DiR release studies

In vitro release of DiR from PEG-MAL – thiol gel was determined by incubating the DiR NCs loaded gel with SIPF at 37 °C. 50 µL gels were incubated in 1.25 mL of SIPF, yielding 1:25 dilution. At each time point, 50 µL samples were collected and diluted with ethanol accordingly. Fluorescence intensity was recorded with the same procedure as described in section 3.2.1.3. Three repeat samples were undertaken at each time point.

4.2.3 *In vivo* local residence and biodistribution studies

4.2.3.1 Animals and image acquisition

All experiments were performed on immunodeficient BALB/c nude mice (Janvier laboratories, France) under the animal protocol no. 15005AE/07/FUN01/FIS02/JACP1. Mice were housed in specific pathogen-free (SPF) conditions, according to Federation of European Laboratory Animal Science Associations (FELASA) guidelines.

Images were acquired after inducing sedation with isoflurane from XGI-8 Gas Anesthesia Unit (Caliper Life Sciences, USA). Fluorescence (λ_{exc} = 745 nm/ λ_{em} = 820 nm) was acquired with IVIS® spectrum imaging system (Caliper Life Sciences, Perkin-Elmer, USA) at different time intervals.

4.2.3.2 Determination of local residence and biodistribution

Local residence and biodistribution were evaluated in 20 mice, dividing them into 2 sets. The first set of 7 mice were randomized into one of the following groups (n = 2 animals per group): DiR alone, DiR NCs and DiR NCs + PEG-MAL – thiol gel groups, while 1 mouse acts as a negative control, which

received isotonic trehalose solution. Second set of 13 mice were randomized into one of the following groups (n = 4 animals per group) DiR alone, DiR NCs and DiR NCs + PEG-MAL – thiol gel groups, while 1 mouse acts as a negative control (isotonic trehalose solution). Whole body images were captured at 0, 4 and 24 h for the first set, while images for the second set were captured at 0, 4 and 24, 48, 96 h and 1 week after administration. Animals were sacrificed and organs were collected after 24 h for the first set, while it was performed after 1 week for the second set. DiR alone, DiR NCs and negative control (isotonic trehalose solution) were administered through IP injection (100 µL/mice, 5 ppm DiR concentration), while DiR NCs + PEG-MAL – thiol gel was implanted after making a surgical incision of approximately 1 cm over the peritoneal cavity, which was further closed by stainless steel wound clips.

4.2.4 Incorporation of DCX into NCs

4.2.4.1 Optimization of DCX loading

DCX was incorporated into HA NCs as a model chemotherapeutic agent. A stock solution of DCX in ethanol (100 mg/mL) was first prepared. This was then added to the mixture of Tween® 80, Labrafac, Lipocol™ and ethanolic solution of BZT. After thorough mixing for 5 min, purified water was added to form a nanoemulsion. Further steps to prepare NCs were as described in section 2.2.1.1. Optimum DCX loading was identified by preparing NCs at DCX final concentrations of 3, 7.5 and 12 mg/mL, followed by microscopic evaluation of NCs for any traces of recrystallization.

4.2.4.2 Determination of colloidal properties of DCX NCs

Particle size, PDI and zeta potential of DCX NCs were determined using the same method as mentioned in section 2.2.1.2. Entrapment efficiency was determined by isolating the NCs using centrifugation at 18,000 for 1 h at 15 °C (Harrier 18/80 refrigerated centrifuge, MSE centrifuges Ltd., UK).

4.2.4.3 Determination of entrapment efficiency of DCX NCs

The amount of DCX in supernatant (isolated NCs), liquid underneath and the non-isolated (before centrifugation) NCs were quantified by HPLC after extraction of DCX from respective samples. To extract DCX from each of these samples, a pre-weighed quantity (approx. 20 mg) of the respective sample was

diluted to 1mL with ethanol, followed by vortex mixing for 3 min. The HPLC consisted of an Agilent system equipped with a UV detector set at 227 nm and a reverse phase Zorbax, Eclipse XDB- C8 column (4.6 ID × 150 mm, pore size 5 μm), Agilent, UK. The mobile phase was a mixture of ultrapure water and acetonitrile, each containing 0.1 %v/v orthophosphoric acid (55:45), isocratic, with the flow rate of 1 mL/min. The column was set at 25 °C and the injection volume was 20 μL. The standard calibration curves of DXM were linear in the range of 1-1000 μg/mL (r^2 = 0.999). The concentration of DCX obtained from these samples was used to calculate the % EE and drug loading using equation 4.1 and 4.2 respectively.

$$\% \text{ EE} = \frac{\text{Amount of DCX in isolated destructed NCs}}{\text{Total DCX added}} \times 100 \quad \text{.....Equation 4.1}$$

$$\text{Drug loading} = \frac{\text{Amount of DCX in NCs}}{\text{Amount of NCs (mg)}} \quad \text{.....Equation 4.2}$$

4.2.4.4 Preparation of DCX NCs loaded PEG-MAL – thiol gel

DCX NCs loaded PEG-MAL – thiol gels were prepared at 5% and 10% w/w concentrations of PEG-MAL. DCX NCs that contain 3 mg/mL of DCX were selected to incorporate into the gel. The method of incorporation of DCX NCs and preparation of the gel are similar to the incorporation of DiR NCs as described in section 5.2.1.4. Once the gel was prepared, percentage DCX recovery was determined by incubating the PEG-MAL – thiol gel in a solution of porcine esterase in 1 M Tris buffer (pH 8.0), followed by estimation of DCX concentration using HPLC as mentioned in section 4.2.4.3. Additionally, samples were centrifuged after addition of ethanol at room temperature, 18000×*g* for 10 min to remove any unwanted precipitate and clear supernatant was collected and injected into the HPLC.

4.2.4.5 In vitro release of DCX from DCX NCs loaded PEG-MAL – thiol gel

In vitro release studies of DCX was determined by incubating the hydrogel with SIPF containing 0.5 %w/v Tween® 80 at 37 °C. Being a hydrophobic molecule, poor aqueous solubility of DCX might be a rate-limiting step to release the drug into the medium. Hence, Tween® 80 was added to the medium to maintain sink condition. 50 μL of PEG-MAL – thiol gel was placed in a glass vial and 1.25 mL of media was added to achieve 1:25 dilution. At each time point, the whole

volume of media was collected and replaced with fresh media. DCX was then extracted from these samples by evaporating the water from 1 mL of sample using a nitrogen evaporator, followed by addition of 1 mL of ethanol to dissolve the DCX. This ethanolic solution was then centrifuged at room temperature, 18000×*g* for 10 min to remove any unwanted precipitate and clear supernatant was collected and injected into the HPLC as descibed in section 4.2.4.3, to determine DCX released at each time point.

4.3 Results and discussion

4.3.1 Preparation and optimization of covalently cross-linked hydrogels

PEG based covalently crosslinked hydrogels were optimized to incorporate DiR NCs. First, the PEG-SH crosslinker was synthesized, which was then used to synthesize PEG-NB – thiol and PEG-MAL – thiol hydrogels.

4.3.1.1 Synthesis of PEG-SH crosslinker

PEG-SH crosslinker was synthesized by modifying a linear PEG (MW: 3350) to incorporate a thiol-end group, linked to PEG chain via a propionate linkage. Free thiol-end group is expected to react with PEG-NB polymer to undergo a thiol-ene photoclick reaction to form a covalently cross-linked hydrogel. Alternatively, it can react with PEG-MAL polymer to undergo a Michael addition reaction to form another covalently cross-linked hydrogel. Chemical structure of PEG-SH is represented in Figure 4.1. Hydrogels that are formed by these thiol-ene photoclick and Michael addition reactions have found multiple applications in tissue engineering and drug delivery (233).

The role of propionate group in PEG-SH is to favour hydrolysis driven *in vivo* degradation of PEG gel, which would render biodegradability of the formulation. Modification of covalent cross-linker in order to tune the hydrolysis and degradation rate of hydrogels is widely reported in the literature. For example, Schoenmakers *et al.* have conjugated a model drug, paclitaxel, to PEG via hydrolysable crosslinker, which controlled the release of active through gradual degradation of the ester bond. Moreover, they were able to tune the rate of degradation by changing the carbon chain length of the cross-linker (234).

In this study, we have modified the linear PEG based on the protocol reported by Nie *et al.*, (235). *p*-toluene sulfonic acid acts as a catalyst in the reflux reaction of hydroxy-functionalized linear PEG with mercaptopropionic acid in toluene. DTT was used as a reducing agent to prevent disulfide bond formation. After the completion of reaction, the formation of PEG-SH was confirmed by 1H NMR, where chemical shifts were observed to be: δ = 4.32 (4H, CH_2-O-C(O)), 3.92 - 3.52 ((CH_2-CH_2-O)$_n$), 2.83 - 2.72 (8H, CH_2-CH_2-SH). After isolation and drying, 90 % yield was observed, which was similar to Nie *et al*. Thus formed PEG-SH was further used to prepare PEG-NB – thiol and PEG-MAL – thiol gels through UV-photoinitiation and Michael addition reactions respectively.

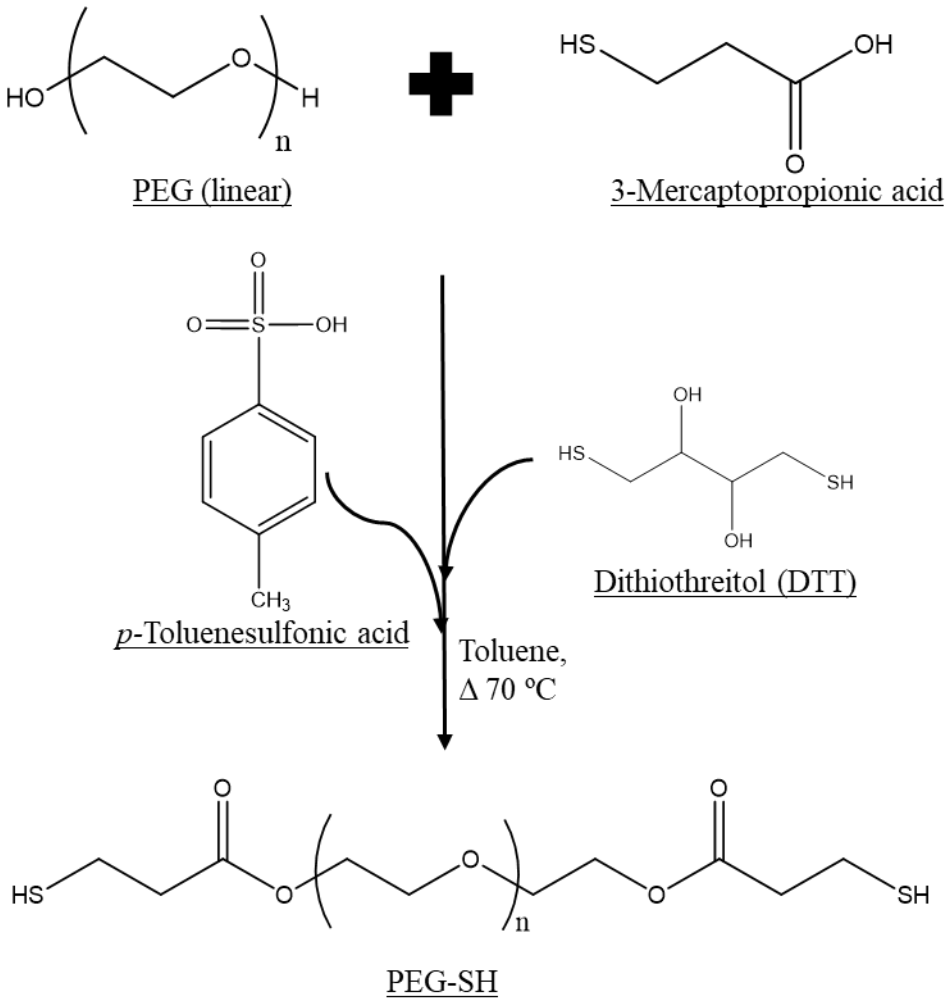


Figure 4.1 Schematic representation of chemical reaction involved in the synthesis of PEG-SH crosslinker. The linear PEG (MW: 3350, n = 74.7 repeating units) was refluxed with mercaptopropionic acid, in presence of *p*-toluenesulfonic acid and DTT in toluene.

4.3.1.2 Preparation and optimization of UV crosslinkable PEG-NB – thiol gel

UV crosslinkable PEG-NB – thiol gels have been explored for tissue engineering and other biomedical applications (236, 237). Incorporation of fluorescently labelled nanoformulations into this hydrogel is a challenge. Nanoparticles and fluorophores should be chemically stable in the presence of highly reactive photoinitiators and UV light. Freitas *et al.* reported the alteration in colloidal properties of solid lipid nanoparticles (SLN) after UV irradiation. They have observed that poloxamer 188 stabilized Compritol solid lipid nanoparticles (SLN) showed accelerated particle growth and destabilization of the formulation after being irradiated with high energy UV radiation (< 390 nm) (238). Hence, in this study, colloidal stability of NCs and chemical stability of DiR in presence of UV were considered as the primary criteria during the optimization of PEG-NB – thiol gel to incorporate DiR NCs. A suspension of DiR NCs in PBS (0.01 M, pH 7.4, 20 mg/mL) was exposed to UV light as described in section 4.2.1.2. The suspension showed a similar particle size and PDI, after exposure to UV light, as compared to prior to UV exposure, as reported in Table 4.3.

Table 4.3 UV stability of NCs, as determined by incubating the suspension of DiR NCs in PBS, followed by exposing them to UV for 5 min at 25 ºC. No significant changes in colloidal properties ensures the UV stability of NCs. Data represented as Mean ± SD (n = 3)

Media for DiR NCs	UV exposure	Size (nm)	PDI
Milli-Q water	No	243 ± 15	0.1
PBS (0.01 M, pH 7.4)	No	230 ± 20	0.1
PBS (0.01 M, pH 7.4)	Yes	230 ± 25	0.1

Once the colloidal stability of DiR NCs after UV exposure was confirmed, the stability of DiR after the incorporation of DiR NCs into the PEG-NB – thiol gel was determined by fluorimetry. This was performed by first identification of an appropriate solvent or media that can dissolve the hydrogel, followed by estimation of DiR released into the media after dissolution of the hydrogel. 50 µL of PEG-NB – thiol gel was immersed in 1 mL of ethanol or acetonitrile or dimethyl sulfoxide or pH 3 citrate buffer or 1 M HCl or 1 M NaOH. NaOH, was

the only solvent that dissolved the gel. In addition, it was observed that DiR was not detectable in the dissolved gel mixture as determined by fluorimetry. This could be due to its degradation either during the manufacture or its interaction with dissolving media, NaOH.

To identify if NaOH contributes to the degradation of DiR, DiR NCs were incubated in 1 M NaOH (15 mg/mL) for 30 min and fluorescence intensity was evaluated. It was observed that DiR only showed 30 % of initial fluorescence after suspending in NaOH. This indicates that NaOH has contributed to the degradation of DiR. Liu *et al.* reported that the fluorescent properties of DiR loaded nanocarriers was influenced by pH. They observed that stearic acid grafted polyethyleneimine and HA nanoparticles containing DiR showed stable fluorescence emission in the pH range of 5-9, while the intensity was reduced at higher pH (239).

To identify an alternative media that can dissolve the gel without degrading the DiR, enzyme mediated degradation was chosen. Porcine esterase, which is isolated from livers of pigs, is an enantioselective serine hydrolase with wide specificity to ester hydrolysis (240). Pancreatin is a lyophilized powder of various enzymatic components that include trypsin, amylase, lipase, ribonuclease and protease, produced by exocrine cells of pancreas. Although non-specific, pancreatin might also contribute to the hydrolysis of ester bonds. Hence, esterase and pancreatin obtained from porcine liver and pancreas were evaluated for their potential to breakdown the propionate bonds to dissolve the PEG-NB – thiol gel. Gels were incubated in the buffer solutions of esterase and pancreatin as discussed in section 4.2.1.3. It was found that porcine esterase dissolved the gel completely in 1 M Tris buffer, pH 8 at room temperature, while pancreatin did not dissolve the gel.

Raghupathi *et al.* have used porcine esterase for understanding the release of fluorescent hydroxycoumarin derivative, 4-methylumbelliferone, from their amphiphilic dendrimer system. The guest molecule, 4-methylumbelliferone, was non-covalently sequestered within an enzyme responsive dendrimer system. The extent of release of fluorescent molecule was directly proportional to enzymatic activity of porcine esterase (241). We have also observed that

porcine esterase was able to degrade the hydrogel, which might be due to the cleavage of propionate linkage on PEG-SH. Similar phenomenon could also occur *in vivo* due to the presence of indigenous esterases in the peritoneal and ascites fluids. Hence, porcine esterase was selected as an alternative to NaOH.

Further, DiR NCs loaded PEG-NB – thiol gel was prepared and dissolved in porcine esterase, to determine the percentage recovery of DiR. In contrast to NaOH, a suspension of DiR NCs incubated with porcine esterase had 99 % DiR recovery. This indicates that porcine esterase was successful in dissolving the gel without the degradation of DiR. Hence, we can conclude that this DiR degradation might have happened during the preparation of PEG-NB – thiol gel.

To understand DiR's degradation further, a compatibility study was performed to trace any potential interactions of DiR with other gel components, which might lead to its degradation. Different gel components were mixed in the same proportions as used for gel preparation. Table 4.4 shows the results of the compatibility study. A suspension of DiR NCs in PBS did not show any degradation after UV exposure (mixture I). Similarly, a mixture of PEG-NB and PEG-SH with DiR NCs did not show any degradation of DiR after UV exposure, in the absence of LAP (mixture V). However, mixtures containing LAP led to strong degradation of DiR after UV exposure, as seen by reduction in fluorescence intensity values (mixtures II, III and IV). Mixture VI that contains LAP did not show degradation of DiR as this mixture was not exposed to UV. Hence, it can be concluded that LAP in presence of UV is responsible for DiR degradation.

Table 4.4 Compatibility study to determine the photostability of DiR NCs with individual gel components before and after exposure to UV. Each mixture was prepared in same proportions as present in the gel, at 25 ºC (n=1). Incompatibility was evaluated by reduction in fluorescence intensity units after exposure to UV. (*Composition indicates respective mixtures prepared in 0.01 M PBS, pH 7.4)

Mixture	Composition*	UV exposure	Fluorescence units (FU)
I	DiR NCs	Yes	55324
II	LAP + DiR NCs	Yes	1481
III	PEG-NB + LAP + DiR NCs	Yes	3026
IV	PEG-SH + LAP +DiR NCs	Yes	2722
V	PEG-NB + PEG-SH + DiR NCs	Yes	48065
VI	PEG-NB + PEG-SH + LAP + DiR NCs	No	50014

To minimise the DiR degradation, concentration of LAP and UV exposure time were reduced. An alternative photoinitiator, Irgacure® 2959 was also evaluated. Table 4.5 shows various concentrations of LAP and Irgacure® 2959 at different UV exposure times that were evaluated to minimise DiR degradation. Unfortunately, in all the cases DiR degradation was observed. In principle, both LAP and Irgacure® 2959 produce free radicals in presence of UV, which favours the formation of hydrogels through step-growth thiol-ene photoclick reactions (242). DiR is a near IR carbocyanine fluorophore, rich in conjugated double bonds, as seen in its chemical structure (Figure 4.2). These conjugated double bonds are susceptible to cleavage in presence of free radicals. Cleavage of these conjugated double bonds might lead to the loss of its fluorescence activity. Moreover, chemotherapeutic agents, which contain double bonds might also act as potential targets for these photoinitiators. The ability of LAP and Irgacure® 2959 to generate free radicals that can potentially degrade chemotherapeutic agents such as doxorubicin was observed by Fairbanks *et al.* (243).

Based on these observations it can be concluded that photocrosslinkable PEG-NB – thiol gel was not be suitable for incorporation of DiR NCs, as the photoinitiators were incompatible with DiR, leading to loss of its fluorescence activity. Moreover, these photoinitators might not guarantee successful incorporation of chemotherapeutic agents in future as they could potential

interact with double bonds. Hence, an alternative covalently cross-linked hydrogel that can be prepared without the use of photoinitiators was required.

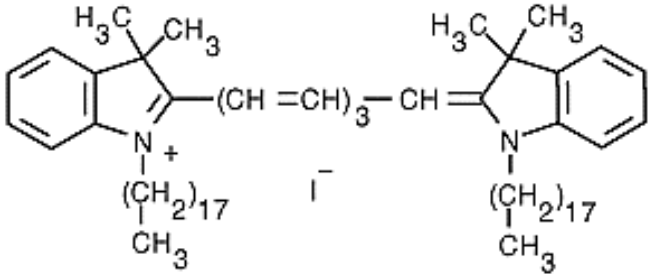


Figure 4.2 Chemical structure of fluorescent dye, DiR, showing the conjugated double bonds, which are susceptible to degradation by photoinitiators, LAP and Irgacure® 2959 in the presence of UV

Table 4.5 Experimental parameters evaluated to determine the influence of nature and concentration of photoinitiators and UV exposure times on photostability of DiR NCs

Photoinitiator	Concentration (% w/w of gel)	UV exposure time
LAP	0.02	5 min
LAP	0.05	2 min
LAP	0.05	30 s
Irgacure® 2959	0.05	2 min
Irgacure® 2959	0.05	45 s

4.3.1.3 Preparation and optimization of PEG-MAL – thiol gel

Covalently crosslinked hydrogels prepared by Michael addition reaction do not require photoinitiators or any external stimuli. Maleimides, acrylates, vinyl sulfones and methacrylates react with thiols to form covalent bonds through a Michael addition reaction (233, 244). PEG has been modified with these groups to form functionalized polymers that can react with thiol crosslinkers to form hydrogels. Phelphs *et al.* have prepared and evaluated various polymers that can crosslink through Michael addition, to encapsulate and support cellular activity of murine myoblast cells. They have found that PEG-MAL hydrogels have improved cross-linking and encapsulation efficiencies, and higher cell viability in comparison to vinyl sulfone and acrylate equivalents (244). Similarly, PEG-MAL hydrogels have found various applications in protein and cell delivery in

regenerative medicine (245). These hydrogels have also been explored for local drug delivery. Yu *et al.* incorporated Avastin® into a covalently crosslinked hydrogel prepared from 4-arm PEG-MAL (MW: 10 kDa) and 4-arm PEG-SH (MW: 20 kDa) for controlled drug delivery. They have achieved a sustained drug delivery up to 14 days *in vitro* with no apparent cytotoxicity found in L-929 cell cultures (246). Despite multiple applications of PEG-MAL – thiol gels, incorporation of nanoparticle formulations in these hydrogels to further prolong the release for local drug delivery has not been explored extensively. In this study, we have used PEG-SH crosslinker to form covalently crosslinked hydrogel with PEG-MAL and incorporate DiR NCs. Figure 4.3 shows the schematic representation of this reaction to form a hydrogel.

Optimization of this hydrogel was performed to identify the appropriate concentration of PEG-MAL that can incorporate DiR NCs and show slow release of DiR. 5% and 10% w/w PEG-MAL concentrations at equimolar PEG-SH were explored in this study. It was known from the literature that the rate of maleimide – thiol reaction is strongly influenced by the pH of the medium. Indeed, Jansen *et al.* have evaluated various parameters that control the reaction kinetics of PEG-MAL (MW: 20 kDa) hydrogel networks. They explored a range of crosslinkers, which include PEG-SH (MW: 1 kDa) and a number of different dithiol terminated peptide sequences. They observed that lowering the pH of reaction medium, reducing the polymer weight percentage and buffer concentration reduces the reaction kinetics. This was due to the base catalysis of nucleophilic addition onto alkene group of maleimide, which favoured the formation of stable polymeric networks. They found that strong bases such as triethanolamine (pKa 7.76) catalyzes the reaction much faster than weak acids such as a citrate buffer (pKa 6.40) (247). In addition, Darling *et al.* observed that faster reaction kinetics of PEG-MAL gel might lead to heterogeneity. They have suggested that lower pH reduces the rate of reaction, which is favourable to ensure homogenous incorporation (248). Hence, a lower pH was considered for gel preparation. However, colloidal stability of NCs and photostability of DiR at lower pH must be ensured. Riehl *et al.* found that the fluorescence emission of DiR was stable at pH 4 and 7, while further reduction in pH has shown significant loss of fluorescence with time (249). As it was known that

DiR was stable at pH ≥ 4, DiR NCs were incubated in different low pH buffers to identify the impact of pH on colloidal stability. Table 4.6 shows the particle size and PDI of DiR NCs incubated with different buffers. It was found that the particle size did not change significantly from pH 7.4 until pH 4.0. Further reduction to pH 3.0 lead to increased particle size and PDI. As pH 4.0 is the lowest threshold, pH 5.0 was chosen as an optimum pH for preparation of the PEG-MAL – thiol gels.

Table 4.6 Determination of colloidal stability of DiR NCs up on incubation in buffers with different pH, at 25 ºC. Data is represented as mean ± SD (n = 3)

Media to incubate NCs	Size (nm)	PDI
Milli-Q water	243 ± 18	0.1
PBS (0.01 M, pH 7.4)	230 ± 15	0.1
Citrate buffer (0.1 M, pH 6)	228 ± 38	0.1
Citrate buffer (0.1 M, pH 5)	221 ± 20	0.1
Citrate buffer (0.1 M, pH 4)	226 ± 28	0.1
Citrate buffer (0.1 M, pH 3)	449 ± 80	0.3

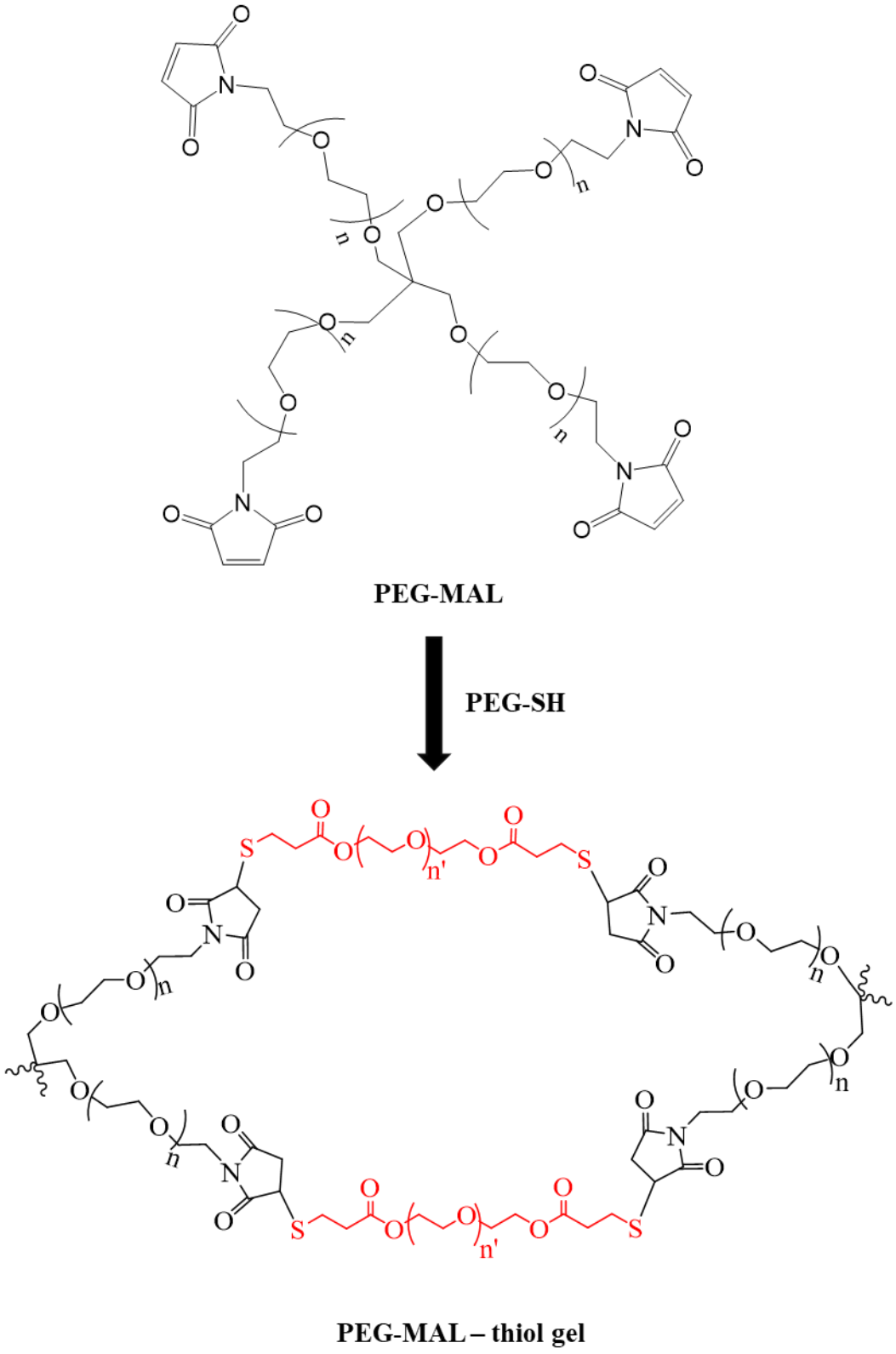


Figure 4.3 Schematic representation of Michael-type addition reaction involved in formation of PEG-MAL – thiol gel (MW of PEG-MAL = 10 kDa, n = 53.3 repeatiting units; MW of PEG-SH = 3350, n' = 74.7 repeating units)

Once optimum pH was identified, PEG-MAL – thiol gels were prepared at 5 and 10% w/w concentrations of PEG-MAL and equimolar concentrations of PEG-SH, incorporating 30% w/w DiR NCs. Gel formation was observed at both the concentrations, without any visual leakage of NCs. To determine the percentage recovery of DiR, gels were incubated in porcine esterase medium as described in section 4.2.1.3. Unlike PEG-NB – thiol gel, 99 % of DiR was recovered after preparation and degradation of the gel. Hence, we achieved a covalently crosslinked PEG-MAL – thiol gel that can incorporate 30 % w/w DiR NCs.

4.3.2 Characterization of PEG-MAL – thiol gels

4.3.2.1 Cryogenic focussed ion beam scanning electron microscopy (cryo-FIB-SEM)

FIB-SEM is an advanced electron microscopy, which involves use of finely focussed ion beams to acquire images at low current while samples can be milled at high currents to reveal the internal structures (250). Operation of FIB-SEM in cryogenic mode favours the imaging of hydrogels in its native state to identify essential structural features (251). It is known that cryo-TEM offers better resolution to image hydrogels and NCs in comparison to SEM techniques. However, sample preparation for cryo-TEM is not suitable to handle preformed hydrogels with high mechanical strengths. Cryoplunge®, which is used to obtain thin frozen samples for cryo-TEM was unable to hold the preformed PEG-MAL – thiol gel. Hence, FIB-SEM was chosen, which offered better sample processing than cryo-TEM. Samples were prepared with slight modification of the protocol developed by Parmenter *et al.*, which involves freezing the samples in metal mirror freezer as explained in section 4.2.2.4 (252). Figure 4.4 shows the FIB-SEM images of frozen PEG-MAL – thiol gel. NCs were found to be entrapped in the hydrogel matrix, in clusters. These images provide an idea about distribution of NCs within the hydrogel. However, because of lower resolution, better contrast was not achieved to differentiate aggregates versus individual NCs. Hence, to elucidate further on the nature of incorporated NCs, cryo-TEM analysis in combination with better sample processing techniques such as microtoming is required.

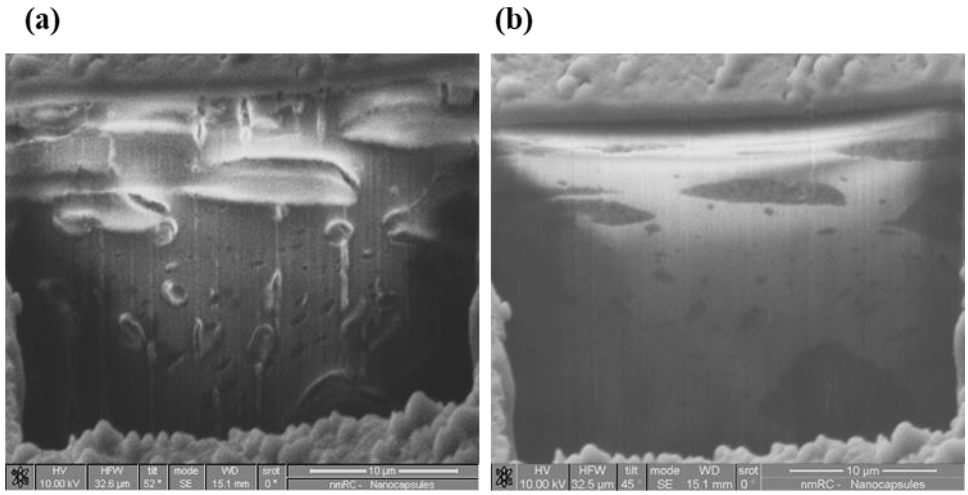


Figure 4.4 FIB-SEM images of (a) PEG-Mal – thiol gel frozen under liquid nitrogen using metal mirror freezer (b) PEG-MAL – thiol gel milled at higher beam currents, showing the clusters of NCs. Scale bar indicates 10 µm

4.3.2.2 Determination of gelation kinetics through rheology

The kinetics of gelation was performed on PEG-MAL – thiol gel containing DiR NCs using rheology, as mentioned in section 4.2.2.2. Gelation kinetics are conventionally evaluated by following the change in storage (G') and loss modulus (G") with time. Darling *et al.* reported the gelation kinetics of PEG-MAL gels at different temperatures, and concentrations of maleimide and thiol, as observed by increasing G' and G" (248). Similarly, Holmes *et al.* also reported the gelation kinetics of thiol-ene photoclick PEG gel through the increase of G' and G" as a function of time (253). In our study, G' and G" was found to gradually increase with time as shown in Figure 4.5 (a). No crossover point of G' and G' was observed, which is generally considered to be the point of initiation of gelation. As the gels were prepared at pH 5.0, gelation kinetics are expected to be rapid (247). Hence, the initiation of gelation might be too fast, which made it difficult to trace during the study. Further reduction in pH of the preparation buffer could reduce the gelation time. However, colloidal properties of NCs would be compromised at lower pH as seen in section 4.3.1.3. Highest G' and G" were seen at 30 min, indicating the complete gelation. These values are comparable to 2′-dC-N_4-C_8 gel, but higher than Fn-HA gel, as shown in Figure 4.5 (b).

Higher mechanical properties would help to withstand dynamic environment in IP cavity. Similar observations were made by Yeo *et al.*, where poly(lactic-

coglycolic acid) (PLGA) nanoparticles were incorporated in covalently cross-linked HA hydrogel designed for prolonged retention in IP cavity. The reported G' obtained from osciallatory amplitude sweep test was approximately 420 Pa, which was comparable to PEG-MAL – thiol gel and it favoured the prolonged retention in IP cavity (254). Another covalently crosslinked hydrogel prepared by crosslinking N, O-carboxymethyl chitosan and aldehyde HA was found to be retained up to 2 weeks in rats after IP administration. G' and G" of this hydrogel, as observed from gelation kinetics experiments, were found to be approximately 10 fold lower than PEG-MAL – thiol gel (255). Based on these data, we can consider that PEG-MAL gel has appropriate mechanical properties suitable for IP administration.

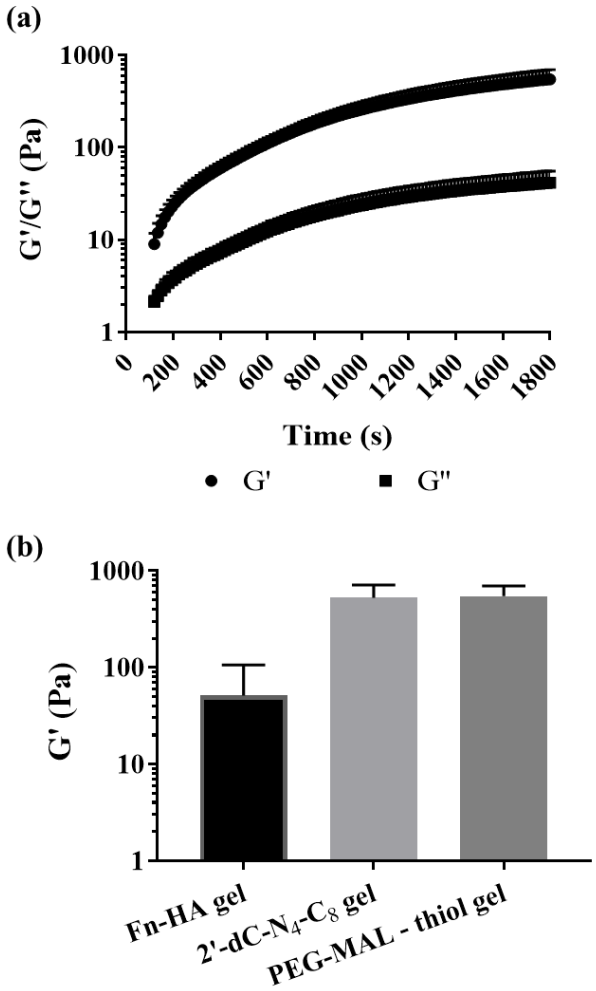


Figure 4.5 (a) Gelation kinetics of PEG-MAL – thiol gel as determined by oscillatory rheology performed on parallel plate assembly at 0.5 Hz frequency, 0.5% strain, 0.5 mm gap and 25 ºC, showing the increase of G' and G" with time. (b) A comparison of Fn-HA, 2′-dC-N4-C8 and PEG-MAL – thiol gels, showing a significant difference of G' ($p < 0.05$, Tukey's multiple comparison test). Data represented as mean ± SD (n = 3)

4.3.2.3 Resistance to dilution

Resistance to dilution is one of the important parameters to be evaluated for hydrogels directed to IP cavity. DiR NCs loaded PEG-MAL – thiol gels prepared with 5% and 10% w/w concentrations of PEG-MAL were incubated with SIPF at 37 °C. As observed visually, both 5 and 10% w/w gels were swollen initially. Interestingly, gels containing 10% w/w PEG-MAL were remained intact up to 3 weeks, while gels containing 5% w/w PEG-MAL were intact up to 2 weeks at 1:25 dilution. This is in contrast to the observations made in section 3.3.3.3, where Fn-HA and 2′-dC-N_4-C_8 gels did not tolerate dilutions higher than 1:3 and 1:9 respectively. Higher resistance to dilution would be favourable for retention longer in the IP cavity, as it would help the formulation to withstand the high fluid turnover rates. Physically assembled hydrogels dissociate rapidly through dissolution in aqueous environments (256). In contrary, covalently cross-linked systems cannot be diluted and instead swell. A covalently cross-linked HA gel containing cisplatin was reported to retain after 28 days of IP administration, exhibiting a significant reduction in peritoneal tumour nodules (231). With being chemically cross-linked, PEG-MAL – thiol gel would have a high potential to be retained longer in the IP cavity.

4.3.2.4 In vitro DiR release studies

Once resistance of PEG-MAL – thiol gel to high dilution was ensured, *in vitro* release of DiR was determined from DiR NCs loaded gels, prepared at 5% and 10% w/w PEG-MAL concentrations. Figure 4.6 shows the release profiles of DiR at both concentrations. The *in vitro* release obtained from PEG-MAL-thiol gels at both 5 and 10% w/w PEG-MAL concentrations was more sustained in comparison to Fn-HA and 2′-dC-*N*4-C_8 gels. As described in section 3.3.3.4, Fn-HA gel showed a 40% release in 48 h at 1:3 dilution, whereas 2′-dC-*N*4-C_8 gel showed 100% release in 24 h at 1:9 dilution. In contrast, PEG-MAL – thiol gels containing 5 and 10% w/w PEG-MAL showed a cumulative release of approximately 80% and 45% after 5 days respectively. Gels were physically retained after the study, showing > 85% recovery of DiR, as determined by dissolving the gel in porcine esterase, followed by fluorescence measurements. It should be noted that the release profile is an indicative of the sum of free DiR

and DiR NCs released into the media, as it was difficult to isolate NCs from free DiR as described in section 2.3.2.1. Presence of DiR NCs in the release media was confirmed by obtaining DLS measurements of the media after incubation with PEG-MAL – thiol gel.

The high concentration of PEG-MAL would naturally provide higher crosslinking density of the hydrogel, which would further control the release from the hydrogel. Fu *et al.* studied the influence of extent of higher crosslinking density in PEG-MAL – thiol gels. They incorporated gelatin into PEG-MAL – thiol gel, prepared from PEG-maleimide (MW: 2 kDa) and PEG-dithiol (MW: 2 kDa), to achieve higher crosslinking density as a result of semi-interpenetrating networks. The *in vitro* release profile of fluorescein isothiocyanate (FITC)-labelled dextran showed that the gels with higher crosslinking density did not show burst release, whereas gels with regular crosslinks showed a burst release up to 80% in 1 h (257). Release of NCs occurs in tandem with the degradation of the hydrogel. As discussed earlier, PEG-MAL – thiol gel has higher probability to degrade via ester hydrolysis (234). SIPF is an aqueous media, which was under constant stirring and replacement during the study. Such fluid dynamics might favour ester hydrolysis, eventually degrading the gel. Gradual degradation might lead to pore formation, which further releases NCs into the media. *In vitro* release of self-emulsifying NCs from a hydrogel was studied by Štaka *et al.* They evaluated the release of nile red loaded HA NCs (80 nm and 40 nm particle size) from self-assembling 2′-dC-*N*4-C_8 gel and found that gels with 8% w/v NCs showed 80% release in 48 h, while gels with 4% w/v NCs showed 60% release in 48 h (205). Interestingly, the release profile obtained with PEG-MAL – thiol gel containing 10% w/w PEG-MAL showed only 40% release in 5 days.

Based on resistance to dilution and *in vitro* release studies, the PEG-MAL – thiol gels containing 10% w/w PEG-MAL concentration have shown better control over the release in comparison to its 5% w/w equivalent. Hence, 10% w/w PEG-MAL concentration was chosen to evaluate the *in vivo* local residence in the IP cavity and biodistribution of NCs from the PEG-MAL – thiol gel.

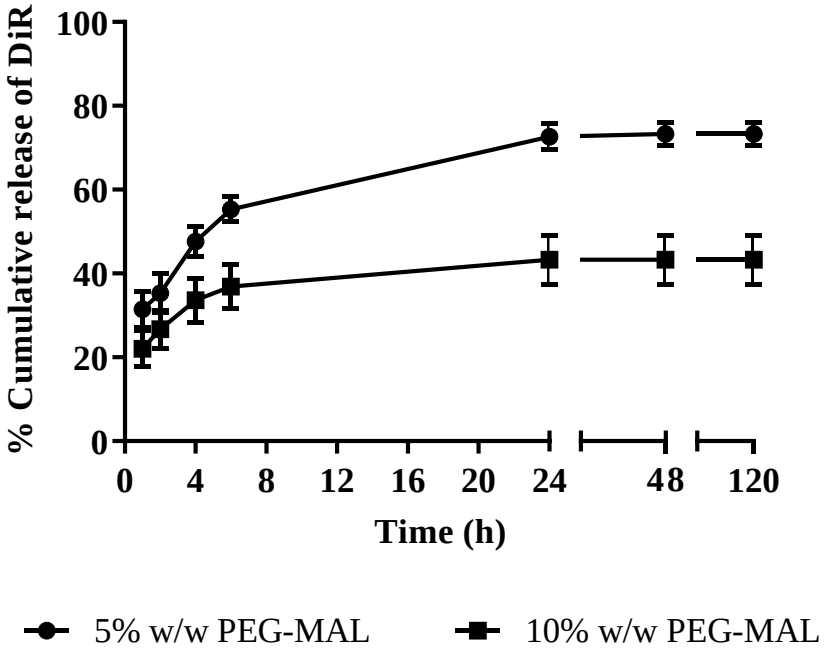


Figure 4.6 *In vitro* release study showing the release of DiR from PEG-MAL – thiol gels, as estimated by fluorescence analysis from each time point. Gels were prepared at 5 and 10% w/w concentrations of PEG-MAL and equimolar concentrations of PEG-SH, followed by incubation under 1:25 dilution in SIPF at 37 ºC. Data represented as mean ± SD (n=3)

4.3.3 *In vivo* local residence and biodistribution studies

In vivo local residence and biodistribution was evaluated in immunodeficient nude mice through IVIS® imaging. In contrast to the IVIS® experiments performed in chapter 4, animals were classified into two sets in order to obtain biodistribution data at an earlier time points after administration. The first set of animals were sacrificed after 24 h, while the second set were sacrificed after 1 week. Sacrificing the animals at an earlier time point, 24 h, was helpful to understand the earlier events related to biodistribution. Moreover, the method of administration was also different from the protocol described in section 3.2.4.3. PEG-MAL – thiol gel is a preformed hydrogel in contrast to Fn-HA gel, which was an *in situ* forming system. Hence, PEG-MAL – thiol gel was administered through surgical intervention, opening the peritoneal cavity of the mice, followed by physically placing the hydrogel in the cavity. While, negative control (isotonic trehalose solution), DiR alone and DiR NCs were administered as IP injections as performed in section 3.2.4.3. Although, the method of administration is more complicated than *in situ* forming system, this approach finds clinical relevance. PEG-MAL – thiol gel can be placed as an implant after

tumour resection in the cavity after cytoreductive surgery, aiming at targeting microscopic, metastatic remnant tumour nodules. Clinical findings have evaluated the benefit of IP chemotherapy in conjugation with cytoreductive surgery (92, 93). Hence, this composite hydrogel can be suitable for highly dissociative cancers such as ovarian and peritoneal carcinomatosis, which are associated with peritoneal cavity.

Figure 4.7 (a) shows the compilation of images of first set of mice, captured from the ventral side. Fluorescence was observed from the site of administration up to 24 h. Further, sacrificing the mice after 24 h showed the presence of hydrogel in the peritoneal cavity, which showed significant fluorescence (Figure 4.7 (b)). This indicates that the hydrogel not only withstands the dynamic IP environment, but also retained the DiR NCs. The biodistribution pattern of DiR NCs, as seen in Figure 4.9, indicates that they were preferentially taken up by the liver as expected. It is well known in the literature that nanoparticles tend to escape from the peritoneal cavity through both lymph duct and capillary openings. Doxorubicin loaded poly(butyl cyanoacrylate) nanoparticles administered through IP route rapidly distributed into blood and to the organs of reticuloendothelial system (258). However, tissue concentrations of IP administered doxorubicin nanoparticles were significantly higher than IV administered equivalent. This has also signified the higher bioavailability and therapeutic efficacy through IP administration. Kohane *et al.* compared the retention of 250 µm and 265 nm particles made of PLGA after IP administration. They have found that microparticles were retained in the peritoneum up to 2 weeks, while nanoparticles were cleared and accumulated in the liver and spleen within 2 days of IP administration (114). In another study, IP administration of superparamagnetic iron oxide nanoparticles have also shown accumulation in liver, spleen and omentum (259). This paper also reported the influx of macrophages as an indication of sequestration and clearance of nanoparticles.

As the retention of PEG-MAL – thiol gel was confirmed after 24 h, it was interesting to assess whether the gel was retained in the cavity up to 1 week. Figure 4.8 (a) shows the compilation of set 2 images, sacrificed after 1 week. Interestingly, no traces of hydrogel were found in the IP cavity, indicating that the hydrogel has completely degraded between 24 h and 1 week. Degradation

of the gel signifies the biodegradability of the system. The dynamic, fluid rich IP cavity might have degraded the gel through ester hydrolysis and enzymatic degradation. Moreover, the succimidyl thioether formed by the Michael addition might undergo degradation *in vivo*. Fontaine *et al.* worked on understanding and stabilizing the maleimide-thiol conjugates *in vivo*. They explained that succimidyl thioether could undergo thiol-exchange reaction or ring-opening hydrolysis in the biological environments. The rate of thiol-exchange and hydrolysis reactions was determined and found that thiol-exchange reaction is more predominant than ring-opening hydrolysis (260).

Biodistribution after 1 week showed a similar pattern to 24 h, showing average radiance from the liver (Figure 4.9). However, no traces of hydrogel were observed in the peritoneal cavity. Based on this data, it can be concluded that the hydrogel was retained in the IP cavity between 24 h to 1 week, while NCs escaped from the cavity and accumulated in the liver after being released from the hydrogel. It was observed that the radiant efficiency from the liver after 1 week was similar to 24 h time point, which further supported the liver accumulation. No significant fluorescence was observed from kidneys, which indicated that neither DiR nor DiR NCs were eliminated through urine. Schädlich *et al.* reported the excretion of DiR and DiR-loaded PEG-PLA nanoparticles through bioconjugation in liver, followed by excretion via gall into intestine, eventually clearing through faeces. They confirmed the faecal excretion through presence of fluorescence in the intestine (261). Interestingly, fluorescence was also seen in the lungs after 24 h, as observed with DiR NCs + PEG-MAL – thiol gel group (Figure 4.7 (b)). This might be due to macrophage-assisted migration of NCs to the lung tissue, after IP administration. Parayath *et al.* demonstrated the macrophage specific targeting of HA nanoparticles through CD_{44} residues, which favoured the accumulation of nanoparticles in lung tissue after IP administration. They exploited this phenomenon of lung accumulation to transfect microRNAs to tumour-assisted macrophages in nonsmall cell lung cancer model after IP administration (262).

This study also demonstrates the tolerability of PEG-MAL gel in the IP cavity of mice within the experimental timeframe. As explained earlier, covalently crosslinked HA gel containing cisplatin was retained even after 28 days of IP

administration, exhibiting a significant reduction in peritoneal tumour nodules (231). This formulation was a hydrogel which contained a chemotherapeutic agent in solution state in contrast to PEG-MAL – thiol gel which contains NCs. Presence of NCs might alter the extent of crosslinking at a sub-microscopic level of the hydrogel. However, presence of NCs opens further possibilities of functionalising the NCs with tumour targeting ligands. Further optimization of PEG-MAL – thiol gel is also possible to alter molecular weights and crosslinking sites of PEG-MAL and PEG-SH. Alternatively, the number of hydrolysable groups on the cross-linker chains could also be manipulated to reduce the rate of hydrolysis in order to further enhance the *in vivo* residence.

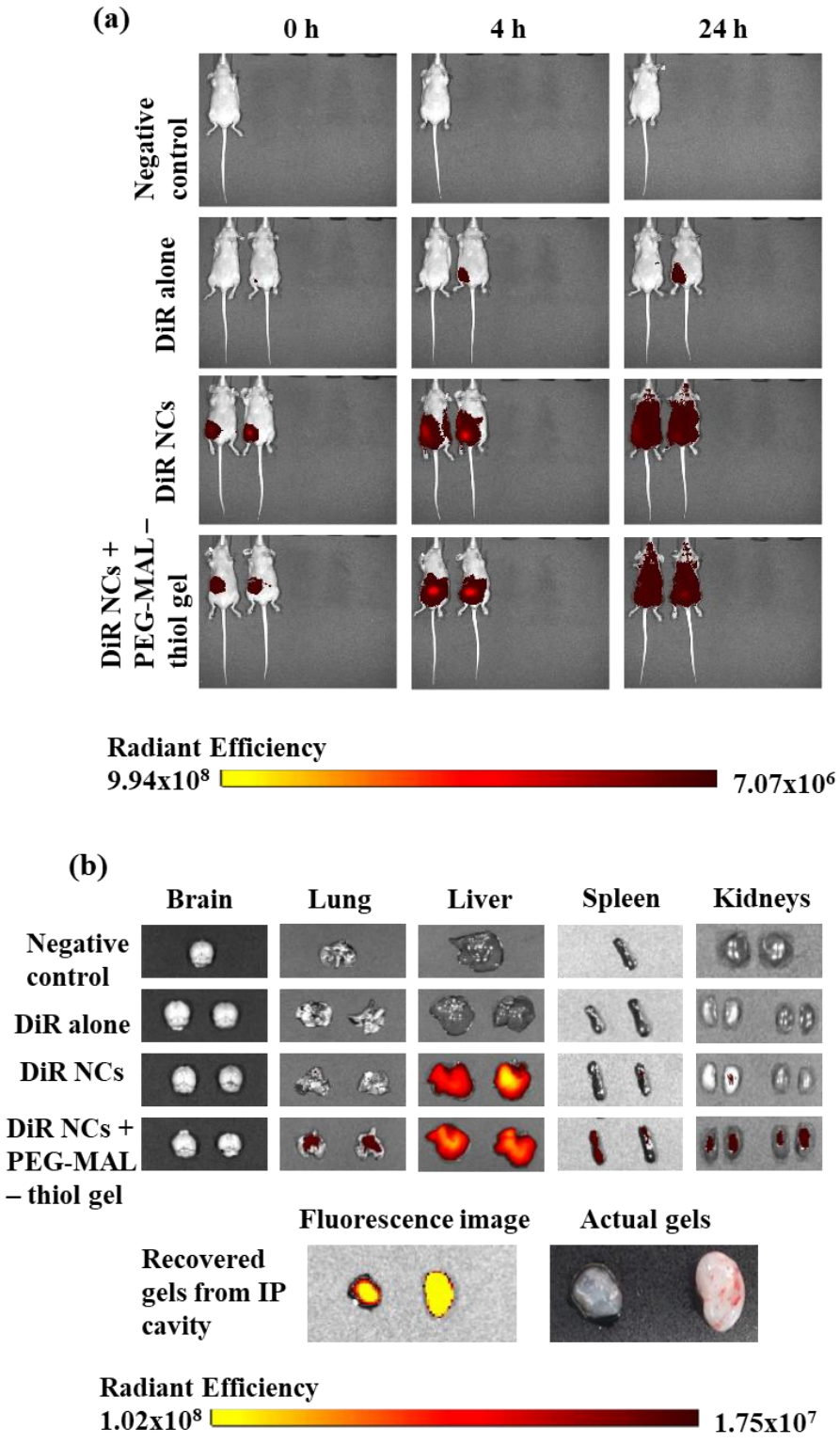


Figure 4.7 *In vivo* IVIS® imaging study performed on mice (set 1) (a) Compilation of images acquired after 0, 4 and 24 h of administration, showing the fluorescence obtained from DiR alone, DiR NCs and DiR NCs + PEG-MAL – thiol gel groups. Mouse administered with isotonic trehalose solution as negative control is also represented in the image (b) Compilation of images acquired from organs obtained after sacrificing the mice at 24 h time point, showing the fluorescence prominently from liver in case of DiR NCs and DiR NCs + PEG-MAL – thiol gel groups. Gels retrieved from the peritoneal cavity after 24 h, indicating the fluorescence, are also shown here.

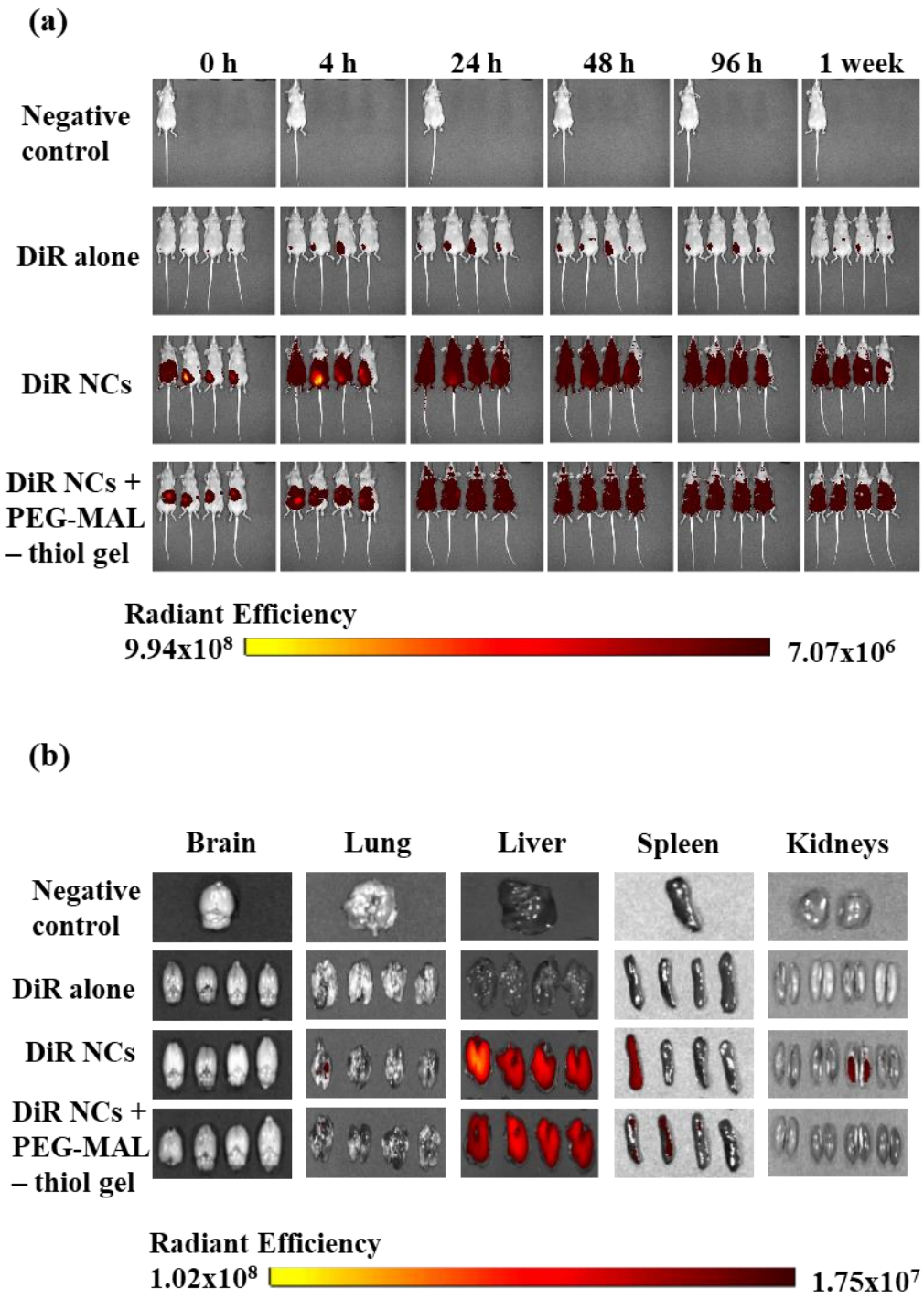


Figure 4.8 *In vivo* IVIS® imaging study performed on mice (set 2) (a) Compilation of images acquired after 0, 4, 24, 48, 96 h and 1 week of administration, showing the fluorescence obtained from DiR alone, DiR NCs and DiR NCs + PEG-MAL – thiol gel groups. Mouse administered with isotonic trehalose solution as negative control is also represented in the image (b) Compilation of images acquired from organs obtained after sacrificing the mice at 1 week time point, showing the fluorescence prominently from liver in case of DiR NCs and DiR NCs + PEG-MAL – thiol gel groups.

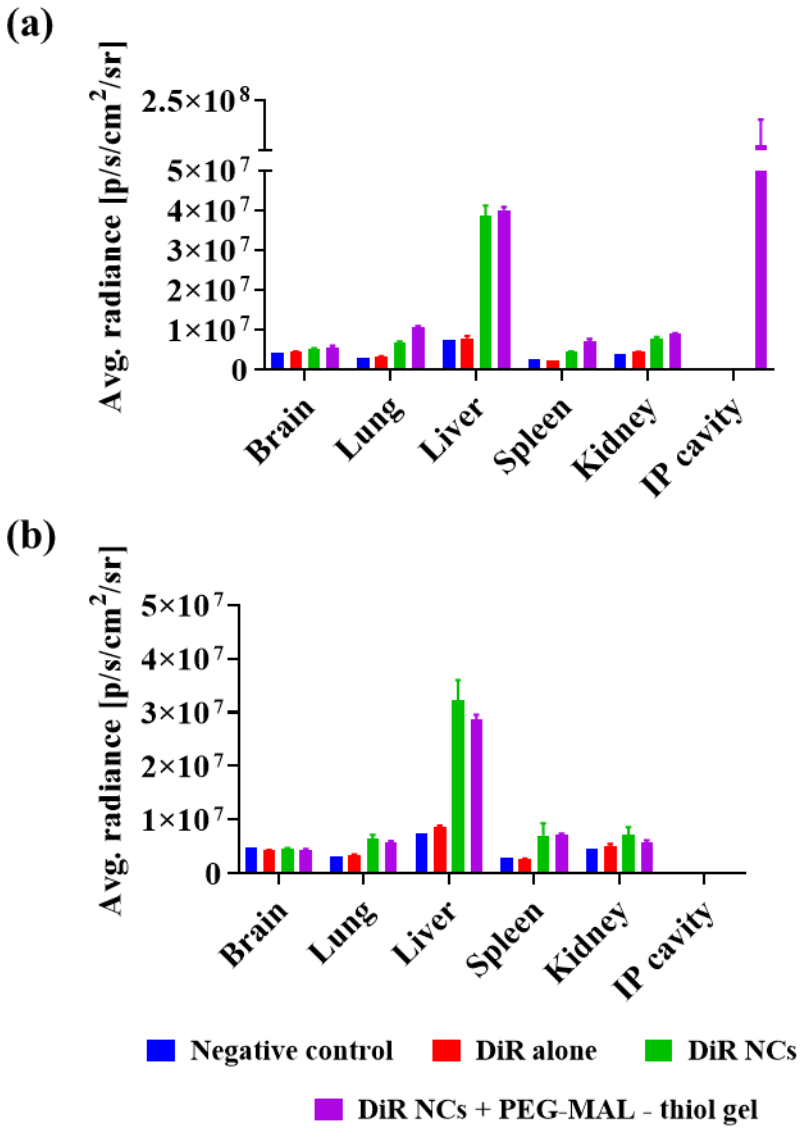


Figure 4.9 Biodistribution obtained from IVIS® imaging study after administration of negative control, DiR alone, DiR NCs and DiR NCs + PEG-MAL – thiol gel after IP administration. (a) Average radiance obtained from various organs acquired after sacrificing the mice up on 24 h of IP administration. IP cavity has shown remnants of DiR NCs + PEG-MAL – thiol gel, whose average radiance is also represented here. Data represented is mean ± SEM (n = 2). (b) Average radiance obtained from various organs acquired after sacrificing the mice up on 1 week of IP administration. Data represented is mean ± SEM (n = 4).

4.3.4 Incorporation of DCX into NCs

As the IP residence of PEG-MAL – thiol gel was established, it would to interesting to incorporate DCX as a model chemotherapeutic agent in order to establish its clinical application for the treatment of peritoneal tumours. In this section, DCX was incorporated into NCs and these DCX NCs were further loaded into PEG-MAL – thiol gel to characterise and evaluate their *in vitro* release.

4.3.4.1 Preparation and optimization of DCX loaded NCs

DCX was incorporated into NCs to achieve the final drug loading of 3, 7.5 and 12 mg/mL, using the procedure described in section 4.2.4.1. Entrapment efficiency and drug loading were determined by isolating the NCs through centrifugation. It was found that the formulations incorporated with 7.5 and 12 mg/mL have shown recrystallization of DCX after centrifugation, as seen by the presence of precipitate. Moreover, microscopic images have shown presence of birefringence, an indicator of recrystallization (Figure 4.10). Hence, DCX NCs containing 3 mg/mL of DCX were only characterized to determine colloidal properties, % EE and drug loading. Incorporation of DCX in the NCs was not found to influence its colloidal properties. Table 4.7 shows the colloidal properties, % EE and drug loading of DCX NCs.

DCX NCs have shown a % EE of 45 ± 5, while drug loading was found to be 3.0 ± 0.3 mg/mL. Based on the achieved drug loading of DCX NCs, the concentration of DCX that can be obtained with PEG-MAL – thiol gel was found to be 0.9 mg/mL (30% w/w NCs in the gel). Rivera-Rodriguez *et al.* reported the % EE of 75 – 90 % in poly-L-asparagine NCs (263). In another study, % EE of 90 % was observed by Lollo *et al.* in polyglutamic acid-PEG NCs (264). Both these studies have reported higher % EE than DCX NCs. However, it should be noted that the method of preparation of those NCs was solvent evaporation in contrast to self-emulsification that was used for preparation of the DCX NCs. Unlike self-emulsification, solvent evaporation technique involves repeated evaporation cycles, which concentrates the NCs. Self-emulsification is a simple manufacturing technique where evaporation is not required. Considering the maximum amount of hydrogel that can be administered to IP cavity of mice as 200 µL, the dose of DCX that can be

administered to mice (approx. 25 g body weight) through PEG-MAL – thiol gel was 7.2 mg/kg. Shimada *et al.* administered 8 mg/kg of DCX IP and demonstrated the pharmacokinetic advantage over IV administration (98). In another study by Yonemura *et al.*, DCX was IP administered at 8, 2 and 0.5 mg/kg doses to investigate the therapeutic effect on peritoneal dissemination of gastric cancer (265). They have reported median survival times of 90, 63 and 49.5 days in comparison to 32 days of control group. These studies suggest that the dose of DCX that can be delivered through PEG-MAL – thiol gel is sufficient to elicit significant therapeutic effect.

Table 4.7 Colloidal properties, % EE and drug loading of DCX loaded NCs. Data represented as mean ± SD (n = 3)

Sample	Size (nm)	PDI	Zeta potential (mV)	% EE	Drug loading (mg/mL)
DCX NCs	235 ± 20	0.2	-17 ± 2	45 ± 5	3.0 ± 0.3

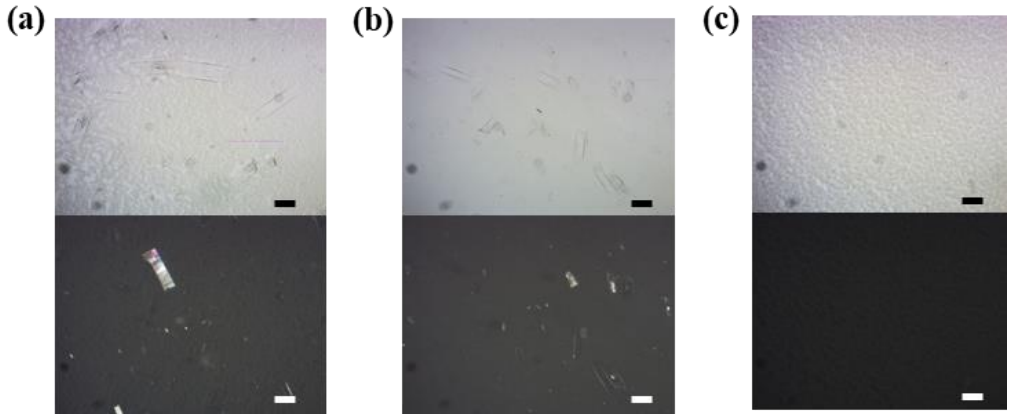


Figure 4.10 Optimization of DCX loading in NCs. Incorporation of DCX at (a) 12 mg/mL and (b) 7.5 mg/mL has shown recrystallization as seen by birefringence, while (c) 3 mg/mL did not show any recrystallization

4.3.4.2 In vitro release of DCX from DCX NCs

Once DCX NCs were optimized, *in vitro* release of DCX from DCX NCs loaded PEG-MAL – thiol gel was determined by incubating the gels in SIPF as described in section 4.2.4.5. 0.5 %w/v Tween® 80 was used to attain sink conditions in the media. Figure 4.11 shows the release profile of DCX from DCX NCs loaded PEG-MAL – thiol gel. Approximately 45 % of DCX was released from the gel within 48 h. However, as explained with DiR, the estimated release of DCX is the sum of free DCX and DCX bound to NCs. Isolation of DCX NCs from free DCX in the release media was not possible because of the instability of NCs upon centrifugation of media and binding tendency of DCX to dialysis membranes as explained in section 2.3.3.1. Hydrogels were still present in swollen state after 48 h, containing the remaining amount of DCX, as recovered by dissolving the gel in porcine esterase. Hence, it can be concluded that PEG-MAL – thiol gel has a control over the release of DCX also. Fan *et al.* explored the thermosensitive hydrogels prepared with polylactic acid (PLA)-Pluronic L35-PLA, containing DCX loaded nanoparticles for IP chemotherapy. This hydrogel was designed to form *in situ* through sol-gel transition. The nanoparticles were 100 – 140 nm diameter containing a tumour cell penetration enhancing peptide, LL37. The *in vitro* release profile obtained from this hydrogel has shown a cumulative release over > 20 days (129). However, they have employed dialysis tubing to determine the release of free DCX in contrast to our estimations, where the sum of free DCX and DCX NCs released from the hydrogel was reported. In our case, use of dialysis tubing has shown very high variation in release profile because of adherence of DCX to the dialysis tubing, yielding poor recovery (< 30 %). Although the techniques used to evaluate the *in vitro* release are different, we can still find that the PEG-MAL – thiol gel has a potential to control the release of chemotherapeutic agent DCX.

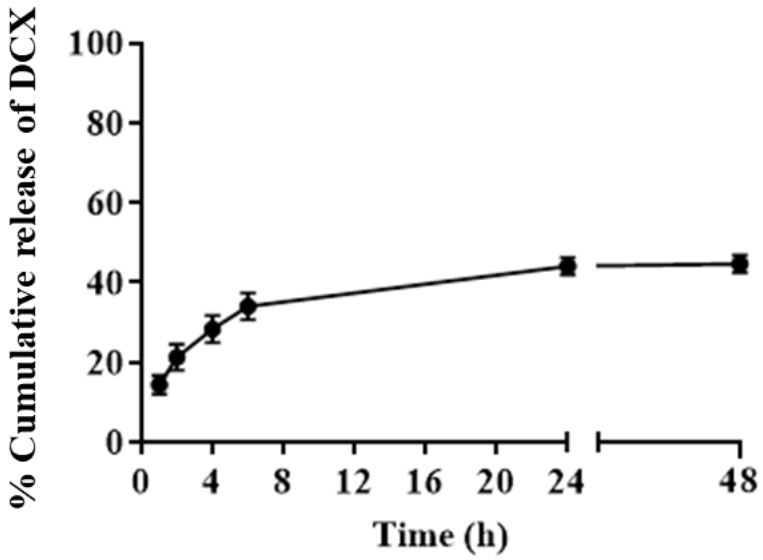


Figure 4.11 *In vitro* release study showing the release of DCX from PEG-MAL – thiol gel, as determined by extracting the DCX from the media, followed by HPLC analysis from each time point. Gels contain 10% w/w PEG-MAL and an equimolar concentration of PEG-SH, incubated under 1:25 dilution in SIPF at 37 ºC. Data represented as mean ± SD (n = 3)

4.4 Conclusions

In this chapter, covalently crosslinked hydrogels were developed to incorporate NCs. Branched 4-arm PEGs, PEG-NB and PEG-MAL were cross-linked with a linear PEG with thiol-end groups (PEG-SH). The reaction between PEG-NB and PEG-SH was a photocrosslinking reaction, mediated by a photoinitators LAP or Irgacure® 2959 in presence of UV. Alternatively, PEG-MAL and PEG-SH undergo Michael-type addition reaction to form covalent crosslinks through simple mixing. Both PEG-NB – thiol and PEG-MAL – thiol hydrogels were optimized to incorporate fluorescent DiR NCs. However, it was found that photoinitiators used to prepare PEG-NB – thiol gel were incompatible with DiR, as they reduced the fluorescence activity of the molecule. Hence, it was concluded that PEG-NB – thiol gel was not suitable to incorporate DiR NCs.

Alternatively, PEG-MAL – thiol gel successfully incorporated DiR NCs without degradation of DiR at pH 5. Hydrogels formed at two concentrations of PEG-MAL, 5 and 10% w/w, were initially evaluated for stability upon dilution at 1:25 in SIPF, which was found to be for 2 and 3 weeks respectively. An *in vitro* release study showed that 10% w/w PEG-MAL concentration showed better control over the release in comparison to its 5 %w/w equivalent, showing 45%

cumulative DiR release in 5 days. Hence, 10% w/w PEG-MAL concentration was selected to evaluate *in vivo* local residence and biodistribution of NCs from the PEG-MAL hydrogel.

IVIS® imaging study performed on immunodeficient nude mice, showed that PEG-MAL – thiol gel resided in the IP cavity between 24 h and 1 week, after implantation in the cavity through a surgical procedure. Complete degradation of the hydrogel was observed within a week highlighting the biodegradability of the formulation. Biodistribution of NCs has shown preferential accumulation in the liver, which is in accordance with the published literature. This *in vivo* study also demonstrated the tolerability of PEG-MAL hydrogel within the experimental timeframe.

As the IP residence of PEG-MAL – thiol gel was confirmed, DCX, a model chemotherapeutic agent was incorporated into NCs first, followed by incorporation of these NCs into the gel, which gave a therapeutically relevant final DCX concentration of 0.9 mg/mL. *In vitro* release study showed a cumulative DCX release of 45 % in 2 days, indicating that the hydrogel has shown control over the DCX release. In summary, this data establishes the potential residence of PEG-MAL – thiol gel in the IP cavity, and proves the capability of controlling the release of DCX. This opens the possibility of performing an *in vivo* efficacy study to evaluate the performance of DCX NCs loaded PEG-MAL – thiol gel in a peritoneal cancer bearing animal model.

Acknowledgements

Development of PEG-SH crosslinker and synthesis of PEG based hydrogels was performed in collaboration with Emanuele Russo[1], Rebeca Obenza Otero[1] and Mischa Zelzer[1]

Fluorescence assisted IVIS® imaging study for determination of *in vivo* local residence and biodistribution was performed in collaboration with Irene Golán Cancela[2] and José A. Costoya[2]

[1] School of Pharmacy, University of Nottingham, University park campus, Nottingham, United Kingdom, NG7 2RD

[2] Molecular oncology laboratory, Departamento de Fisioloxia, Facultade de Medicina and Centro de Investigación en Medicina Molecular y Enfermedades Crónicas (CiMUS), Instituto de investigación Sanitaria de Santiago de Compostela (IDIS), Universidade de Santiago de Compostela, Santiago de Compostela, 15706, Spain

5. Conclusions and Future work

5.1 Conclusions

Local drug delivery, achieved through administration of pharmacologically active compounds within a restricted area of the body or specific tissue, is advantageous for better drug accessibility and reduced side effects. The focus of this thesis is the local delivery in the management of osteoarthritis (OA) and peritoneal malignancies, using intra-articular (IA) and intra-peritoneal (IP) injections.

IA injections are not first-line treatments for OA. They are preferred as the last non-operative alternatives when oral or topical medications have failed to manage the pain or joint degeneration. Currently approved IA injections are either corticosteroids or hyaluronic acid (HA) injections. Despite the long history of clinical use and cost-effectiveness, IA administered corticosteroids are rapidly clear from the joint. The residence times of commonly used corticosteroids in the joint range from hours to a few days. Hence, various formulation strategies such as suspensions, hydrogels, nano, and microparticles have been employed to achieve longer retention and sustained release of IA injections. The particle size of the delivery system has been reported as one of the crucial factors for determining the extent of retention in the joint after IA injection. Smaller particles tend to escape from the cavity faster than the larger particles. Synovial macrophages tend to phagocytose the particles < 10 µm without eliciting neutrophil response, whereas microparticles > 10 µm tend to reside longer in the joint. However, efficacy of microparticles is limited by the release of the drug from the formulation, which is again dependent on the degradation of the polymer matrix. Once released, the drug molecules must penetrate into the local tissues such as synovium and cartilage in order to interact with local inflammatory cascade to elicit anti-inflammatory action. Microparticles cannot dictate the further interaction of drug molecules with the inflammatory cascade in the tissues. However, nanoparticles have the capability to penetrate into the synovial membrane and interact with tissue-associated inflammatory reactions. Hence, nanoparticles have also gained importance for IA drug delivery despite their relatively higher clearance rates. To overcome the

rapid clearance, nanoparticles have been incorporated into hydrogels to form composite systems for sustained release. Hence, in this study, we aimed to formulate a composite system of nanocapsules (NCs) loaded into a hydrogel.

In contrast to IA delivery, IP delivery is not routine practice in the clinic for peritoneal malignancies. Routine strategy for the treatment of these peritoneal malignancies is a cytoreductive surgery of macroscopic tumours, followed by perioperative or postoperative IV chemotherapy. It has been demonstrated that IP administration of chemotherapeutic drugs offers pharmacokinetic advantages in comparison to the IV route. Although no chemotherapeutic products are approved for IP administration, many compounds including, doxorubicin, fluorouracil, paclitaxel and platinum-based compounds have been explored for IP therapy. In the current clinical practice, IP administration is achieved by repeated instillation through catheters. These procedures involve perfusion of chemotherapeutic agents under hyperthermic conditions or pressurized aerosol pumps. It is extremely challenging to provide long-term repeated administrations through indwelling catheters, due to pain and infection-related problems for the patient. Moreover, peritoneal cavity is highly dynamic with high fluid turnover rates, which clears the small molecules rapidly from the joint. This challenge poses a need for developing sustained release chemotherapeutic formulations for IP delivery, which can avoid installation of catheters. Novel drug delivery systems, aimed at prolonging the duration of action of these agents were developed as hydrogels, micro or nanoparticles. Microparticles show relatively slow dissolution than nanoparticles because of their lower surface area to volume ratio. Moreover, they do not undergo phagocytosis and hence clearance from the cavity because of their relatively larger size. However, microparticles pose potential risks to form adhesions and inflammation in the peritoneal cavity. In contrast, nanoparticles do not cause peritoneal adhesions and they are relatively tunable to offer higher tumour penetration. However, nanoparticles can be rapidly cleared from peritoneal cavity through phagocytosis and fluid driven convective transport. Incorporation of nanoparticles in the hydrogel delays their clearance from the IP cavity, as the rate of release of nanoparticles into the cavity depends on the

degradation of the hydrogel. Hence, there is a need for exploring composite systems incorporated with nanoparticles, aiming for prolonged IP delivery.

5.1.1 Development of NCs-loaded hydrogel for IA delivery

To develop a composite formulation, polymeric nanocapsules (NCs) were first developed with hyaluronic acid (HA). Dexamethasone (DXM) was used as a model anti-inflammatory agent to incorporate into NCs. Two different approaches for the development of NCs, solvent displacement and self-emulsification, were evaluated for development and optimization of DXM NCs. Solvent displacement led to precipitation of DXM, while self-emulsification method yielded a DXM loading up to 6 mg/mL. During the optimization, the influence of molecular weight and concentration of HA on the particle size and drug loading of DXM NCs was studied. HA (40 kDa) was evaluated at 0.1, 0.25 and 0.5% w/w concentrations, while HA (700 kDa) was evaluated at 0.1% w/w. It was identified that HA (40 kDa) at 0.25% w/w formed relatively stable NCs in terms of particle size and drug loading. These DXM NCs were found to have a particle size, PDI and zeta potential of 250 ± 30 nm, 0.2 and -17 ± 3 mV respectively. DXM NCs were further characterized for *in vitro* release through centrifugation, gel chromatography columns and dialysis bags. However, none of these approaches were successful to reflect the release profile because of the instability of NCs during the experimental procedures or adherence of DXM to the dialysis membrane.

Once prepared and characterized, DXM NCs were incorporated into a hydrogel. Fn-HA gel, which was previously developed in our group, was selected to incorporate DXM NCs. The concentrations of fibrinogen and thrombin were optimized to incorporate at least 34% w/w of DXM NCs in order to meet the anti-inflammatory dose requirement of DXM (1 mg/kg). Further, DXM NCs-loaded Fn-HA gel was characterized for rheology and *in vitro* release studies. Oscillatory amplitude and frequency sweep tests performed on Fn-HA gel showed a viscoelastic behaviour. A crossover point of storage modulus (G') and loss modulus (G") was observed in osciallatory amplitude sweep study, at approximately 10% strain, indicating the mechanical breakdown of the gel. An *in vitro* release study performed on DXM NCs-loaded Fn-HA gel exhibited a DXM release of up to 70% in 48 h. However, the release obtained was an

additive of free DXM and DXM NCs, as isolation of DXM NCs from the media was not feasible. Hence, this release study was found to be reflective of gel degradation, rather than estimation of the release of free DXM.

After the development, characterization and *in vitro* evaluation, Fn-HA gel containing DXM NCs was evaluated for *in vivo* local residence and biodistribution studies using a radiolabel marker, ^{111}In. The radioactivity obtained from the knee joint with time showed that Fn-HA gel did not retain ^{111}InNCs as there was no difference in % ID values between ^{111}InNCs group and Fn-HA gel + ^{111}InNCs group. Biodistribution of ^{111}InNCs to the popliteal lymph nodes was observed after 6 h of IA administration, which indicated their preferential clearance through lymph duct openings in the synovial cavity. Further, a long and short-term anti-inflammatory efficacy study was performed in antigen induced arthritis (AIA) rats. We found that DXM did not show any beneficial anti-inflammatory activity, as observed from knee diameters and synovial histology. Failure to show anti-inflammatory activity was consistent with marketed DXM formulation, DXM NCs and Fn-HA gel containing DXM NCs. Developed formulation did not overcome the current challenge associated with ineffective steroid anti-inflammatory IA injections. However, its role in the management of prevention of disease progression and chronic arthritis is yet to be evaluated in suitable chronic and preventive care OA models respectively.

5.1.2 Development of NCs-loaded hydrogel for IP delivery

To further explore the potential of this formulation, another route of administration, IP delivery, was evaluated. Chapters 3 and 4 describes the development, optimization, and evaluation of NCs-loaded hydrogels for IP delivery. To evaluate the *in vivo* local residence and biodistribution of these hydrogels, IVIS® fluorescence imaging was chosen. Hence, a fluorescent dye, DiR, was incorporated into HA NCs. The incorporation of DiR reduced the size of NCs as a function of its concentration, which was attributed to its amphiphilic properties. As described in chapter 3, two different hydrogels, Fn-HA, and 2′-dC-*N*4-C_8 gels were optimized to incorporate 30% w/w of DiR NCs. Both Fn-HA and 2′-dC-*N*4-C_8 gels were not resistant to rapid dissolution at higher dilutions in SIPF. Rheology of 2′-dC-*N*4-C_8 gel has shown higher G' and G" values, indicating its higher mechanical properties over Fn-HA gel. However,

G' values of 2′-dC-*N*4-C_8 gel containing 30% w/w NCs were significantly lower than previously reported gels, which contain 2-8% w/v of NCs. Reduction in mechanical properties was attributed to the interaction between gelator and NCs. *In vitro* release studies suggest that the release of DiR was rapid from 2′-dC-*N*4-C_8 gel, showing a complete release in 24 h. Based on its proven *in vivo* tolerability, Fn-HA gel was chosen for *in vivo* study for the determination of *in vivo* local residence and biodistribution upon IP administration. Two pilot studies were performed in immunodeficient BALB/c nude mice to determine the optimum concentration of DiR for IVIS® imaging, which was found to be 5 ppm. A pivotal local residence and biodistribution study performed in 20 mice showed a strong fluorescence signal from the mice which have received DiR NCs and Fn-HA + DiR NCs up to 2 weeks, in contrast to DiR alone which was not traceable after 24 h. Upon sacrificing the mice after 2 weeks, the liver showed the highest fluorescence amongst the organs that were imaged. As IVIS® is a qualitative technique, where it was difficult to differentiate the fluorescence between the peritoneal cavity and the liver. However, based on the results obtained from *in vitro* release and resistance to dilution studies, it was highly unlikely that the Fn-HA gel could retain up to 2 weeks in the IP cavity. Hence, the fluorescence signal at 2 weeks time point was considered majorly from the liver, which was the most probably the uptake of NCs. Therefore, it was understood that combating the dynamic IP environment requires a robust hydrogel that is resistant to high dilutions and retains NCs for longer. Hence, hydrogels formed by covalent crosslinking were further developed and evaluated.

In chapter 4, covalently crosslinked hydrogels were developed with branched poly(ethylene glycol) (PEG) polymers, PEG-NB and PEG-MAL. A linear PEG (MW: 3350) was chemically modified to incorporate thiol-end groups to form PEG-SH, which can interact with PEG-NB and PEG-MAL to form covalent crosslinks. The reaction between PEG-NB and PEG-SH was a photocrosslinking reaction, mediated by photoinitators LAP or Irgacure® 2959 in presence of UV. Alternatively, PEG-MAL and PEG-SH undergo Michael-type addition reaction to form covalent crosslinks through simple mixing. Both PEG-NB – thiol and PEG-MAL – thiol hydrogels were optimized to incorporate

fluorescent DiR NCs. However, it was found that photoinitiators used to prepare PEG-NB – thiol gel were incompatible with DiR, as they reduced the fluorescence activity of the molecule. The reduction of UV exposure time from 5 min to 30 s did not prevent degradation of DiR. Hence, it was concluded that PEG-NB – thiol gel was not suitable to incorporate DiR NCs.

Alternatively, the PEG-MAL – thiol gel successfully incorporated DiR NCs without degradation of DiR. However, the formation of this hydrogel was influenced by pH of the media. Lower pH favoured the slower rate of reaction, which allowed homogeneous mixing of gel components, which would not happen at neutral or higher pH. Based on the colloidal stability of DiR NCs, pH 5.0 was selected as the optimum pH for the preparation of the hydrogel. Two concentrations of PEG-MAL, 5 and 10% w/w, were initially evaluated for stability upon dilution and NCs' release studies. Both 5 and 10% w/w concentrations were stable at 1:25 dilution in SIPF for 2 and 3 weeks respectively. *In vitro* release studies showed that 10% w/w PEG-MAL concentration had better control over the release in comparison to its 5 %w/w equivalent, showing 45% cumulative DiR release in 5 days. Hence, 10% w/w PEG-MAL concentration was selected to evaluate the *in vivo* local residence and biodistribution of NCs from the PEG-MAL hydrogel.

IVIS® imaging study performed on immunodeficient BALB/c nude mice showed that PEG-MAL – thiol gel resided in the IP cavity between 24 h and 1 week, after implantation in the cavity through a surgical procedure. Complete degradation of the hydrogel was observed within a week highlighting the biodegradability of the formulation. Biodistribution of NCs has shown preferential accumulation in the liver, which is in accordance with the published literature. This *in vivo* study also demonstrated the tolerability of PEG-MAL hydrogel within the experimental timeframe.

As the IP residence of PEG-MAL – thiol gel was confirmed, DCX, a model chemotherapeutic agent was incorporated into NCs first, followed by incorporation of these NCs into the gel. Incorporation of DCX NCs into the PEG-MAL – thiol gel yielded a final DCX concentration of 0.9 mg/mL, which would be sufficient to elicit a significant therapeutic effect. The *in vitro* release

study showed a cumulative DCX release of 45 % in 2 days, indicating that the hydrogel has shown control over the DCX release. In summary, this data establishes the potential residence of PEG-MAL – thiol gel in the IP cavity and proves the capability of controlling the release of DCX.

5.2 Future work

5.2.1 Further development & evaluation of DXM NCs-loaded Fn-HA gel

It was observed that DXM NCs loaded Fn-HA gel did not show expected anti-inflammatory efficacy against the AIA rat model. However, the nature of the animal model also influences the study outcomes. AIA is an acute inflammation model, which is considered to be highly aggressive on rat knees. Alternative models such as anterior cruciate ligament transection (ACLT) model and mechanical knee injury model are considered to be less aggressive than AIA (28, 266). These models might yield positive outcomes, as IA DXM is usually recommended for moderate stage rather than severe stage of OA. Another approach for further efficacy evaluation is through using the preventive care model, where IA therapy is administered along with the disease-inducing agent. This model represents the role of IA corticosteroids in prevention of disease progression. The clinical relevance of this model is the use of IA corticosteroids before advancing to moderate stage of the disease (267, 268).

Another possible development is to evaluate *in situ* forming covalently crosslinked hydrogels to incorporate DXM NCs. The knee joint is the weight-bearing joint characterized by high fluid turnover. Covalently cross-linked hydrogels are usually stable to high dilution caused by fluid turnover and mechanical forces provided by the body weight, as proven by commercial HA injections (269). Hence, we can expect a slow degradation profile and controlled release of NCs from these hydrogels. For example, covalently cross-linked HA gel can be synthesized by chemically modifying HA to attach aldehyde (HA-CHO) and dihydrazide (HA-ADH) functionality. HA-CHO and HA-ADH can form an *in situ* covalently cross-linked hydrogel upon mixing and IA administration (270). Molecular weights and concentrations of HA can be

optimized to incorporate DXM NCs. Being an HA hydrogel, it could also act as a viscosupplement to the joint.

5.2.2 Further development & evaluation of DCX NCs-loaded PEG-MAL – thiol gel

From chapter 5 it was observed that PEG-MAL – thiol gel retained in the peritoneal cavity between 1 – 7 days. It was implanted through surgical procedure, which is clinically relevant, as it is possible to implant the hydrogel after the tumour resection from the peritoneal cavity by the surgeon. However, further optimization of the hydrogel is feasible to further enhance the residence time in the cavity. For example, the molecular weights and concentrations of PEG-MAL and PEG-SH can be modified in order to obtain various mesh sizes that could control the release of chemotherapeutic agent from the hydrogel. There is a possibility to modify the cross-linker by altering the functional groups. For example, PEG-SH has two ester functionalities on either side of linear PEG, which could act as potential sites for degradation of the hydrogel through hydrolysis. The number of ester groups on the linear PEG-SH could be reduced to one, which could prolong the residence time in the cavity. Alteration of molecular weights, concentration and functional groups of the polymer and cross-linker would be helpful to customize the swellability and degradation rates of the resulting hydrogel.

As DCX NCs-loaded PEG-MAL – thiol gel showed its potential to control the release of DCX *in vitro*, it can be tested in a suitable peritoneal cancer-bearing animal model. Orthotropic cancer models are available for ovarian (271), gastric (272), pancreatic (273) and colon cancers (274). These cancers are generally highly dissociative and metastasize very rapidly. DCX NCs-loaded PEG-MAL – thiol gel could be surgically implanted in the peritoneal cavity of one of these models to evaluate the rate of tumour progression and survival. Moreover, a pharmacokinetic study can also be performed after IP administration in order to evaluate the area under curve of DCX in the peritoneal cavity and plasma. This study would be helpful to understand the potential of IP administration to reduce the systemic side effects of DCX. Moreover, the rate of clearance from the IP

cavity can also be estimated from this pharmacokinetic study, which would be helpful to identify the therapeutic window upon IP administration.

6. References

1. Wang Y, Kohane DS. External triggering and triggered targeting strategies for drug delivery. Nature Reviews Materials. 2017;2(6):1-14.
2. Wen H, Jung H, Li X. Drug delivery approaches in addressing clinical pharmacology-related issues: opportunities and challenges. The AAPS Journal. 2015;17(6):1327-1340.
3. Langer R. New methods of drug delivery. Science. 1990;249(4976):1527-1533.
4. Türker S, Onur E, Ózer Y. Nasal route and drug delivery systems. Pharmacy world and science. 2004;26(3):137-142.
5. Gaudana R, Ananthula HK, Parenky A, Mitra AK. Ocular drug delivery. The AAPS Journal. 2010;12(3):348-360.
6. Evans CH, Kraus VB, Setton LA. Progress in intra-articular therapy. Nature Reviews Rheumatology. 2014;10(1):11-22.
7. Bajaj G, Yeo Y. Drug delivery systems for intraperitoneal therapy. Pharmaceutical Research. 2010;27(5):735-738.
8. Narayanaswamy R, Torchilin VP. Hydrogels and their applications in targeted drug delivery. Molecules. 2019;24(3):603-621.
9. Sershen S, West J. Implantable, polymeric systems for modulated drug delivery. Advanced Drug Delivery Reviews. 2002;54(9):1225-1235.
10. Kanwar N, Sinha VR. In situ forming depots as sustained release drug delivery systems. Critical Reviews™ in Therapeutic Drug Carrier Systems. 2019;36(2):93-136.
11. Kohane DS. Microparticles and nanoparticles for drug delivery. Biotechnology and bioengineering. 2007;96(2):203-209.
12. Ji T, Kohane DS. Nanoscale systems for local drug delivery. Nano Today. 2019: DoI: 10.1016/j.nantod.2019.100765 (In press).
13. Buzea C, Pacheco II, Robbie K. Nanomaterials and nanoparticles: sources and toxicity. Biointerphases. 2007;2(4):MR17-MR71.
14. Weldon C, Ji T, Nguyen M-T, Rwei A, Wang W, Hao Y, Zhao C, Mehta M, Wang BY, Tsui J. Nanoscale Bupivacaine Formulations To Enhance the Duration and Safety of Intravenous Regional Anesthesia. ACS Nano. 2018;13(1):18-25.

15. Verma A, Stellacci F. Effect of surface properties on nanoparticle–cell interactions. Small. 2010;6(1):12-21.
16. Ruoslahti E. Peptides as targeting elements and tissue penetration devices for nanoparticles. Advanced Materials. 2012;24(28):3747-3756.
17. Boeneman K, Delehanty JB, Blanco-Canosa JB, Susumu K, Stewart MH, Oh E, Huston AL, Dawson G, Ingale S, Walters R. Selecting improved peptidyl motifs for cytosolic delivery of disparate protein and nanoparticle materials. ACS Nano. 2013;7(5):3778-3796.
18. El-Sherbiny IM, Villanueva DG, Herrera D, Smyth HD. Overcoming lung clearance mechanisms for controlled release drug delivery. In. Controlled pulmonary drug delivery: Springer; 2011. p. 101-126.
19. Date AA, Halpert G, Babu T, Ortiz J, Kanvinde P, Dimitrion P, Narayan J, Zierden H, Betageri K, Musmanno O. Mucus-penetrating budesonide nanosuspension enema for local treatment of inflammatory bowel disease. Biomaterials. 2018;185:97-105.
20. Kaldybekov DB, Filippov SK, Radulescu A, Khutoryanskiy VV. Maleimide-functionalised PLGA-PEG nanoparticles as mucoadhesive carriers for intravesical drug delivery. European Journal of Pharmaceutics and Biopharmaceutics. 2019;143:24-34.
21. Berrada M, Serreqi A, Dabbarh F, Owusu A, Gupta A, Lehnert S. A novel non-toxic camptothecin formulation for cancer chemotherapy. Biomaterials. 2005;26(14):2115-2120.
22. Palmese LL, Thapa RK, Sullivan MO, Kiick KL. Hybrid hydrogels for biomedical applications. Current Opinion in Chemical Engineering. 2019;24:143-157.
23. Lin Z, Gao W, Hu H, Ma K, He B, Dai W, Wang X, Wang J, Zhang X, Zhang Q. Novel thermo-sensitive hydrogel system with paclitaxel nanocrystals: High drug-loading, sustained drug release and extended local retention guaranteeing better efficacy and lower toxicity. Journal of Controlled Release. 2014;174:161-170.
24. Harper E, Dang W, Lapidus RG, Garver RI. Enhanced efficacy of a novel controlled release paclitaxel formulation (PACLIMER delivery

system) for local-regional therapy of lung cancer tumor nodules in mice. Clinical Cancer Research. 1999;5(12):4242-4248.

25. Chow AH, Tong HH, Chattopadhyay P, Shekunov BY. Particle engineering for pulmonary drug delivery. Pharmaceutical Research. 2007;24(3):411-437.
26. Ungaro F, d'Angelo I, Miro A, La Rotonda MI, Quaglia F. Engineered PLGA nano-and micro-carriers for pulmonary delivery: challenges and promises. Journal of Pharmacy and Pharmacology. 2012;64(9):1217-1235.
27. Stewart SA, Domínguez-Robles J, Donnelly RF, Larrañeta E. Implantable polymeric drug delivery devices: Classification, manufacture, materials, and clinical applications. Polymers. 2018;10(12):1379-1403.
28. Holyoak DT, Tian YF, van der Meulen MC, Singh A. Osteoarthritis: pathology, mouse models, and nanoparticle injectable systems for targeted treatment. Annals of Biomedical Engineering. 2016;44(6):2062-2075.
29. Woolf AD, Pfleger B. Burden of major musculoskeletal conditions. Bulletin of the World Health Organization. 2003;81:646-656.
30. Martín-Millán M, Castañeda S. Estrogens, osteoarthritis and inflammation. Joint Bone Spine. 2013;80(4):368-373.
31. Martini F. Anatomy and Physiology. Ed: 1; Pearson Education Inc., Singapore, 2006:189-208.
32. Onodera S, Suzuki K, Matsuno T, Kaneda K, Takagi M, Nishihira J. Macrophage migration inhibitory factor induces phagocytosis of foreign particles by macrophages in autocrine and paracrine fashion. Immunology. 1997;92(1):131-137.
33. Müller-Ladner U, Gay RE, Gay S. Cellular pathways of joint destruction. Current Opinion in Rheumatology. 1997;9(3):213-220.
34. Knight A, Levick J. Morphometry of the ultrastructure of the blood-joint barrier in the rabbit knee. Quarterly Journal of Experimental Physiology: Translation and Integration. 1984;69(2):271-288.

35. Goldring MB, Goldring SR. Articular cartilage and subchondral bone in the pathogenesis of osteoarthritis. Annals of the New York Academy of Sciences. 2010;1192(1):230-237.
36. Hunter DJ. Osteoarthritis. British Medical Journal. 2006;332:639-642.
37. Felson DT. Risk factors for osteoarthritis: understanding joint vulnerability. Clinical Orthopaedics and Related Research. 2004;427:S16-S21.
38. Kidd BL. Osteoarthritis and joint pain. Pain. 2006;123(1):6-9.
39. Fitzcharles MA, Almahrezi A, Shir Y. Pain: understanding and challenges for the rheumatologist. Arthritis & Rheumatism. 2005;52(12):3685-3692.
40. Ji R-R, Befort K, Brenner GJ, Woolf CJ. ERK MAP kinase activation in superficial spinal cord neurons induces prodynorphin and NK-1 upregulation and contributes to persistent inflammatory pain hypersensitivity. Journal of Neuroscience. 2002;22(2):478-485.
41. Sofat N, Ejindu V, Kiely P. What makes osteoarthritis painful? The evidence for local and central pain processing. Rheumatology. 2011;50(12):2157-2165.
42. Pontes-Quero GM, García-Fernández L, Aguilar MR, San Román J, Cano JP, Vázquez-Lasa B. Active viscosupplements for osteoarthritis treatment. Seminars in Arthritis and Rheumatism. 2019;49(2):171-183.
43. Knop E, de Paula LE, Fuller R. Platelet-rich plasma for osteoarthritis treatment. Revista Brasileira de Reumatologia (English Edition). 2016;56(2):152-164.
44. Ahmad Z, Howard D, Brooks RA, Wardale J, Henson F, Getgood A, Rushton N. The role of platelet rich plasma in musculoskeletal science. Journal of the Royal Society of Medicine Short Reports. 2012;3(6):1-9.
45. Harrison S, Vavken P, Kevy S, Jacobson M, Zurakowski D, Murray MM. Platelet activation by collagen provides sustained release of anabolic cytokines. The American Journal of Sports Medicine. 2011;39(4):729-734.
46. Hochberg MC, Altman RD, April KT, Benkhalti M, Guyatt G, Mcgowan J, Towheed T, Welch V, Wells G, Tugwell P.

Recommendations for the use of nonpharmacologic and pharmacologic therapies in osteoarthritis of the hand, hip, and knee. Arthritis Care & Research. 2012;64(4):455-474.

47. Jevsevar DS. Treatment of osteoarthritis of the knee: evidence-based guideline. JAAOS-Journal of the American Academy of Orthopaedic Surgeons. 2013;21(9):571-576.
48. Zhang W, Moskowitz R, Nuki G, Abramson S, Altman RD, Arden N, Bierma-Zeinstra S, Brandt K, Croft P, Doherty M. OARSI recommendations for the management of hip and knee osteoarthritis, Part II: OARSI evidence-based, expert consensus guidelines. Osteoarthritis and Cartilage. 2008;16(2):137-162.
49. Hollander JL, Brown EM, Jessar RA, Brown CY. Hydrocortisone and cortisone injected into arthritic joints: comparative effects of and use of hydrocortisone as a local antiarthritic agent. Journal of the American Medical Association. 1951;147(17):1629-1635.
50. Maudens P, Jordan O, Allémann E. Recent advances in intra-articular drug delivery systems for osteoarthritis therapy. Drug Discovery Today. 2018;23(10):1761-1775.
51. Rosen J, Sancheti P, Fierlinger A, Niazi F, Johal H, Bedi A. Cost-effectiveness of different forms of intra-articular injections for the treatment of osteoarthritis of the knee. Advances in Therapy. 2016;33(6):998-1011.
52. Losina E, Daigle ME, Suter L, Hunter D, Solomon D, Walensky R, Jordan J, Burbine SA, Paltiel AD, Katz JN. Disease-modifying drugs for knee osteoarthritis: can they be cost-effective? Osteoarthritis and Cartilage. 2013;21(5):655-667.
53. Jevsevar DS, Brown GA, Jones DL, Matzkin EG, Manner PA, Mooar P, Schousboe JT, Stovitz S, Sanders JO, Bozic KJ. The American Academy of Orthopaedic Surgeons evidence-based guideline on: treatment of osteoarthritis of the knee. The Journal of Bone and Joint Surgery. 2013;95(20):1885-1886.
54. Edwards SH. Intra-articular drug delivery: the challenge to extend drug residence time within the joint. The Veterinary Journal. 2011;190(1):15-21.

55. Schurman DJ, Kajiyama G. Antibiotic absorption from infected and normal joints using a rabbit knee joint model. Journal of Orthopaedic Research. 1985;3(2):185-188.
56. Park CW, Ma KW, Jang SW, Son M, Kang MJ. Comparison of piroxicam pharmacokinetics and anti-inflammatory effect in rats after intra-articular and intramuscular administration. Biomolecules & Therapeutics. 2014;22(3):260.
57. Owen S, Francis H, Roberts M. Disappearance kinetics of solutes from synovial fluid after intra-articular injection. British Journal of Clinical Pharmacology. 1994;38(4):349-355.
58. Wernecke C, Braun HJ, Dragoo JL. The effect of intra-articular corticosteroids on articular cartilage: a systematic review. Orthopaedic Journal of Sports Medicine. 2015;3(5):2325967115581163.
59. Clyne M. Pathogenesis of degenerative joint disease. Equine Veterinary Journal. 1987;19(1):15-18.
60. Nagaya H, Ymagata T, Ymagata S, Iyoda K, Ito H, Hasegawa Y, Iwata H. Examination of synovial fluid and serum hyaluronidase activity as a joint marker in rheumatoid arthritis and osteoarthritis patients (by zymography). Annals of the Rheumatic Diseases. 1999;58(3):186-188.
61. Zhong S, Campoccia D, Doherty P, Williams R, Benedetti L, Williams D. Biodegradation of hyaluronic acid derivatives by hyaluronidase. Biomaterials. 1994;15(5):359-365.
62. Maheu E, Bannuru RR, Herrero-Beaumont G, Allali F, Bard H, Migliore A. Why we should definitely include intra-articular hyaluronic acid as a therapeutic option in the management of knee osteoarthritis: results of an extensive critical literature review. Seminars in Arthritis and Rheumatism. 2019;48(4):563-572.
63. Creamer P. Intra-articular corticosteroid injections in osteoarthritis: do they work and if so, how? Annals of the Rheumatic Diseases. 1997;56(11):634-635.
64. Ho MJ, Kim SR, Choi YW, Kang MJ. Recent advances in intra-articular drug delivery systems to extend drug retention in joint. Journal of Pharmaceutical Investigation. 2019;49(1):9-15.

65. Kang ML, Im G-I. Drug delivery systems for intra-articular treatment of osteoarthritis. Expert Opinion on Drug Delivery. 2014;11(2):269-282.
66. Butoescu N, Jordan O, Doelker E. Intra-articular drug delivery systems for the treatment of rheumatic diseases: a review of the factors influencing their performance. European Journal of Pharmaceutics and Biopharmaceutics. 2009;73(2):205-218.
67. Wehling P, Evans C, Wehling J, Maixner W. Effectiveness of intra-articular therapies in osteoarthritis: a literature review. Therapeutic Advances in Musculoskeletal Disease. 2017;9(8):183-196.
68. Larsen C, Østergaard J, Larsen SW, Jensen H, Jacobsen S, Lindegaard C, Andersen PH. Intra-articular depot formulation principles: Role in the management of postoperative pain and arthritic disorders. Journal of Pharmaceutical Sciences. 2008;97(11):4622-4654.
69. Pradal J, Maudens P, Gabay C, Seemayer CA, Jordan O, Allémann E. Effect of particle size on the biodistribution of nano-and microparticles following intra-articular injection in mice. International Journal of Pharmaceutics. 2016;498(1-2):119-129.
70. Spitzer AI, Richmond JC, Kraus VB, Gomoll A, Jones DG, Huffman KM, Peterfy C, Cinar A, Lufkin J, Kelley SD. Safety and efficacy of repeat administration of triamcinolone acetonide extended-release in osteoarthritis of the knee: a phase 3b, open-label study. Rheumatology and Therapy. 2019;6(1):109-124.
71. Horisawa E, Kubota K, Tuboi I, Sato K, Yamamoto H, Takeuchi H, Kawashima Y. Size-dependency of DL-lactide/glycolide copolymer particulates for intra-articular delivery system on phagocytosis in rat synovium. Pharmaceutical Research. 2002;19(2):132-139.
72. Yang X, Du H, Zhai G. Progress in intra-articular drug delivery systems for osteoarthritis. Current Drug Targets. 2014;15(9):888-900.
73. Burt HM, Tsallas A, Gilchrist S, Liang LS. Intra-articular drug delivery systems: overcoming the shortcomings of joint disease therapy. Expert Opinion on Drug Delivery. 2009;6(1):17-26.

74. Periyasamy PC, Leijten JC, Dijkstra PJ, Karperien M, Post JN. Nanomaterials for the local and targeted delivery of osteoarthritis drugs. Journal of Nanomaterials. 2012;2012:5-18.
75. Morgen M, Tung D, Boras B, Miller W, Malfait A-M, Tortorella M. Nanoparticles for improved local retention after intra-articular injection into the knee joint. Pharmaceutical Research. 2013;30(1):257-268.
76. Kang M-L, Jeong S-Y, Im G-I. Hyaluronic acid hydrogel functionalized with self-assembled micelles of amphiphilic PEGylated kartogenin for the treatment of osteoarthritis. Tissue Engineering Part A. 2017;23(13-14):630-639.
77. Kim SR, Ho MJ, Kim SH, Cho HR, Kim HS, Choi YS, Choi YW, Kang MJ. Increased localized delivery of piroxicam by cationic nanoparticles after intra-articular injection. Drug Design, Development and Therapy. 2016;10:3779-3787.
78. Fernández MJA, Lopez DT, Rodriguez GR, Ampuero FAO, Lollo G, Lázaro TG, Fuentes MG. Nanocapsules with a polymer shell. 2016: US9415019B2.
79. Liakakos T, Thomakos N, Fine PM, Dervenis C, Young RL. Peritoneal adhesions: etiology, pathophysiology, and clinical significance. Digestive Surgery. 2001;18(4):260-273.
80. Yeo Y, Kohane DS. Polymers in the prevention of peritoneal adhesions. European Journal of Pharmaceutics and Biopharmaceutics. 2008;68(1):57-66.
81. Yeo Y, Adil M, Bellas E, Astashkina A, Chaudhary N, Kohane DS. Prevention of peritoneal adhesions with an in situ cross-linkable hyaluronan hydrogel delivering budesonide. Journal of Controlled Release. 2007;120(3):178-185.
82. Siegel R, Ma J, Zou Z, Jemal A. Cancer statistics, 2014. CA: a Cancer Journal for Clinicians. 2014;64(1):9-29.
83. Ceelen WP, Flessner MF. Intraperitoneal therapy for peritoneal tumors: biophysics and clinical evidence. Nature Reviews Clinical Oncology. 2010;7(2):108-115.

84. Siegel R, Jemal A. Cancer facts & figures 2014. American Cancer Society. 2014;1-68.
85. Sadeghi B, Arvieux C, Glehen O, Beaujard AC, Rivoire M, Baulieux J, Fontaumard E, Brachet A, Caillot JL, Faure JL. Peritoneal carcinomatosis from non-gynecologic malignancies: Results of the EVOCAPE 1 multicentric prospective study. Cancer: Interdisciplinary International Journal of the American Cancer Society. 2000;88(2):358-363.
86. Jayne D, Fook S, Loi C, Seow-Choen F. Peritoneal carcinomatosis from colorectal cancer. British Journal of Surgery. 2002;89(12):1545-1550.
87. Senger DR. Vascular endothelial growth factor: much more than an angiogenesis factor. Molecular Biology of the Cell. 2010;21(3):377-379.
88. Senger DR, Galli SJ, Dvorak AM, Perruzzi CA, Harvey VS, Dvorak HF. Tumor cells secrete a vascular permeability factor that promotes accumulation of ascites fluid. Science. 1983;219(4587):983-985.
89. Feldman GB, Knapp RC, Order SE, Hellman S. The role of lymphatic obstruction in the formation of ascites in a murine ovarian carcinoma. Cancer Research. 1972;32(8):1663-1666.
90. Group GM-aTG. Chemotherapy in adult high-grade glioma: a systematic review and meta-analysis of individual patient data from 12 randomised trials. The Lancet. 2002;359(9311):1011-1018.
91. Bijelic L, Yan TD, Sugarbaker PH. Failure analysis of recurrent disease following complete cytoreduction and perioperative intraperitoneal chemotherapy in patients with peritoneal carcinomatosis from colorectal cancer. Annals of Surgical Oncology. 2007;14(8):2281-2288.
92. Glehen O, Kwiatkowski F, Sugarbaker P, Elias D, Levine E, De Simone M, Barone R, Yonemura Y, Cavaliere F, Quenet F. Cytoreductive surgery combined with perioperative intraperitoneal chemotherapy for the management of peritoneal carcinomatosis from colorectal cancer: a multi-institutional study. Journal of Clinical Oncology. 2004;22(16):3284-3292.

93. Sugarbaker PH. Intraperitoneal chemotherapy and cytoreductive surgery for the prevention and treatment of peritoneal carcinomatosis and sarcomatosis. Seminars in Surgical Oncology. 1998;14:254-261.
94. Armstrong DK, Bundy B, Wenzel L, Huang HQ, Baergen R, Lele S, Copeland LJ, Walker JL, Burger RA. Intraperitoneal cisplatin and paclitaxel in ovarian cancer. New England Journal of Medicine. 2006;354(1):34-43.
95. Flessner MF. The transport barrier in intraperitoneal therapy. American Journal of Physiology-Renal Physiology. 2005;288(3):F433-F442.
96. Van der Speeten K, Stuart OA, Sugarbaker PH. Pharmacokinetics and pharmacodynamics of perioperative cancer chemotherapy in peritoneal surface malignancy. The Cancer Journal. 2009;15(3):216-224.
97. Dedrick RL, Myers CE, Bungay PM, DeVita V. Pharmacokinetic rationale for peritoneal drug administration. Cancer Treatment Reports. 1978;62:1-13.
98. Shimada T, Nomura M, Yokogawa K, Endo Y, Sasaki T, Miyamoto Ki, Yonemura Y. Pharmacokinetic advantage of intraperitoneal injection of docetaxel in the treatment for peritoneal dissemination of cancer in mice. Journal of Pharmacy and Pharmacology. 2005;57(2):177-181.
99. Mohamed F, Marchettini P, Stuart OA, Sugarbaker PH. Pharmacokinetics and tissue distribution of intraperitoneal paclitaxel with different carrier solutions. Cancer Chemotherapy and Pharmacology. 2003;52(5):405-410.
100. Li X-F, Carlin S, Urano M, Russell J, Ling CC, O'Donoghue JA. Visualization of hypoxia in microscopic tumors by immunofluorescent microscopy. Cancer Research. 2007;67(16):7646-7653.
101. Jacquet P, Averbach A, Stuart OA, Chang D, Sugarbaker PH. Hyperthermic intraperitoneal doxorubicin: pharmacokinetics, metabolism, and tissue distribution in a rat model. Cancer Chemotherapy and Pharmacology. 1997;41(2):147-154.
102. Harada S, Ping L, Obara T, Oikawa H, Miyata M, Matsuo M, Takahashi T, Yanagisawa T. The antitumor effect of hyperthermia

combined with fluorouracil and its analogues. Radiation Research. 1995;142(2):232-241.

103. Kuh H-J, Jang SH, Wientjes MG, Weaver JR, Au JL-S. Determinants of paclitaxel penetration and accumulation in human solid tumor. Journal of Pharmacology and Experimental Therapeutics. 1999;290(2):871-880.

104. Van de Vaart P, Van der Vange N, Zoetmulder F, Van Goethem A, Van Tellingen O, ten Bokkel Huinink W, Beijnen J, Bartelink H, Begg A. Intraperitoneal cisplatin with regional hyperthermia in advanced ovarian cancer: pharmacokinetics and cisplatin–DNA adduct formation in patients and ovarian cancer cell lines. European Journal of Cancer. 1998;34(1):148-154.

105. Dakwar GR, Shariati M, Willaert W, Ceelen W, De Smedt SC, Remaut K. Nanomedicine-based intraperitoneal therapy for the treatment of peritoneal carcinomatosis—Mission possible? Advanced Drug Delivery Reviews. 2017;108:13-24.

106. Walker JL, Armstrong DK, Huang HQ, Fowler J, Webster K, Burger RA, Clarke-Pearson D. Intraperitoneal catheter outcomes in a phase III trial of intravenous versus intraperitoneal chemotherapy in optimal stage III ovarian and primary peritoneal cancer: a Gynecologic Oncology Group Study. Gynecologic Oncology. 2006;100(1):27-32.

107. Hasovits C, Clarke S. Pharmacokinetics and pharmacodynamics of intraperitoneal cancer chemotherapeutics. Clinical Pharmacokinetics. 2012;51(4):203-224.

108. Dedrick RL, Flessner MF. Pharmacokinetic problems in peritoneal drug administration: tissue penetration and surface exposure. Journal of the National Cancer Institute. 1997;89(7):480-487.

109. Esquivel J. Current status of colorectal cancer with peritoneal carcinomatosis. Annals of Surgical Oncology. 2010;17(7):1968-1969.

110. Flessner M, Fenstermacher J, Blasberg R, Dedrick R. Peritoneal absorption of macromolecules studied by quantitative autoradiography. American Journal of Physiology-Heart and Circulatory Physiology. 1985;248(1):H26-H32.

111. Ellam T, Wilkie M. Peritoneal dialysis. Medicine. 2015;43(8):484-488.

112. Figueiredo A, Goh B-L, Jenkins S, Johnson DW, Mactier R, Ramalakshmi S, Shrestha B, Struijk D, Wilkie M. Clinical practice guidelines for peritoneal access. Peritoneal Dialysis International. 2010;30(4):424-429.
113. Kipps E, Tan DS, Kaye SB. Meeting the challenge of ascites in ovarian cancer: new avenues for therapy and research. Nature Reviews Cancer. 2013;13(4):273-282.
114. Kohane DS, Tse JY, Yeo Y, Padera R, Shubina M, Langer R. Biodegradable polymeric microspheres and nanospheres for drug delivery in the peritoneum. Journal of Biomedical Materials Research Part A: An Official Journal of The Society for Biomaterials, The Japanese Society for Biomaterials, and The Australian Society for Biomaterials and the Korean Society for Biomaterials. 2006;77(2):351-361.
115. Tsai M, Lu Z, Wang J, Yeh T-K, Wientjes MG, Au JL-S. Effects of carrier on disposition and antitumor activity of intraperitoneal paclitaxel. Pharmaceutical Research. 2007;24(9):1691-1701.
116. Hirano K, Hunt CA. Lymphatic transport of liposome-encapsulated agents: effects of liposome size following intraperitoneal administration. Journal of Pharmaceutical Sciences. 1985;74(9):915-921.
117. Shih W, Coupal J, Chia H. Communication between peritoneal cavity and mediastinal lymph nodes demonstrated by Tc-99m albumin nanocolloid intraperitoneal injection. Proceedings of the National Science Council, Republic of China Part B, Life sciences. 1993;17(3):103-105.
118. Kohane DS, Langer R. Biocompatibility and drug delivery systems. Chemical Science. 2010;1(4):441-446.
119. Ernsting MJ, Murakami M, Roy A, Li S-D. Factors controlling the pharmacokinetics, biodistribution and intratumoral penetration of nanoparticles. Journal of Controlled Release. 2013;172(3):782-794.
120. Huo S, Ma H, Huang K, Liu J, Wei T, Jin S, Zhang J, He S, Liang X-J. Superior penetration and retention behavior of 50 nm gold nanoparticles in tumors. Cancer Research. 2013;73(1):319-330.

121. Simón-Gracia L, Hunt H, Scodeller PD, Gaitzsch J, Braun GB, Willmore A-MA, Ruoslahti E, Battaglia G, Teesalu T. Paclitaxel-loaded polymersomes for enhanced intraperitoneal chemotherapy. Molecular Cancer Therapeutics. 2016;15(4):670-679.
122. Nguyen MK, Lee DS. Injectable biodegradable hydrogels. Macromolecular Bioscience. 2010;10(6):563-579.
123. Pereira RF, Bártolo PJ. Photopolymerizable hydrogels in regenerative medicine and drug delivery. Hot Topics in Biomaterials. 2014;6-28.
124. Wang Y, Gong C, Yang L, Wu Q, Shi S, Shi H, Qian Z, Wei Y. 5-FU-hydrogel inhibits colorectal peritoneal carcinomatosis and tumor growth in mice. BMC Cancer. 2010;10(1):402-409.
125. Bajaj G, Kim MR, Mohammed SI, Yeo Y. Hyaluronic acid-based hydrogel for regional delivery of paclitaxel to intraperitoneal tumors. Journal of Controlled Release. 2012;158(3):386-392.
126. Sun B, Taha MS, Ramsey B, Torregrosa-Allen S, Elzey BD, Yeo Y. Intraperitoneal chemotherapy of ovarian cancer by hydrogel depot of paclitaxel nanocrystals. Journal of Controlled Release. 2016;235:91-98.
127. Bae WK, Park MS, Lee JH, Hwang JE, Shim HJ, Cho SH, Kim D-E, Ko HM, Cho C-S, Park I-K. Docetaxel-loaded thermoresponsive conjugated linoleic acid-incorporated poloxamer hydrogel for the suppression of peritoneal metastasis of gastric cancer. Biomaterials. 2013;34(4):1433-1441.
128. Xu S, Fan H, Yin L, Zhang J, Dong A, Deng L, Tang H. Thermosensitive hydrogel system assembled by PTX-loaded copolymer nanoparticles for sustained intraperitoneal chemotherapy of peritoneal carcinomatosis. European Journal of Pharmaceutics and Biopharmaceutics. 2016;104:251-259.
129. Fan R, Tong A, Li X, Gao X, Mei L, Zhou L, Zhang X, You C, Guo G. Enhanced antitumor effects by docetaxel/LL37-loaded thermosensitive hydrogel nanoparticles in peritoneal carcinomatosis of colorectal cancer. International Journal of Nanomedicine. 2015;10:7291-7305.
130. Cho EJ, Sun B, Doh K-O, Wilson EM, Torregrosa-Allen S, Elzey BD, Yeo Y. Intraperitoneal delivery of platinum with in-situ crosslinkable

hyaluronic acid gel for local therapy of ovarian cancer. Biomaterials. 2015;37:312-319.

131. Zhang Z, Wei X, Gao J, Zhao Y, Zhao Y, Guo L, Chen C, Duan Z, Li P, Wei L. Intra-articular injection of cross-linked hyaluronic acid-dexamethasone hydrogel attenuates osteoarthritis: an experimental study in a rat model of osteoarthritis. International Journal of Molecular Sciences. 2016;17(4):411-425.

132. Petit A. *In situ* forming hydrogels for intra-articular delivery of celecoxib: from polymer design to *in vivo* studies. Utrecht University; 2014.

133. Li Y, Meng H, Liu Y, Lee BP. Fibrin gel as an injectable biodegradable scaffold and cell carrier for tissue engineering. The Scientific World Journal. 2015;685690:1-10.

134. Janmey PA, Winer JP, Weisel JW. Fibrin gels and their clinical and bioengineering applications. Journal of the Royal Society Interface. 2008;6(30):1-10.

135. Kirilak Y, Pavlos NJ, Willers CR, Han R, Feng H, Xu J, Asokananthan N, Stewart GA, Henry P, Wood D. Fibrin sealant promotes migration and proliferation of human articular chondrocytes: possible involvement of thrombin and protease-activated receptors. International Journal of Molecular Medicine. 2006;17(4):551-558.

136. Lee F, Kurisawa M. Formation and stability of interpenetrating polymer network hydrogels consisting of fibrin and hyaluronic acid for tissue engineering. Acta Biomaterialia. 2013;9(2):5143-5152.

137. Lei Y, Rahim M, Ng Q, Segura T. Hyaluronic acid and fibrin hydrogels with concentrated DNA/PEI polyplexes for local gene delivery. Journal of Controlled Release. 2011;153(3):255-261.

138. Zhang Y, Heher P, Hilborn J, Redl H, Ossipov DA. Hyaluronic acid-fibrin interpenetrating double network hydrogel prepared in situ by orthogonal disulfide cross-linking reaction for biomedical applications. Acta Biomaterialia. 2016;38:23-32.

139. Urban MCC, Mainardes RM, Gremião MPD. Development and validation of HPLC method for analysis of dexamethasone acetate in

microemulsions. Brazilian Journal of Pharmaceutical Sciences. 2009;45(1):87-92.

140. Marques MR, Loebenberg R, Almukainzi M. Simulated biological fluids with possible application in dissolution testing. Dissolution Technologies. 2011;18(3):15-28.

141. Riveiro-Naveira RR, Valcarcel-Ares MN, Almonte-Becerril M, Vaamonde-García C, Loureiro J, Hermida-Carballo L, López-Peláez E, Blanco FJ, Lopez-Armada MJ. Resveratrol lowers synovial hyperplasia, inflammatory markers and oxidative damage in an acute antigen-induced arthritis model. Rheumatology. 2016;55(10):1889-1900.

142. Benito MJ, Sánchez-Pernaute O, José López-Armada M, Hernández P, Palacios I, Egido J, Herrero-Beaumont G. Cyclosporin A prevents the histologic damage of antigen arthritis without inducing fibrosis. Arthritis & Rheumatism: Official Journal of the American College of Rheumatology. 2000;43(2):311-319.

143. El-Hakim I, Abdel-Hamid I, Bader A. Tempromandibular joint (TMJ) response to intra-articular dexamethasone injection following mechanical arthropathy: a histological study in rats. International Journal of Oral and Maxillofacial Surgery. 2005;34(3):305-310.

144. Son AR, Park SH, Jang JY, Kim K, Kim BJ, Yin XY, Kim JH, Min BH, Han DK, Kim MS. Direct chemotherapeutic dual drug delivery through intra-articular injection for synergistic enhancement of rheumatoid arthritis treatment. Scientific Reports. 2015;5:14713.

145. Heard BJ, Barton KI, Chung M, Achari Y, Shrive NG, Frank CB, Hart DA. Single intra-articular dexamethasone injection immediately post-surgery in a rabbit model mitigates early inflammatory responses and post-traumatic osteoarthritis-like alterations. Journal of Orthopaedic Research. 2015;33(12):1826-1834.

146. Storozhylova N. New potential nanotechnology-based therapies for the tratment of rheumatoid arthritis. Université de Nantes; 2018.

147. Staff RH, Landfester K, Crespy D. Recent advances in the emulsion solvent evaporation technique for the preparation of nanoparticles and nanocapsules. Advances in Polymer Science. 2013;262:329-344.

148. Gonzalo T, Lollo G, Garcia-Fuentes M, Torres D, Correa J, Riguera R, Fernandez-Megia E, Calvo P, Avilés P, Guillén MJ. A new potential nano-oncological therapy based on polyamino acid nanocapsules. Journal of Controlled Release. 2013;169(1-2):10-16.

149. Abellan-Pose R, Teijeiro-Valiño C, Santander-Ortega MJ, Borrajo E, Vidal A, Garcia-Fuentes M, Csaba N, Alonso MJ. Polyaminoacid nanocapsules for drug delivery to the lymphatic system: effect of the particle size. International Journal of Pharmaceutics. 2016;509(1-2):107-117.

150. Kohli K, Chopra S, Dhar D, Arora S, Khar RK. Self-emulsifying drug delivery systems: an approach to enhance oral bioavailability. Drug Discovery Today. 2010;15(21-22):958-965.

151. Moghimipour E, Salimi A, Karami M, Isazadeh S. Preparation and characterization of dexamethasone microemulsion based on pseudoternary phase diagram. Jundishapur Journal of Natural Pharmaceutical Products. 2013;8(3):105.

152. Macfarlane R. An enzyme cascade in the blood clotting mechanism and its function as a biochemical amplifier. Nature. 1964;202(4931):498-499.

153. Breen A, O'Brien T, Pandit A. Fibrin as a delivery system for therapeutic drugs and biomolecules. Tissue Engineering Part B: Reviews. 2009;15(2):201-214.

154. Zhou W, Zhao M, Zhao Y, Mou Y. A fibrin gel loaded with chitosan nanoparticles for local delivery of rhEGF: preparation and *in vitro* release studies. Journal of Materials Science: Materials in Medicine. 2011;22(5):1221-1230.

155. Losi P, Briganti E, Errico C, Lisella A, Sanguinetti E, Chiellini F, Soldani G. Fibrin-based scaffold incorporating VEGF-and bFGF-loaded nanoparticles stimulates wound healing in diabetic mice. Acta Biomaterialia. 2013;9(8):7814-7821.

156. Furmaniak-Kazmierczak E, Cooke T, Manuel R, Scudamore A, Hoogendorn H, Giles AR, Nesheim M. Studies of thrombin-induced proteoglycan release in the degradation of human and bovine cartilage. Journal of Clinical Investigation. 1994;94(2):472-480.

157. Chiu Y-C, Fong Y-C, Lai C-H, Hung C-H, Hsu H-C, Lee T-S, Yang R-S, Fu W-M, Tang C-H. Thrombin-induced IL-6 production in human synovial fibroblasts is mediated by PAR1, phospholipase C, protein kinase Cα, c-Src, NF-kappaB and p300 pathway. Molecular Immunology. 2008;45(6):1587-1599.
158. Ghosh K, Shu XZ, Mou R, Lombardi J, Prestwich GD, Rafailovich MH, Clark RA. Rheological characterization of *in situ* cross-linkable hyaluronan hydrogels. Biomacromolecules. 2005;6(5):2857-2865.
159. Barnes HA, Hutton JF, Walters K. An introduction to rheology, Elsevier Science Publishers B.V, Amsterdam, 1989:37-54.
160. Borzacchiello A, Ambrosio L. Structure-property relationships in Hydrogels. Springer, Milano, 2009:9-20.
161. Modi S, Anderson BD. Determination of drug release kinetics from nanoparticles: overcoming pitfalls of the dynamic dialysis method. Molecular Pharmaceutics. 2013;10(8):3076-3089.
162. Xie L, Beyer S, Vogel V, Wacker MG, Mäntele W. Assessing the drug release from nanoparticles: Overcoming the shortcomings of dialysis by using novel optical techniques and a mathematical model. International Journal of Pharmaceutics. 2015;488(1-2):108-119.
163. Nair C, Shah G, Dhall D. Effect of temperature, pH and ionic strength and composition on fibrin network structure and its development. Thrombosis Research. 1986;42(6):809-816.
164. Chiu CL, Hecht V, Duong H, Wu B, Tawil B. Permeability of three-dimensional fibrin constructs corresponds to fibrinogen and thrombin concentrations. BioResearch Open Access. 2012;1(1):34-40.
165. de Barros AB, Tsourkas A, Saboury B, Cardoso VN, Alavi A. Emerging role of radiolabeled nanoparticles as an effective diagnostic technique. EJNMMI Research. 2012;2(1):39-54.
166. Kamkaew A, Ehlerding EB, Cai W. Nanoparticles as Radiopharmaceutical Vectors: Radiopharmaceutical Chemistry, Springer, Cham; 2019: 181-203.
167. Ocampo-García B, Gibbens-Bandala B, Morales-Avila E, Melendez-Alafort L, Khoobchandani M, Trujillo-Nolasco M, Katti KV. Dual-Targeted Therapy and Molecular Imaging with Radiolabeled

Nanoparticles: Biotechnology Products in Everyday Life, Springer Cham, 2019: 201-219.

168. Edwards SH, Cake MA, Spoelstra G, Read RA. Biodistribution and clearance of intra-articular liposomes in a large animal model using a radiographic marker. Journal of Liposome Research. 2007;17(3-4):249-261.

169. Abellan-Pose R, Rodríguez-Évora M, Vicente S, Csaba N, Évora C, Alonso MJ, Delgado A. Biodistribution of radiolabeled polyglutamic acid and PEG-polyglutamic acid nanocapsules. European Journal of Pharmaceutics and Biopharmaceutics. 2017;112:155-163.

170. Torchilin VP, Trubetskoy VS, Wolf GL. Amphipathic polychelating compounds and methods of use.1996;US5534241A.

171. Castronovo Jr FP, Wagner Jr HN. Comparative toxicity and pharmacodynamics of ionic indium chloride and hydrated indium oxide. Journal of Nuclear Medicine. 1973;14(9):677-682.

172. von Lospichl B, Hemmati-Sadeghi S, Dey P, Dehne T, Haag R, Sittinger M, Ringe J, Gradzielski M. Injectable hydrogels for treatment of osteoarthritis–A rheological study. Colloids and Surfaces B: Biointerfaces. 2017;159:477-483.

173. Ahmed TA, Griffith M, Hincke M. Characterization and Inhibition of Fibrin Hydrogel–Degrading Enzymes During Development of Tissue Engineering Scaffolds. Tissue Engineering. 2007;13(7):1469-1477.

174. Gonen-Wadmany M, Oss-Ronen L, Seliktar D. Protein–polymer conjugates for forming photopolymerizable biomimetic hydrogels for tissue engineering. Biomaterials. 2007;28(26):3876-3886.

175. Billinghurst R, Fretz P, Gordon J. Induction of intra-articular tumour necrosis factor during acute inflammatory responses in equine arthritis. Equine Veterinary Journal. 1995;27(3):208-216.

176. Haywood L, Walsh D. Vasculature of the normal and arthritic synovial joint. Histology and Histopathology. Universidad de Murica; 2001.

177. Kennedy A, Fearon U, Veale DJ, Godson C. Macrophages in synovial inflammation. Frontiers in Immunology. 2011;2:52-61.

178. Winter CA, Nuss GW. Treatment of adjuvant arthritis in rats with anti-inflammatory drugs. Arthritis & Rheumatism: Official Journal of the American College of Rheumatology. 1966;9(3):394-404.
179. Elron-Gross I, Glucksam Y, Margalit R. Liposomal dexamethasone–diclofenac combinations for local osteoarthritis treatment. International Journal of Pharmaceutics. 2009;376(1-2):84-91.
180. Otterness I, Pazoles P, Moore P, Pepys M. C-reactive protein as an index of disease activity. Comparison of tenidap, cyclophosphamide and dexamethasone in rat adjuvant arthritis. The Journal of Rheumatology. 1991;18(4):505-511.
181. Čeponis A, Waris E, Mönkkönen J, Laasonen L, Hyttinen M, Solovieva SA, Hanemaaijer R, Bitsch A, Konttinen YT. Effects of low-dose, noncytotoxic, intraarticular liposomal clodronate on development of erosions and proteoglycan loss in established antigen-induced arthritis in rabbits. Arthritis & Rheumatism. 2001;44(8):1908-1916.
182. Schade R, Göhler K, Bürger W, Hirschelmann R. Modulation of rat C-reactive protein serum level by dexamethasone and adrenaline-comparison with the response of α 2 phase globulin. Agents and Actions. 1987;22(3-4):280-287.
183. Yang B, Gong C, Qian Z, Zhao X, Li Z, Qi X, Zhou S, Zhong Q, Luo F, Wei Y. Prevention of post-surgical abdominal adhesions by a novel biodegradable thermosensitive PECE hydrogel. BMC biotechnology. 2010;10(1):65-73.
184. Yang B, Gong C, Zhao X, Zhou S, Li Z, Qi X, Zhong Q, Luo F, Qian Z. Preventing postoperative abdominal adhesions in a rat model with PEG-PCL-PEG hydrogel. International Journal of Nanomedicine. 2012;7:547-557.
185. Yeo Y, Highley CB, Bellas E, Ito T, Marini R, Langer R, Kohane DS. In situ cross-linkable hyaluronic acid hydrogels prevent post-operative abdominal adhesions in a rabbit model. Biomaterials. 2006;27(27):4698-4705.
186. Ward BC, Panitch A. Abdominal adhesions: current and novel therapies. Journal of Surgical Research. 2011;165(1):91-111.

187. Markman M, Walker JL. Intraperitoneal chemotherapy of ovarian cancer: a review, with a focus on practical aspects of treatment. Journal of clinical oncology. 2006;24(6):988-994.
188. Chan DL, Morris DL, Rao A, Chua TC. Intraperitoneal chemotherapy in ovarian cancer: a review of tolerance and efficacy. Cancer Management and Research. 2012;4:413-422.
189. Yan TD, Cao CQ, Munkholm-Larsen S. A pharmacological review on intraperitoneal chemotherapy for peritoneal malignancy. World journal of Gastrointestinal Oncology. 2010;2(2):109-116.
190. Lengyel E. Ovarian cancer development and metastasis. The American Journal of Pathology. 2010;177(3):1053-1064.
191. Le T, Krepart G, Lotocki R, Heywood M. Does debulking surgery improve survival in biologically aggressive ovarian carcinoma? Gynecologic Oncology. 1997;67(2):208-214.
192. Jacquet P, Sugarbaker PH. Peritoneal-plasma barrier. Peritoneal carcinomatosis: principles of management. Springer, Boston, MA. 1996:53-63.
193. Mikkelsen MS, Christiansen T, Petersen LK, Blaakaer J, Iversen LH. Morbidity after cytoreductive surgery and hyperthermic intraperitoneal chemotherapy with carboplatin used for ovarian, tubal, and primary peritoneal cancer. Journal of Surgical Oncology. 2019;120(3):550-557.
194. Hurst D, Owusu-Agyemang P. Perioperative Management of the Oncologic Patient Undergoing Cytoreductive Surgery with Hyperthermic Intraperitoneal Chemotherapy (HIPEC). Oncologic Critical Care. 2019:1-9.
195. Horvath P, Yurttas C, Struller F, Bösmüller H, Lauer UM, Nadalin S, Königsrainer A, Reymond MA. Pressurized Intraperitoneal Aerosol Chemotherapy (PIPAC) for Peritoneal Metastases in Solid Organ Graft Recipients: First Experience. Annals of Transplantation. 2019;24:30-35.
196. Horvath P, Beckert S, Struller F, Königsrainer A, Reymond MA. Pressurized intraperitoneal aerosol chemotherapy (PIPAC) for peritoneal metastases of pancreas and biliary tract cancer. Clinical & Experimental Metastasis. 2018;35(7):635-640.

197. Amoozgar Z, Wang L, Brandstoetter T, Wallis SS, Wilson EM, Goldberg MS. Dual-layer surface coating of PLGA-based nanoparticles provides slow-release drug delivery to achieve metronomic therapy in a paclitaxel-resistant murine ovarian cancer model. Biomacromolecules. 2014;15(11):4187-4194.
198. Yang K, Gong H, Shi X, Wan J, Zhang Y, Liu Z. In vivo biodistribution and toxicology of functionalized nano-graphene oxide in mice after oral and intraperitoneal administration. Biomaterials. 2013;34(11):2787-2795.
199. De Smet L, Colin P, Ceelen W, Bracke M, Van Bocxlaer J, Remon JP, Vervaet C. Development of a nanocrystalline Paclitaxel formulation for HIPEC treatment. Pharmaceutical research. 2012;29(9):2398-2406.
200. Sadzuka Y, Hirota S, Sonobe T. Intraperitoneal administration of doxorubicin encapsulating liposomes against peritoneal dissemination. Toxicology letters. 2000;116(1-2):51-59.
201. Li Y, Rodrigues J, Tomas H. Injectable and biodegradable hydrogels: gelation, biodegradation and biomedical applications. Chemical Society Reviews. 2012;41(6):2193-2221.
202. Silveira CP, Apolinário LM, Fávaro WJ, Paula AJ, Durán N. Doxorubicin-functionalized silica nanoparticles incorporated into a thermoreversible hydrogel and intraperitoneally administered result in high prostate antitumor activity and reduced cardiotoxicity of doxorubicin. ACS Biomaterials Science & Engineering. 2016;2(7):1190-1199.
203. Johnson L, Faidra Angelerou MG, Surikutchi BT, Allen S, Zelzer M, Marlow M. Low molecular weight nucleoside gelators: A platform for protein aggregation inhibition. Molecular pharmaceutics. 2018;16(1):462-467.
204. Skilling KJ, Kellam B, Ashford M, Bradshaw TD, Marlow M. Developing a self-healing supramolecular nucleoside hydrogel. Soft Matter. 2016;12(43):8950-8957.
205. Štaka I, Cadete A, Surikutchi BT, Abuzaid H, Bradshaw TD, Alonso MJ, Marlow M. A novel low molecular weight nanocomposite

hydrogel formulation for intra-tumoural delivery of anti-cancer drugs. International Journal of Pharmaceutics. 2019;565:151-161.

206. Skilling KJ, Ndungu A, Kellam B, Ashford M, Bradshaw TD, Marlow M. Gelation properties of self-assembling *N*-acyl modified cytidine derivatives. Journal of Materials Chemistry B. 2014;2(47):8412-8417.

207. El-Kamel RS, Ghoneim AA, Fekry AM. Electrochemical, biodegradation and cytotoxicity of graphene oxide nanoparticles/polythreonine as a novel nano-coating on AZ91E Mg alloy staple in gastrectomy surgery. Materials Science and Engineering: C. 2019;103(109780):1-9.

208. Xu L, Yu H, Yin S, Zhang R, Zhou Y, Li J. Liposome-based delivery systems for ginsenoside Rh2: *in vitro* and *in vivo* comparisons. Journal of Nanoparticle Research. 2015;17(10):415-428.

209. Zhang L, Zhou H, Belzile O, Thorpe P, Zhao D. Phosphatidylserine-targeted bimodal liposomal nanoparticles for in vivo imaging of breast cancer in mice. Journal of controlled release. 2014;183:114-123.

210. Chen X, Huang W, Wong BC, Yin L, Wong YF, Xu M, Yang Z. Liposomes prolong the therapeutic effect of anti-asthmatic medication via pulmonary delivery. International journal of nanomedicine. 2012;7:1139-1148.

211. Bastiat G, Pritz CO, Roider C, Fouchet F, Lignières E, Jesacher A, Glueckert R, Ritsch-Marte M, Schrott-Fischer A, Saulnier P. A new tool to ensure the fluorescent dye labeling stability of nanocarriers: a real challenge for fluorescence imaging. Journal of Controlled Release. 2013;170(3):334-342.

212. Yu Y, Tan S, Zhao S, Zhuang X, Song Q, Wang Y, Zhou Q, Zhang Z. Antitumor activity of docetaxel-loaded polymeric nanoparticles fabricated by Shirasu porous glass membrane-emulsification technique. International Journal of Nanomedicine. 2013;8:2641-2652.

213. Skilling KJ, Citossi F, Bradshaw TD, Ashford M, Kellam B, Marlow M. Insights into low molecular mass organic gelators: a focus on drug delivery and tissue engineering applications. Soft Matter. 2014;10(2):237-256.

214. Skilling KJ. Low molecular mass nucleoside gelators for intra-tumoural drug delivery. University of Nottingham; 2016.
215. Chen L, Raeburn J, Sutton S, Spiller DG, Williams J, Sharp JS, Griffiths PC, Heenan RK, King SM, Paul A. Tuneable mechanical properties in low molecular weight gels. Soft Matter. 2011;7(20):9721-9727.
216. Wright M. Nanoparticle tracking analysis for the multiparameter characterization and counting of nanoparticle suspensions. In. Nanoparticles in biology and medicine: Springer; 2012. p. 511-524.
217. Carr B, Wright M. Nanoparticle tracking analysis. Innovations in Pharmaceutical Technology. 2008;26:38-40.
218. Flessner MF. Peritoneal transport physiology: insights from basic research. Journal of the American Society of Nephrology. 1991;2(2):122-135.
219. Hirst AR, Coates IA, Boucheteau TR, Miravet JF, Escuder B, Castelletto V, Hamley IW, Smith DK. Low-molecular-weight gelators: elucidating the principles of gelation based on gelator solubility and a cooperative self-assembly model. Journal of the American Chemical Society. 2008;130(28):9113-9121.
220. Hutteman M, Mieog J, Van der Vorst J, Dijkstra J, Kuppen P, van der Laan A, Tanke H, Kaijzel E, Que I, van de Velde C. Intraoperative near-infrared fluorescence imaging of colorectal metastases targeting integrin αvβ3 expression in a syngeneic rat model. European Journal of Surgical Oncology. 2011;37(3):252-257.
221. Feng M, Zhang J, Anver M, Hassan R, Ho M. *In vivo* imaging of human malignant mesothelioma grown orthotopically in the peritoneal cavity of nude mice. Journal of Cancer. 2011;2:123-131.
222. Yu J, Lee H-J, Hur K, Kwak MK, Han TS, Kim WH, Song S-C, Yanagihara K, Yang H-K. The antitumor effect of a thermosensitive polymeric hydrogel containing paclitaxel in a peritoneal carcinomatosis model. Investigational new drugs. 2012;30(1):1-7.
223. Vassileva V, Moriyama E, De Souza R, Grant J, Allen C, Wilson B, Piquette-Miller M. Efficacy assessment of sustained intraperitoneal paclitaxel therapy in a murine model of ovarian cancer using

bioluminescent imaging. British Journal of Cancer. 2008;99(12):2037-2043.

224. Patenaude M, Smeets NM, Hoare T. Designing Injectable, Covalently Cross-Linked Hydrogels for Biomedical Applications. Macromolecular Rapid Communications. 2014;35(6):598-617.

225. Hoffman AS. Hydrogels for biomedical applications. Advanced Drug Delivery Reviews. 2012;64:18-23.

226. Nguyen QV, Park JH, Lee DS. Injectable polymeric hydrogels for the delivery of therapeutic agents: A review. European Polymer Journal. 2015;72:602-619.

227. Parhi R. Cross-Linked Hydrogel for Pharmaceutical Applications: A Review. Advanced Pharmaceutical Bulletin. 2017;7(4):515-530.

228. Kuo CK, Ma PX. Ionically crosslinked alginate hydrogels as scaffolds for tissue engineering: Part 1. Structure, gelation rate and mechanical properties. Biomaterials. 2001;22(6):511-521.

229. Sun HW, Feigal R, Messer H. Cytotoxicity of glutaraldehyde and formaldehyde in relation to time of exposure and concentration. Pediatric Dentistry. 1990;12(5):303-307.

230. Nguyen AK, Goering PL, Reipa V, Narayan RJ. Toxicity and photosensitizing assessment of gelatin methacryloyl-based hydrogels photoinitiated with lithium phenyl-2,4,6-trimethylbenzoylphosphinate in human primary renal proximal tubule epithelial cells. Biointerphases. 2019;14(2):021007(1-8).

231. Emoto S, Yamaguchi H, Kamei T, Ishigami H, Suhara T, Suzuki Y, Ito T, Kitayama J, Watanabe T. Intraperitoneal administration of cisplatin via an in situ cross-linkable hyaluronic acid-based hydrogel for peritoneal dissemination of gastric cancer. Surgery Today. 2014;44(5):919-926.

232. Zhu J. Bioactive modification of poly (ethylene glycol) hydrogels for tissue engineering. Biomaterials. 2010;31(17):4639-4656.

233. Nair DP, Podgorski M, Chatani S, Gong T, Xi W, Fenoli CR, Bowman CN. The thiol-Michael addition click reaction: a powerful and widely used tool in materials chemistry. Chemistry of Materials. 2013;26(1):724-744.

234. Schoenmakers RG, Van De Wetering P, Elbert DL, Hubbell JA. The effect of the linker on the hydrolysis rate of drug-linked ester bonds. Journal of Controlled Release. 2004;95(2):291-300.
235. Nie T, Baldwin A, Yamaguchi N, Kiick KL. Production of heparin-functionalized hydrogels for the development of responsive and controlled growth factor delivery systems. Journal of Controlled Release. 2007;122(3):287-296.
236. Lin CC, Ki CS, Shih H. Thiol–norbornene photoclick hydrogels for tissue engineering applications. Journal of Applied Polymer Science. 2015;132(8):41563(1-11).
237. McGann CL, Dumm RE, Jurusik AK, Sidhu I, Kiick KL. Thiol-ene Photocrosslinking of Cytocompatible Resilin-Like Polypeptide-PEG Hydrogels. Macromolecular bioscience. 2016;16(1):129-138.
238. Freitas C, Müller RH. Effect of light and temperature on zeta potential and physical stability in solid lipid nanoparticle (SLN™) dispersions. International journal of pharmaceutics. 1998;168(2):221-229.
239. Liu H, Li K, Xu L, Wu D. Bilayered near-infrared fluorescent nanoparticles based on low molecular weight PEI for tumor-targeted in vivo imaging. Journal of nanoparticle research. 2014;16(12):2784.
240. Tamm C. Pig liver esterase catalyzed hydrolysis: substrate specificity and stereoselectivity. Pure and applied chemistry. 1992;64(8):1187-1191.
241. Raghupathi KR, Azagarsamy MA, Thayumanavan S. Guest-Release Control in Enzyme-Sensitive, Amphiphilic-Dendrimer-Based Nanoparticles through Photochemical Crosslinking. Chemistry–A European Journal. 2011;17(42):11752-11760.
242. Shih H, Lin C-C. Cross-linking and degradation of step-growth hydrogels formed by thiol–ene photoclick chemistry. Biomacromolecules. 2012;13(7):2003-2012.
243. Fairbanks BD, Schwartz MP, Bowman CN, Anseth KS. Photoinitiated polymerization of PEG-diacrylate with lithium phenyl-2,4,6-trimethylbenzoylphosphinate: polymerization rate and cytocompatibility. Biomaterials. 2009;30(35):6702-6707.

244. Phelps EA, Enemchukwu NO, Fiore VF, Sy JC, Murthy N, Sulchek TA, Barker TH, García AJ. Maleimide cross-linked bioactive peg hydrogel exhibits improved reaction kinetics and cross-linking for cell encapsulation and in situ delivery. Advanced Materials. 2012;24(1):64-70.
245. García AJ. PEG–Maleimide Hydrogels for Protein and Cell Delivery in Regenerative Medicine. Annals of Biomedical Engineering. 2014;42(2):312-322.
246. Yu J, Xu X, Yao F, Luo Z, Jin L, Xie B, Shi S, Ma H, Li X, Chen H. In situ covalently cross-linked PEG hydrogel for ocular drug delivery applications. International Journal of Pharmaceutics. 2014;470(1-2):151-157.
247. Jansen LE, Negrón-Piñeiro LJ, Galarza S, Peyton SR. Control of thiol-maleimide reaction kinetics in PEG hydrogel networks. Acta Biomaterialia. 2018;70:120-128.
248. Darling NJ, Hung Y-S, Sharma S, Segura T. Controlling the kinetics of thiol-maleimide Michael-type addition gelation kinetics for the generation of homogenous poly (ethylene glycol) hydrogels. Biomaterials. 2016;101:199-206.
249. Riehl M, Harms M, Göttel B, Kubas H, Schiroky D, Mäder K. Acid-induced degradation of widely used NIR dye DiR causes hypsochromic shift in fluorescence properties. European Journal of Pharmaceutical Sciences. 2019;132:27-33.
250. Stevie F, Giannuzzi L, Prenitzer B. The Focused Ion Beam Instrument. Introduction to Focused Ion Beams. Springer, Heidelberg, 2005:1-12.
251. Al-Abboodi A, Fu J, Doran PM, Chan PP. Three-dimensional nanocharacterization of porous hydrogel with ion and electron beams. Biotechnology and Bioengineering. 2013;110(1):318-326.
252. Parmenter C, Baki A, Shakesheff K. Application of Cryogenic Focused Ion Beam Scanning Electron Microcopy to Hydrogel Characterisation. In.European Microscopy Congress 2016: Proceedings: Wiley Online Library; 2016:682-683.
253. Holmes R, Yang X-B, Dunne A, Florea L, Wood D, Tronci G. Thiol-ene photo-click collagen-PEG hydrogels: impact of water-soluble

photoinitiators on cell viability, gelation kinetics and rheological properties. Polymers. 2017;9(6):226-242.

254. Yeo Y, Ito T, Bellas E, Highley CB, Marini R, Kohane DS. *In situ* cross-linkable hyaluronan hydrogels containing polymeric nanoparticles for preventing postsurgical adhesions. Annals of Surgery. 2007;245(5):819-824.

255. Li L, Wang N, Jin X, Deng R, Nie S, Sun L, Wu Q, Wei Y, Gong C. Biodegradable and injectable in situ cross-linking chitosan-hyaluronic acid based hydrogels for postoperative adhesion prevention. Biomaterials. 2014;35(12):3903-3917.

256. Vintiloiu A, Leroux J-C. Organogels and their use in drug delivery—a review. Journal of Controlled Release. 2008;125(3):179-192.

257. Fu Y, Kao WJ. In situ forming poly (ethylene glycol)-based hydrogels via thiol-maleimide Michael-type addition. Journal of Biomedical Materials Research Part A. 2011;98(2):201-211.

258. Reddy LH, Murthy R. Pharmacokinetics and biodistribution studies of doxorubicin loaded poly (butyl cyanoacrylate) nanoparticles synthesized by two different techniques. Biomed Pap Med Fac Univ Palacky Olomouc Czech Repub. 2004;148(2):161-166.

259. Pham B, Colvin E, Pham N, Kim B, Fuller E, Moon E, Barbey R, Yuen S, Rickman B, Bryce N. Biodistribution and clearance of stable superparamagnetic maghemite iron oxide nanoparticles in mice following intraperitoneal administration. International Journal of Molecular Sciences. 2018;19(1):205.

260. Fontaine SD, Reid R, Robinson L, Ashley GW, Santi DV. Long-term stabilization of maleimide–thiol conjugates. Bioconjugate Chemistry. 2014;26(1):145-152.

261. Schädlich A, Rose C, Kuntsche J, Caysa H, Mueller T, Göpferich A, Mäder K. How stealthy are PEG-PLA nanoparticles? An NIR in vivo study combined with detailed size measurements. Pharmaceutical Research. 2011;28(8):1995-2007.

262. Parayath NN, Parikh A, Amiji MM. Repolarization of tumor-associated macrophages in a genetically engineered nonsmall cell lung cancer model by intraperitoneal administration of hyaluronic acid-

based nanoparticles encapsulating microRNA-125b. Nano Letters. 2018;18(6):3571-3579.

263. Rivera-Rodriguez GR, Lollo G, Montier T, Benoit JP, Passirani C, Alonso MJ, Torres D. *In vivo* evaluation of poly-l-asparagine nanocapsules as carriers for anti-cancer drug delivery. International Journal of Pharmaceutics. 2013;458(1):83-89.

264. Lollo G, Rivera-Rodriguez GR, Bejaud J, Montier T, Passirani C, Benoit J-P, García-Fuentes M, Alonso MJ, Torres D. Polyglutamic acid–PEG nanocapsules as long circulating carriers for the delivery of docetaxel. European Journal of Pharmaceutics and Biopharmaceutics. 2014;87(1):47-54.

265. Yonemura Y, Endou Y, Bando E, Kuno K, Kawamura T, Kimura M, Shimada T, Miyamoto K-i, Sasaki T, Sugarbaker PH. Effect of intraperitoneal administration of docetaxel on peritoneal dissemination of gastric cancer. Cancer Letters. 2004;210(2):189-196.

266. Kuyinu EL, Narayanan G, Nair LS, Laurencin CT. Animal models of osteoarthritis: classification, update, and measurement of outcomes. Journal of Orthopaedic Surgery and Research. 2016;11(1):19-46.

267. Jones MD, Tran CW, Li G, Maksymowych WP, Zernicke RF, Doschak MR. In vivo microfocal computed tomography and micro–magnetic resonance imaging evaluation of antiresorptive and antiinflammatory drugs as preventive treatments of osteoarthritis in the rat. Arthritis & Rheumatism. 2010;62(9):2726-2735.

268. Furman BD, Mangiapani DS, Zeitler E, Bailey KN, Horne PH, Huebner JL, Kraus VB, Guilak F, Olson SA. Targeting pro-inflammatory cytokines following joint injury: acute intra-articular inhibition of interleukin-1 following knee injury prevents post-traumatic arthritis. Arthritis Research & Therapy. 2014;16(3):R134-R149.

269. Bowman S, Awad ME, Hamrick MW, Hunter M, Fulzele S. Recent advances in hyaluronic acid based therapy for osteoarthritis. Clinical and Translational Medicine. 2018;7(1):6-17.

270. A Peattie R, P Grentzmann I, A Firpo M. Recent Advances in Delivery of Cytokines, Growth Factors, and Molecules of Therapeutic Interest

from Hyaluronan-based Hydrogels. Current Tissue Engineering. 2015;4(1):47-56.

271. Connolly DC. Animal models of ovarian cancer. Ovarian Cancer. Springer, Boston, MA. 2009:353-391.

272. Bhargava S, Hotz B, Buhr HJ, Hotz HG. An orthotopic nude mouse model for preclinical research of gastric cardia cancer. International Journal of Colorectal Disease. 2009;24(1):31-39.

273. Zhang ZX, Li DC, Zhao H, Zhu DM. Suppressive Effect of Recombinant Adenovirus-mediated Endostatin Gene by Intraperitoneal Injection on Pancreatic Cancer in an Orthotropic Nude Mouse Model. Suzhou University Journal of Medical Science. 2009;1-11.

274. Li Z, Zhao L, Liu L, Ding Y. Monitoring changes of serum protein markers in metastatic colorectal carcinoma model. Chinese Journal of Pathology. 2007;36(1):48-52.